Author:
Salim, Wijaya

Title:
Punching shear failure in reinforced concrete slabs with membrane restraint

ACKNOWLEDGEMENTS

I am deeply grateful to Dr. Wendel Sebastian, who stimulated my interest in the present research, for his supervision and for his critical reading of the thesis.

My deep appreciation to all the technical staff of both the Concrete as well as the Structures Laboratories. In particular, I thank Mr. Dave Hooper and Peter Whereat for their assistance and advice on the set-up of the experiments. Further thanks are due to my colleagues, Mr. Jun Kim and Mr. Shivendren Ananadakrishnan for their help with the preparation and the testing of the concrete specimens.

This research programme was funded by the Bristol Postgraduate Scholarship and the Overseas Research Scholarship (ORS) from the Committee of Vice-Chancellors and Principals of the Universities of the United Kingdom. I am indeed very grateful.

Finally, I want to share my happiness with my mother and brother. Their unconditional love and full support to me is always in my mind. My beloved wife, Grace, who has accompanied me throughout the sorrow and joyful days studying abroad. I cherish her from the bottom of my heart. Her love and patience enriched my life and gave me the trust in which we can support each other for the rest of our lives.

Wijaya Salim

Bristol, England

DECLARATION

The research presented in this thesis was conducted between October 2000 and September 2003, under the supervision of Dr. Wendel Sebastian of Bristol University. The work described was carried out by the author, except where indicated in the text. Parts of Chapters 3 and 4 have been published in international journals, see references (2) and (3) below. In addition, the material presented in Chapter 5 was also presented and well-received at a conference, see reference (1) below. None of this work has been submitted in support of any other degree or qualification.

Papers published based on some of the work of this thesis

1. Salim, W., and Sebastian, W.M., "Simplified model for estimating punching resistance of reinforced concrete slabs", *Proceedings of the First FIB Congress – Concrete Structures in the 21st Century*, Osaka, Japan, October, 2002.

2. Salim, W., and Sebastian, W.M., "A plasticity model for predicting punching shear strengths of reinforced concrete slabs", *ACI Structural Journal*, American Concrete Institute, Vol. 99, Issue. 6, Nov., 2002, pp. 827-835.

3. Salim, W., and Sebastian, W.M., "Punching shear failure in reinforced concrete slabs with compressive membrane action", *ACI Structural Journal*, American Concrete Institute, Vol. 100, Issue 4, July 2003, pp. 471-479.

Signed:..... Date: 21/06/06

ABSTRACT

In this study, three important and previously unresolved issues surrounding the prediction and experimental study of punching shear failure of reinforced concrete flat slabs have been investigated, namely: (1) Investigation of the roles of effectiveness factors for prediction of punching failure loads via both the work method and an equilibrium approach; (2) Experimental study of the stiffness (from various sources), and enhancing effect on failure load, of the surround restraint ; and (3) Experimental study of the effect, on the punching failure load, of deviation from axi-symmetry of the punching failure surface in a nominally axi-symmetric slab under central loading.

The work method along with plastic theory was employed to predict the punching shear failure loads of reinforced concrete slabs without shear reinforcement and with little in-plane restraint. An improved material model which accounts for the variation in angle of friction of the concrete with stress state has been incorporated into this analysis. A key focus of this analytical work was the study of the sensitivities of the predicted failure loads to variations in the tension and compression effectiveness factors used for the concrete. This theory was also extended to incorporate the effect of compressive membrane action for the prediction of the enhanced punching shear strength of restrained reinforced concrete slabs. This incorporated sensitivity studies to establish the effects – on both surround stiffness and failure load – of varying quantities of surround concrete and also of steel hoops and straight bars. In addition, an alternative to the work method, namely the equilibrium approach incorporating a purpose-calibrated size effect factor, was developed and successfully applied to a wide range of published test data.

A total of five large-scale flat slabs, comprising both square and circular specimens, were also designed and tested to punching failure. It was found that the predicted failure loads correlate well with the test results conducted within this PhD study, despite disparities between the predicted and measured failure surfaces.

Generally, it was found that the predictions from the work and equilibrium approaches correlate well with a range of experimental data. Most importantly, a further investigation of the work method reveals that the plastic approach may well incorporate membrane enhancements to some extent. It is concluded that, provided the effectiveness factors are properly calibrated, the work method provides reliable predictions of punching shear capacity. It is also concluded that moderate deviations of the punching failure surface from the commonly assumed axi-symmetric failure surface may not necessarily impact significantly on predictions of failure load.

CONTENTS

PUNCHING SHEAR FAILURE IN REINFORCED CONCRETE SLABS WITH MEMBRANE RESTRAINT

WIJAYA SALIM

Dissertation submitted to the University of Bristol in partial fulfilment of the requirements for the degree of Doctor of Philosophy

UNIVERSITY OF BRISTOL

2006

NOTATION

a	radius of slab
c	diameter/side length of loaded area
c_k	parameter related to ratio of compressive to tensile strengths of concrete
c_t	column perimeter
d	effective depth of slab
d_0	punch diameter
d_1	outer diameter of punched cone
d_h	diameter of cross-section of hoop steel bar
ds	increment of length along the generatrix of the failure surface
D	diameter of support
D_A	rate of dissipation of internal energy per unit area
E_c	young modulus of concrete
E_s	young modulus of steel
e	radial displacement of slab
f_c	uniaxial cube strength of concrete
f_{cu}	effective uniaxial compressive strength of concrete
f'_c	cylinder strength of concrete, taken as 80% of concrete cube strength f_{cu}
f_t	effective uniaxial tensile strength of concrete
f_y	yield strength of steel reinforcement
F_{ct}	radial resultant of the tangential forces in the concrete
F_{cr}	radial force in the concrete at the column face

F_{dowel}	dowel forces of steel cutting across the inclined crack
F_{sr}	radial force in the steel cutting across the shear crack
F_{st}	resultant of the tangential forces in the steel
h	slab thickness
L	clear span of slab panels
n_a	compressive membrane force actng at boundary
n_r	radial compressive membrane force in slab
n_c	stress concentration factor
n_s	modular ratio
N_{rs}	sum of radial compressive membrane forced acting on failure surface
P	punching shear load
P_{ACI}	punching load predicted by American code ACI 318-89
P_{BS8110}	punching load predicted by British code BS 8110
P_C	predicted punching load based on curved generatrix
P_E	experimental punching load
P_L	predicted punching load based on linear generatrix
P_P	predicted simplified punching load
r	radial (horizontal) coordinate of generatrix of failure surface
r_0	radius of a coulmn or loaded area
r_3	radius of slab
r_p	radius of a peripheral load or reaction
r_s	radius within which all steel is yielding

r_w	punching radius
S	stiffness parameter of laterally restrained slab
S_b	slab-self stiffness
S_s	total surround stiffness
u	relative displacement rate
υ	poisson ratio for conrete = 0.2
w_0	critical central deflection
w_i	an initial elastic delfection at which membrane force starts
W_A	total rate of dissipation of internal energy
W_E	rate of working of external load
x	vertical coordinate/neutral axis depth
z	lever arm
α	angle between normal to $\tau - \sigma$ failure surface and τ axis
α'	angle between tangent to generatrix of failure surface and relative displacement rate vector
β	angle between elative displacement and vetical
γ_{nt}	shear strain
Δ	middle surface extension of radial segment of slab
Δ_a	middle surface extension at support
Δ_b	middle surface extension at centre of slab
δ	thickness of a plane homogeneous strain field
ε_n	normal strain
ε_{st}	tangential steel strain

ε_t	tangential strain
η	dimensional distance from middle surface to axis of rotation
η_a	dimensional distance from middle surface to axis of rotation at support
η_b	dimensional distance from middle surface to axis of rotation at centre of slab
θ	rotation of radial segment of slab
θ_a	rotation at support
θ_b	rotation at centre of slab
λ	angle of inclination of inclined crack
σ	normal stress on an arbitrary plane
σ_1, σ_3	principal stresses
σ_b	bearing capacity
τ	shear stress on an arbitrary plane
φ	angle of internal friction
ϕ	flexibility factor of laterally restrained slab
ρ	tension steel reinforcement ratio (A_s / bd)
ρ_r	percentage of radial steel reinforcement
$\Delta\phi$	small sectorial angle of a radial element
ξ	size effect coefficient
ψ_f	rotation at failure
μ_c	ratio of effective compressive strength to actual compressive strength of concrete
μ_t	ratio of effective tensile strength to effective compressive strength of concrete

1

INTRODUCTION

1.1 Background

1.2 Objectives of this study

1.3 Structure of the thesis

Chapter One

INTRODUCTION

1.1 BACKGROUND

Reinforced concrete *flat* slabs are used largely in car parks and residential buildings. Flat slabs can sometimes be advantageous over conventional slab-beam construction from both architectural and economic points of view. The following points highlight some of the advantages of using flat slab construction:

- Reduction in formwork;
- Flush soffit and hence minimum construction depth
- Simplicity of construction which facilitates reduction of the construction time;
- Reduction of the storey height, allowing an increase in the number of floors within a fixed height or, alternatively, saving on cladding;
- Reduction in finishing material;
- Maximum flexibility for horizontal service distribution.

One of the most significant modes of failure in flat slab construction is *punching shear failure*. Punching shear failure occurs in reinforced concrete slabs subjected to concentrated loading when a cone of concrete is suddenly pushed through the slab by the load, as shown in Fig. 1.1(b). This mode of failure can occur in *flat slabs* around columns, in *pad footings* underneath columns and in *bridge deck slabs* under concentrated wheel loads. This thesis focuses on punching shear failure of ***flat slabs***. Fig. 1.2 shows a typical punching shear failure of a reinforced concrete slab-column connection with axial column load.

A recent dramatic example of flat slab punching shear failure occurred in 1997, when a 120 tonne, 15m x 15m top floor flat slab of the Pipers Row multi-storey car park in Wolverhampton collapsed at about 3 am on 20th March due to punching shear failure at one column leading to partial progressive collapse throughout the structure. For this failure, Figure 1.3 shows the partially collapsed 4th floor, while Figure 1.4 shows the punching local to one of the interior slab-column connections.

Research on punching shear strength since the 1960s has focused on deriving analytical approaches. Two representative theoretical approaches, namely the work approach based on Plasticity Theory, and an alternative approach founded on satisfying equilibrium requirements, have enjoyed encouraging success despite assuming different failure mechanisms.

Each theory incorporates approaches which could be further refined to significantly enhance its predictive capabilities. In particular, the following highlights some of the areas which require further exploration:

- Effectiveness factors used in previous work to align the predictions with the experimental results have been determined almost purely by comparison with test data. The issue of the general robustness of these factors, in particular the sensitivities of the failure load predictions to variations in these factors as a *generic* issue has been left largely unaddressed.
- Investigation of the validity of the plastic approach in terms of its predictive capabilities against experimental results and in particular, verification of the *assumed failure surface profile* via extensive comparison against experimental results.
- Investigation of the effect of loss of axisymmetry – in a nominally axisymmetric slab under central loading – on both the shape of the failure surface and the punching failure load.

In addition to the above issues, it is to be noted that the effect of compressive membrane action has been found to result in significant enhancement to the ultimate load capacity of reinforced concrete slabs with lateral restraint. Although the theory for compressive membrane action is developing, little work has so far focused on quantification of the surround restraint in detail. As a result, there is significant scope for more thoroughly addressing the issue of the existence of a threshold restraint magnitude beyond which there is little or no further enhancement on punching failure load. This important facet of the effects of membrane restraint on punching capacity requires more in-depth study from the point of view of both *limits on the restraint*

stiffness with increasing amounts of surrounding material and *limits on the strength-enhancing effect of this stiffness*. This is significantly crucial for the case of say *corner* columns in flat slab construction, where additional surrounding material can be specified to achieve a desirable strength.

1.2 OBJECTIVES OF THIS STUDY

The main concern of this thesis is to improve the present understanding of the principal factors which influence the punching shear strength of reinforced concrete slabs. There were seven primary objectives to this study, as follows:

1) Introduction of a suitable set of effectiveness factors together with the application of plastic theory for prediction of the punching shear strengths of both unrestrained and restrained reinforced concrete slabs.

2) Investigation of the ranges within which the effectiveness factors may be varied without significantly influencing the plastic predictions.

3) Simplification of the plastic analysis (work method) whilst still retaining the reliable predictive capabilities of this approach.

4) Introduction of a simplified equilibrium model with an appropriate size effect factor as an alternative to the work method tied in with plastic theory.

5) Investigation of the effects of different degrees of restraint inherent in reinforced concrete slab-column systems, with restraint provided via incorporating hoop reinforcement as well as by providing extra surrounding

material outside the punching failure zone.

6) Discussion of the effect of loss of axisymmetry – in a nominally axisymmetric slab under a central point load – on both the shape of the failure surface and the punching failure load.

7) Verification of the appropriateness of applying the plastic theory for prediction of punching failure loads of restrained reinforced concrete slabs via extensive comparison against test results reported in the literature and also with the experimental results obtained in the present research.

A brief description of the remaining chapters of the thesis, where these research results are discussed, is given in the next section.

1.3 STRUCTURE OF THE THESIS

This thesis is constructed in 7 chapters. In the next chapter, the historical background to the analysis and design of reinforced concrete slabs subjected to concentrated loading is presented and the relevant literature on both punching shear failure and compressive membrane action is reviewed. Subsequently, in Chapter 3, a method of analysis for predicting the punching shear strength of reinforced concrete slabs using the application of plasticity theory with alternative failure material models for concrete, including proposals for appropriate effectiveness factors for the concrete, is presented. It is worth noting that much of the presentation and discussion of the theoretical analyses given in Chapter 3 has been published in the ACI Structural Journal (Salim & Sebastian (2002)). The proposed theoretical model for the upper bound

analysis is then extended to incorporate the effect of compressive membrane action for the prediction of the enhanced punching shear strength of laterally restrained reinforced concrete slabs in Chapter 4. In addition, an attempt to quantify the surrounding restraint is also pursued using Lame axi-symmetric analysis. It is also worth noting that the content of Chapter 4 has also been published in the ACI Structural Journal (Salim & Sebastian (2003)).

In Chapter 5, an equilibrium model which incorporates the influence of the size effect is presented. The material forming the basis of that Chapter was published in the Proceedings of the first FIB congress, Japan, (Salim & Sebastian 2002). Subsequently, an experimental programme conducted to investigate the behaviour of reinforced concrete slabs with inherent membrane restraint, and the effect of different degrees of restraint on ultimate load capacity of the slabs, are presented in Chapter 6. Most importantly, a verification of the proposed plastic analysis presented in Chapter 4 was pursued in order to validate the assumptions made in the proposed analysis.

In the course of the thesis, the proposed models are verified by extensive comparisons of the predicted failure loads with measured failure loads from a wide range of tests reported in the literature. At the end of each chapter, the major points of importance are summarised. General conclusions are finally drawn from an overall perspective of the study in Chapter 7.

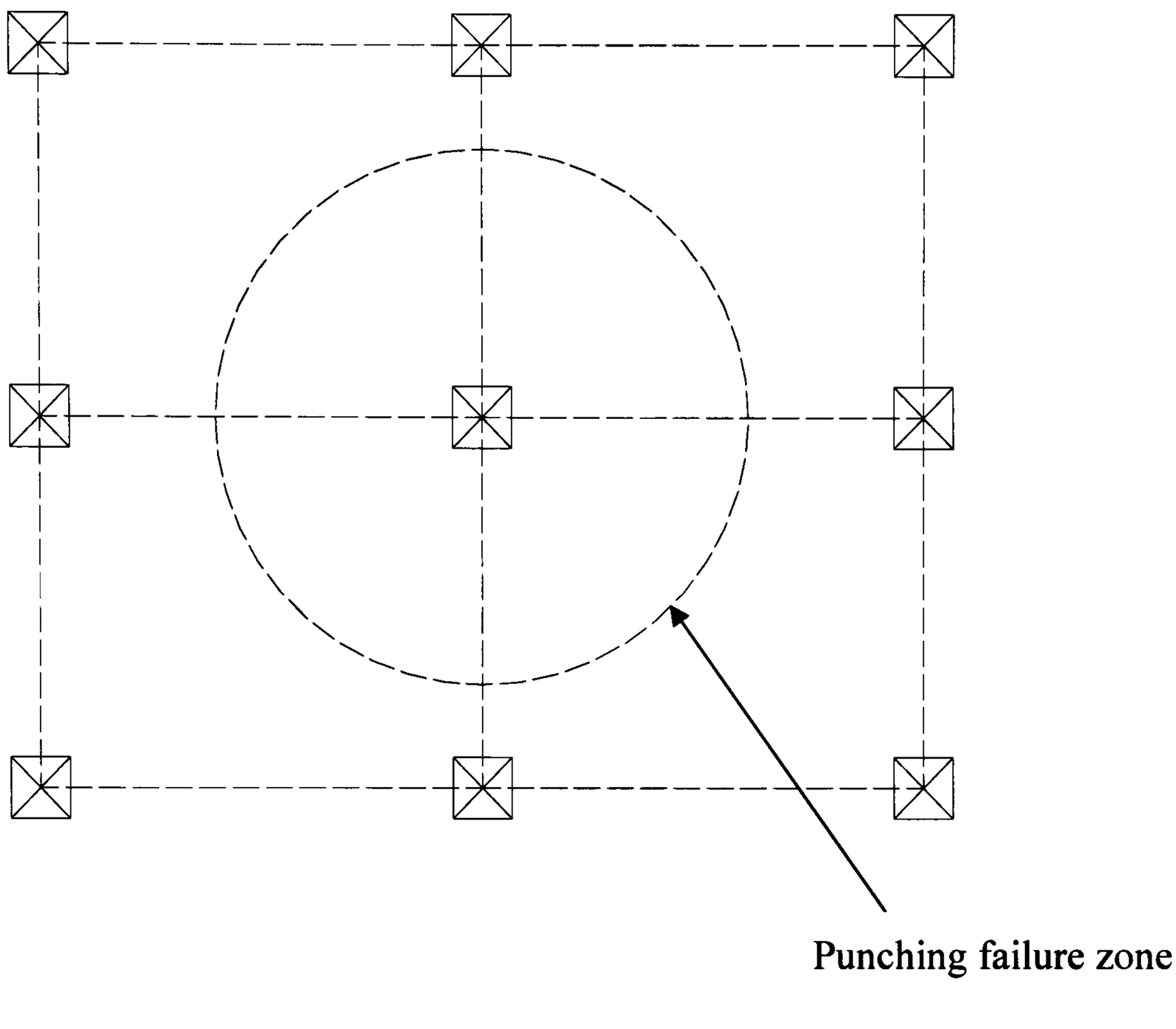

FIG. 1.1(a) Plan layout of a flat slab monolithic with supporting columns

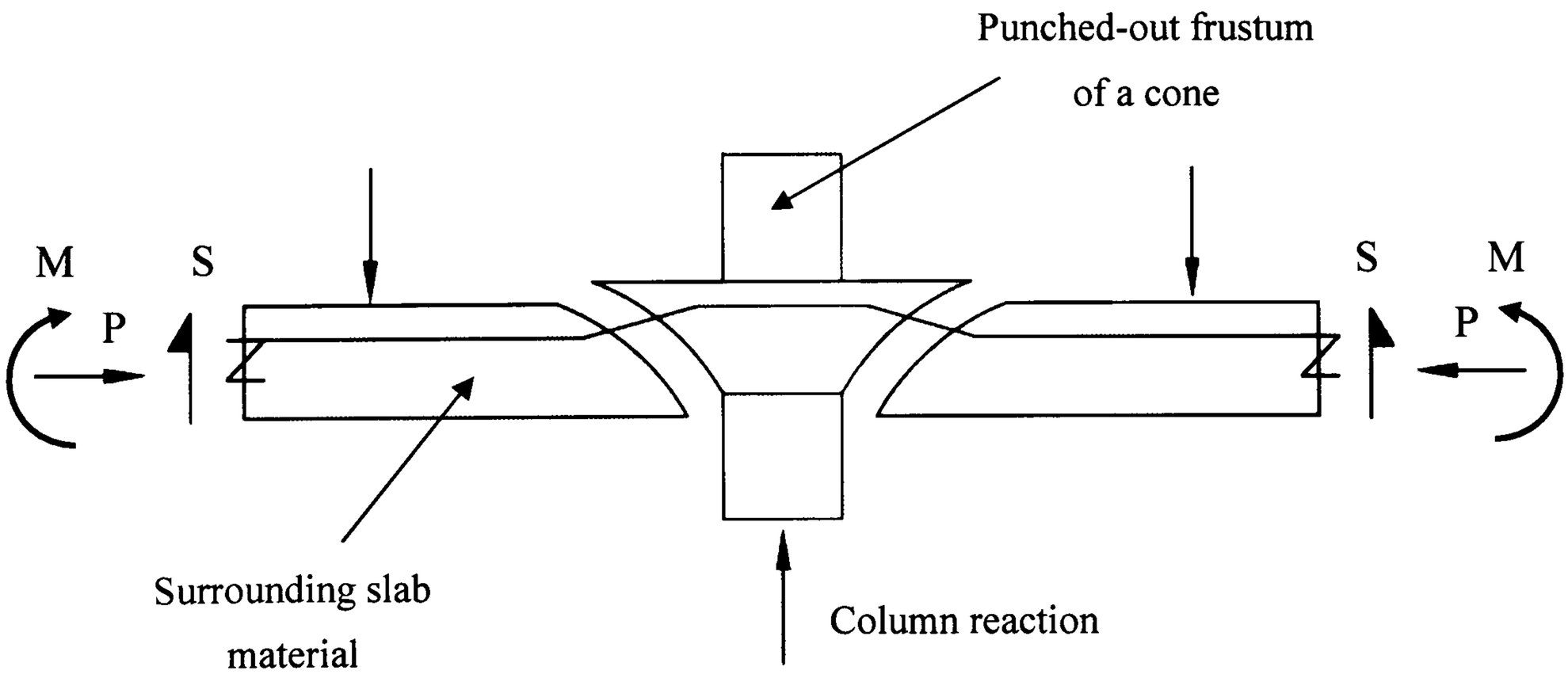

FIG. 1.1(b) Typical punching shear failure at interior bay

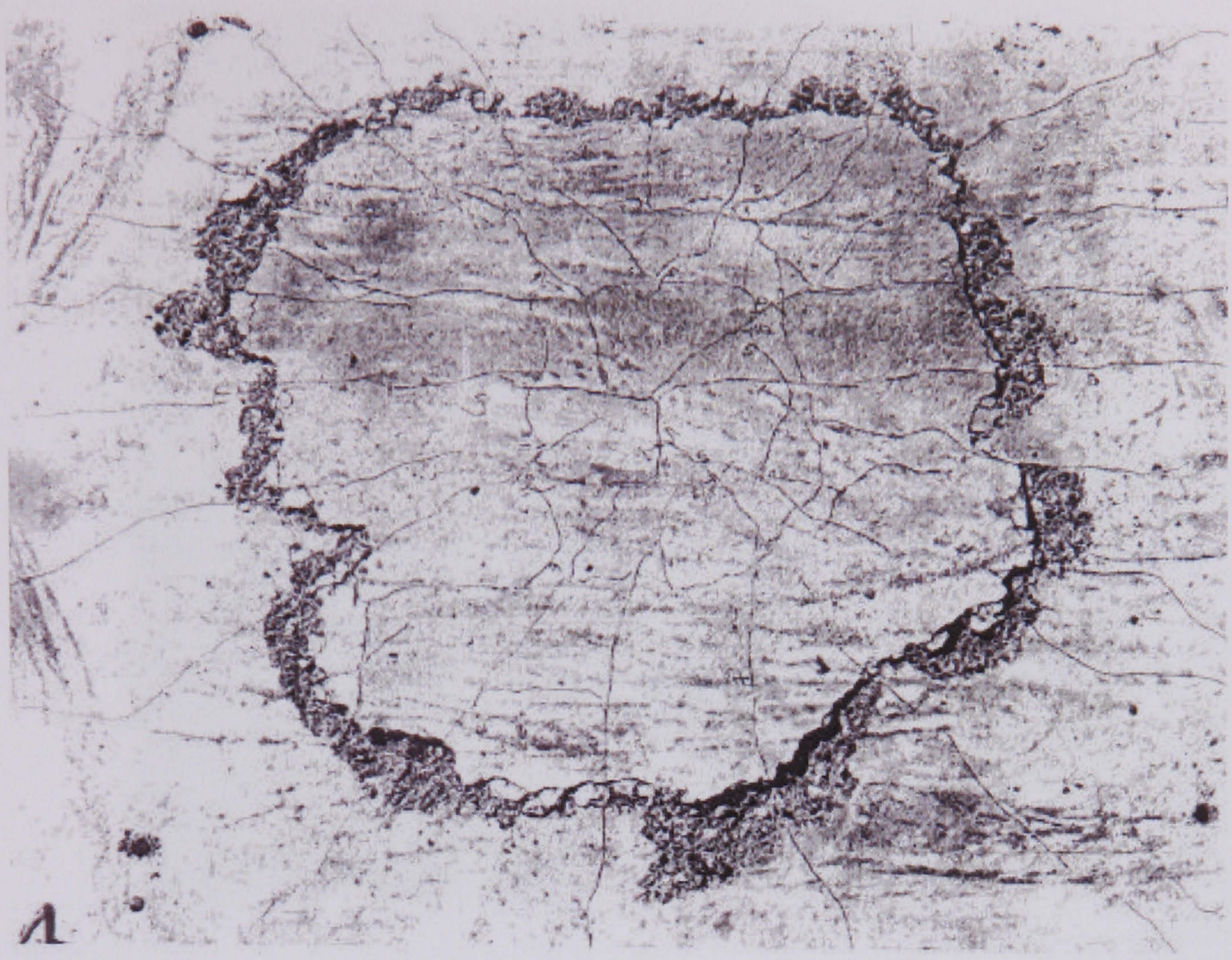

FIG. 1.2 Punching shear failure of reinforced concrete slab-column connection due to axial column load [34]

FIG. 1.3 Collapsed 4th floor slab at Pipers Row Car Park, Wolverhampton [106]

FIG. 1.4 Punching shear failure at interior slab-column connection at Pipers Row Car Park, Wolverhampton [106]

2

HISTORICAL REVIEW

2.5 Areas for Further Exploration

2.5.1 Lack of focus on Simplification on Existing Theoretical Approaches

2.5.2 Influence of Variation in Effectiveness Factors Employed in Plastic Analysis

2.5.3 Experimental Approach to Determination of Surround Restraint

2.6 Summary

Chapter Two

HISTORICAL REVIEW

2.1 INTRODUCTION

This Chapter reviews research into the punching shear failure of reinforced concrete slabs. Emphasis is placed on the investigation of the enhancing effect of surround restraint on punching capacities as a result of compressive membrane action. Research on punching shear since the 1960s revealed the existence of 2 representative analytical approaches, which were employed to provide predictions namely: upper bound or lower bound analyses and in some cases, semi-empirical approaches. The review aims to demonstrate that although much research effort has been focused on the development towards a more rational theoretical treatment of the punching shear problem as well as a better understanding of the contribution to the enhancement in punching capacities as a result of compressive membrane action, there still exist some important issues which require further investigation. In particular, this chapter highlights the urgent need for further work in the following areas:

- Use of *both* (as opposed to *either*) upper and lower bound approaches to enhance the reliability of prediction of punching shear failure loads in reinforced concrete slabs subjected to concentrated loading.

- Investigation of the *sensitivity* of the predicted punching capacities via the application of plasticity theory to the effectiveness factors used for the concrete material as a *generic* issue.

- Simplification of the plastic approach whilst still retaining the predictive capabilities of the mathematical models.

- Incorporation of the influence of the *size effect* in the equilibrium approach.

- Consideration of both the enhancing effect by surrounding concrete and additional surround restraint from hoop steel as the basis of an experimental programme for this PhD study.

- Investigation of the use of hoop reinforcement to simulate the surrounding concrete restraint in an attempt to facilitate laboratory experiments.

- Investigation of the effect of loss of axisymmetry – in the critical region of nominally axisymmetric slab under central concentrated loading – on the shape of the failure surface and on the punching shear failure load.

The remainder of Chapter 2 is divided into 3 main sections, namely a section on upper and lower Bound *theoretical* treatments of punching shear where in-plane restraint is insignificant, another on *empirical* approaches for the unrestrained cases, and a final section on previous work into the modelling and experimental investigations into

membrane restraint effects on punching shear capacity of *restrained* slabs.

This helps to put the new ideas covered in the present PhD study into a suitable context. The outstanding issues raised in the bullet points above are discussed and emphasized in greater depth, which leads to an establishment for the work reported in the remaining chapters of this thesis. Finally, conclusions are drawn from the extensive discussions of this chapter.

2.2 THEORETICAL TREATMENT OF PUNCHING SHEAR STRENGTH OF SLABS

2.2.1 Upper Bound/Plasticity Approach

The yield line theory developed by Johansen for flexural failure of slabs was popular. In 1970, Gesund [34] employed this theory to analyse punching failure in slabs. He assumed a yield line fan mechanism around the column as shown in Fig. 2.1. The ultimate load calculated for that mechanism was considered to be the ultimate punching load for the case of an interior circular column, i.e.,

$$P_{u,p} = \frac{6\pi m(1+u)A_{slab}/A_0 \cdot \eta}{3(\eta-1)\frac{A_{slab}}{A_0} - (\eta^3 - 1)} \tag{2.1}$$

where:

$$\eta = \frac{r}{r_0} = \sqrt[3]{\frac{3}{2}\cdot\frac{A_{slab}}{A_0} - \frac{1}{2}}$$

u = percentage of steel reinforcement

The approach was limited to slabs with reinforcement ratios normally accepted in design. For slabs with high reinforcement ratio, punching might take place before yield [66] and so the above expressions may not be valid.

Another application of plastic theory to estimate the punching resistance of axisymmetric concrete slabs without shear reinforcement was presented by Nielsen et al [70]. This theory is in contrast with Gesund method, as the failure mechanism adopted (Fig. 2.2) is totally independent of the flexural properties of the slab. The mechanism is one of the punching out of a solid of revolution attached to the column, while the rest of the slab remains rigid. Using the minimisation of work together with the modified failure criterion and the normality flow rule in a plane strain condition, the minimum upper bound solution for the ultimate punching load can be obtained.

In 1986, Jiang & Shen [46] presented a theoretical solution for predicting the punching shear strength of concrete slabs followed by a discussion in 1987 [47]. The problem was treated as a three-dimensional axi-symmetrical one with the material assumed to be rigid-plastic. A parabolic failure criterion was suggested.

A more recent attempt at using the plasticity theory was made by Kuang & Morley [55] for prediction of punching shear failure of reinforced concrete slabs, in which a parabolic Mohr failure criterion for concrete was adopted. Predictions made by the proposed analysis showed good agreement with experimental results.

2.2.2 Lower Bound/Equilibrium Approach

The original slab equilibrium model developed by Kinnunen and Nylander [50,51] about 40 years ago, remains one of the most reliable equilibrium models for slabs. In the derivation of this theory, a mechanical model of failure, as shown in Fig. 2.3 was assumed on the basis of observations from a series of tests on circular slab-column specimens. It was assumed that the slab is divided into rigid segments, each bounded by two radial crack lines, a part of initial circumferential crack and the slab boundary or the lines of contra-flexure around the column. The radial segments rotate around the centre of rotation, C.R., at the face of the column and on the level of neutral axis. Failure is assumed to occur when the tangential strains at the bottom of the slab below the root of the shear crack reach a characteristic value which was determined from tests on slabs with ring reinforcement only. The punching load was calculated by applying the conditions of equilibrium and then following a convergent iterative process. Kinnunen and Nylander found that the predictions made by the proposed method above showed satisfactory agreement with the results of their own tests and those of Elstner and Hognestad [30]. Kinnunen [50] later extended the method to cover slabs with two-way reinforcement, with reasonable accuracy.

In the 1980s, Shehata [92,93,94] presented a mechanical model based on the work by Kinnunen & Nylander for predicting the punching resistance of axi-symmetric reinforced concrete slabs subjected to concentrated loads or reactions. Material characteristics are defined by generally accepted stress-strain relationships with failure criteria expressed in terms of the limit at which tension is developed in the critical region of concrete. In particular, the influence of *size effect* on punching shear, in terms of the effective depth of slab was taken into account based on the test results of

Regan [86]. The range of data used in determining the size effect factor was very limited.

In 1999, Yankelevsky [107] presented a new model, based on rigid post-fractured behaviour, utilizing the post fracture properties of concrete at the rough crack interfaces that are developed. The model predicts the force-displacement resistance during punching, the stress distributions along the crack interfaces, as well as the shape of the punched concrete plug. Comparison of the model showed good correlation with various data.

Recently, Marzouk et al [60] proposed a numerical model which incorporates a fictitious crack model together with equilibrium considerations to predict the punching load and the deformations of reinforced concrete slabs. Important features which include concrete strength, aggregate type, reinforcement ratio as well as the fracture strength properties were taken into account in developing the model. They pointed out that despite the low tensile strength of concrete, it has considerable fracture energy which contributes to the flexural concrete strength.

Research on the theoretical treatment of punching shear failure of reinforced concrete slabs was based on either Plasticity Theory or Equilibrium Approaches. In this PhD study, in addition to the use of Plasticity Theory for prediction of punching capacities of reinforced concrete slabs, research into the application of Equilibrium analysis based on the work by Kinnunen and Nylander is also pursued. In particular, a simplified model together with consideration of the size effect will be presented in Chapter 5. The aim of considering both approaches as opposed to only one of them is to provide a fairly narrow range of predictions of punching capacity.

2.2.3 Numerical Approach

In 1996, Menetrey [62] presented an analytical expression to compute the punching shear strength of reinforced concrete slabs, derived from results obtained with numerical simulation of the failure phenomenon. The simulation revealed that punching can be computed by integration of assumed constant *vertical* stresses around the assumed truncated cone shape punching crack. The punching strength expression is expressed in terms of the tensile strength of concrete, percentage of reinforcement, slab thickness and radius of punching crack initiation. In the following year, Menetrey et al [63] developed a numerical model to reproduce the punching shear failure in reinforced concrete structures. The model is characterized by an efficient triaxial strength criterion for concrete, a non-associated flow rule and a cracking model accounting for the brittleness of concrete failure under various states of stress. Three important characteristics were demonstrated: (1) punching failure is due to tensile failure of concrete along the inclined punching crack rather than due to compressive failure; (2) increasing the percentage of reinforcement reduces the state of internal cracking resulting in an increase in failure load and a reduction of the ductility; and (3) the size effect observed experimentally is reproduced and a size effect law is proposed.

In 1998, Polak [77] examined the applicability of using layered finite elements to model punching shear of reinforced concrete slabs. The formulation incorporates quadratic, degenerate, isoparametric shell elements which are capable of taking out-of-plane shear response into account. The proposed finite element formulation was used for the analysis of several slabs subjected to highly concentrated transverse forces.

2.2.4 Empirical Approach and Previous Experimental Work

Punching shear has been a subject which stimulated the interest of many researchers since 1909, when Talbot made his study of this problem in footings. In 1913, at the end of his experimental programme, he proposed a method for design against punching shear failure suggesting an expression in terms of the nominal shear stress at a critical perimeter distant d from the face of the column:

$$\tau_n = \frac{P}{2\pi(r_0 + d)z} \tag{2.2}$$

According to Talbot, punching shear failure is due to diagonal tension and hence the limit for τ_n should be proportional to f_t and, consequently, proportional to f_c.

Since the lever arm z decreases when the ratio of reinforcement increases, the estimated punching resistance obtained using Equation 2.2 decreases with the increase of the ratio of flexural steel reinforcement. In fact, this actually contradicts the experimental findings of Criswell [22] and Regan [86].

During the following three decades, extensive experimental tests [33,36,37,42,68,69,88-91,96] were conducted on slabs and footings, from which empirical relationships were derived and proposed. In 1938 Graf [37], and subsequently Forsell and Holmberg [33] in 1946, investigated the problem of punching shear failure in concrete slabs subjected to concentrated loads. They proposed a similar formulation to the one proposed by Talbot, but disagreed on the location of the critical perimeter and, consequently, on the limiting shear stress. In addition, they also

replaced the lever arm z of Equation 2.2 by the slab thickness h. According to Graf, the critical perimeter is at the column periphery, while Forsell and Holmberg suggested that it should be at $h/2$ from the column. In the latter case, the shear stress distribution over the slab thickness is assumed to be parabolic.

$$\tau_n = \frac{P}{2\pi r_0 h} \qquad \text{(Graf)} \qquad (2.3)$$

$$\tau_n = \frac{1.5P}{2\pi(r_0 + 0.5h)h} \qquad \text{(Forsell and Holmberg)} \qquad (2.4)$$

Fig. 2.4 illustrates the effect of the chosen critical perimeter on the punching resistance for the ratio $2r_0/d = 1$, together with some tests results. Experimental work conducted by Elstner and Hognestad excluded the case $2r_0/d = 1$; hence their results are plotted so that the inner most point for $2r_0/d \approx 2$ coincides with Kinnunen . The figure suggests that the test results are most consistent with the line obtained from the critical perimeter situated at a distance d from the periphery of the loaded area.

In 1948, Richart [88,89] presented the results of a very extensive investigation on reinforced concrete footings. He concluded that the shearing stresses rather than the bond stresses between the steel reinforcement and the concrete could be a critical feature of the design of a slab subjected to concentrated loading. In a re-evaluation of Richart tests results of column footings, Hognestad [42] suggested that the ultimate strength of slabs failing in shear is mainly dependent on the following factors:

(1) Properties of the materials used in the slab: quality of concrete as expressed by cylinder strength f'_c; amount, type and quality of steel reinforcement.

(2) Size and shape of loaded area as compared to the slab thickness.

(3) Span, support conditions and edge restraints of the slab.

The final failure of a slab was believed to take place by shearing of the compression zone directly around the loaded area, hence Hognestad proposed a formula to calculate the shear stress:

$$v = \frac{V}{sd} \tag{2.5}$$

where s is the perimeter of the loaded area. It was found that the ultimate shearing stress of a variety of slabs could be expressed by the empirical equation:

$$v = 0.00689\left[\left(0.035 + \frac{0.07}{\phi}\right) \cdot f'_c + 130\right] \quad N/mm^2 \tag{2.6}$$

where ϕ is the ratio of the ultimate shearing capacity to the ultimate flexural capacity of the slab and f'_c is concrete cylinder strength. Equation (2.6) recognized the influence of flexural strength on the ultimate shearing stress, and provided reasonable predictions of the punching shear strengths of all the slabs tested.

On consideration of the failure mechanism and from the analysis of previously reported test results, Whitney [107] stated that the punching strength was dependent upon the section moment of resistance.

In 1953, Elstner and Hognestad [30] proposed that the problem of punching shear is more complicated than just limiting a nominal shear stress at a critical perimeter away

from the column. Based on their experimental research programme together with Richart [88,89] footing tests, they introduced an empirical formulation for the punching resistance of concrete slabs without shear reinforcement, including the flexural parameter $P_{u,p}/P_{u,f}$. This formulation was revised by them in 1956 taking the form:

$$\frac{P_{u,p}}{\frac{7}{8}u_0 df_c} = \frac{2.98}{f_c} + \frac{0.046}{P_{u,p}/P_{u,f}} \qquad \text{in S.I. units} \tag{2.7}$$

Fig. 2.5 shows how the flexural parameter $P_{u,p}/P_{u,f}$ affects the results given by Equation (2.7). Although this approach is in a better form than those of Equations (2.1, 2.2, 2.3), in it the effect of column size coincides with that of Graf [37], which overestimates the punching resistances as the column size increases.

Another extensive experimental programme on studying the punching shear failure was conducted by Moe [65] and an empirical equation for the punching strength of slabs without shear reinforcement was given as below:

$$P_{u,p} = 0.083\left[15\left(1-0.075\frac{a_1}{d}\right)-5.25\frac{P_{u,p}}{P_{u,f}}\right]\cdot\sqrt{f_c}\cdot u_0\cdot d \tag{2.8}$$

where a_1 is the side dimension of a square column.

In analyzing the test results, Moe suggested that the shearing strength is proportional to the square root of the concrete compressive strength given by Equation (2.8). He then proposed a new set of empirical formulae to evaluate the shearing strength of reinforced concrete slabs and footings under concentrated loads. This

significant work of Moe has formed the basis of punching shear design provisions of the present ACI building code in the United States.

In 1974 Regan [83] reviewed the existing knowledge on punching shear in the context of British design codes and made a comparison of British and American treatments of punching shear. Important recommendations were made [79] for the design of punching shear. Design approaches for punching shear of slabs in British codes [16,17] were primarily based on the work of Regan.

At about the same time, following a review of the existing knowledge up to the 1970s, a comprehensive state-of-the-art report on the shear strength of reinforced concrete slabs was published by the ASCE-ACI Committee 426 [5]. In this report, existing methods of analysis for shear strength of slabs were thoroughly discussed and contrasted with the current understanding of the failure mechanisms. Limitations were also imposed on these failure mechanisms by employing general principles governing the behaviour of slabs.

In the same year, Masterson and Long [61] presented a flexural approach for investigating the punching strength of flat slabs via a simplified finite element model. Their idealized representation of slab-column connections resembled the theory of development of local plasticity at the column periphery. By relating the applied load to the internal moment at failure together with an allowance for dowel and tensile membrane effects, the punching strength could then be accurately computed. The predicted results were compared with those from the majority of slab-column specimens tested by various researchers.

Later, Long [59] formulated a two-phase design approach for flat slab construction in which the punching strength was computed as the lesser of either a flexural or shear criterion of failure. For the flexural mode of failure, the predicted punching load for a slab is given by:

$$P_v = \frac{\rho \cdot f_y d^2 \left(1 - 0.59\rho \frac{f_y}{f'_c}\right)}{\left(0.2 - 0.9\frac{c}{L}\right)} \quad \textit{Newtons} \qquad (2.9)$$

and for the shear mode,

$$P_v = \frac{1.66(c+d)d(100)^{0.25}\sqrt{f'_c}}{\left(0.75 + 4\frac{c}{L}\right)} \quad \textit{Newtons} \qquad (2.10)$$

where c is the side length of a square column; d is the effective depth of the slab; L is the span between columns and ρ is the reinforcement ratio. In the proposed procedure, there was a strong analytical basis for the flexural mode whereas the empirical part of the procedure was related to the shear mode.

In 1987, following an improvement of the two-phase approach [59] by a more rational treatment of the flexural mode of punching failure, Rankin and Long [80] developed a method of analysis for predicting the punching strength of flat slabs from rational concepts of the various modes of failure exhibited by model tests.

These modes of failure could be broadly classified as either flexural or shear, depending on whether failure was indicated by the yielding of the reinforcement (flexural), crushing of the concrete (flexural) or by internal cracking (shear). The

ultimate load capacity in the flexural mode was related to the yield moment by an analytically based linear interpolative moment factor, and the ultimate load capacity in the shear mode was based on a semi-empirical relationship for vertical shear stress on a critical section close to the perimeter of the loaded area. The proposed approach was shown to give good correlation with a wide range of test results from various sources.

In 1986, Regan [87] reported punching tests on 28 reinforced concrete slab specimens. The tests were carefully designed and divided into different series primarily concerned with the effect of:

- Arrangement of reinforcement
- Absolute depth
- Concrete strength and reinforcement ratio
- Boundary restraint
- Size of loaded area

The test results were compared with the predictions of four codes of practice ? ACI 318-83 [1], BS 8110 [16], CP 110 [18] and CEB-FIB Model Code [19]. Regan pointed out that the expression for punching resistance given by BS 8110, did not achieve the required level of safety and in fact gave significant overestimates of the punching strength.

Soon after this, Bazant and Cao [9] employed fracture mechanics to investigate the size effect on punching shear strength. The model used was essentially a modified perimeter approach, and it was assumed that the shear strength was directly proportional to the concrete strength. With consideration of the size effect, a formula for

calculating the punching shear load was proposed:

$$P = v_u \cdot \pi \cdot d_0 \cdot h \tag{2.11}$$

where d_0 is the punch diameter; h is the slab thickness and v_u is the nominal shear stress at failure,

$$v_u = 0.00168 f'_c \cdot \frac{1 + 0.35 \frac{h}{d_0}}{\sqrt{1 + \frac{h}{28.5 d_{agg}}}} \qquad N/mm^2 \tag{2.12}$$

in which d_{agg} is the maximum aggregate size.

In 1999, Gomes and Regan [35] conducted 12 experiments on reinforced concrete slabs with shear reinforcement. The primary variables under consideration were the area, number and distribution of the shear elements. Results indicated that the failure load of the specimen with the most reinforcement was more than twice than those of the slabs without shear reinforcement.

This literature review on both the analytical and experimental research reveals a lack of focus on the comparison of the experimentally observed *failure surfaces* against the theoretically assumed or calculated failure profiles, an issue which will be addressed in Chapter 6 of this thesis.

2.2.5 Present Design Specifications

In all of the major codes of practice, the design provisions to guard against punching shear failure still rely on the original concept of a nominal ultimate shear stress on a critical perimeter around the loaded area.

The British code BS 8110 is based primarily on the work of Regan [84], while the American code ACI 318 is based primarily on the work of Moe [65]. Therefore, there exist various inconsistencies between the two codes. For example, different control perimeters for slabs subjected to concentrated loading are adopted in the two codes, as shown in Fig. 2.6. In the British code, the control perimeter is at a distance $1.5d$ from the load and has square corners whether the loaded area is square or circular; whereas, in the American code the control perimeter is at a distance $0.5d$ from the load and is taken to have the same shape as the loaded area. Consequently, different maximum permissible shear stresses are taken on the control perimeter. In BS 8110, the shear stress depends on both the level of reinforcement and the cube root of concrete compressive strength:

$$v_{ck} = 0.79 \cdot \sqrt[3]{100\rho} \cdot \sqrt[3]{\frac{f_{cu}}{25}} \cdot \sqrt[4]{\frac{400}{d}} \quad N/mm^2 \tag{2.13}$$

in which the partial safety factor for materials $\gamma_m = 1.25$ is removed and the limits on f_{cu} are neglected; whereas in ACI 318-319, the shear stress is only dependent on the square root of concrete compressive strength:

$$v_{ck} = 0.332\sqrt{f'_c} \quad N/mm^2$$

in which the capacity reduction factor $\phi = 0.85$ is omitted.

Fig. 2.7 illustrates the main differences between the British and American design provisions for predicting punching shear strength of slabs [55]. It is obvious that the basic inconsistencies may result in different predictions of the punching shear strength in the same slab.

For bridge deck construction, all deck slabs are generally designed by flexural methods in the British [17,25] and North American [2,74,75] bridge codes. In the UK, the methods of Westergaard [105] or Pucher [78] are used for the derivation of the local bending moments due to wheel loads. These are then added to the global moments and the slab is designed flexurally. However, it is interesting to note that almost all the bridge deck-slab models with normal steel reinforcement, including even those with relatively low percentage of steel, failed in a punching shear mode in actual tests.

In BS 5400, the prediction of the punching shear capacity of typical bridge slabs subjected to concentrated loading resembles that given in BS 8110; while in the Ontario Highway Bridge Design Code [74,75] and also in the Amendment for Design of M-beam Bridge Decks in Northern Ireland [24], a less conservative approach is adopted in which the strength enhancement due to compressive membrane action is allowed for.

Clearly, the wide divergences existing between different design recommendations are indications of the unsatisfactory situation concerning the present understanding of punching failure in reinforced concrete slabs.

2.3. PREVIOUS WORK IN GENERAL FIELD OF THE USE OF EFFECTIVENESS FACTORS FOR PREDICTION OF SHEAR FAILURE

Recent work into the investigation of the general role of effectiveness factors for concrete was pursued by Ashour & Morley [6] in continuous deep beams via the application of plasticity theory. Calibration of the computed failure loads against experimental failure loads for 20 test beams produced the value of effectiveness factor for concrete in compression for this particular type of structure. They concluded that parameters such as concrete strength, geometric dimensions and reinforcement ratio affect the effectiveness factor for concrete in compression.

In these plastic analyses, the level of success achieved in predicting the shear failure loads has been significantly influenced by the concrete material models used. In particular, the effectiveness factors used for concrete in tension and compression play important roles in determining the reliability of the plastic approach for predicting punching shear capacities [6]. Therefore, it is worth investigating the sensitivity to effectiveness factors as a *generic* issue, which has not been addressed to date but is crucially important. In addition, research into plastic analysis was focused on failure criteria where little attention was paid into the simplification of the existing analyses. Therefore, another prime objective of this PhD study is an attempt to simplify the plastic analysis. All of these important features will be discussed in Chapter 3.

2.4. COMPRESSIVE MEMBRANE ACTION

2.4.1 Membrane Action in Slabs

Flexure of unrestrained slabs is associated with in-plane movements at the supports which are compatible with the vertical deflections of the slab. However, by restraining the lateral movement of a concrete panel against stiff boundary elements, membrane forces are induced in the plane of the slab. This occurs in the following sequences: as load is applied, cracking of the concrete causes the edges of the slab to tend to move outward or in the other case, yielding of the reinforcement causes the slab edges to tend to move inward and to react against the bounding elements. This membrane effect has been found to result in substantial enhancement in the ultimate load capacity of reinforced concrete slabs with lateral restraint.

An illustration of the compressive membrane action and the enhanced behaviour of a laterally restrained slab is shown in Fig. 2.8. It can be seen that after the onset of cracking in the slab, most of the rotational deformation is concentrated along narrow bands which represent the incipient yield-lines. As a result of the migration of the neutral axis at these cracked sections, the centres of rotation are close to the compression surface of the slab, and are at different levels for the sagging and hogging moments. Consequently, vertical deflection of the panel is accompanied by a tendency for lateral expansion, which if restrained, is responsible for the development of compressive membrane forces (arching forces), as shown in Fig. 2.8(a). In this way, the ultimate capacity of the slab is increased beyond the normal flexural strength up until the sudden collapse of the inherent arching mechanism, as shown in Fig. 2.8(b). Subsequently, the load carried by the slab decreases rapidly because of a reduction in the compressive membrane forces and/or the rise of the arch. The load may then again

increase with the development of tensile membrane action under further deformation, until fracture of the reinforcement occurs.

The phenomenon of arching action was appreciated by the pioneers of slab construction from relatively early on in the application of reinforced concrete technology. In 1909, Turner [104] quoted the following descriptions:

> *"Such a slab will at first act somewhat like a flat dome and slab combined, but as the deflection gradually increases it will gradually act like a suspension system in which rods will merely hold the concrete together and distribute the load over them."*

This fact was also recognized by the early codes of practice, but was incorporated into design by the dubious procedure of using moments that did not satisfy equilibrium conditions [98].

The arching action was also mentioned in the works of Westergaard and Slater [106] and Taylor et al [100]. In addition, the arching effect was acknowledged many years ago in the USSR, where Gvozdev [37] allowed for a twenty percent reduction in the calculated reinforcement percentages for interior panels in continuous slab floors in the Russian code of practice for design of reinforced concrete structures.

However, with the extensive development of the yield line theory by Johansen [48], the arching effect was largely forgotten in later years. Instead, research efforts were concentrated on validation of the yield line approach for ultimate strength design. It was not until the historic tests by Ockleston [72] on a complete concrete building – the

Old Dental Hospital in Johannesburg – that interest in compressive membrane action was revived. These full scale tests indicated that the collapse loads were three or four times those predicted by Johansen's yield line theory. In a later publication [73], Ockleston correctly attributed this strength enhancement to the development of compressive membrane forces caused by the restraint against lateral expansion of the panels. He demonstrated this potential load carrying capability by means of a simple Perspex model which was severed along the yield lines, but restrained within a stiff surround.

Probably the earliest theoretical treatment of arching action was that of McDowell et al [64], in which a method was proposed for predicting the relationship between the load and deflection of masonry walls constrained between rigid supports. The theory was based on the assumption that the principal resistance to lateral load stemmed from a crushing action at the end supports and centre of the panel. It was therefore necessary to include an idealization of the stress-strain properties of masonry materials. The theory was offered as a means of explaining and predicting the relatively great strength of masonry walls constrained between rigid supports.

A significant step forward into appreciating the benefits of incorporating membrane action was taken when a document was introduced into the UK Design Manual for roads and bridges BD81/02 in 2002 [26], which relates the use of compressive membrane action in the design and assessment of reinforced concrete bridge deck slabs. Many criteria given in the Standard are based on experimental evidence [53], which has been conservatively interpreted for use in design and assessment. However, this document does not define the enhancing effect quantitatively. Clearly, more work is to be done to fully utilise the enhancing effect as

a result of compressive membrane action, as has been done in this PhD study.

2.4.2 Slabs Subjected to Concentrated Loading

Although much theoretical and experimental work has been carried out on the investigation of compressive membrane action in laterally restrained reinforced concrete slabs subjected to uniformly distributed loading, less has been reported on the study of compressive membrane action in such slabs under the action of concentrated loading. Owing to this lack of focus on the issue of compressive membrane action in slabs loaded under concentrated conditions, another part of this PhD study will investigate the effect of surrounding restraint via a carefully designed experimental programme presented in Chapter 6. A detailed consideration of restraint provided by surrounding concrete together with the enhancing effect of surround restraint by hoop steel will be investigated in Chapter 4. In addition, the effect of uneven distribution of support reactions on the symmetry of the failure surface will be addressed in Chapter 6.

Probably the earliest experimental study of laterally restrained reinforced concrete slabs subjected to concentrated loading was reported by Taylor and Hayes [101], in which the results of tests on square slabs failing in punching shear were presented, although no theoretical analysis was proposed. As a consequence of compressive membrane action the punching load capacity of a laterally restrained slab is much greater than that of an equivalent unrestrained slab. The test results showed that the influence of the level of reinforcement on the load-carrying capacity is small in normally reinforced slabs with restrained boundaries.

A popular approach for predicting the enhanced punching shear strength of laterally restrained slabs was to incorporate the compressive membrane effect into existing method which was applicable to conventional unrestrained slabs. Based on their own tests, Aoki and Seki [4] derived a semi-empirical equation for evaluating the ultimate shear strength of restrained slabs:

$$V = 0.67(d + d_0) \cdot d \cdot \sqrt{f'_c} \quad Newtons \tag{2.14}$$

where d is the effective depth of slabs and d_0 is the punch diameter (diameter of loaded area). The proposed equation is a modification of Moe equations [65] for punching shear strength of conventional unrestrained slabs and allows for the enhancement in strength due to membrane effect. It was found that membrane action was insignificant in slabs with high concrete compressive strength and/or low level of steel reinforcement. A slightly different method was presented by Hyttinen [44], who assumed that the effect of compressive membrane action was to increase the shear resistance in the same proportion as it increased the depth of the compression zone at the periphery of the loaded area.

The ultimate strength of continuous two-way bridge slabs subjected to concentrated loading was investigated by Tong and Batchelor [102]. On the basis of the results from a series of tests on small scale bridge panel models, an empirical relationship between the enhanced punching shear strength and the slab flexural capacity, which included contribution due to compressive membrane action, was developed:

$$\frac{V}{b_0 \cdot d \cdot \sqrt{f'_c}} = 2.18 + 0.603 \frac{V_{total}}{b_0 \cdot d \cdot \sqrt{f'_c}} \qquad \textit{(Newtons)} \qquad (2.15)$$

where b_0 is the periphery of the loaded area; V is the ultimate load and V_{total} is the total ultimate flexural capacity of the slab which is the sum of the ultimate flexural capacity of the slab, calculated using yield-line theory, and the estimated maximum flexural capacity due to compressive membrane action. The compressive membrane effects enhanced both the flexural and shear capacity of the slabs and ensured that all slabs failed at loads higher than those predicted by the yield line theory regardless of the actual mode of failure.

In 1975, Hewitt and Batchelor [40] presented a theoretical approach for investigating the punching strength of restrained slabs subjected to concentrated loading. The boundary restraining forces and moments were incorporated into Kinnunen and Nylander idealized model of failure [51], as shown in Fig. 2.9. This involved an iterative procedure for the prediction of the punching load of slab with known boundary restraints. For practical situations, it was suggested that a boundary restraint factor could be estimated and this was accordingly evaluated from previously reported test results. On this basis, the restraint factors for a variety of slabs were determined and limiting values tentatively recommended for use in estimating the punching strength. Clearly, the ability of quantifying the surround restraint proves invaluable for accurate predictions of enhanced punching capacities of restrained concrete slabs.

The enhanced punching strength of two-way bridge slabs was further investigated by Batchelor and Tissington [7], who introduced some modifications to the earlier method of analysis proposed by Tong and Batchelor [102]. The main experimental

aspects of this study were related to the influence of model scale, boundary conditions and percentage of slab reinforcement. It was suggested that bridge slabs provided with minimum isotropic reinforcement could be expected to perform satisfactorily in service.

The results of the various studies on the enhanced punching shear strength of bridge slabs were verified by an extensive series of field tests on existing structures by the Ontario Ministry of Transportation and Communications in Canada. Consequently, an empirical method of design was permitted in the Ontario Highway Bridge Design Code [74,75] in which a minimum isotropic reinforcement (only 0.3 percent) was specified in bridge decks provided that certain boundary conditions were fulfilled. The background to this successful approach has been reviewed by Csagoly [23].

Soon after this, Ekeberg et al [29] carried out *in-situ* punching tests in a four storey warehouse building and the surrounding quay deck. These full scale tests indicated that the punching failure loads were much higher than those predicted by both elastic theory and the Norwegian code NS-3473. The test results provide valuable information on the punching shear failure of actual continuous structures.

In 1984, Kirkpatrick, Rankin and Long [53] reported an investigation into the strength of M-beam bridge decks, which are commonly used in the United Kingdom. As part of this study, a model bridge deck was constructed and tested under simulated concentrated wheel loading. A detailed analysis of test results showed that the ultimate capacity of bridge slabs was significantly enhanced by compressive membrane action, as shown in Fig. 2.10, and the failure load was virtually independent of the percentage of transverse reinforcement. A semi-empirical method of predicting the ultimate capacity was proposed in which it was assumed that bridge slabs were fully

restrained laterally. This was based on the punching shear equation in a previously reported two-phase approach by Long [59], with the consideration of the enhancement due to compressive membrane action accounted for by an equivalent percentage reinforcement parameter with the actual slab reinforcement being neglected. The punching strength of a rigidly restrained slab is predicted by the following equation:

$$P = 1.36(d_0 + d) \cdot d \cdot \sqrt{f_{cu}} \cdot (100\rho_e)^{0.25} \qquad f_{cu} \text{ in } N/mm^2 \tag{2.16}$$

where d_0 is the diameter of a circular loaded area and ρ_e is the effective reinforcement ratio which represents an equivalent percentage of flexural reinforcement, derived from the arching characteristics of the slabs, in the simplified shear criterion proposed by Long [59].

Kirkpatrick et al [54] also investigated the influence of compressive membrane action on the serviceability of M-beam bridge decks from the series of full-scale tests on an M-beam bridge deck. The investigation illustrated that the initial cracking of the slab occurred at a load well in excess of the design service load and was independent of reinforcement bar size. It was suggested that compressive membrane forces play an important part in the control of the cracking in the slab. As a result, a simplified design procedure was proposed for both the ultimate and serviceability limit states.

A research effort has been devoted to the investigation of the enhanced punching strength of interior slab-column connections by Rankin [79,82] and Rankin and Long [80,81]. In their studies, tests on full panel specimens were carried out, and the punching strength was found to be enhanced by the development of compressive membrane action. A rational semi-empirical method for predicting the enhanced

flexural and shear punching strengths of interior slab-column connections was proposed, which was also based on the punching equations given in the reported two-phase approach [59]. In this method the portion of slab inside the nominal line of contraflexure was considered to be laterally restrained by the surrounding zone of slab and therefore compressive membrane action was induced when the slab deflected, as shown in Fig. 2.11.

In 1989, Fenwick and Dickson [32] carried out tests on three one-way reinforced concrete slabs subjected to concentrated loading. The model slabs were simply supported, flexurally restrained and fully fixed respectively. The test results indicated that the effect of the in-plane restraint provided by slab boundaries on the enhancement in punching strength was very evident. Although no theoretical analysis was presented, the investigation provided basic experimental information on the behaviour of slabs subjected to concentrated loading for the establishment of a rational method of analysis that allows for the beneficial effect of compressive membrane action.

In the following year, Jackson [45] reported tests on two half-scale M-beam-type deck models under HB loads. The test results showed that global transverse moments could significantly reduce the load strength of bridge deck slabs. It is suggested that the punching shear failure observed in deck slabs is primarily brittle compressive failure.

In 1991, Kuang [55,57] presented a plastic theoretical model for the punching shear failure of laterally restrained concrete slabs, in which a parabolic Mohr failure criterion for concrete is adopted. The method allowed for the effect of compressive membrane action and a membrane-modified flexural theory of elasto-plasticity was used

to calculate the compressive membrane forces. The predictions by the proposed analysis showed good agreement with a wide range of experimental test results. This suggested that the plasticity theory could well incorporate the influence of compressive membrane action. This fact is used in some of the work presented in Chapter 4 of this thesis.

In 2000, Eyre [31] applied the modified rigid-plastic method of analysis to both one-way plain concrete strips and to two-way slabs under a concentrated load which was shown to give fairly good agreement with test data. However, the ability of the theory to make such predictions is not yet particularly valuable owing to the lack of information on the calculation of the in-plane stiffness restraint offered by surrounding areas of slab outside a failure mechanism.

Most recently, Collings [21] outlined a method of analysis for slab structures in bridge decks that takes into account in-plane 'arching' effects. The method utilises current frame and grillage analysis with only minor modification. The method of analysis generally results in a lower reinforcement requirement than conventional techniques for the interior bays of multi-beam or ladder beam decks where external restraint can be relied upon.

The following section highlights potential areas for further exploration on both the theoretical treatment and experimental work on the subject of punching shear failure of reinforced concrete slabs with consideration of compressive membrane action.

2.5 AREAS FOR FURTHER EXPLORATION

2.5.1 Lack of focus on simplification of existing theoretical approaches

Either Plastic Analysis *or* the Equilibrium approach was employed by various researchers to provide predictions for punching shear failure capacities of reinforced concrete slabs reported in the literature. However, the literature review revealed that there is a distinct lack of research aimed at enhancing the quality or reliability of the theoretical approaches and also, on the simplification of existing approaches. This stimulates the interest towards a more in-depth study of the important parameters influencing the accuracy of the predictions. In addition, an attempt towards a more simplified version of existing theoretical approaches for punching shear predictions will be addressed in Chapter 3. *In this PhD study, both approaches namely: Plastic Theory based on the Parabolic Failure Criterion for concrete and the Equilibrium approach based on Kinnunen and Nylander's model were attempted and are presented in Chapter 3 and Chapter 5 respectively.*

2.5.2 Influence of variation in effectiveness factors employed in Plastic Analysis

One major advantage of using the plasticity-based method is that only effectiveness factors relating concrete compressive and tensile strengths have to be determined through calibration of theoretical results against experimental results. However, the important role of the effectiveness factors themselves on the degree of accuracy of predictions as a *generic* issue has not really been addressed and requires further investigation [6]. *Therefore, another prime objective of this PhD study is to*

establish the level of sensitivity of the predictions made by plasticity theory to different combinations of effectiveness factors. In addition, appropriate combinations of effectiveness factors are suggested which will be incorporated in further plastic analysis with consideration of compressive membrane action (Chapter 4).

2.5.3 Experimental approach to determination of surround restraint

It was identified earlier in this chapter that research into some important aspects of the effect of surrounding restraint on punching failure loads remains outstanding. In addition, assessment of the effects on the punching failure surface and load of statical indeterminacy of slab-column systems requires further attention. *For this reason, another major emphasis of this PhD study was the experimental investigation to establish: (1) the influences on the punch loads of increasing levels of surround restraint provided via both steel hoop reinforcement as well as surround concrete material; (2) an assessment of the effect on the punch loads and surfaces of statical indeterminacy (particularly the resulting potential effect on lack of axisymmetry) of the tested slabs.* All of the above considerations are useful for establishing the level of reliability of the predictive model based on symmetry considerations and will be discussed in Chapter 6.

2.6 SUMMARY

From the extensive discussions of this chapter, the following points have emerged:

- It has been shown from the historical review that the present understanding of punching failure in reinforced concrete slabs subjected to concentrated loading is based on experimental studies of the behaviour and strength of simple laboratory specimens.

- Empirical studies have been found to be most fruitful, and have led to simple recommendations which were incorporated into the various codes of practice for the punching shear design of conventional slabs. However, there is still uncertainty over the influence of the primary variables, and the present unsatisfactory situation is reflected in the wide divergences existing between different design provisions.

- Moreover, an appreciation of the important parameters which dictate the level of accuracy achieved by applying the plasticity theory to prediction of punching capacities remains insufficient. As a result, much important work on sensitivity of punching shear predictions to variations in these key parameters remains to be done to clarify these problems.

- While the research on compressive membrane action in reinforced concrete slabs has yielded a relatively clear understanding of the enhancement in flexural strength of slabs under the action of uniformly distributed loads, the picture is not quite so clear on compressive membrane effects on the punching strength of slabs subjected

to concentrated loading. This is primarily because of insufficient knowledge of the degree and influence of edge restraint at the instant of the punching failure. This situation provided the motivation in the presently reported PhD study for a carefully designed experimental programme to investigate the influence of surrounding restraint.

These outstanding issues have guided the approach in the present PhD study. In the following chapter, a detailed discussion of the theoretical work conducted within this study via the application of plasticity theory is presented. Chapter 4 then extends the theoretical model described earlier in Chapter 3 to incorporate the enhancement effect due to compressive membrane action. Chapter 5 presents an equilibrium model based on the Kinnunen and Nylander model for predicting punching failure loads of unrestrained slabs. Chapter 6 describes an experimental study to understand the influence of the degree of surrounding restraint together with an attempt to quantify the magnitude of the restraint stiffness. Another major emphasis of Chapter 6 is to verify the suitability of applying the plasticity model presented in the theoretical chapters together with a study of the effect of loss of axi-symmetry on punching predictions. Finally, Chapter 7 summarises the main findings of this thesis and puts forward suggestions for extension of this work.

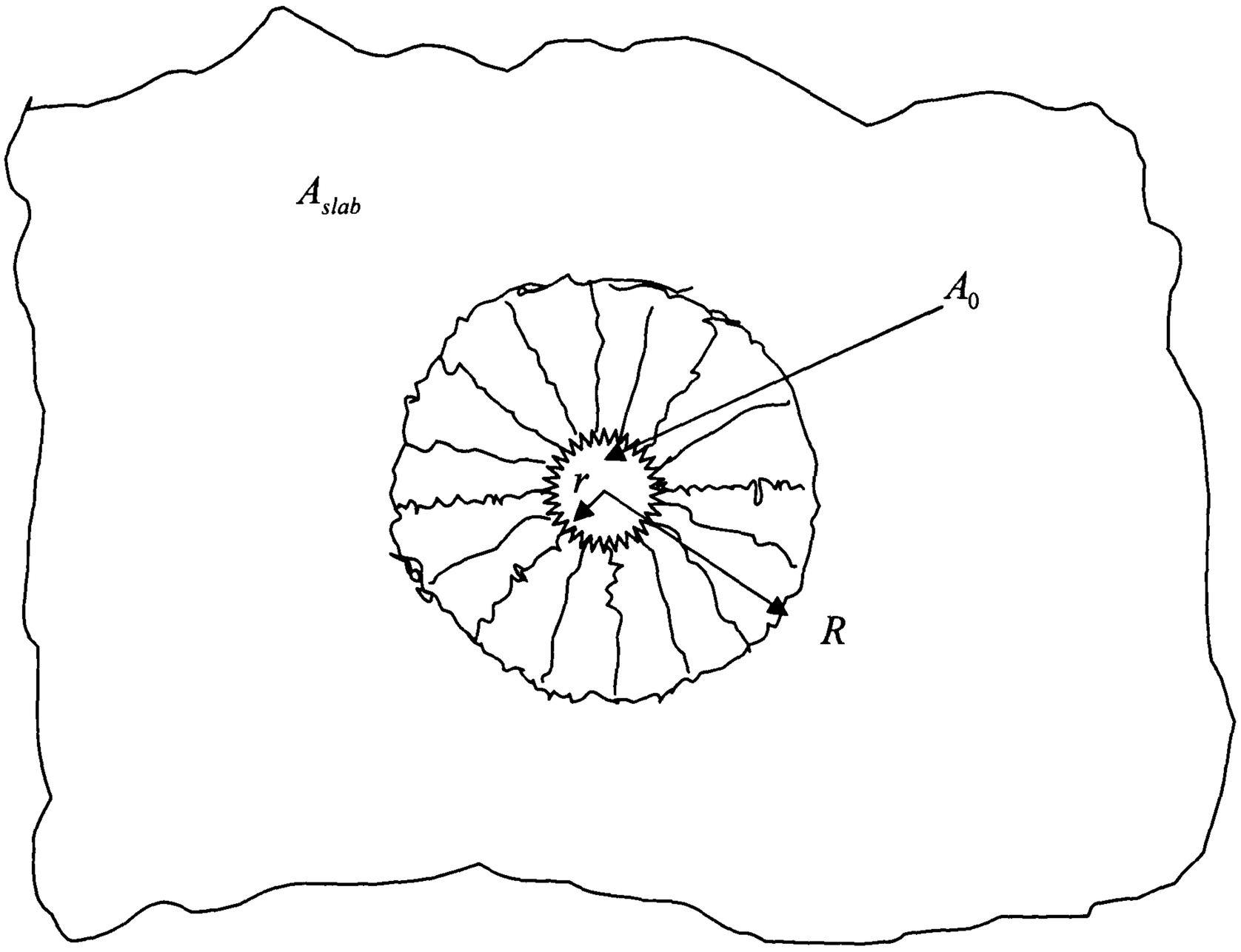

(a) Interior circular column

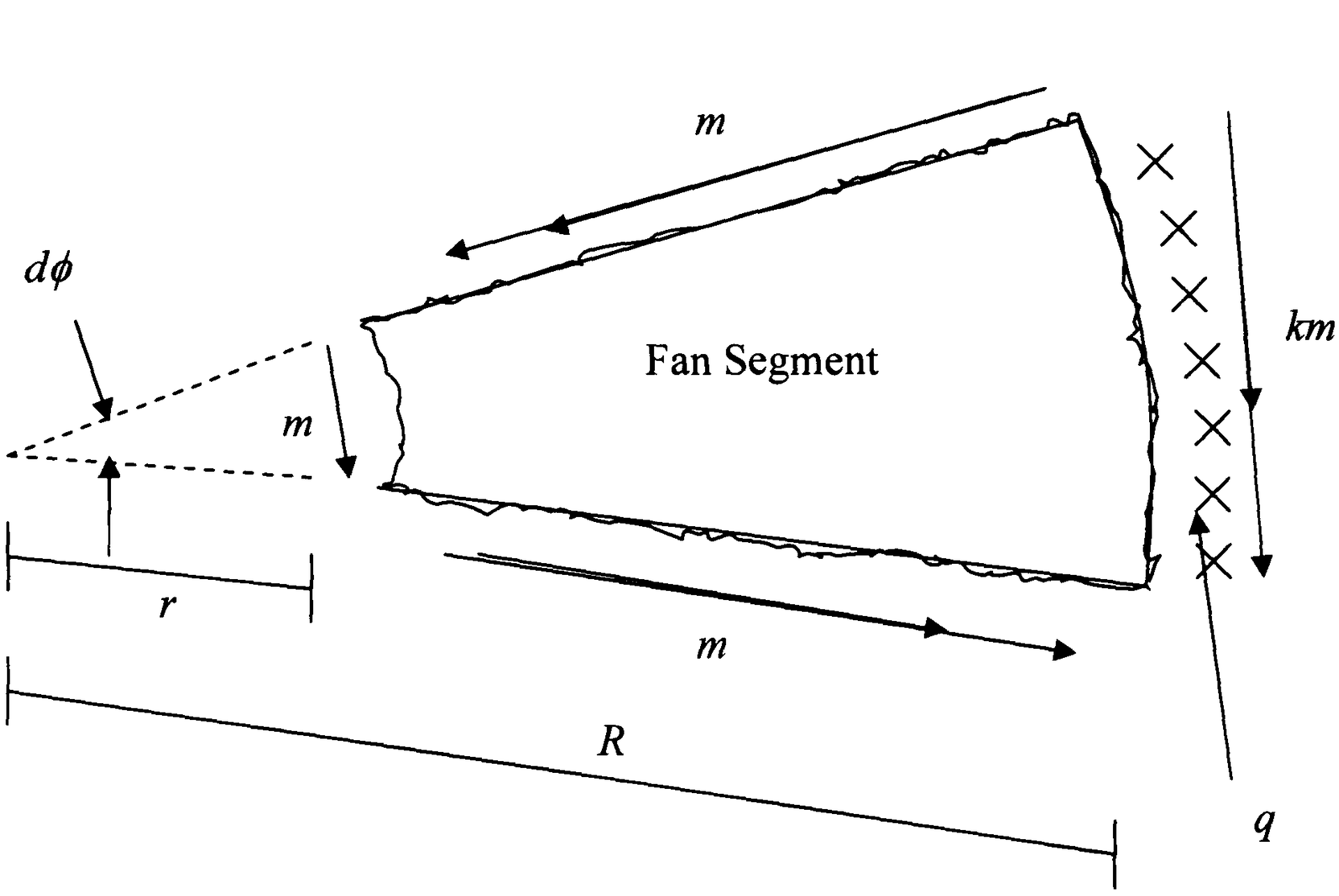

FIG. 2.1(a) Yield-line pattern for punching shear of slabs [34]

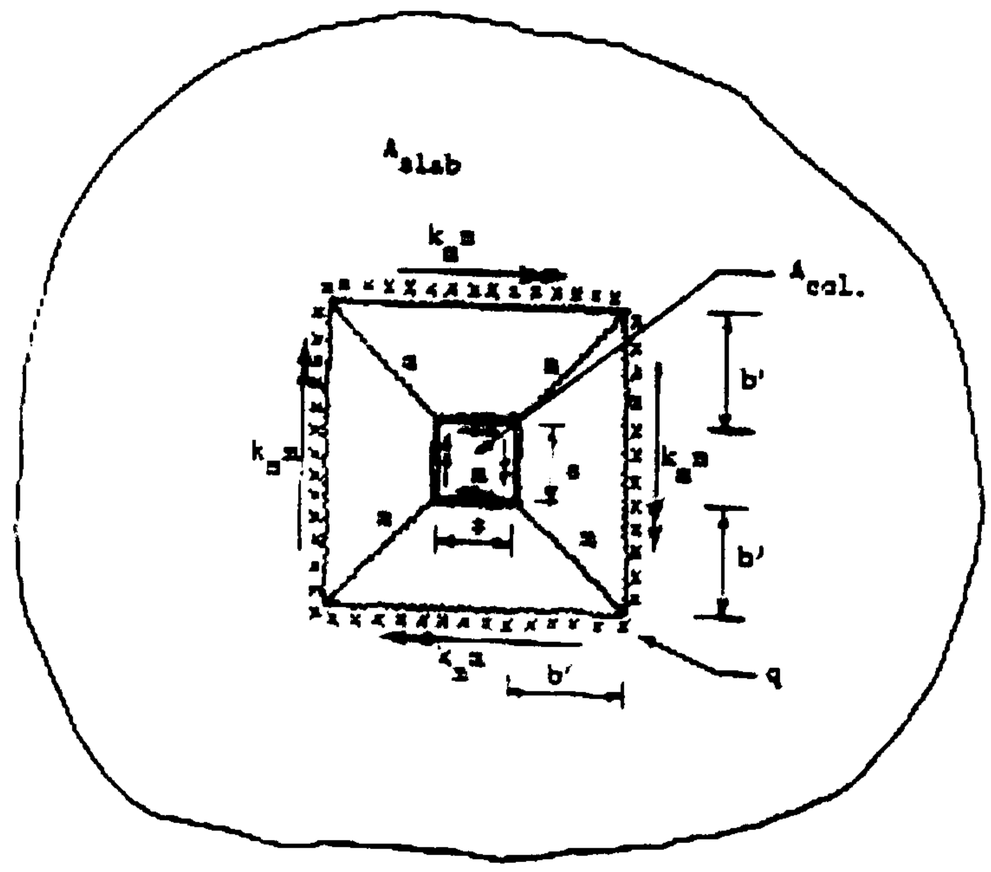

(b) Interior square column

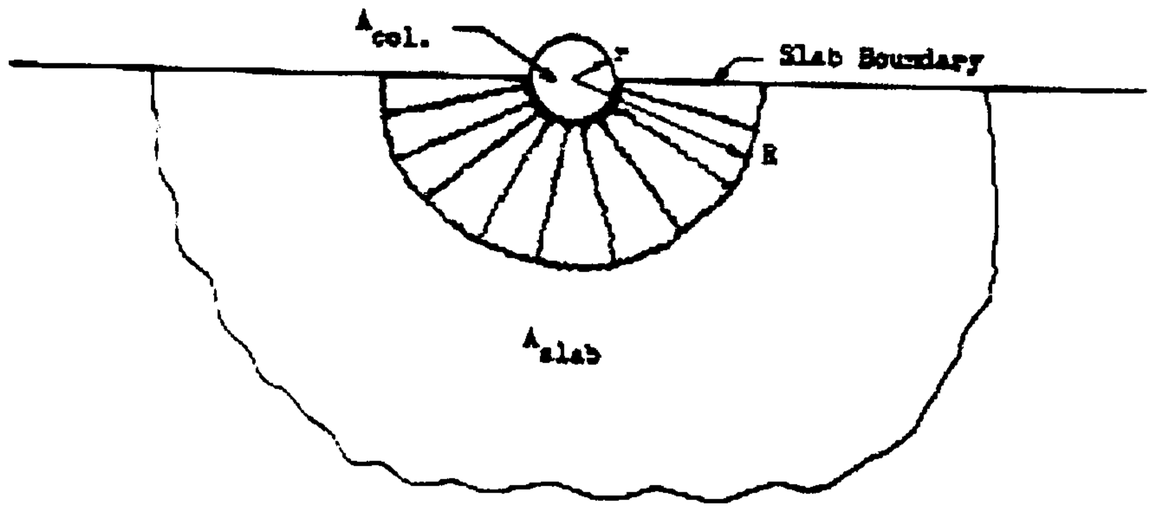

(c) Exterior column bisected by slab boundary

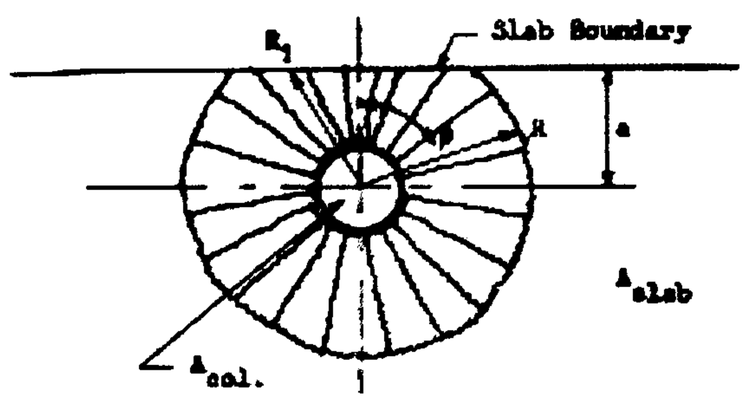

(d) Circular column near slab boundary

Figure 2.1 Yield-line pattern for punching shear of slabs [34]

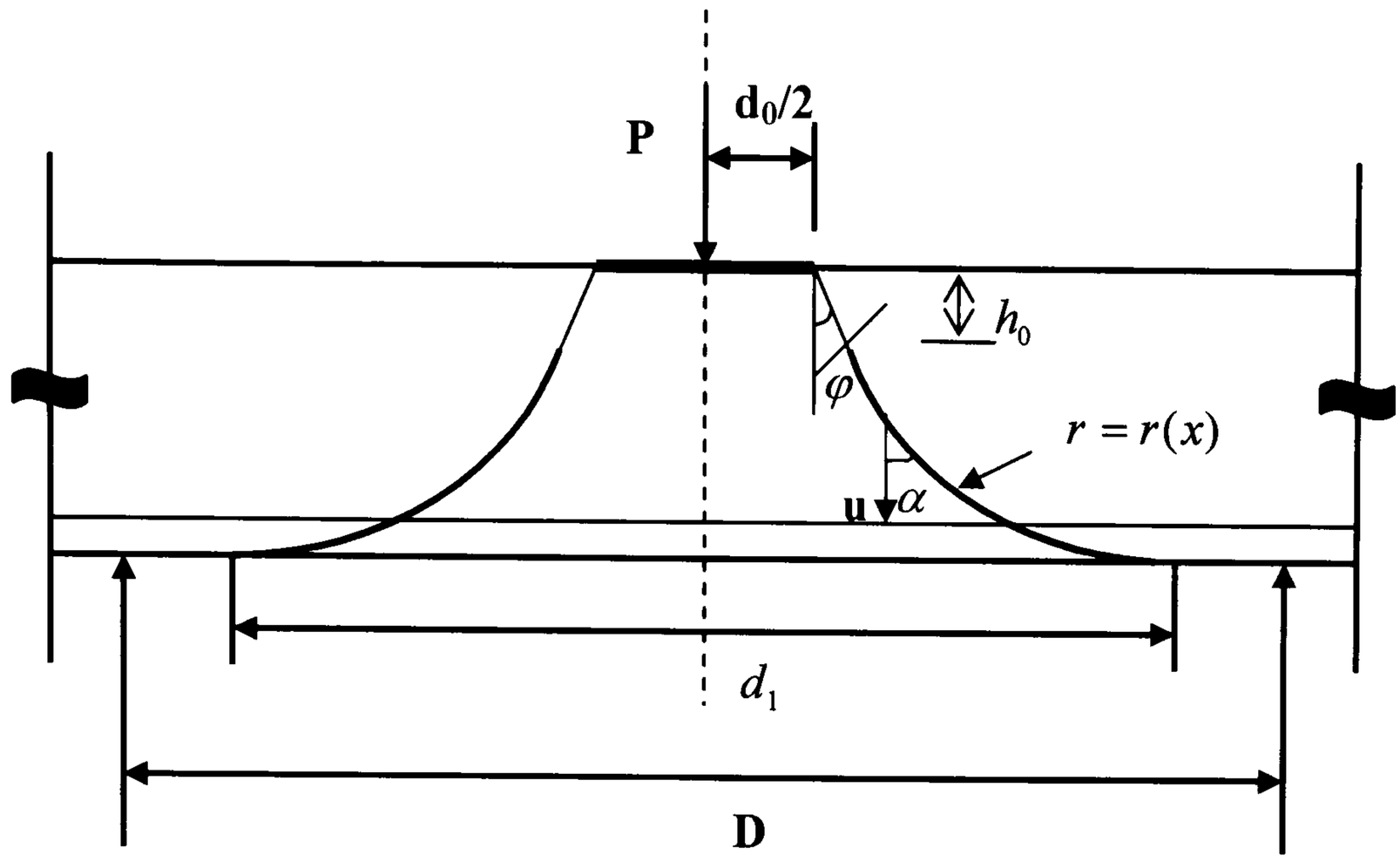

FIG. 2.2 Failure Mechanism of Braestrup

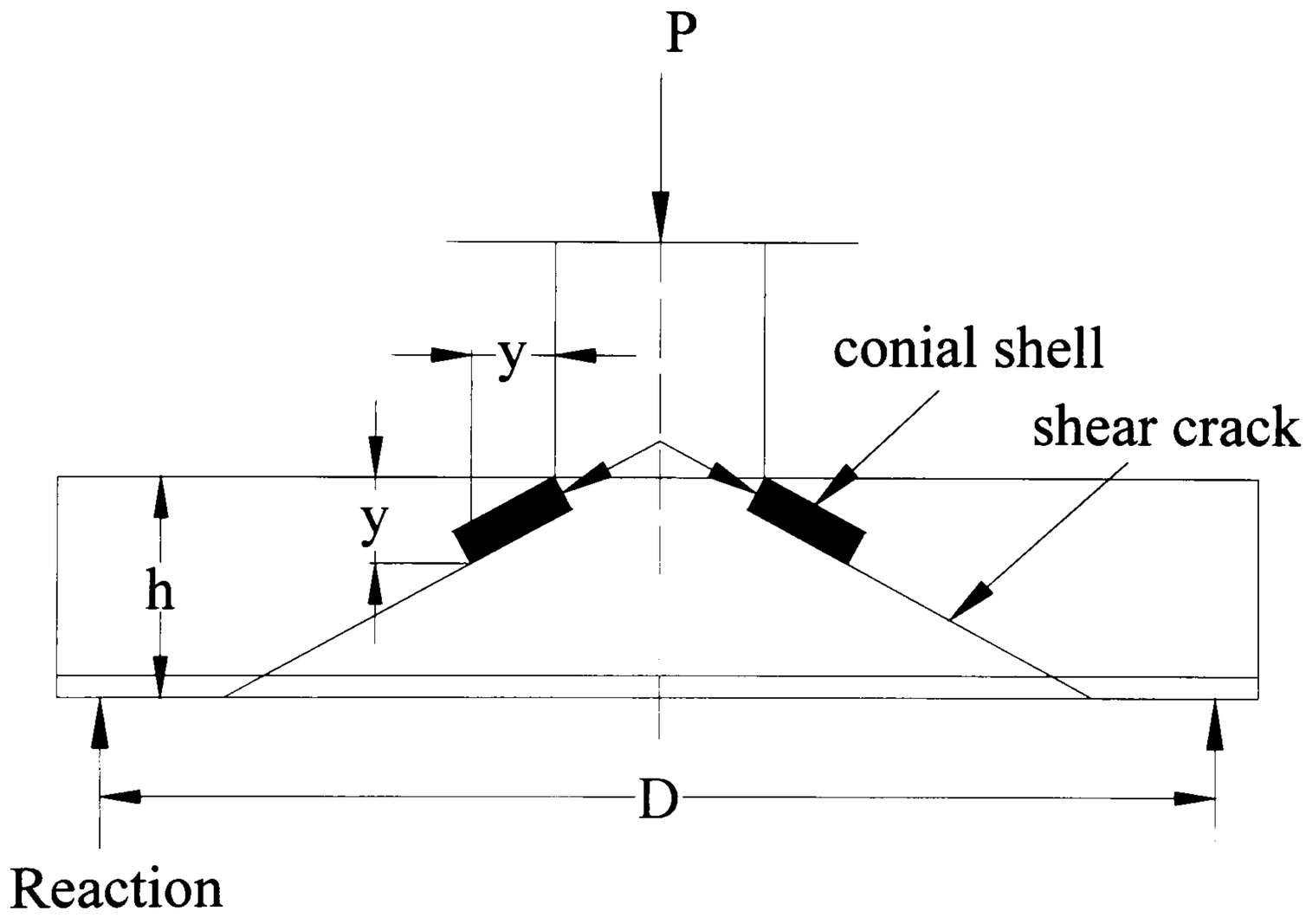

FIG. 2.3(a) Section showing conical shell and shear crack

R_1 and R_2 = Resultant horizontal force in circumferential direction

R_3 = Resultant of horizontal tangential compressive stress in concrete

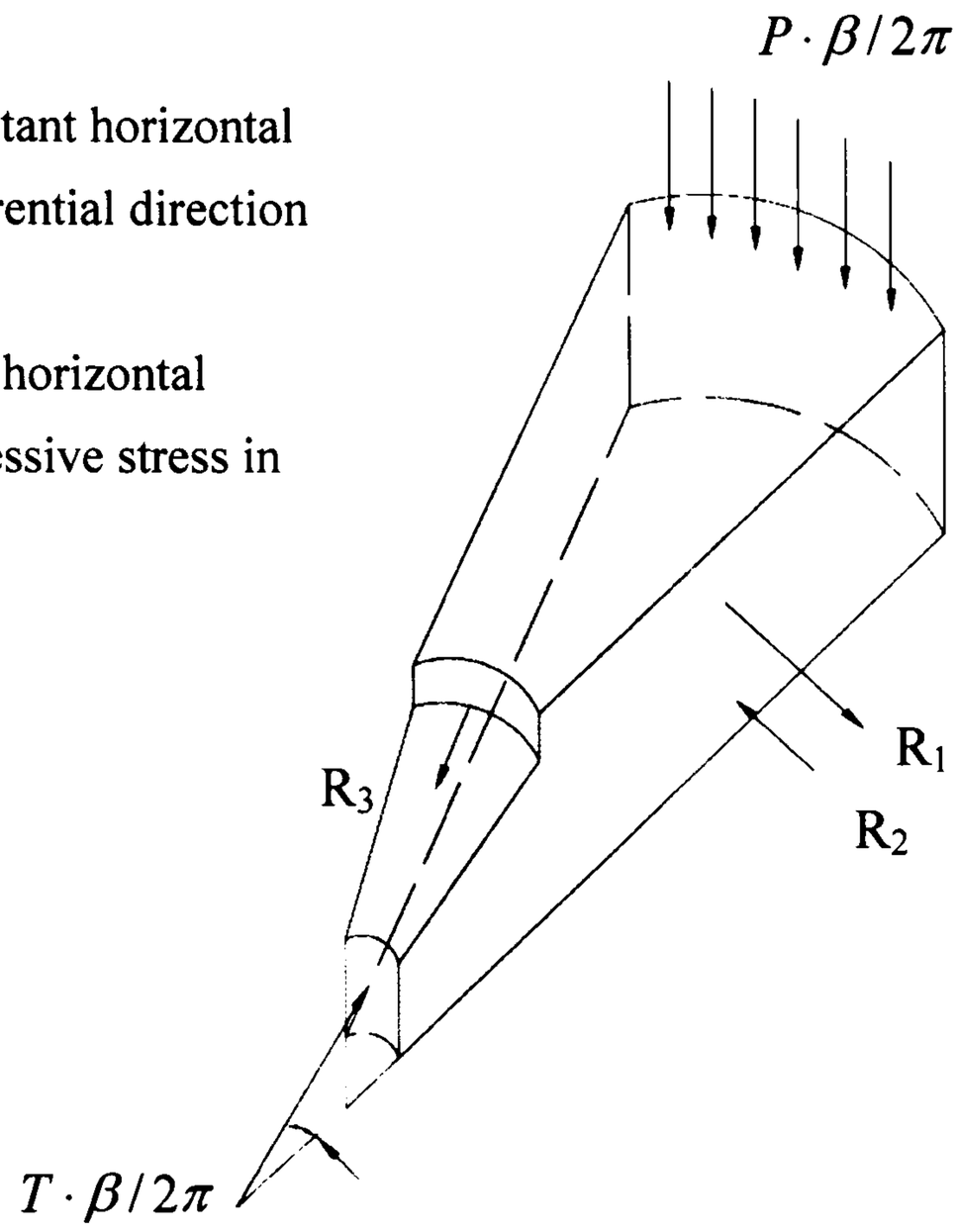

(b) Sector element showing slab forces

FIG. 2.3 Mechanical model of a slab at punching shear failure proposed by Kinnunen and Nylander

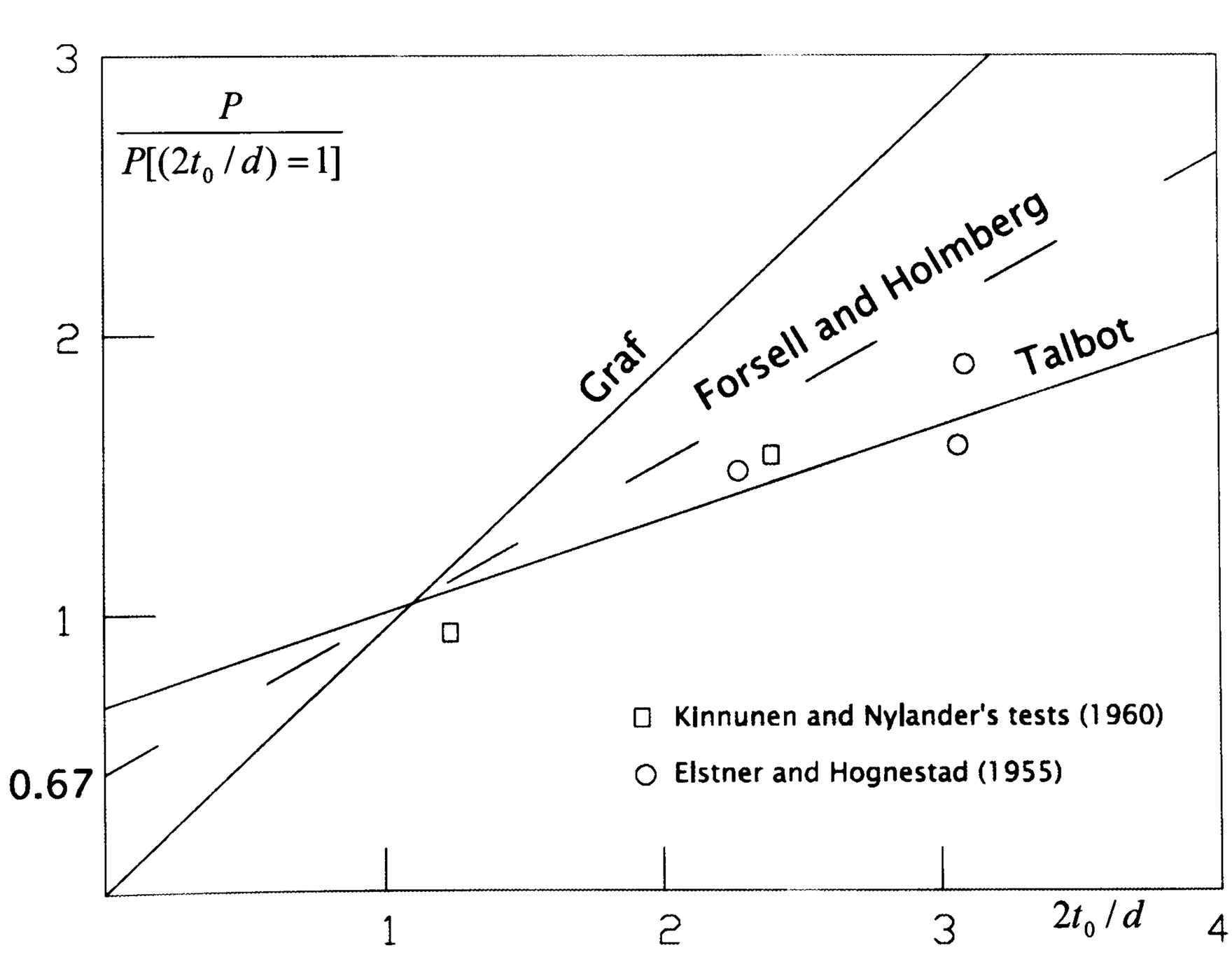

FIG. 2.4 Effect of column size according to Talbot, Graf and Forsell and Holmberg, compared with test results

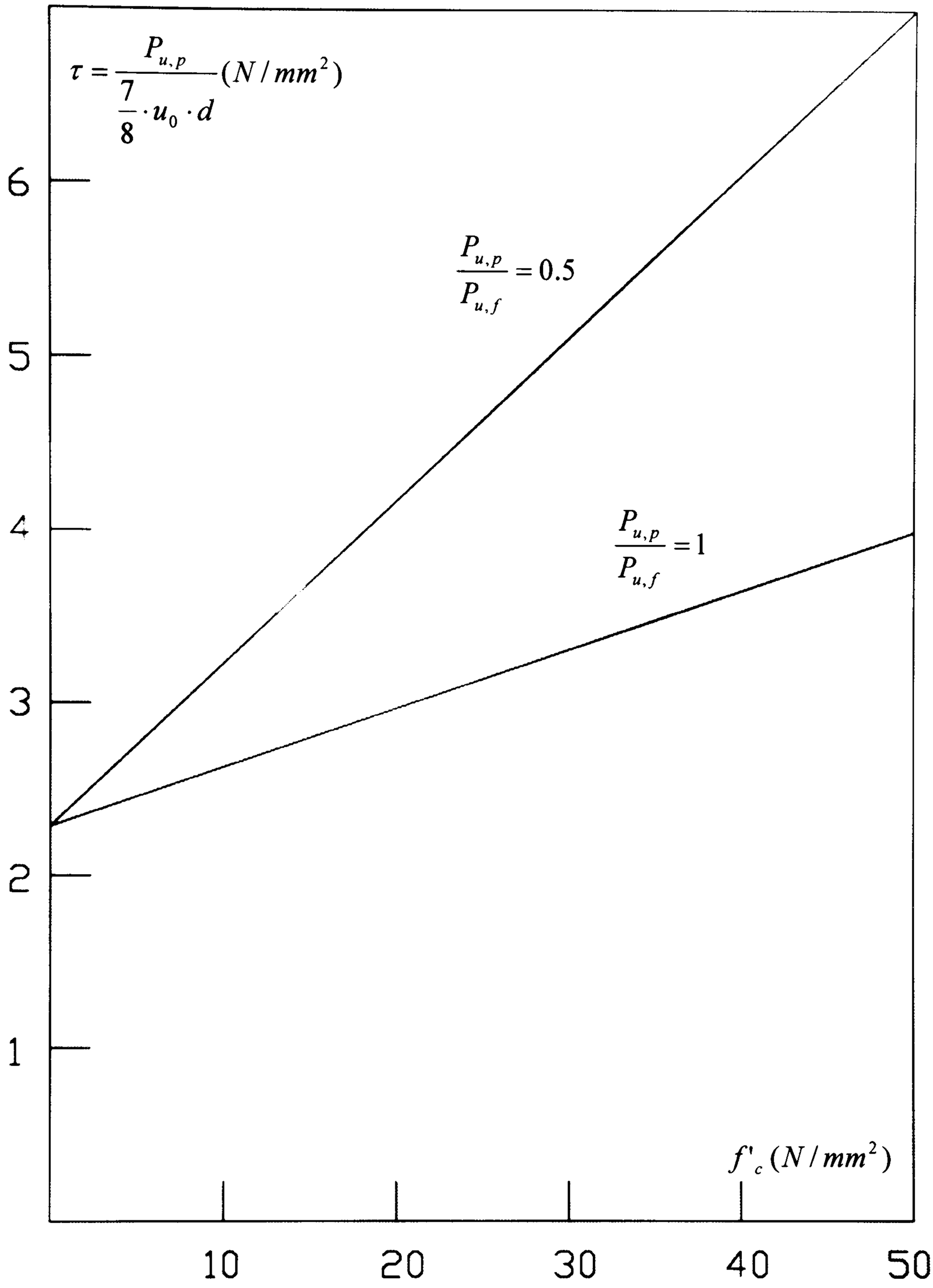

FIG. 2.5 Nominal shear stress-concrete strength relationship given by Equation (2.7)

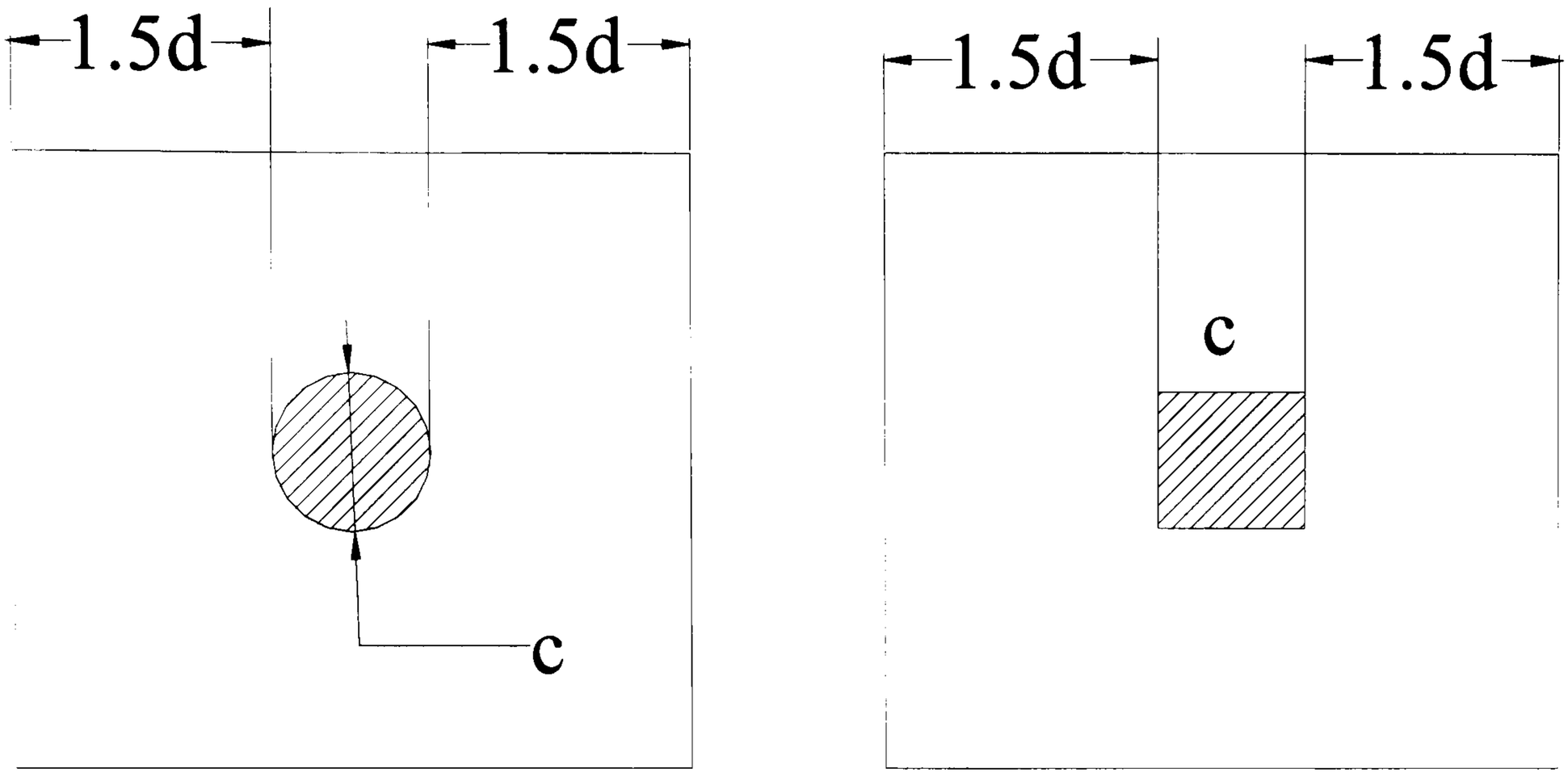

British code: BS 8110

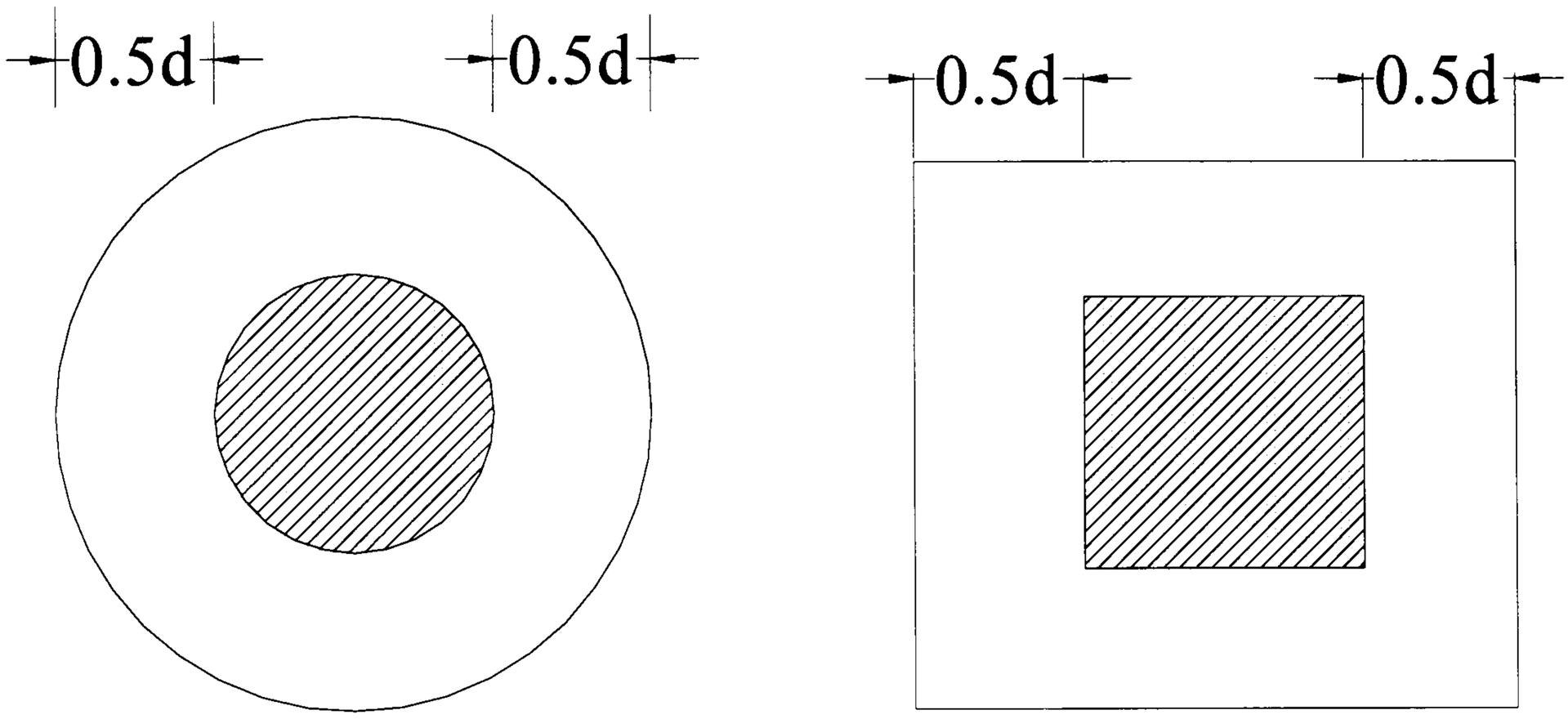

American code: ACI 318-89

FIG. 2.6 Control perimeter adopted by design codes

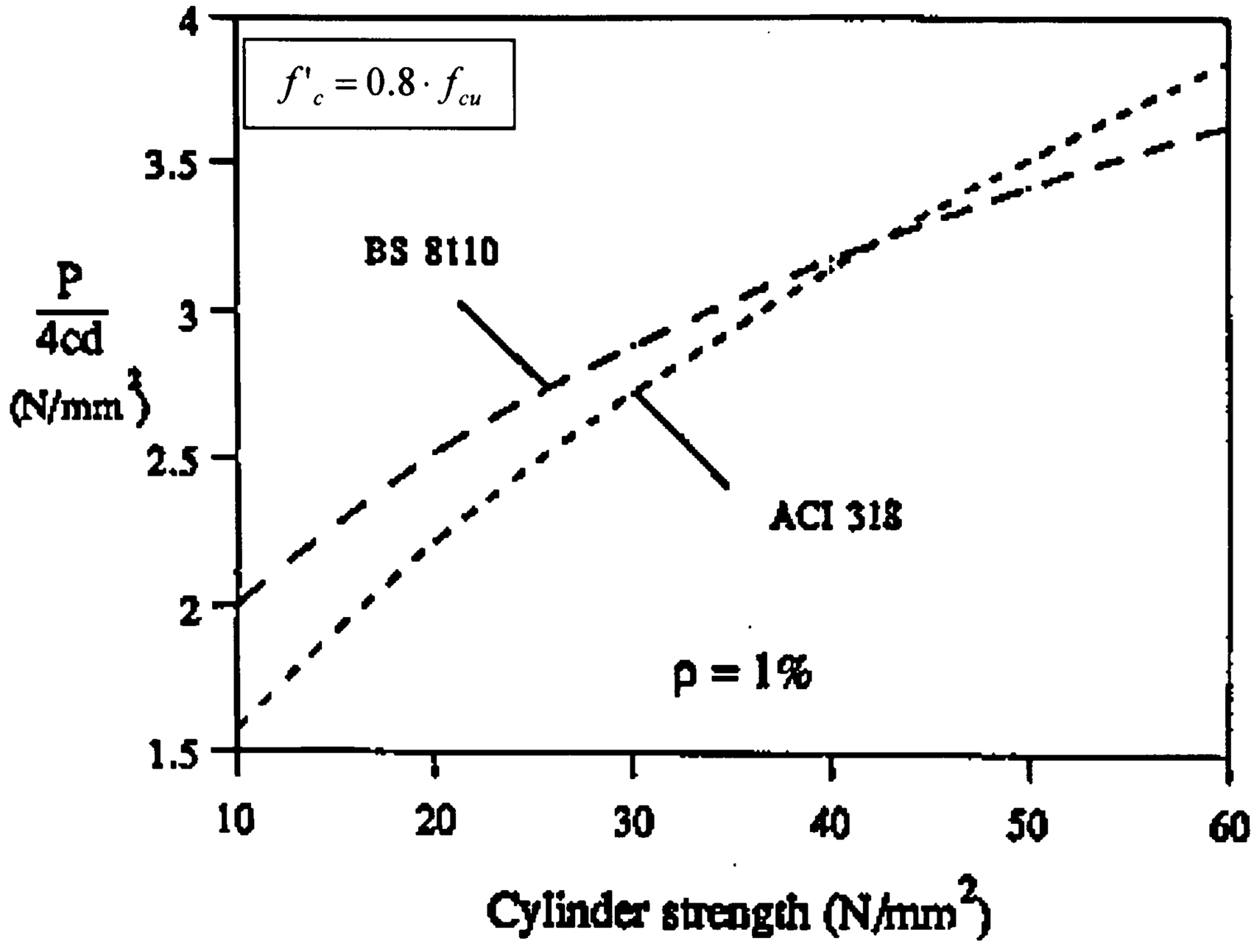

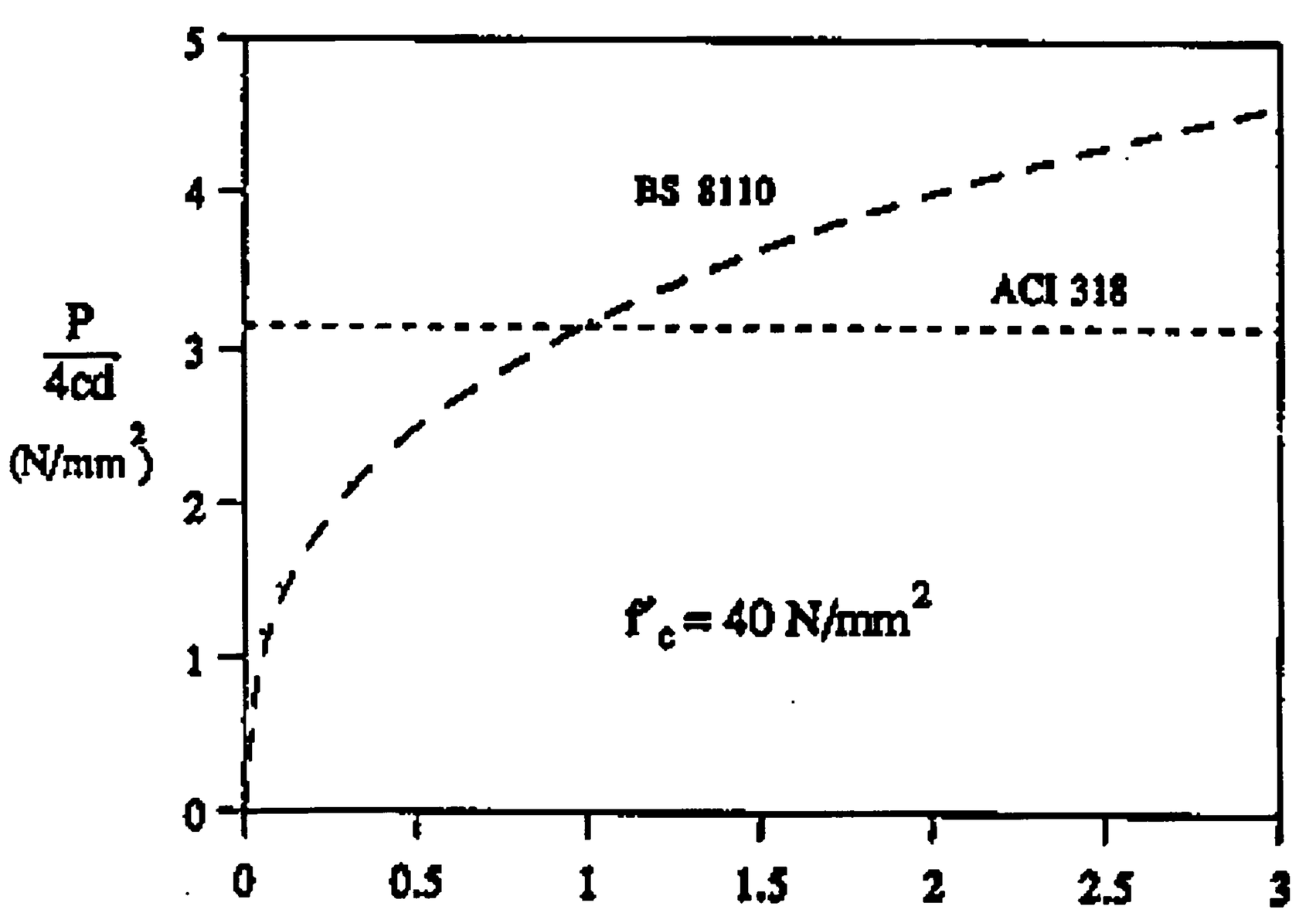

FIG. 2.7 Comparison of design provisions for punching shear strength (d = 150mm, d/c = 0.5) [55]

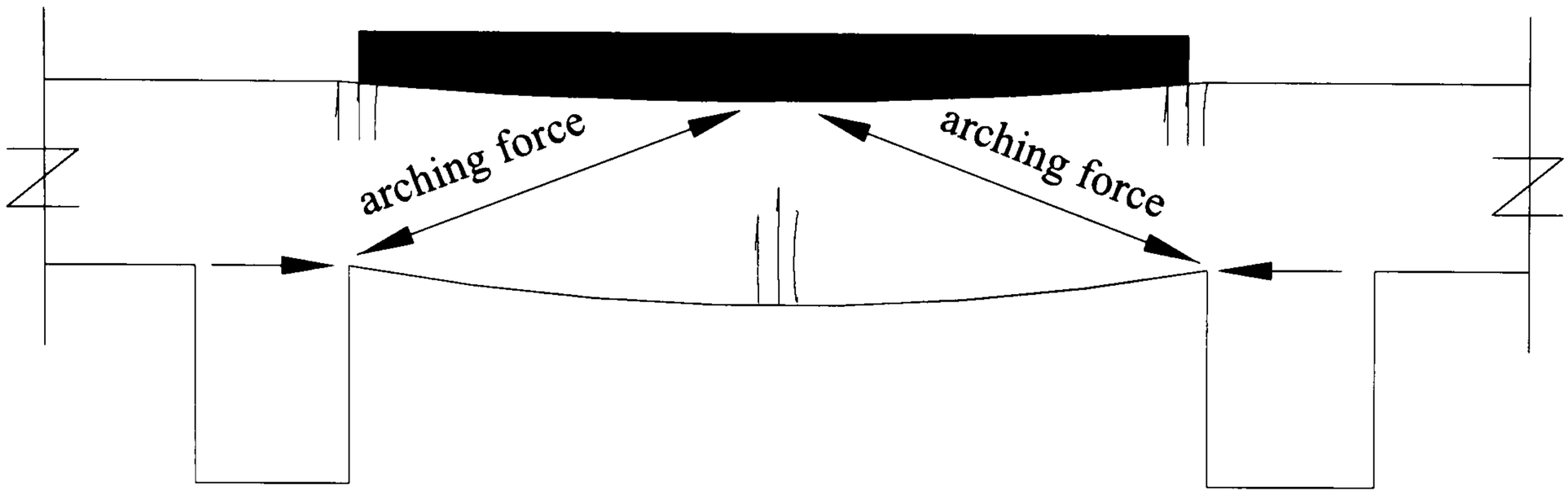

(a) Compressive membrane action in a cracked slab

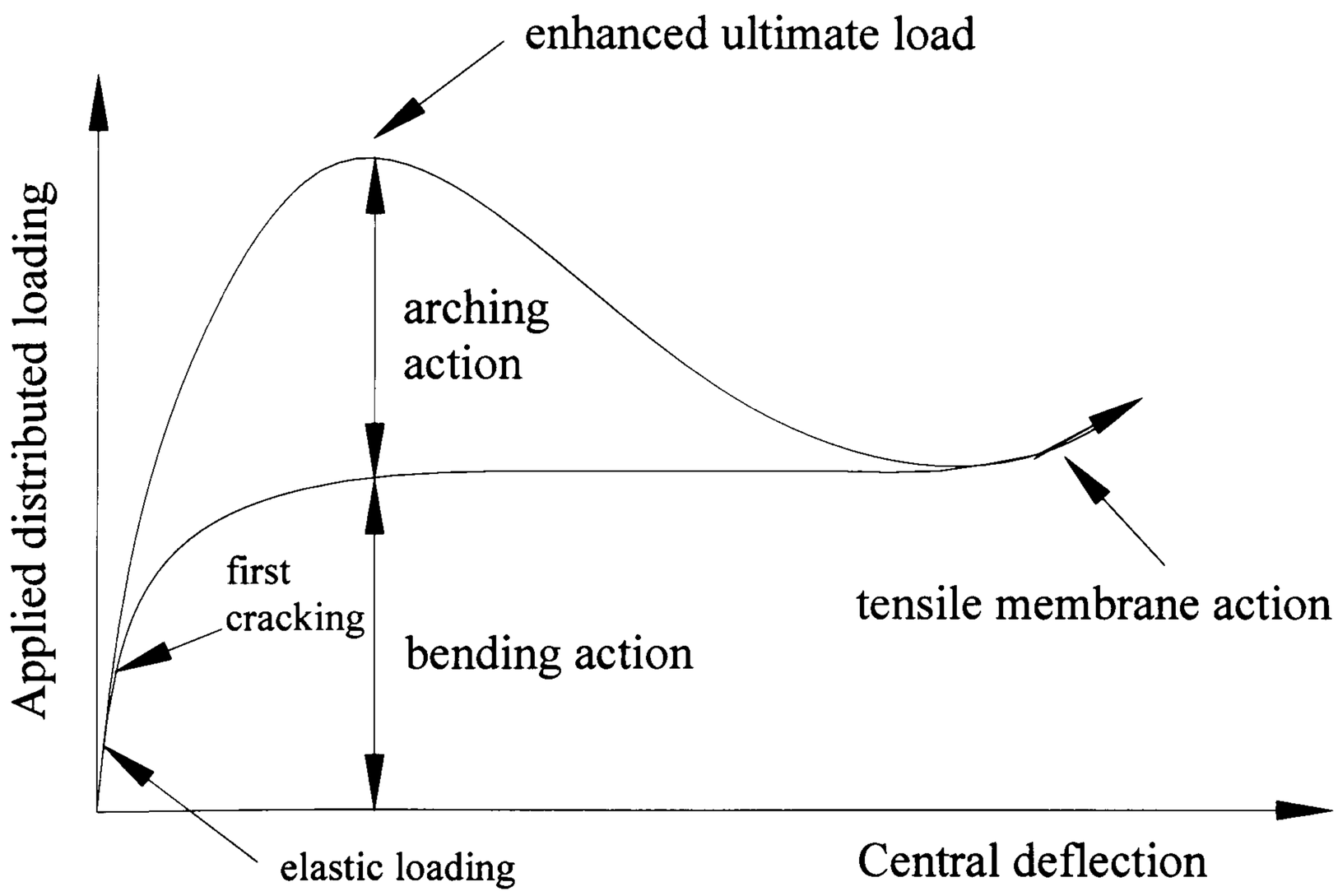

(b) Qualitative illustration of enhanced behaviour of a restrained slab

FIG. 2.8 Structural behaviour of a restrained slab

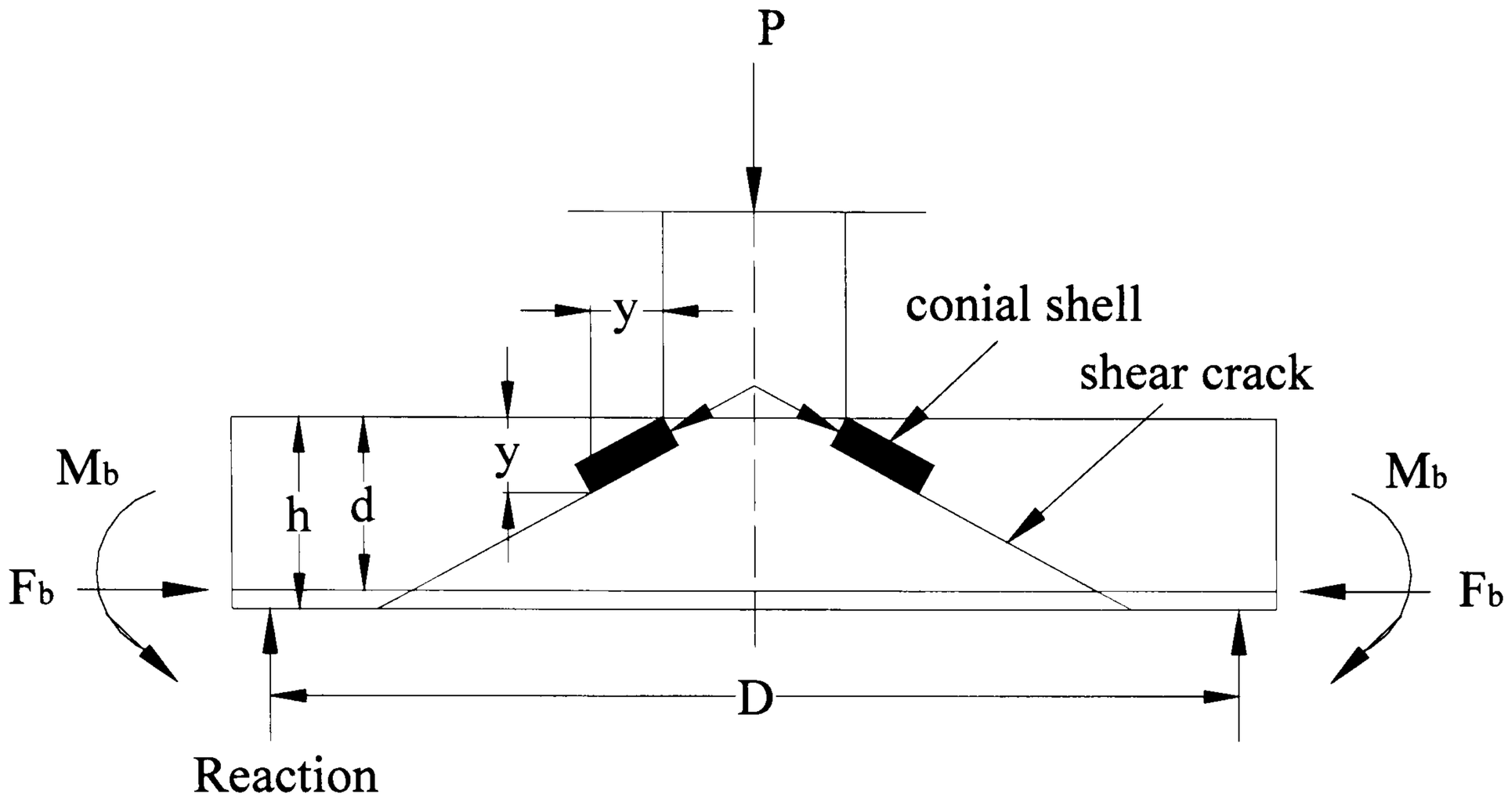

(a) Section showing conical shell and shear crack

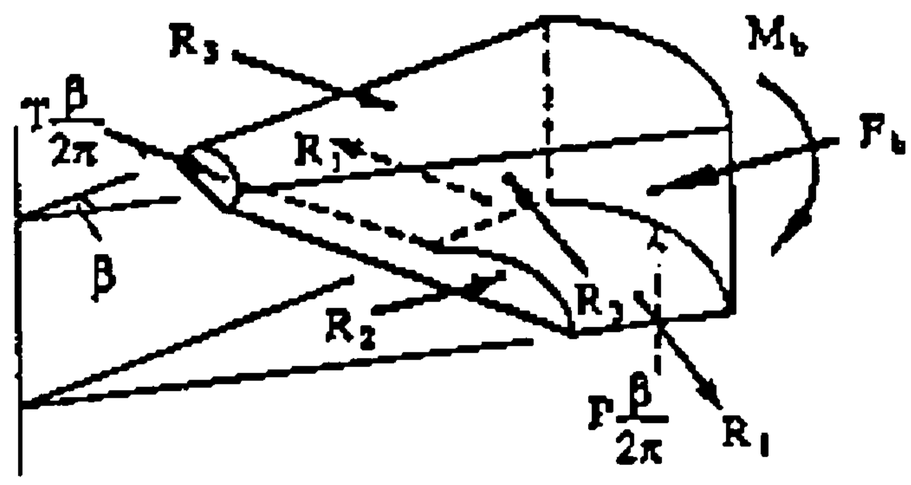

(b) Sector element showing slab forces and boundary forces

FIG. 2.9 Mechanical model of a slab at punching shear failure by Hewitt and Batchelor

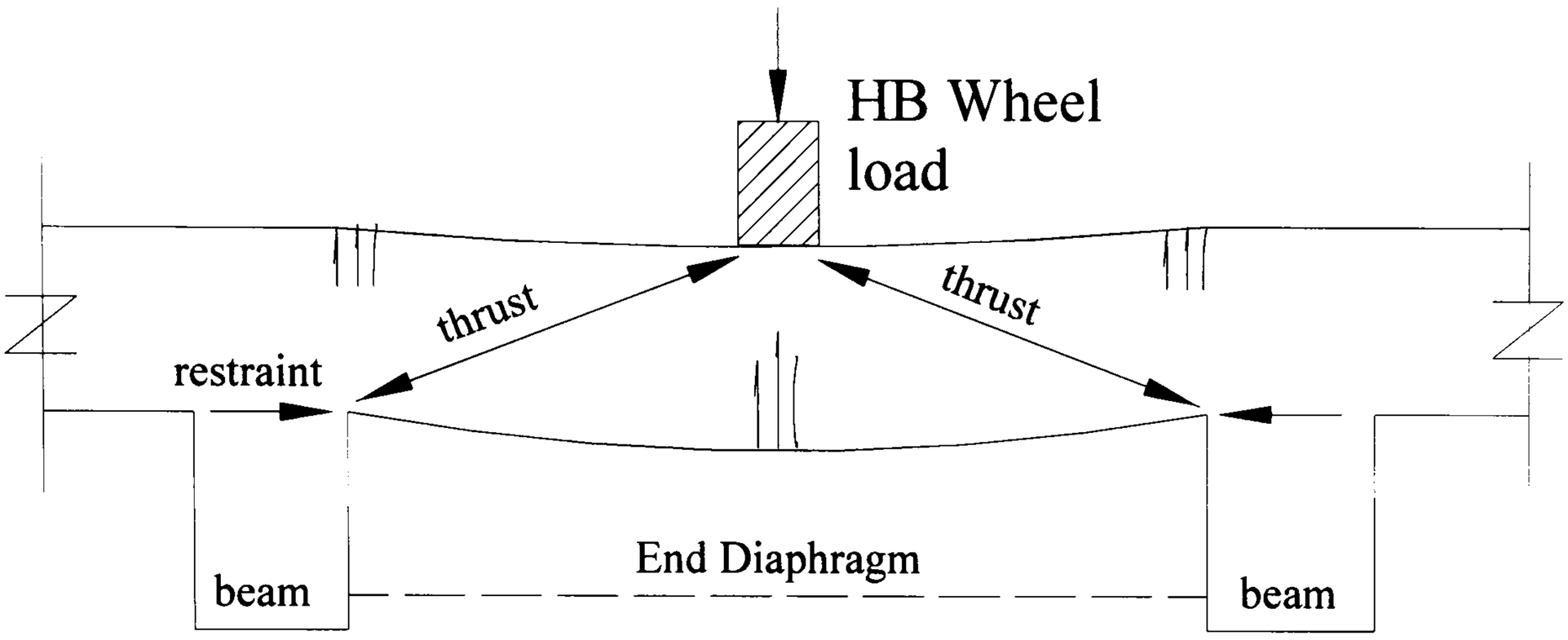

FIG. 2.10 Compressive membrane action in bridge deck [54]

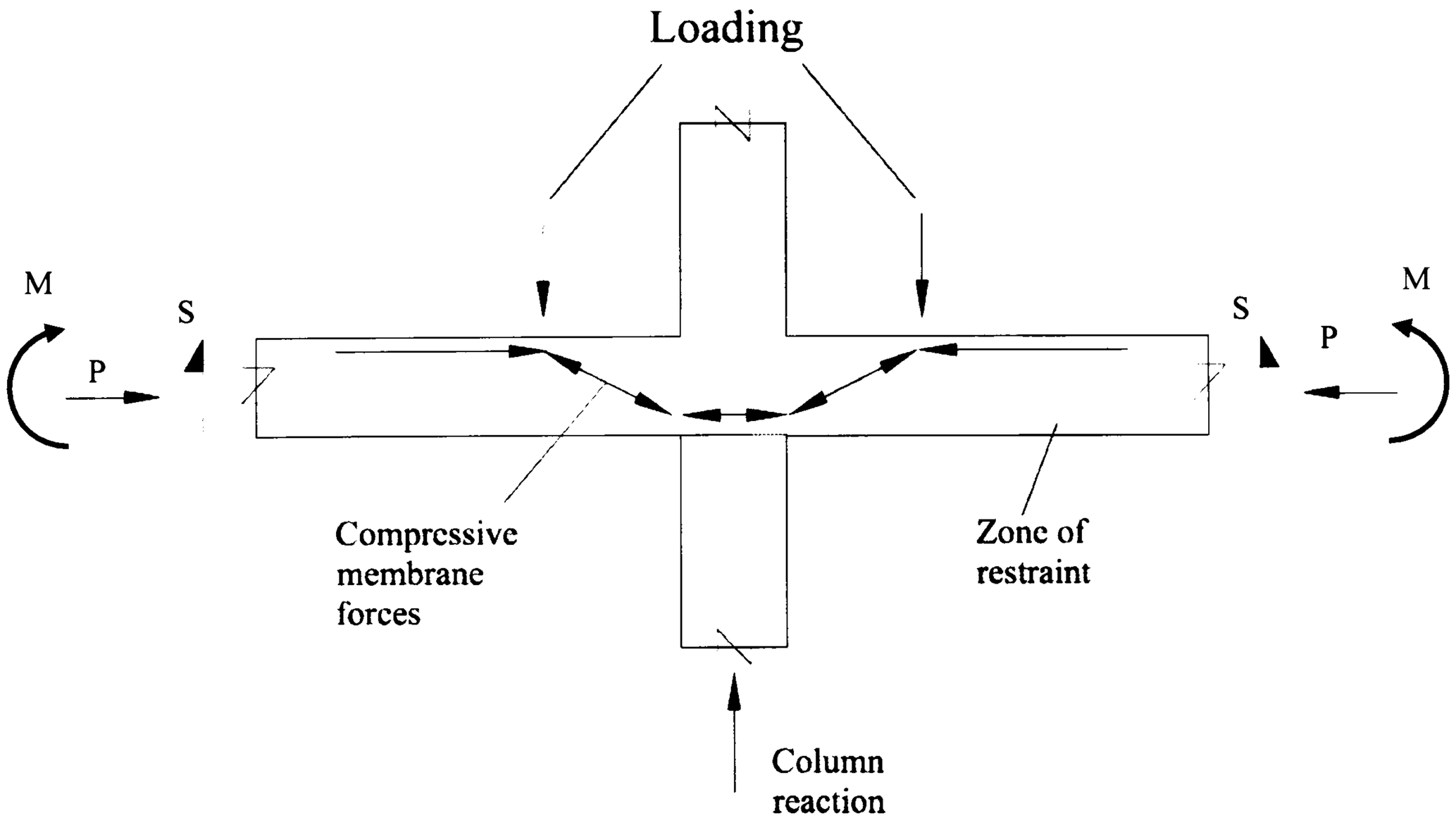

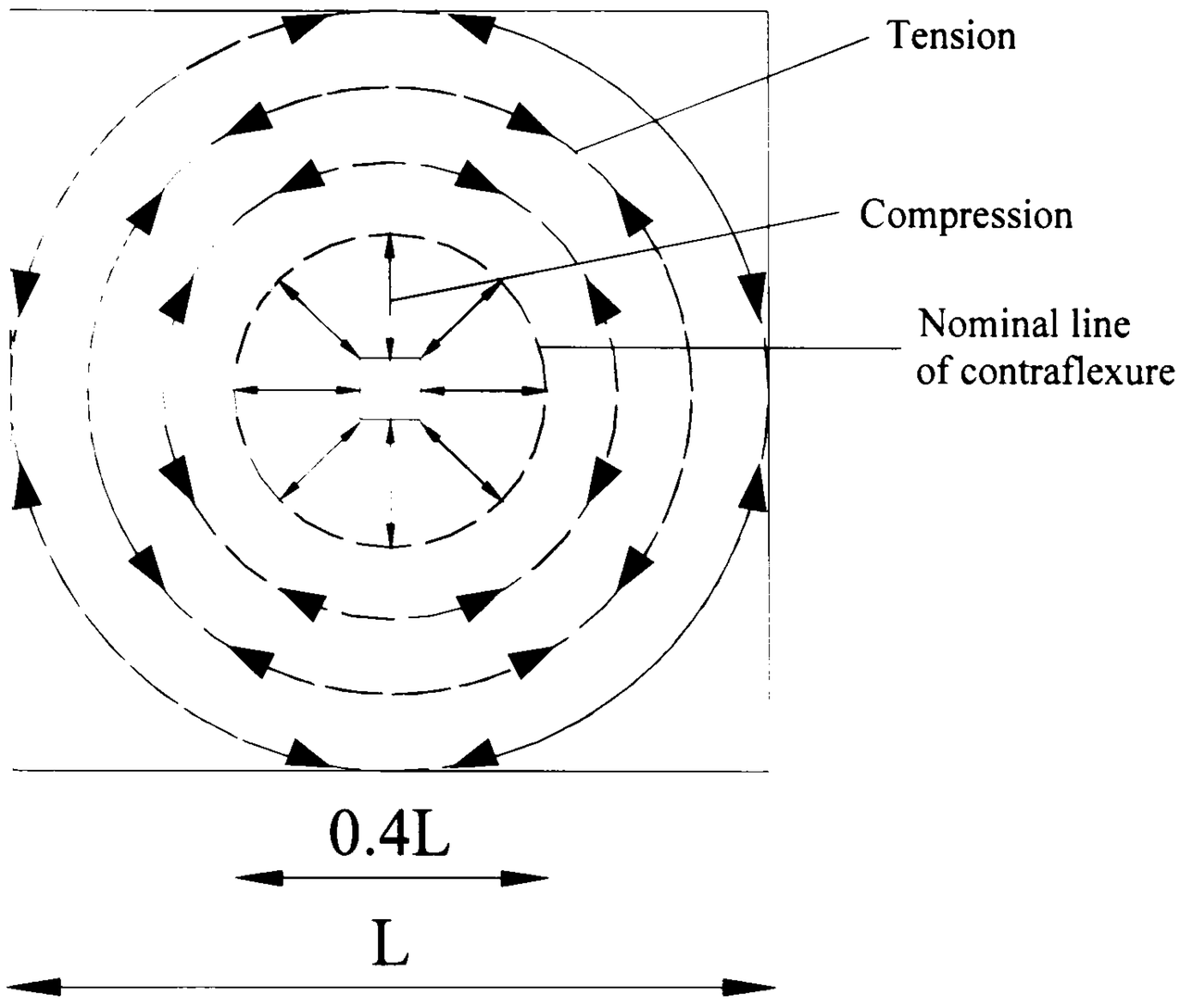

FIG. 2.11 Concept of compressive membrane action at interior slab-column connection [81]

3

SENSITIVITY STUDY OF A PLASTICITY MODEL FOR PREDICTING PUNCHING SHEAR STRENGTHS OF REINFORCED CONCRETE SLABS

Chapter Three

SENSITIVITY STUDY OF A PLASTICITY MODEL FOR PREDICTING PUNCHING SHEAR STRENGTHS OF REINFORCED CONCRETE SLABS

3.1 INTRODUCTION

In Chapter 2, two representative theoretical approaches namely: (1) the upper bound approach based on the theory of plasticity and (2) the lower bound approach based on the Kinnunen and Nylander model, were outlined. This chapter seeks to investigate the possibility of refining the existing plastic approach to significantly enhance its predictive capabilities. One advantage of using the plasticity-based method is that only effectiveness factors relating concrete compressive and tensile strengths have to be determined through calibration of theoretical results against experimental results.

The level of success achieved in predicting the punching failure loads is significantly influenced by the concrete material models used. In particular, the effectiveness factors used for concrete in tension and compression play important roles

in determining the level of accuracy of the predictions. In this chapter, alternative concrete material models are used along with rigid plastic theory to provide new predictive analyses for punching shear. There are three main aspects to these new analyses which are as follows:

- First, concrete material models are used which incorporate the important variation in angle of internal friction with stress state in the concrete.

- Second, two alternative predictive punching shear expressions are presented, one based on using a *curve* for the generatrix of the failure surface, the other a simplified solution based on approximating the failure generatrix to a *straight line*.

- Third, a study to assess the robustness of the plastic predictions in light of the *variability* of the effectiveness factors is investigated. In particular, the range within which effectiveness factors may be varied without significantly influencing the predictions is investigated.

A brief review of previous approaches based on the plasticity theory and specific to the material of this chapter is given in the next section, followed by presentation of the alternative upper bound analysis used in this PhD study.

3.2 UPPER BOUND SOLUTION DERIVED BY BRAESTRUP

3.2.1 Modified Mohr-Coulomb Failure Criterion for Concrete

In Braestrup [13] analysis of punching shear failure of concrete slabs, concrete is regarded as a rigid-perfectly-plastic material, with yielding controlled by the modified Mohr-Coulomb failure criterion in which the Coulomb friction hypothesis is combined with a bound for the maximum tensile strength of concrete. Fig. 3.1 shows the modified criterion. Mohr circles for simple compression and simple tension are also drawn, and the circles intersect the horizontal axis at distances f_c and f_t from the origin respectively, where f_c and f_t are concrete uniaxial compressive and tensile strengths respectively. In the modified Mohr-Coulomb failure criterion, a distinction is made between a sliding failure, when the shear stress in the section reaches the sliding resistance, and a separation failure, when the tensile stress in the section reaches separation resistance. The well-known sliding criterion is given by:

$$|\tau| = c - \sigma \tan \varphi \tag{3.1}$$

and the separation criterion is described as:

$$\sigma = f_t \tag{3.2}$$

where τ and σ are shear and normal stresses on an arbitrary plane; c and φ are cohesion and angle of internal friction of the material.

In the principal-stress coordinate, the sliding condition (3.1) is written as:

$$\frac{1}{2}\sigma_1(1+\sin\varphi)-\frac{1}{2}\sigma_3(1-\sin\varphi)-c\cos\varphi=0 \tag{3.3}$$

where $\sigma_1 \geq \sigma_2 \geq \sigma_3$. Mohr circles showing the principal stresses can be drawn on the $\sigma-\tau$ coordinates shown in Fig. 3.1. It is clear that a sliding failure will occur when the circle with diameter $(\sigma_1-\sigma_3)$ touches the sloping part of the criterion, and a separation failure when the circle touches the vertical part. The sliding condition (3.3) can be written as:

$$k\sigma_1-\sigma_3=2c\sqrt{k} \tag{3.4}$$

where:

$$k=\frac{1+\sin\varphi}{1-\sin\varphi}=\left(\frac{\cos\varphi}{1-\sin\varphi}\right)^2=\frac{f_c}{f_t} \tag{3.5}$$

From equations (3.4) and (3.5), the uniaxial compressive and tensile strengths are expressed by:

$$f_c=\frac{2c\cos\varphi}{1-\sin\varphi} \quad \text{and} \quad f_t=\frac{2c\cos\varphi}{1+\sin\varphi} \tag{3.6}$$

Equation (3.4) is then written as:

$$k\sigma_1-\sigma_3=f_c \tag{3.7}$$

The angle of internal friction φ, was treated as a constant in that study. The yield locus is shown in Fig. 3.2 for cases of plane stress and plane strain.

To allow for the lack of ductility in real concrete, the uniaxial compressive and tensile yield strengths are assumed to be $\mu_c f_c$ and $\mu_t f_t (\mu < 1)$, where μ_c and μ_t are effectiveness factors and are the only parameters which have to be determined experimentally.

3.2.2 Upper Bound Solution

Fig. 3.3 shows the concrete slab which is annularly supported and loaded by a circular punch, and the failure mechanism considered by Braestrup. This consists of the punching out of a solid of revolution at the centre with a vertical downward displacement relative to the rigid surrounding slab. The slab is reinforced in such a way that flexural failure is prevented; dowel action and the contribution of main reinforcement to the punching load-carrying capacity are ignored.

The axi-symmetric failure is described by a function $r = r(x)$, as shown in Fig. 3.3. The relative displacement u at the yield surface is uniform on the whole surface and inclined at a variable angle α to it. Since it is assumed that no direct strain exists in the circumferential direction, the generatrix $r(x)$ can be regarded as a plane-strain yield line. There are tensile and compressive strains in the yield zone, and the normality condition requires that $\alpha \geq \varphi$, otherwise the failure point in Fig. 3.2 would be far to the bottom left. Therefore, the analysis is only valid for the range:

$$D \geq d_0 + 2h\tan\varphi \tag{3.8}$$

where D is the diameter of the annular support.

The upper bound work equation for the assumed failure mechanism is as follows:

$$P \cdot u = \int_0^h \frac{1}{2} f_c u(\zeta - \xi \sin\alpha) \frac{2\pi r}{\cos\alpha} dx \tag{3.9}$$

where P is the ultimate punching load; ζ and ξ are given by:

$$\zeta = 1 - 2\frac{f_t}{f_c}\frac{\sin\varphi}{1-\sin\varphi} \quad \text{and} \quad \xi = 1 - 2\frac{f_t}{f_c}\frac{1}{1-\sin\varphi} \tag{3.10}$$

By considering the relation $\tan\alpha = dr/dx = r'$, the upper bound on the ultimate punching load is expressed as:

$$P = \pi f_c \int_0^h r\left(\zeta\sqrt{1+(r')^2} - \xi r'\right)dx \tag{3.11}$$

Subject to the condition dictated by the plane-strain yield locus that:

$$r' \geq \tan\varphi \tag{3.12}$$

the function $r = r(x)$ which minimises the load P in equation (3.11) can be found using calculus of variations,

$$\begin{aligned} r &= \frac{d_0}{2} + x\tan\varphi (0 \leq x \leq h_0) \\ r &= a\cosh\left(\frac{x-h_0}{c}\right) + b\sinh\left(\frac{x-h_0}{c}\right) (h_0 \leq x \leq h) \end{aligned} \tag{3.13}$$

It is seen that the generatrix consists of a straight line and a catenary curve, as shown in Fig. 3.3. The constants, a, b, c and h_0, are determined by the following equations:

$$a = \frac{d_0}{2} + h_0\tan\varphi \tag{3.14}$$

$$\tan\varphi = \frac{b}{c} \tag{3.15}$$

$$c = \sqrt{a^2 + b^2} \tag{3.16}$$

$$\frac{d_1}{2} = a\cosh\left(\frac{h-h_0}{c}\right) + b\sinh\left(\frac{h-h_0}{c}\right) \tag{3.17}$$

The least upper bound on the failure load is found to be:

$$P = \pi f_c \frac{h_0}{2}\frac{(d_0\cos\varphi + h_0\sin\varphi)(1-\sin\varphi)}{\cos^2\varphi} + \frac{\pi}{2} f_c \left\{\zeta\left[c(h-h_0) + \frac{d_1}{2}\sqrt{\left(\frac{d_1}{2}\right)^2 - c^2 - ab}\right] - \xi\left[\left(\frac{d_1}{2}\right)^2 - a^2\right]\right\} \tag{3.18}$$

In applying equation (3.18) to determine the failure load P, an iterative process has to be used [71].

The analytical results for particular cases have been presented [16, 70]. It is obvious that equation (3.18) involves an iterative procedure which can be easily implemented into readily available computer software. In the next section, an alternative simpler upper bound solution is presented for predicting the punching shear strength of reinforced concrete slabs with no membrane restraint.

3.3 AN ALTERNATIVE UPPER BOUND SOLUTION

3.3.1 Parabolic Mohr's Failure criterion for Concrete

For the concrete material modelling, Braestrup et al (1976) used the modified Coulomb failure criterion, which incorporates a *constant* angle of internal friction (Fig. 3.1), to tackle the punching shear problem. In the present study, a parabolic Mohr failure criterion, shown in Fig. 3.4 and which incorporates the *variation* in angle of internal friction with stress state in the material, is used to represent the real mechanical characteristics of concrete. As shown in Fig. 3.4, the parabola touches the Mohr circles for simple compression and simple tension. It is important to note that the concrete material strengths used in Fig. 3.4 are the *effective* uniaxial tensile (f_t) and compressive (f_c) strengths as required for incorporation within plastic theory, as opposed to the actual measured uniaxial tensile and compressive strengths. This is achieved by applying effectiveness factors to the actual concrete material strengths, and is discussed further in the next section. The parabolic Mohr failure criterion is expressed as:

$$\left(\frac{\tau}{c_k f_t}\right)^2 + \frac{\sigma}{f_t} = 1 \tag{3.19}$$

where τ and σ are shear and normal stresses on an arbitrary plane, and c_k is a parameter related to the ratio of the effective material strengths of concrete as follows:

$$c_k = \sqrt{1 + \frac{f_c}{f_t}} - 1 \tag{3.20}$$

The shear and normal stresses in the parabolic Mohr failure envelope can be given as functions of the parameter α defined in Fig. 3.2 by:

$$\tau = f_t \frac{c_k^{\,2}}{2} \cot\alpha \tag{3.21}$$

$$\sigma = f_t \left(1 - \frac{c_k^{\,2}}{4} \cot^2 \alpha \right) \tag{3.22}$$

From Mohr's circle the maximum and minimum principal stresses can be found to be:

$$\sigma_1 = f_t \left[1 - \frac{c_k^{\,2}}{4} (\csc\alpha - 1)^2 \right] \tag{3.23}$$

$$\sigma_3 = f_t \left[1 - \frac{c_k^{\,2}}{4} (\csc\alpha + 1)^2 \right] \tag{3.24}$$

The yield loci for the cases of plane stress and plane strain are shown in Fig. 3.2.

The above formulation is chosen for convenience. It is possible to re-write this formulation in terms of the effective compressive strength f_c and the effectiveness factor μ_t (ratio of f_t to f_c), as follows :

$$\sigma_1 = f_c \left\{ \mu_t - \left[\frac{\mu_t}{2} + \frac{1}{4} - \frac{1}{2} \sqrt{\mu_t (1 + \mu_t)} \right] (\csc\alpha - 1)^2 \right\} \tag{3.25}$$

$$\sigma_3 = f_c \left\{ \mu_t - \left[\frac{\mu_t}{2} + \frac{1}{4} - \frac{1}{2} \sqrt{\mu_t (1 + \mu_t)} \right] (\csc\alpha + 1)^2 \right\} \tag{3.26}$$

The significances of the effective concrete material strengths and of the effectiveness factors used to determine those strengths, are discussed below.

3.3.2 Effectiveness factors

Rigid-perfectly plastic theory assumes that ultimate conditions are attained along the failure surfaces at zero deformation, and that these ultimate conditions continue to prevail via the normality rule at least up to the deformations corresponding to overall failure of the structure. In other words, the slabs are assumed to be ductile in the shear failure zones. However, concrete shows limited ductility; in compression, concrete is both nonlinear and of limited ductility, while in tension the material exhibits brittle behaviour at low stress and subsequently displays monotonic strain softening behaviour to zero stress at large strains. This is clearly at odds with the assumption of perfectly plastic material, which implies a plateau in the material stress-strain behaviour under uniaxial loading. Fortunately, for the slabs considered in this study, extensive yielding of the tension steel reinforcement occurs during the punching failure regime. As a result, the limited ductility of the concrete is overshadowed by the considerable ductility of steel, so that the slabs exhibit ductile punching failure characteristics overall.

For analytical purposes, these overall ductile characteristics permit fictitious "perfectly plastic" stresses to be assigned to the concrete in both tension and compression, consistent with the requirements of plastic theory. This is done by applying "*effectiveness factors*" to the actual compressive strength of the concrete, to give the *effective* compressive and tensile strengths used in Equations 3.19 – 3.26 above. Henceforth, the effectiveness factors used to determine these effective compressive and tensile strengths will be termed μ_c and μ_t respectively. In general, effectiveness

factors are determined by calibration against test data, with the calibration used depending on the material model under consideration. As illustrated in Fig. 3.5, one method of determining the effectiveness factor is based on retaining the strain to failure of the material and equating the area underneath the actual stress-strain curve to that underneath the effective ultimate stress-strain rectangle.

The next section will investigate the role of effectiveness factors as a *generic* issue, which has to date not been done but is crucially important to the reliability of the plastic approach to punching shear predictions. Specifically, this next section will investigate the sensitivity of punching shear failure load predictions to variability of the effectiveness factors. In so doing, that section uses expressions for failure load derived later on (section 3.3.6) in this chapter. The sensitivity study is presented *before* the derivation, as the overall influence of the effectiveness factors is considered to be a crucial issue in this study.

3.3.3 Sensitivities of Predictions To Variations In Effectiveness Factors

A wider study to investigate the role of the effectiveness factors themselves, in particular the range of values over which these may be varied without significantly influencing the predictions, has not really been done. Therefore, this section is focused on assessing the robustness of the plastic predictions in light of the variability of the effectiveness factors.

Consider the simplified punching shear expression (derived in section 3.3.6 of this chapter), which is as follows:

$$P = \pi \cdot \mu_c \cdot f_c \left(\mu_t \tan\alpha + z\cot\alpha\right)\left(\frac{d_0}{h} + \tan\alpha\right)h^2 \tag{3.27}$$

Differentiation of this expression with respect to the tension and compression effectiveness factors gives the following two expressions:

$$\frac{\partial P}{\partial \mu_t} = \left(\pi \cdot \mu_c \cdot f'_c\right)\cdot\left(\frac{d_0}{h} + \tan\alpha\right)\cdot\left(h^2\right)\cdot\left(\tan\alpha + \frac{\partial z}{\partial \mu_t}\cdot\cot\alpha\right) \tag{3.28}$$

$$\frac{\partial P}{\partial \mu_c} = \left(\mu_t \cdot \tan\alpha + z\cot\alpha\right)\cdot\left(\frac{d_0}{h} + \tan\alpha\right)\cdot\left(h^2\right)\cdot\left(\pi \cdot f'_c\right) \tag{3.29}$$

where:

$$z = 0.5\mu_t + 0.25 - 0.5\left[\mu_t \cdot \left(1 + \mu_t\right)\right]^{\frac{1}{2}} \tag{3.30}$$

For evaluating maximum or minimum values of failure load (P), we have:

$$\frac{\partial P}{\partial \mu_t} = 0 \qquad \& \qquad \frac{\partial P}{\partial \mu_c} = 0$$

By solving the above differential equations, it is found that the equation $\frac{\partial P}{\partial \mu_t} = 0$ gives unreal roots indicating that the solutions have to be rejected. On the other hand, the expression $\frac{\partial P}{\partial \mu_c} = 0$ results in a solution of (μ_t) equal to be $\frac{1}{1021}$ which corresponds to a minimum value of failure load.

The analysis thus shows that the minimum value of punching shear strength occurs when the effectiveness factor for concrete in tension equals to $\mu_t = \frac{1}{1021}$. This

evaluated value of effectiveness factor in tension is relatively smaller than the values of $\mu_t = \frac{1}{400}$ or $\mu_t = \frac{1}{100}$ as suggested in the literature [71]. The boundaries of values to be used in producing a plot which represents the influence of effectiveness factors on the robustness of plastic analysis are as follows:

$$0 \leq \mu_t \leq \frac{1}{3} \tag{3.31}$$

$$0 < \mu_c \leq 1 \tag{3.32}$$

Using this range as a guide, the following steps were taken to generate a normalised plot of punching shear strength against the compression and tension effectiveness factors:

1. Choose a slab of numerically defined span, depth, concrete strength and percentage of reinforcement. In this case a slab of 1.2m span, with an overall thickness of $150mm$, a concrete cube strength of $40N/mm^2$ and a percentage of reinforcement equal to 1.06% is considered.
2. Choose one set of effectiveness factors of specific values which will make the punching shear load quite high using the general formula given by Equation (3.27).
3. Vary the tension and compression effectiveness factors over the range as described above and divide each punching shear load by the one obtained in step (2) to achieve a normalised punching shear load.
4. Use the normalised values from step (3) along with the corresponding tension and compression effectiveness factors to generate a 3D plot.

Figure 3.6 shows a 3-Dimensional plot of normalised punching shear strength against μ_c and μ_t within the boundaries presented in Equation (3.31) and (3.32). The plot shows that the normalised punching shear strength increases as the values of effectiveness factors of concrete in tension and compression increase. The important features of Figure 3.6 fall within the highlighted region which represents the range of effectiveness factors commonly used in the literature.

This highlighted region is reproduced in Figure 3.7 within the range of effectiveness factors used in the literature. The plot suggests that the normalised punching shear strength increases as both effectiveness factors increase; in particular, there exists a non-sensitive region where a minimum normalised punching shear strength is observed. This important feature is reproduced in Figure 3.8 which represents a line diagram in 3-D space, showing clearly a distinct point of minimum value of normalised punching shear strength when the effectiveness factor of concrete in tension (μ_t) equals to $\frac{1}{1021}$ as indicated earlier in the partial differential analysis with different values of μ_c. This new finding suggests that this plastic analysis remains within fairly small bounds provided that the effectiveness factor of concrete in tension is kept within reasonable range of $\mu_t = \frac{1}{1021}$.

Having identified the confident range of effectiveness factors, it seems prudent to establish the level of sensitivity of the present predictions of punching shear failure loads to different effectiveness factors. For that reason, in the work presented throughout the remainder of this chapter, two alternative tension effectiveness factors and two alternative compression effectiveness factors are used. The compression effectiveness factors, taken after Sigurdsson (1991) and Nielsen (2000) respectively, are

as follows:

$$\mu_c = \frac{1.47}{\sqrt{f'_c}}\left(1+\frac{0.48}{\sqrt{0.001h}}\right)(1+0.125\rho) \qquad (h \text{ in metre})$$

or $$\mu_c = 4.22/\sqrt{f'_c} \qquad (3.33a,\ b).$$

Note the dependence of the Sigurdsson factor on the tension steel reinforcement ratio (ρ), the concrete uniaxial cylinder compressive strength and the thickness of the slab. The two alternative tension effectiveness factors considered in this study, both taken from Nielsen (2000), are as follows:

$$\mu_t = f_t / f_c = 1/400$$

or $$\mu_t = f_t / f_c = 1/100 \qquad (3.34a,\ b)$$

One compression and one tension effectiveness factor must be used in the punching shear analysis. Equations (3.33) and (3.34) above permit up to four different potential combinations of factors. Also, it is shown further on in this chapter that the predicted punching shear load depends on the shape of the generatrix of the failure surface. In the present study, one curved generatrix and one straight generatrix are considered. For each generatrix, the predicted punching shear loads emerging from use of the above four combinations of effectiveness factors will be compared. In what follows, it is seen that the effectiveness factors which work well do indeed fall within the range of factors shown to be robust in the sensitivity study of this section. Although this sensitivity study was performed for the failure surface of a *straight* generatrix, the results are seen to be applicable also to failure predictions based on a curved *generatrix*.

3.3.4 Work Equation

The yield zone between adjacent bodies moving in one plane can be investigated by considering rigid moving blocks separated by a homogeneous plane strain field of thickness δ, as shown in Fig. 3.9(a). If the angle between the relative displacement rate u and the surface is α', the strain rates in the deforming zone are:

$$\varepsilon_t = 0 \tag{3.35}$$

$$\varepsilon_n = \frac{u}{\delta}\sin\alpha' \tag{3.36}$$

$$\gamma_{nt} = \frac{u}{\delta}\cos\alpha' \tag{3.37}$$

The principal strain rates can therefore be determined by:

$$\frac{\varepsilon_1}{\varepsilon_3} = \frac{1}{2}\left[(\varepsilon_n + \varepsilon_t) \pm \sqrt{(\varepsilon_n - \varepsilon_t)^2 + \gamma_{nt}}\right] = \frac{u}{2\delta}(\sin\alpha' \pm 1) \tag{3.38}$$

According to the normality flow rule of the theory of plasticity, using Equations (3.23) and (3.24) with plastic strain rates being considered:

$$-\frac{d\sigma_1}{d\sigma_3} = \frac{\varepsilon_3}{\varepsilon_1} = \frac{\sin\alpha - 1}{\sin\alpha + 1} \tag{3.39}$$

From equation (3.38):

$$\frac{\varepsilon_3}{\varepsilon_1} = \frac{\sin\alpha' - 1}{\sin\alpha' + 1} \tag{3.40}$$

It is evident from the comparison between Equations (3.39) and (3.40) that if and only if $\alpha' = \alpha$ can the stress state described by the parabolic Mohr yield condition (Fig. 3.2) produce the strain vector given by expression (3.38). Internal energy dissipation per unit area in the deforming zone for the parabolic material is:

$$D_A = (\sigma_1 \varepsilon_1 + \sigma_3 \varepsilon_3)\delta = u f_t \left(1 + \frac{c_k^{\,2}}{4} \cot^2 \alpha\right) \sin \alpha \tag{3.41}$$

This equation is applicable for any condition of plane strain, and for plane stress on the tension side of points A, A? in Fig. 3.2, i.e. for the ratio $\varepsilon_1 / \varepsilon_3$ exceeding a certain limit. For other strain ratios in plane stress, the stress point will be at A or A? in Fig. 3.2, and the energy dissipation will be correspondingly different.

It is observed from equation (3.41) that the energy dissipation is totally independent of the thickness δ, indicating that a yield line is obtained in the limiting case when the value of δ tends toward zero.

3.3.5 Upper Bound Solution

The Upper-Bound theorem of plasticity states that if, for any assumed failure mechanism, the external rate of work is equated to the rate of dissipation of internal energy, then an upper bound for the collapse load of the structure can be found. The rate of work done by the external load on the slab under punching is:

$$W_E = P * u \tag{3.42}$$

Consistent with the Upper-Bound procedure, we can state work-energy equilibrium as $W_E = W_A = \int_{r=0}^{r=h} D_A (2\pi r ds)$, where ds is the increment of length along the

generatrix of the punching shear failure surface. At this stage, it is important to note that, as shown in Fig 3.9(b), the incremental movement of the punched-out block of concrete is vertically down the page, while the remaining block of peripheral concrete is assumed not to move. As a result, the relative displacement rate vector is oriented vertically along the entire length of the generatrix of the failure surface. This, along with the requirement that $\alpha' = \alpha$, leads to the convenient and useful result that $r' = \tan\alpha' = \tan\alpha$. Insertion of this relationship into the above Upper Bound equation gives the following:

$$P = 2\pi f_t \int_0^h \left(r' + \frac{c_k^{\,2}}{4r'} \right) r dx \tag{3.43}$$

which can also be expressed as:

$$P = 2\pi f_t \int_0^h F(r, r') dx \tag{3.44}$$

where:

$$F(r, r') = r\left(r' + \frac{c_k^{\,2}}{4r'} \right) \tag{3.45}$$

Equation (3.43) shows that the punching shear strength of a slab depends on the shape of the failure surface and the related angle, in other words, it depends upon the generatrix r (Fig. 3.9(b)). The function $r(x)$ which minimizes the ultimate punching load can be found by calculus of variations. To that end, the appropriate form of Euler equation (for function F in Equation (3.45)) is as follows:

$$\frac{\partial F}{\partial r} - \frac{d}{dx}\left(\frac{\partial F}{\partial r'} \right) = 0 \tag{3.46}$$

Since $F(r,r')$ does not contain x, Euler equation has the first integral:

$$F - r'\frac{\partial F}{\partial r'} = C \tag{3.47}$$

where C is a constant.

By substituting equation (3.45) into Euler equation with consideration of the boundary conditions:

$$r(0) = \frac{d_0}{2} \quad \text{and} \quad r(h) = \frac{d_1}{2} \tag{3.48}$$

gives the minimizing function of the generatrix:

$$r = \frac{d_0}{2}\left(\frac{d_1}{d_0}\right)^{x/h} \tag{3.49}$$

Once the minimizing function of the generatrix has been found, the least upper bound solution for the punching load can be obtained from equation (3.43):

$$P = \frac{\pi}{4} f_t \left[{d_1}^2 - {d_0}^2 + \frac{2{c_k}^2 h^2}{\ln(d_1/d_0)} \right] \tag{3.50}$$

Equation (3.50) shows that the collapse load varies with the outer diameter of the punched cone d_1. If the support diameter D is sufficiently large, there is a critical value of d_1 which is found from consideration of $\frac{\partial P}{\partial d_1} = 0$ which gives:

$$\left(\frac{d_1}{d_0}\right)^{d_1} = e^{c_k h} \tag{3.51}$$

3.3.6 Simplified Upper Bound Solution

The upper-bound solution defined in equation (3.50) can be simplified by assuming the yield line to be straight in elevation (Fig. 3.10), in which case the equation of the generatrix simplifies to:

$$r = \frac{d_0}{2} + x\tan\alpha \tag{3.52}$$

By substituting equation (3.52) into equation (3.43) and using equations (3.25 and 3.42) gives:

$$P = \pi f_c\left(\mu_t \tan\alpha + z\cot\alpha\right)\left(\frac{d_0}{h} + \tan\alpha\right)h^2 \tag{3.53}$$

where:

$$z = \frac{\mu_t}{2} + \frac{1}{4} - \frac{1}{2}\sqrt{\mu_t\left(1+\mu_t\right)}$$

$$f_c = \mu_C \cdot f'_c$$

The extreme of the collapse load is found from consideration of $\frac{\partial P}{\partial \alpha} = 0$ which gives:

$$\cot^3\alpha - \frac{\mu_t}{z}\cot\alpha - \frac{2}{z}\cdot\frac{h}{d_0}\cdot\mu_t = 0 \tag{3.54}$$

Equation (3.54) has a real root for α, which is the critical punch angle α_1 given by:

$$\alpha_1 = \operatorname{arcot}\left[\sqrt[3]{\frac{\mu_t\cdot h}{z\cdot d_0}\left(1+\sqrt{1-\frac{\mu_t\cdot {d_0}^2}{27z\cdot h^2}}\right)} + \sqrt[3]{\frac{\mu_t\cdot h}{z\cdot d_0}\left(1-\sqrt{1-\frac{\mu_t\cdot {d_0}^2}{27z\cdot h^2}}\right)}\right] \tag{3.55}$$

Thus, the critical diameter is:

$$d_1 = d_0 + 2h\tan\alpha_1 \tag{3.56}$$

3.4 EXPERIMENTAL VERIFICATION

Predictions from the presently-proposed analyses have been compared with the results of 97 tests conducted by various researchers [Base (1959), Kinnunen & Nylander (1960), Moe (1961), Dragosavic et al (1974), Elstner et al (1956), Criswell (1974), Regan (1978), Rankin & Long (1987), Hallgren & Kinnunen (1996)]. The relevant geometric and material-property details of the slabs are given in Tables 3.1 and 3.2. The comparisons between predicted and measured punching shear failure loads are given in Figs 3.11 and 3.12, while a statistical summary of the correlations of Figs 3.11 and 3.12 are presented in Table 3.3. The data of Figs 3.11 and 3.12 were obtained by implementing the present analyses and associated iterative operations in MATLAB. Note the following points in relation to the implementations of the analyses:

- Concretes over a wide range of cylinder compressive strengths, from 14 N/mm^2 to 109 N/mm^2, and slabs over a wide range of scales, with effective depths from 30mm to 250mm, are considered.

- The value of h is approximated to the effective depths of the slabs.

- The present analyses assume a circular punch, but some of the experiments used square punches. In such cases, an effective diameter (d_0) 10% greater than the side length of the square is assumed. This gives a circular punch of equal plan area to the experimentally-employed square punch.

- In applying the compression effectiveness factor due to Sigurdsson (Equation (3.33a)), the tension steel reinforcement ratio is required. For most of the slabs considered, this ratio was equal along the two main perpendicular directions of the slab. However for Moe's tests, these ratios were different along the two perpendicular directions (this explains why two reinforcement ratios are given for each of Moe's slabs in Table 3.2). This issue was dealt with by using, in Equation (3.33a), the *average* of the tension steel reinforcement ratios along the perpendicular directions.

- Tables 3.1 and 3.2 give the cube strength (f_{cu}) and cylinder compressive strength (f'_c) respectively of the concrete, because these were the data on concrete compressive strength supplied in the literature. However, the present analyses are based on the cylinder strength. For cases where only the cube strength (and not the cylinder strength) was given, the cylinder strength was taken as 80% of the cube strength. This was done before effectiveness factors were applied.

- Figs 3.11 and 3.12 show the comparisons based on the curved and linear generatrices respectively. As explained earlier, four different combinations of compression and tension effectiveness factors, taken from Equations (3.33) and (3.34), have been used with each analytical approach. This accounts for the presence of four plots for each analytical approach in Figs 3.11 and 3.12.

A scrutiny of Tables 3.1 ? 3.3, along with Figs 3.11 and 3.12, reveals the following essential points:

- Both the complex and simplified theoretical analyses show decent correlation with the test data for all possible combinations of effectiveness factors. The closest correlation (based on the mean) occurs for the complex analysis using the Sigurdsson compression effectiveness factor and a value of 1/100 for the tension effectiveness factor. This gives a mean correlation of 1.04, standard deviation of 0.196 and coefficient of variation of 18.85%.

- The mean correlations for the simplified analyses are appreciably sensitive to variation in the tension effectiveness factor, but are virtually insensitive to variation in the compression effectiveness factor (refer to Table 3.3). The reverse is true for the complex analysis using the compression effectiveness factor of $\mu_c = 4.22/\sqrt{f'_c}$, where the analysis is insensitive to change in the tension effectiveness factor.

- The correlation mean (0.85) furthest away from 1 is obtained via use of the complex analysis with the compression effectiveness factor of $\mu_c = 4.22/\sqrt{f'_c}$. Note, however, that the correlation is less than 1 and so points to a conservative approach. This contrasts with the simplified approaches using a tension effectiveness factor of 1/100, where the correlation mean is on average 13% into the non-conservative regime.

- When the Sigurdsson compression effectiveness factor is used along with the tension effectiveness factor of value 1/400, all the correlation data are

virtually identical for both the simplified and complex approaches. This also gives an impressive mean correlation of predicted to experimental data of 0.93.

- The simplified analysis referred to immediately above, namely that which gives a mean correlation of 0.93, also gives the closest (and indeed very encouraging) correlation for the very high strength concrete slabs tested by Hallgren. This is apparent from Figs 3.11 and 3.12, which show that the predicted values for Hallgren slabs are always higher than the test values, and that, of all the analyses, the simplified approach of Fig. 3.12(a) locates the Hallgren points closest to the 45^{o} line.

These results clearly suggest that the complex approach with the Sigurdsson compression effectiveness factor and the tension effectiveness factor of value 1/1100 gives the closest correlation (1.04 mean) overall. The simplified approach with the Sigurdsson compression effectiveness factor and the tension effectiveness factor of value 1/400 is also strongly recommended, as it shows good correlation (mean 0.93) overall, and also because it gives the best correlation for the high strength concrete slabs. The excellent mean of value 0.93 points to a conservative approach. This conservatism, coupled with the ease of implementation in a computer, renders this version of the simplified analysis particularly useful in a design office environment.

Note also that both these recommended approaches use the Sigurdsson compression effectiveness factor, which depends on the tension steel reinforcement ratio, on the depth of the slab and on the compressive strength of the concrete.

3.5 CONCLUSIONS

By adopting a parabolic failure criterion for concrete, an alternative upper-bound rigid - perfectly plastic solution for the punching shear failure of concrete slabs has been derived. Two alternative predictive approaches, namely one complex approach based on a curved generatrix of the failure surface, the other a simplified approach based on a linear generatrix of the failure surface, have been used. In addition, a sensitivity study of the plastic punching predictions to variations in these factors was considered. Two effectiveness factors for the concrete both in compression and tension, giving four different possible combinations of tension and compression effectiveness factors, were employed in the plastic analysis. Eight different analyses in all were performed, based on the use of these four different sets of effectiveness factors with each of the complex and simple approaches.

The predicted failure loads were compared with data from 97 tests in the literature. These tests incorporate a wide range of slab scales, from 30 mm to 250 mm effective depth, and a wide range of concrete cylinder compressive strengths, from 14 N/mm^2 to 109 N/mm^2. The predictions from the analytical approaches broadly show decent agreement with the test data. The approach which gives the closest correlation with test data is based on the curved generatrix of failure surface along with a compression effectiveness factor due to Sigurdsson and a tension effectiveness factor of value 1/100. This analysis gives a mean correlation of predicted to experimental failure loads of 1.04. Also highly recommended is the simplified approach using the Sigurdsson compression effectiveness factor and the tension effectiveness factor of value 1/400, because that approach gives an impressive mean correlation of 0.93, and also because it gives the closest agreement with the test data for the highest strength concrete slabs considered.

Note that a correlation mean of 0.93 signifies a slightly conservative approach. This conservatism, along with the ease of implementation of the analysis, renders this version of the simplified approach eminently suited to use in a design office environment. Finally, note that the Sigurdsson effectiveness factor, which is common to both the above recommended "best" analytical approaches, is dependent on the tension steel reinforcement ratio, on the concrete compressive strength, and on the depth of the slab.

It is seen that the effectiveness factors which work well do indeed fall within that range of factors shown to be robust in the sensitivity study.

In this chapter, no deliberate attempt was made to directly model any enhancing effects of compressive membrane action in the slabs. Such modelling forms the subject of the next chapter.

Researchers & Span	Slab No	d_0 (mm)	d (mm)	ρ %	f_{cu} (N/mm^2)
Base (span = 559 mm)	A	102	57.3	1.083	33.1
	B	102	57.3	1.083	35.7
	C	102	57.3	1.083	32.8
	D	102	57.3	1.083	34.2
	E	102	57.3	0.725	37.3
	F	102	57.3	0.725	34.7
	G	102	57.3	1.635	36.4
	H	102	57.3	1.635	33.0
	J	102	57.3	3.270	35.1
Kinnunen & Nylander (span = 1710 mm)	1A30a24	300	128.0	1.01	32.4
	1A30a25	300	124.0	1.04	30.8
	1A15a5	150	117.0	0.80	32.9
	1A15a6	150	118.0	0.79	32.1
Moe (span = 1778 mm)	S1-60	254	114.3	1.06	29.3
	S5-60	203	114.3	1.06	27.8
	S1-70	254	114.3	1.06	30.6
	S5-70	203	114.3	1.06	28.9
	H1	254	114.3	1.15	32.6
	R2	152	114.3	1.15	33.3
	M1A	305	114.3	1.50	26.1
Regan (span = 1892 mm)	SS2	200	77	1.20	29.3
	SS4	200	77	0.92	40.4
	SS6	200	79	0.75	27.4
	SS7	200	79	0.80	38.0

Table 3.1 Slabs tested by various researchers

Researchers	Slab No	d_0 (mm)	d (mm)	ρ %	f'_c (N/mm^2)
Elstner & Hognestad (span = 1778 mm)	A1a	254	117.6	1.15	14.1
	A1b	254	117.6	1.15	25.3
	A1c	254	117.6	1.15	29.1
	A1d	254	117.6	1.15	36.9
	A1e	254	117.6	1.15	20.3
	A2a	254	114.3	2.47	13.7
	A2b	254	114.3	2.47	19.6
	A2c	254	114.3	2.47	37.5
	A7b	254	114.3	2.47	28.0
	A3a	254	114.3	3.70	12.8
	A3b	254	114.3	3.70	22.7
	A3c	254	114.3	3.70	26.6
	A3d	254	114.3	3.70	34.6
	A4	356	117.6	1.15	26.2
	A5	356	114.3	2.47	27.8
	A6	356	114.3	3.70	25.1
	B4	254	114.3	0.99	47.8
	B9	254	114.3	2.00	44.0
	B11	254	114.3	3.00	13.5
	B14	254	114.3	3.00	50.7
Criswell (span = 2134 mm)	S2075-1	254	120.6	0.75	32.5
	S2075-2	254	122.2	0.75	29.1
	S2150-1	254	124.0	1.50	29.7
	S2150-2	254	122.2	1.50	30.2
	S4150-1	508	125.5	1.50	35.5
	S4150-2	508	125.5	1.50	35.8
Moe - Concentrated reinforcement (span = 2388 mm)	S2-60	254	114.3	1.53, 0.84	22.1
	S3-60	254	114.3	2.3, 0.54	22.7
	S4-60	254	114.3	3.45, 2.65	23.9
	S3-70	254	114.3	2.3, 0.54	25.4
	S4-70	254	114.3	3.45, 2.65	35.2
	S4A-70	254	114.3	3.45, 2.65	20.5

Hallgren & Kinnunen (span = 2540 mm)	HSC0	250	200	0.8	90.3
	HSC2	250	200	0.8	85.7
	HSC4	250	200	1.2	91.6
	HSC6	250	200	0.6	108.8

Table 3.2 Slabs tested by various researchers

	Effectiveness factors	Mean (predicted/experimental)	Standard deviation	Coefficient of variation (%)
Complex approach	Eqs (3.33a & 3.34a)	0.92	0.146	15.87
	Eqs (3.33a & 3.34b)	1.04	0.196	18.85
	Eqs (3.33b & 3.34a)	0.85	0.176	20.70
	Eqs (3.33b & 3.34b)	0.85	0.216	25.41
Simplified approach	Eqs (3.33a & 3.34a)	0.93	0.15	16.13
	Eqs (3.33b & 3.34a)	0.92	0.18	19.56
	Eqs (3.33a & 3.34b)	1.14	0.20	17.54
	Eqs (3.33b & 3.34b)	1.12	0.22	19.64

Table 3.3 Comparison of predictions using different effectiveness factors

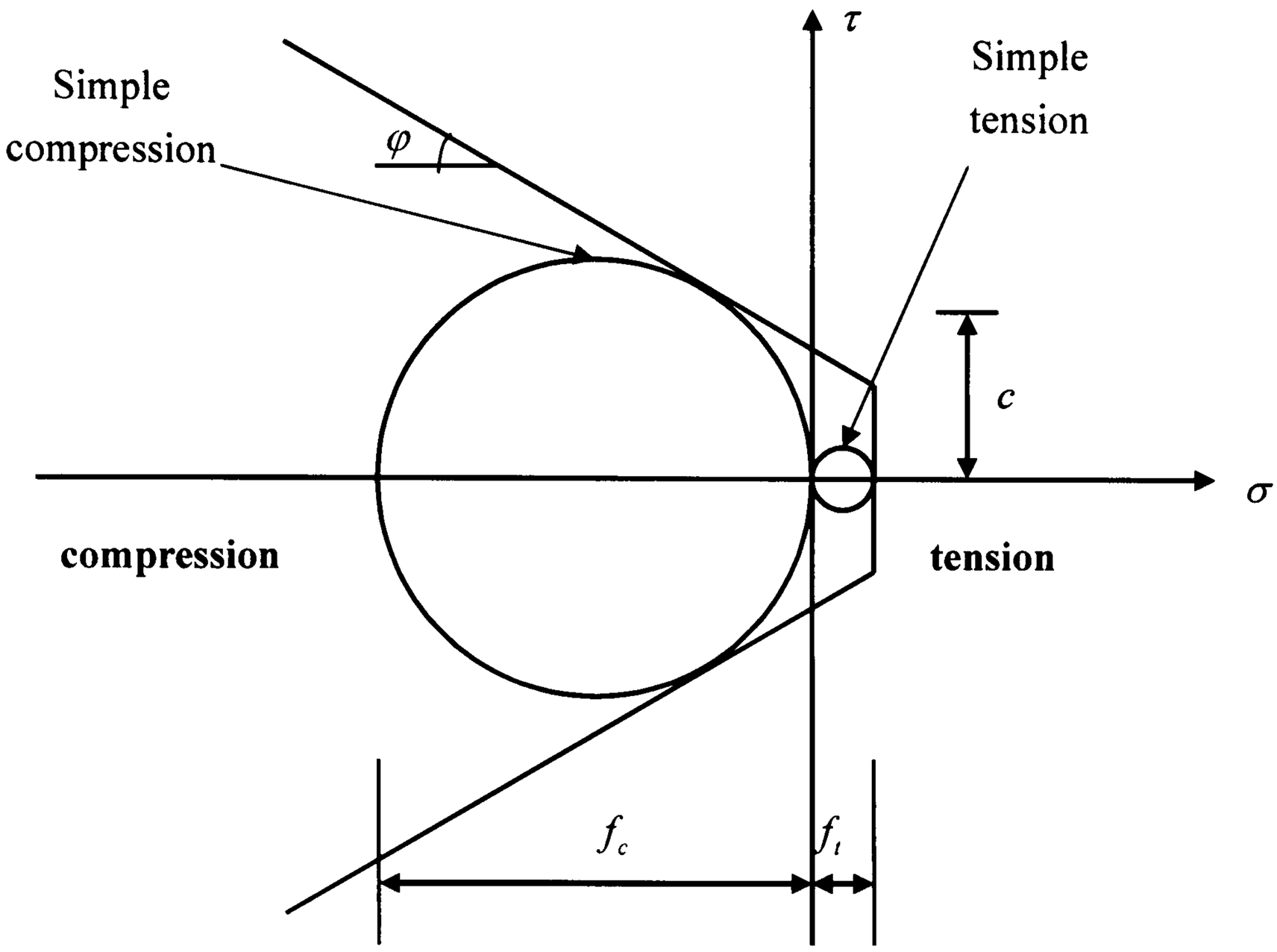

FIG. 3.1 Modified Mohr-Coulomb failure criterion for concrete – sliding condition

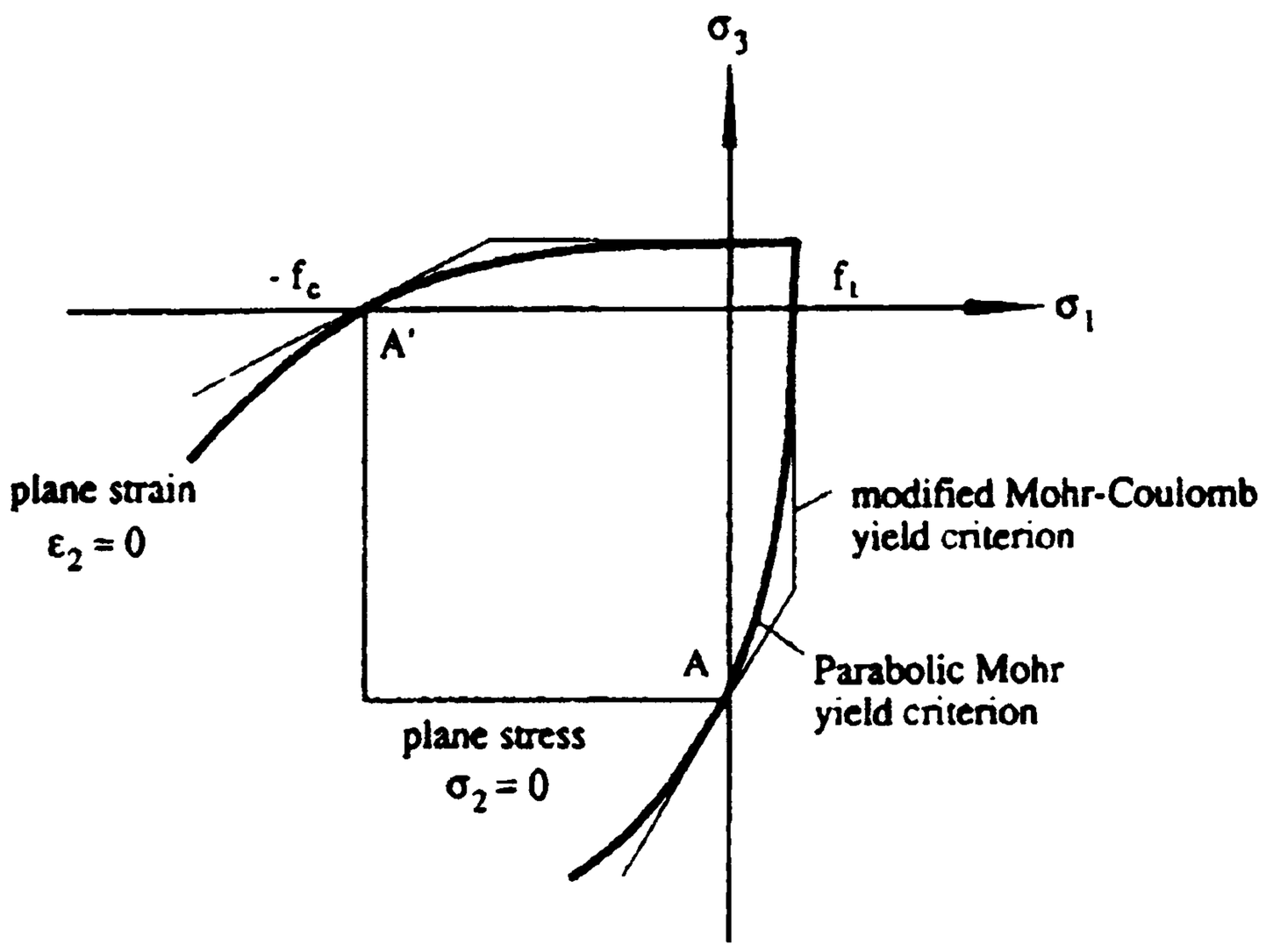

FIG. 3.2 Yield loci in cases of plane stress and plane strain

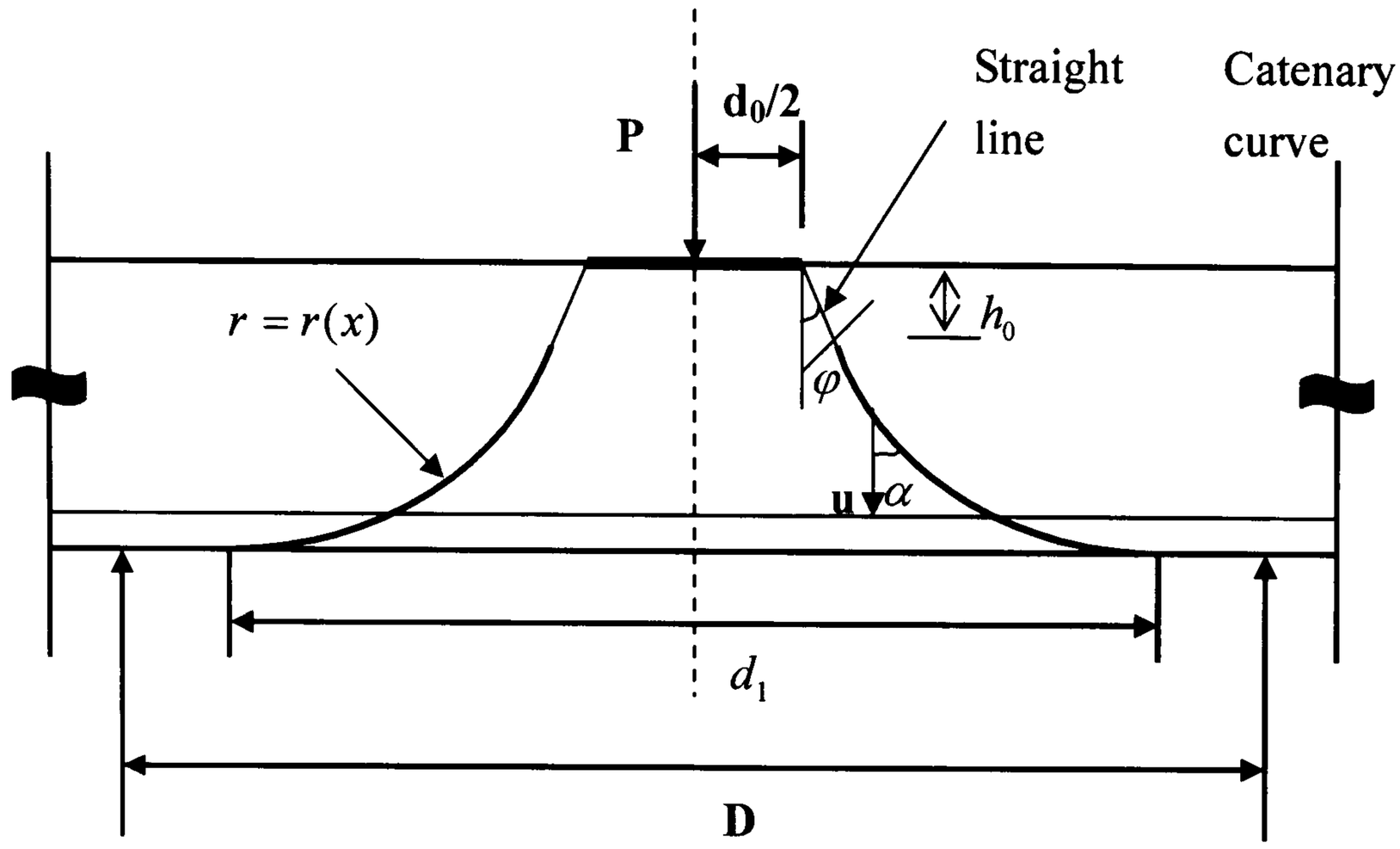

FIG. 3.3 Detailed construction of Failure Generatrix

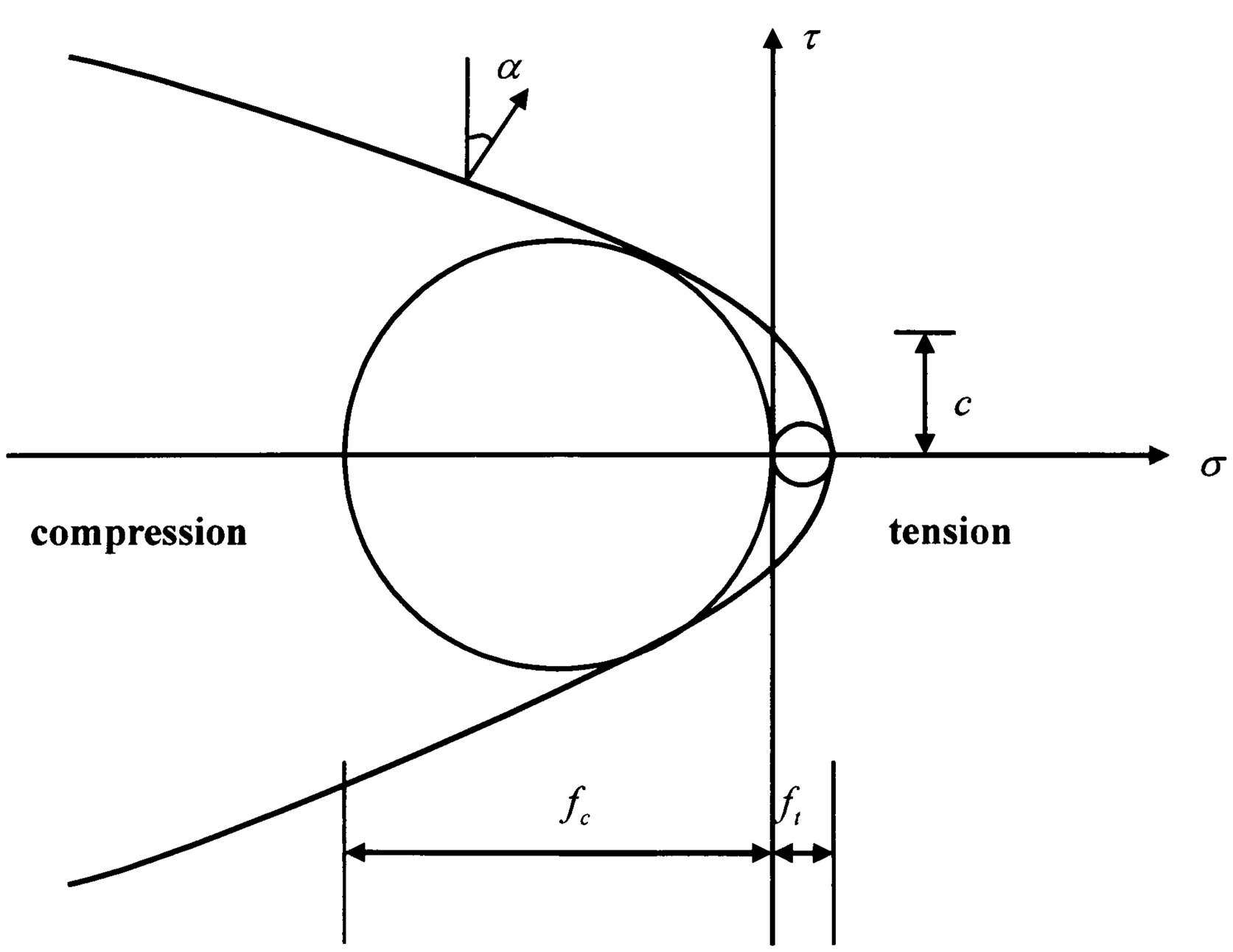

FIG. 3.4 Parabolic Mohr failure criterion for concrete

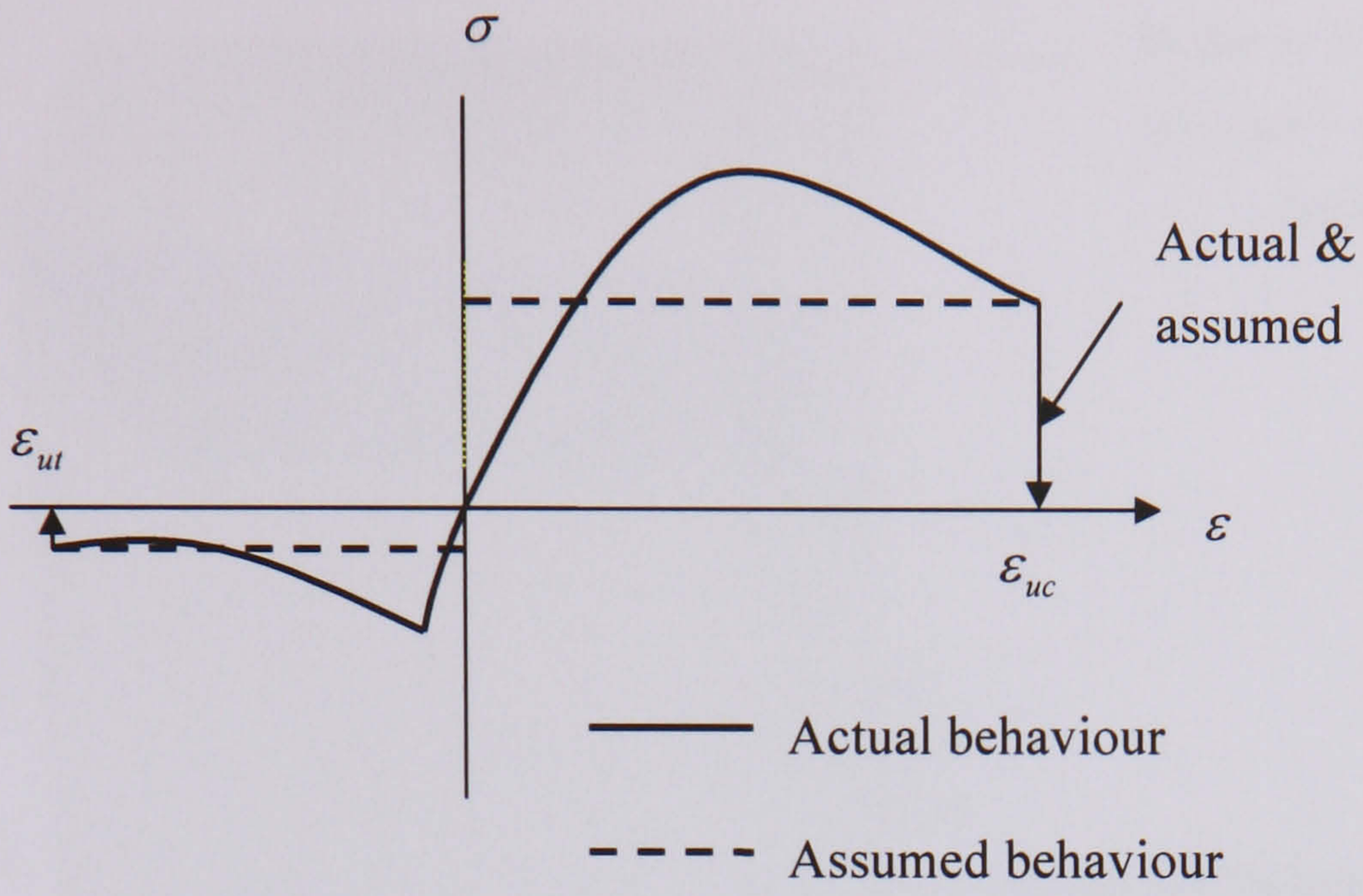

FIG. 3.5 Stress-strain relationship for concrete

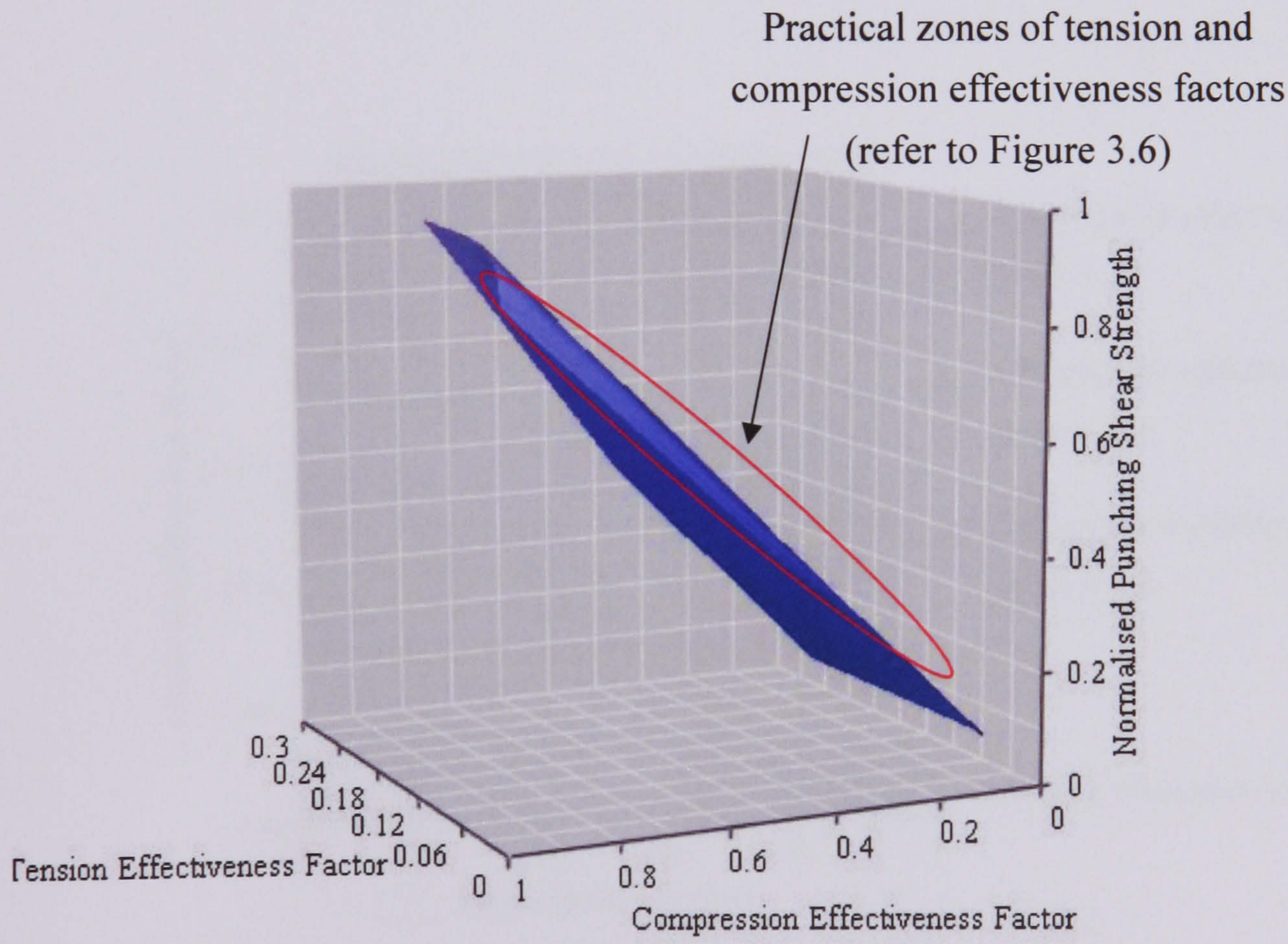

Figure 3.6 A sensitivity plot of Normalised Punching Shear Strength to Effectiveness Factors used in Plastic Analysis

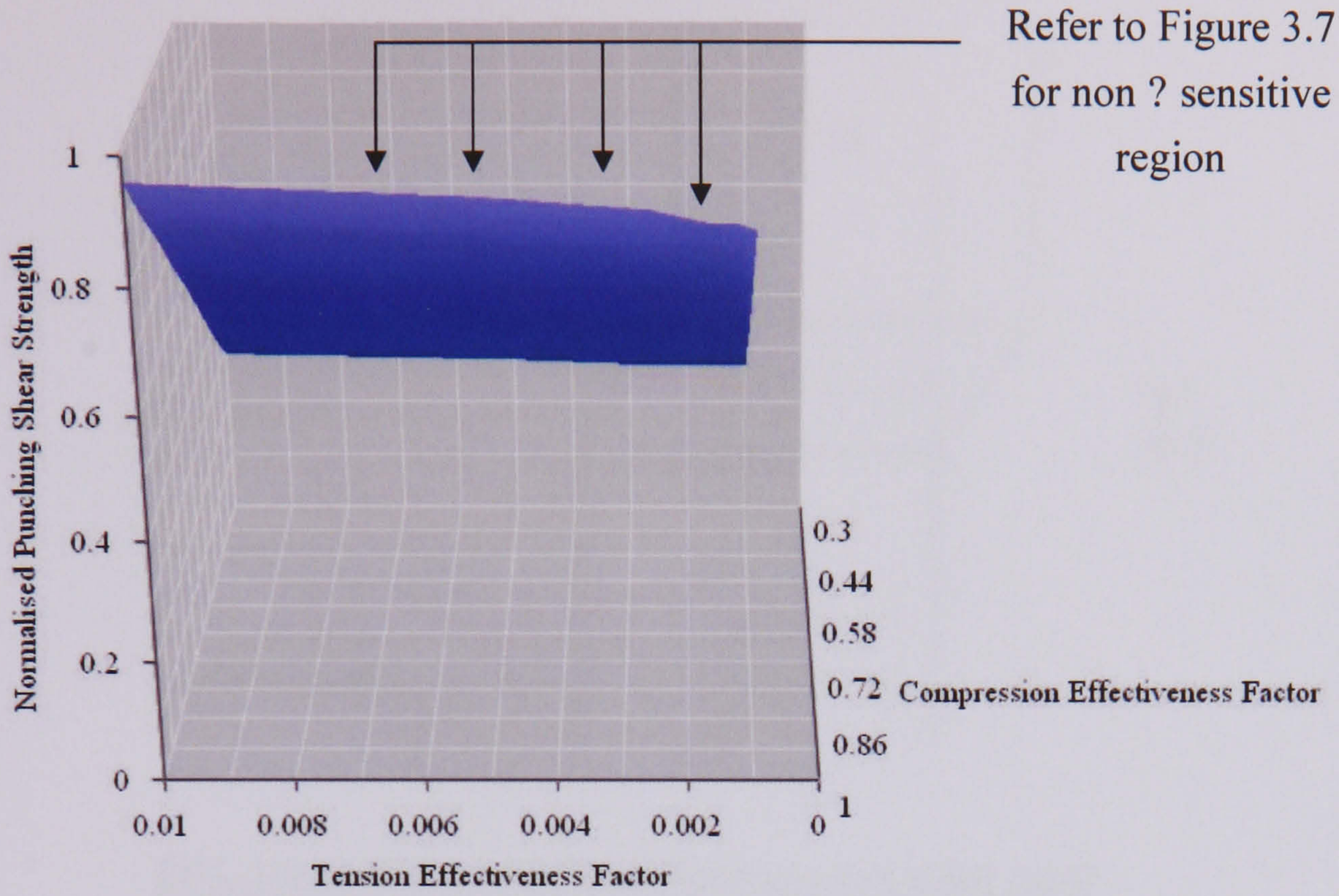

Figure 3.7 A Normalised Plot of sensitivity of Effectiveness factors within the practical ranges

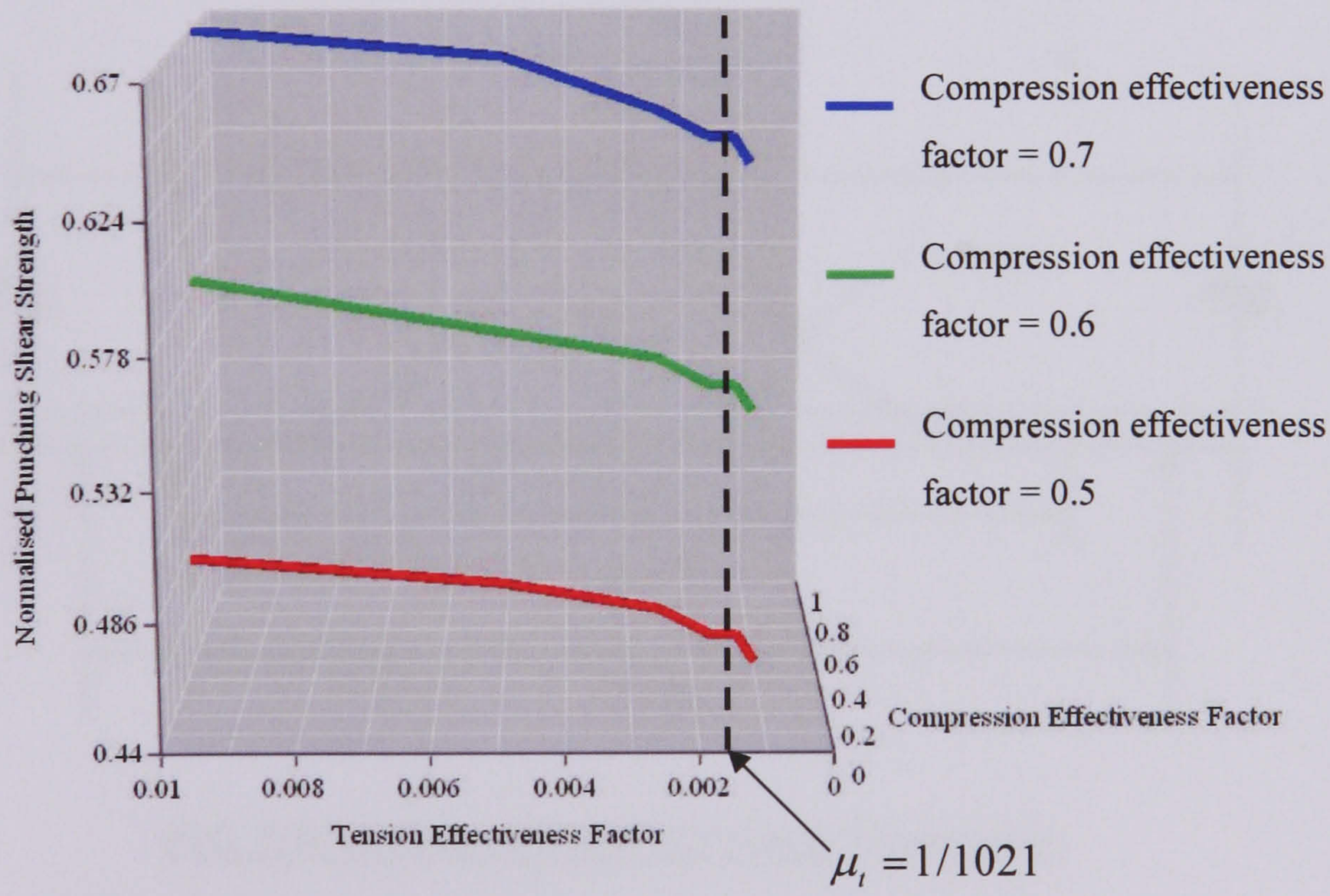

Figure 3.8 A Line Diagram demonstrating the normalised punching shear strength profile

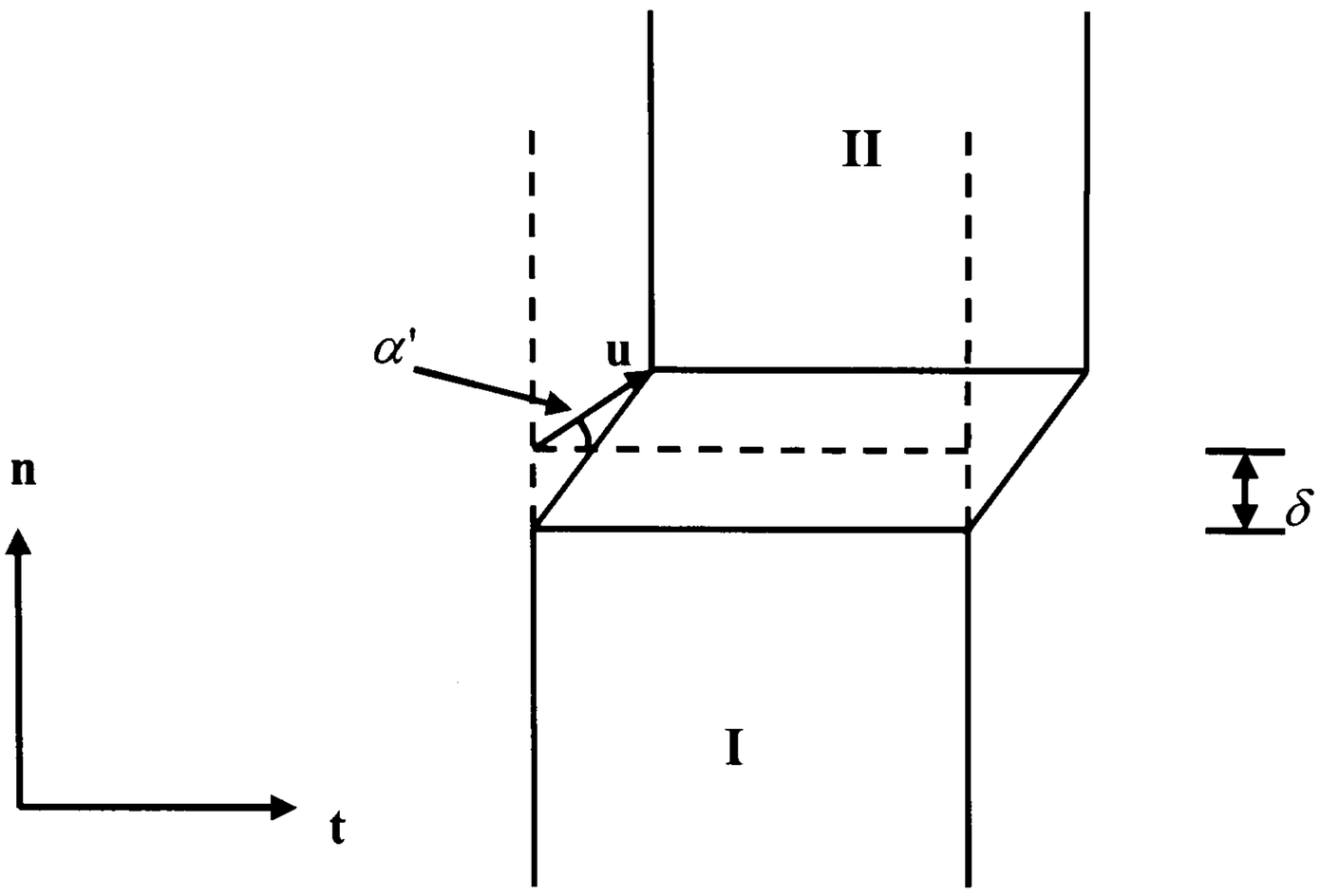

FIG. 3.9(a) Deforming zone between two rigid parts

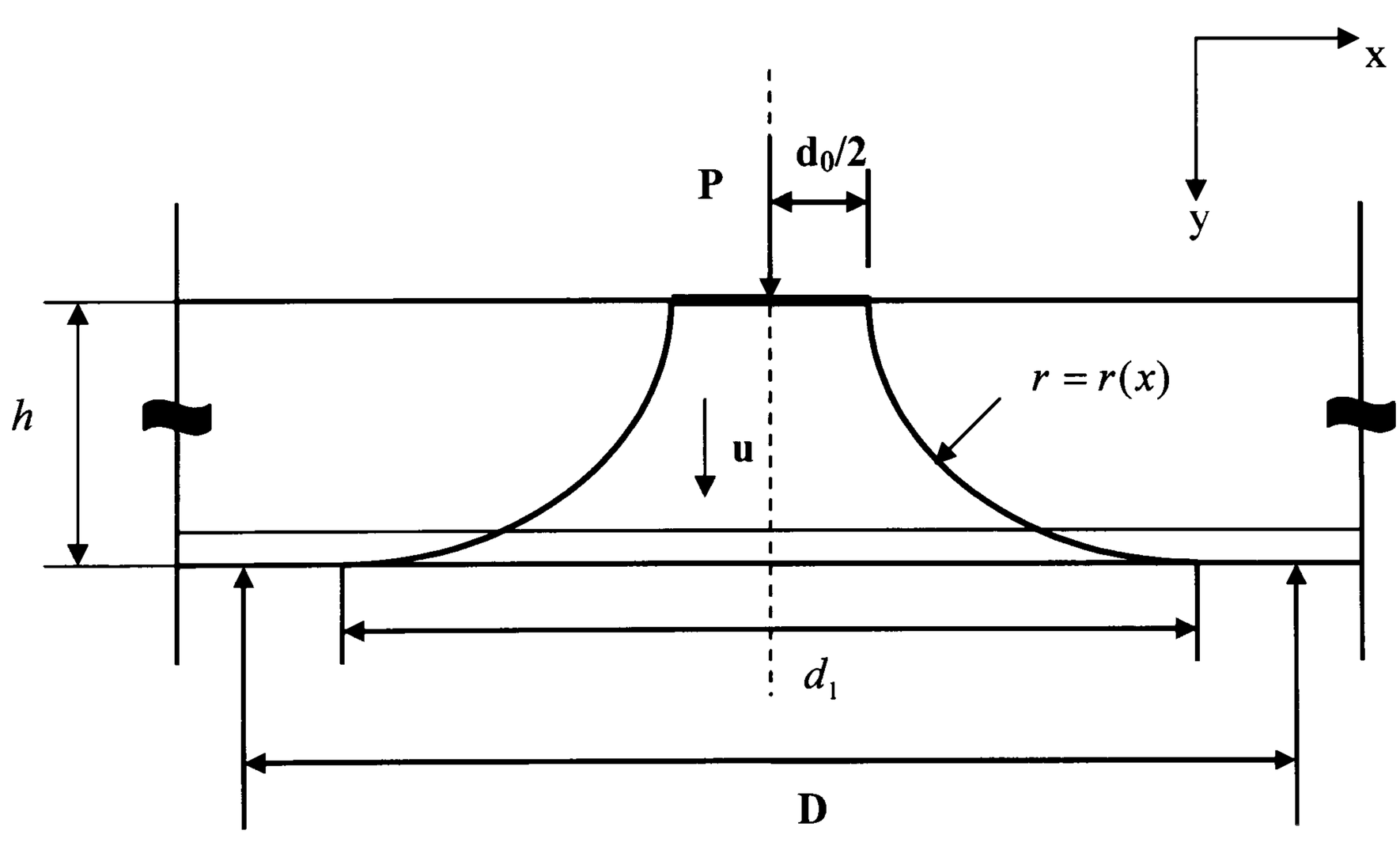

FIG. 3.9(b) General view of Failure Generatrix

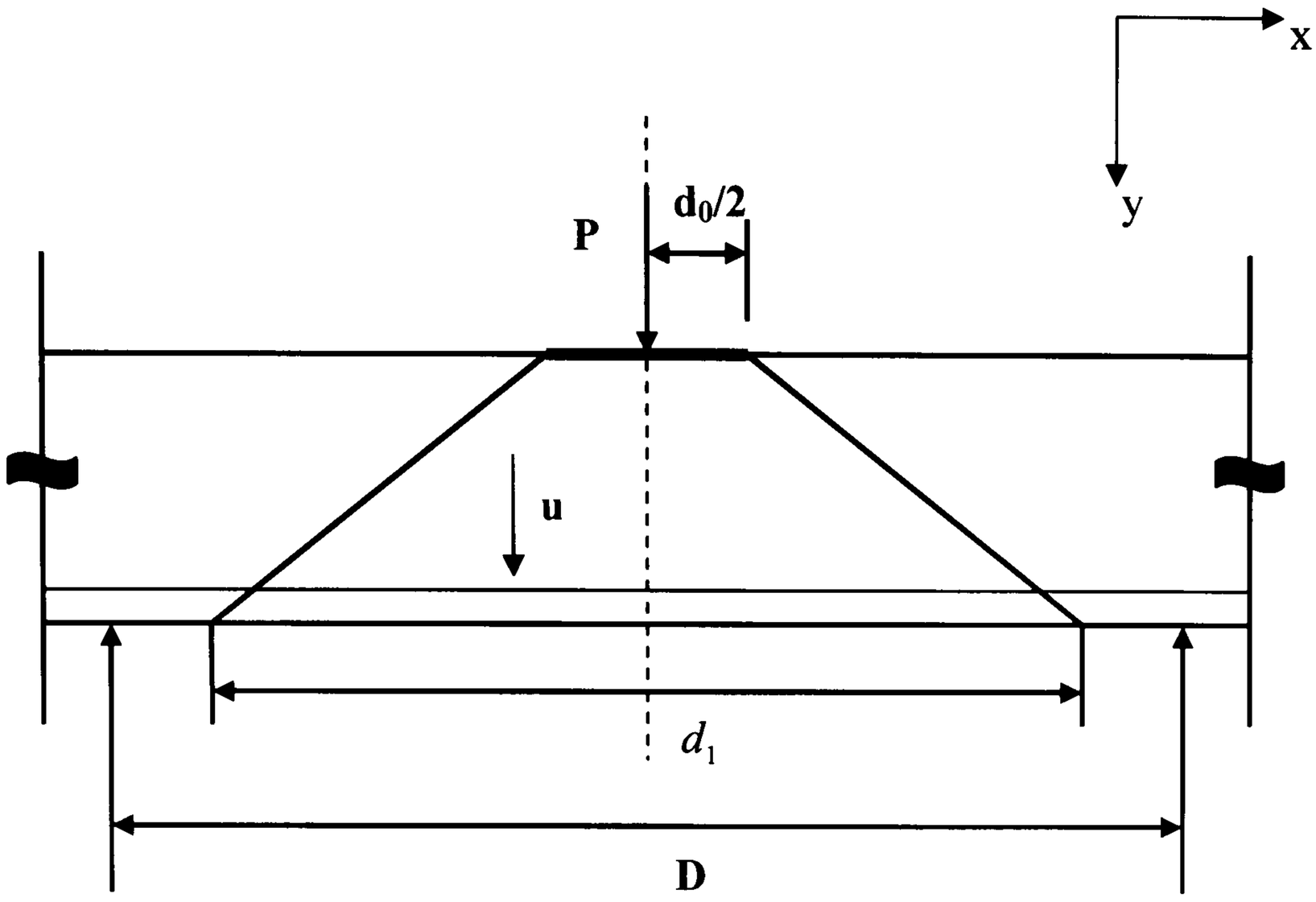

FIG. 3.10 Simplified Solution

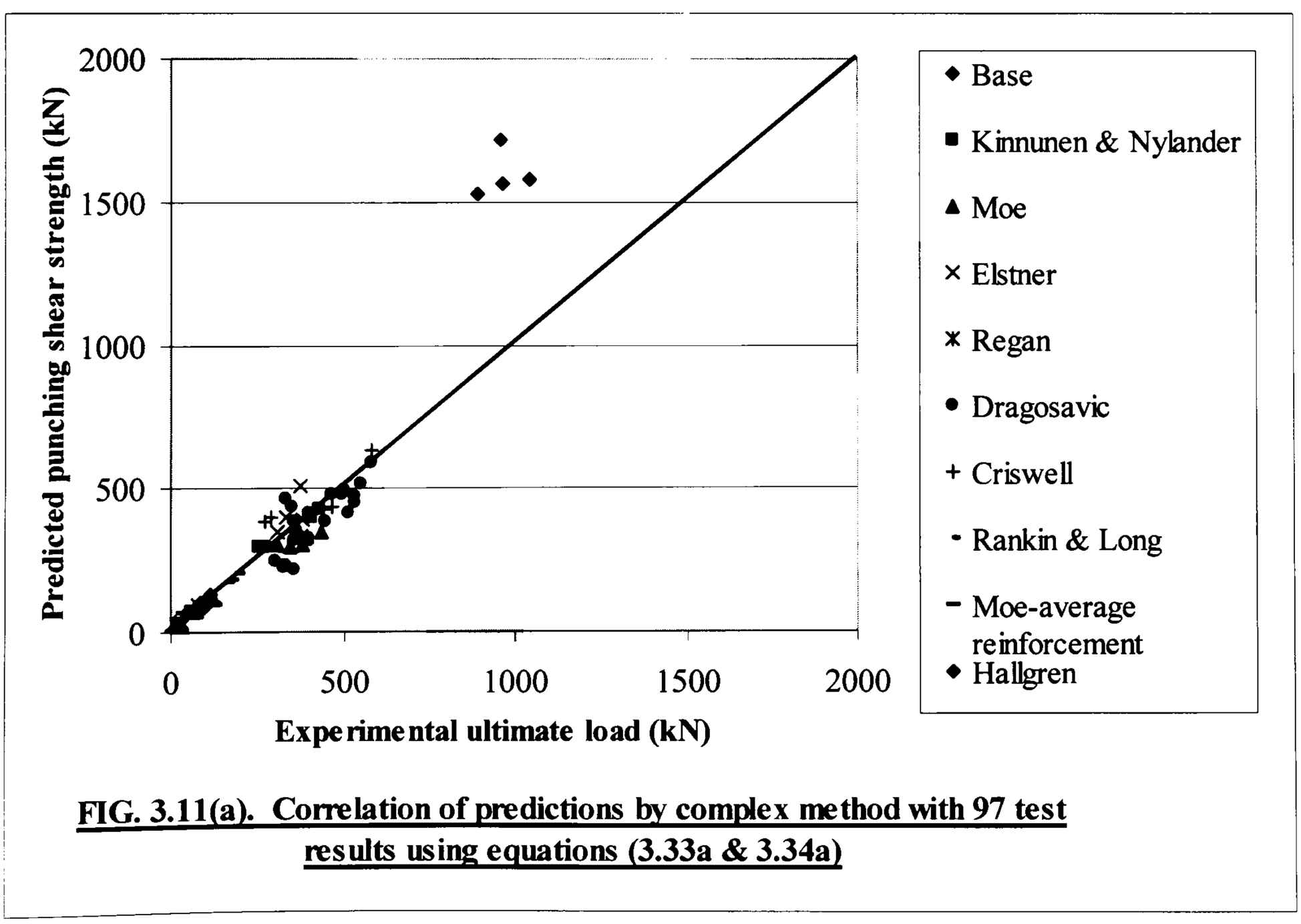

FIG. 3.11(a). Correlation of predictions by complex method with 97 test results using equations (3.33a & 3.34a)

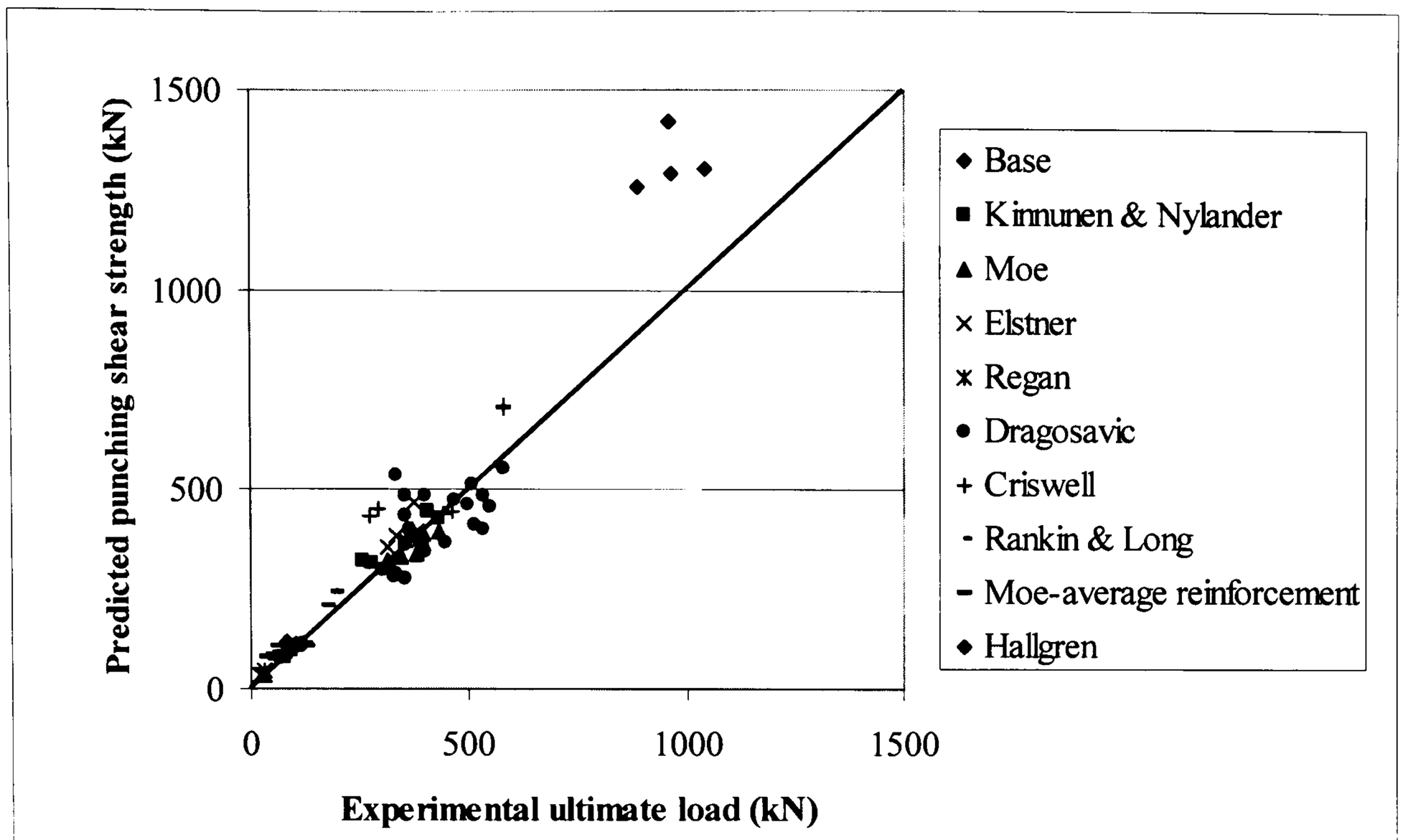

FIG. 3.11(b). Correlation of predictions by complex method with 97 test results using equations (3.33a & 3.34b)

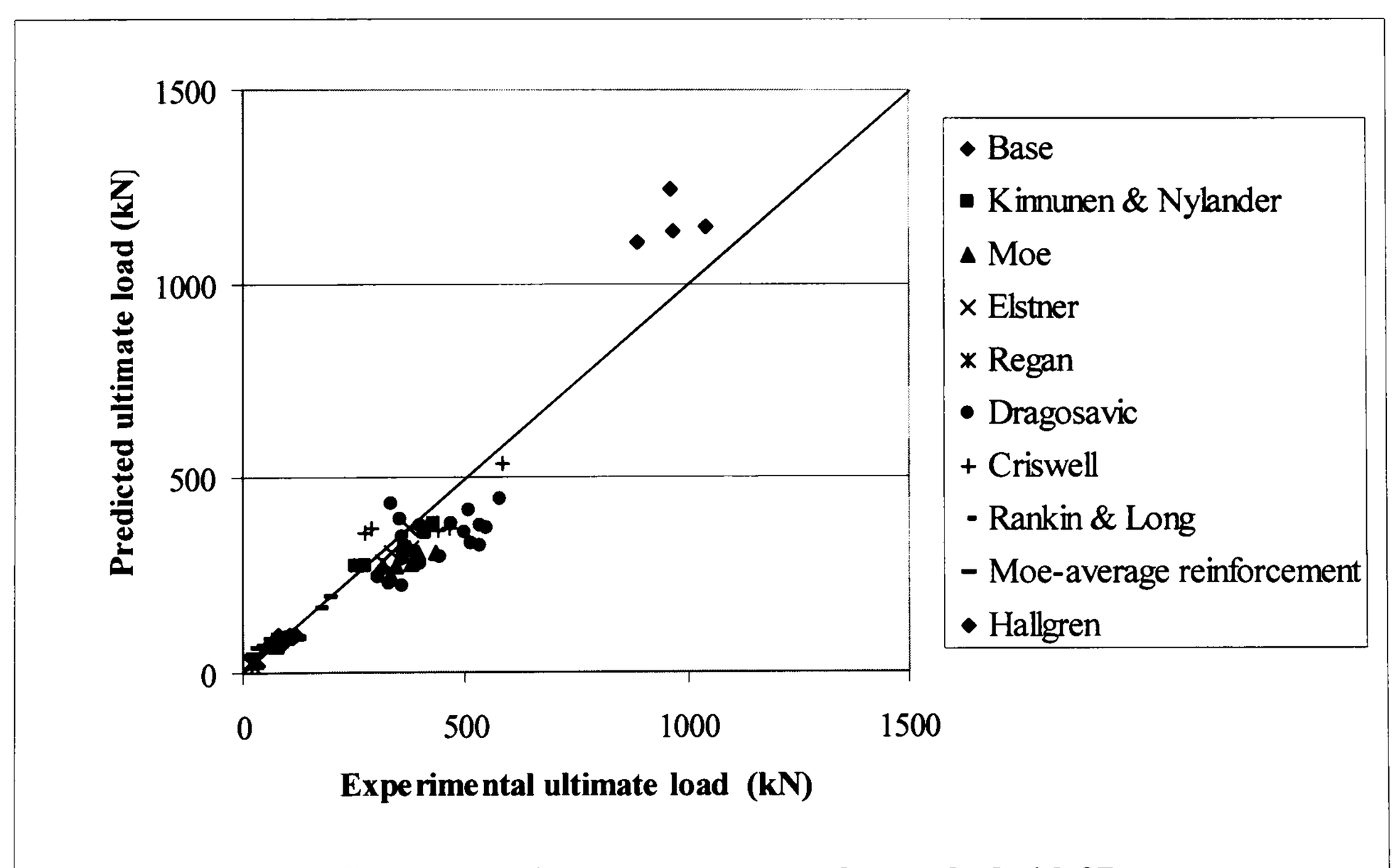

FIG. 3.11(c). Correlation of predictions by complex method with 97 test results using equations (3.33b & 3.34a)

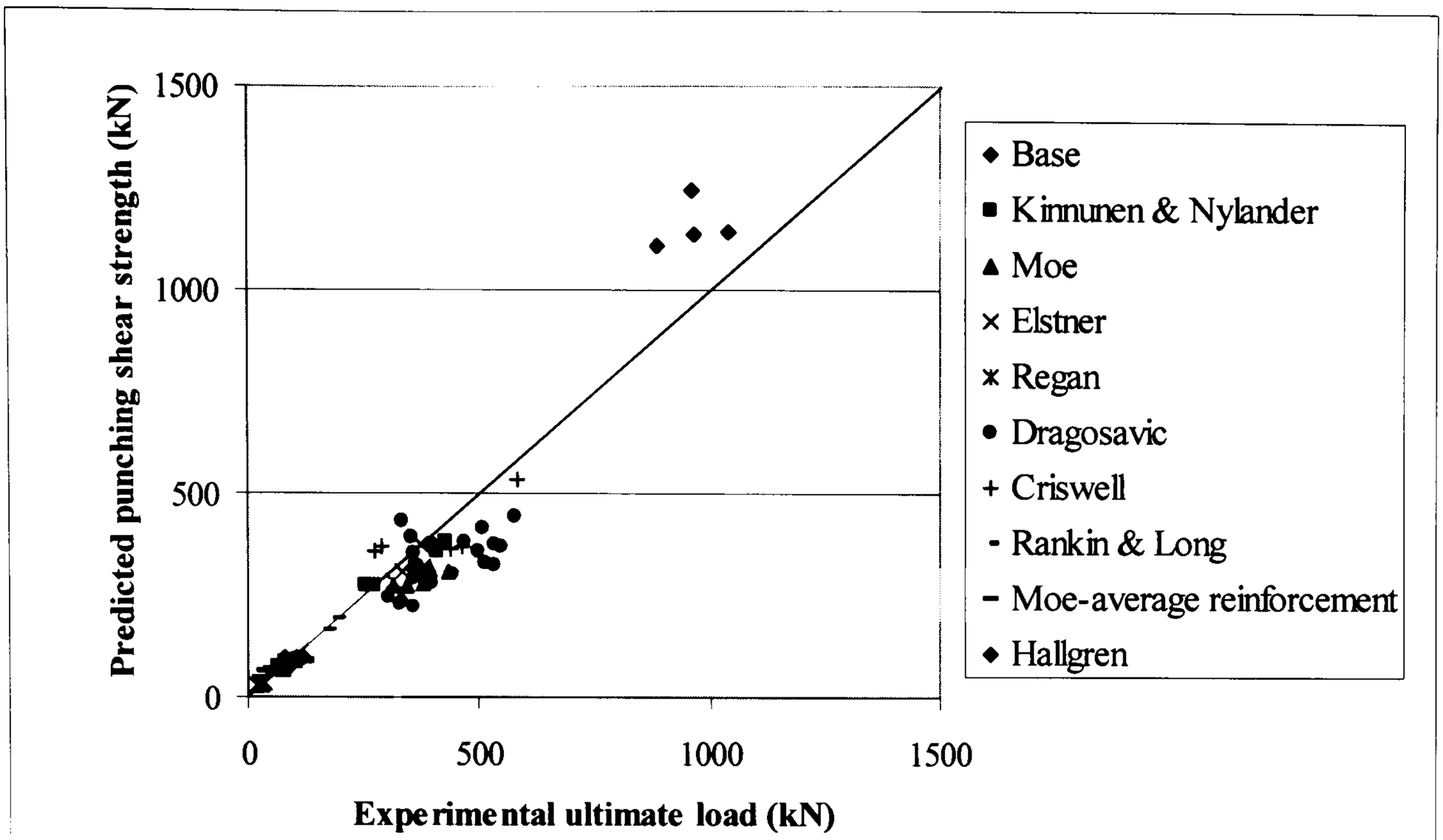

FIG. 3.11(d). Correlation of predictions by complex method with 97 test results using equations (3.33b & 3.34b)

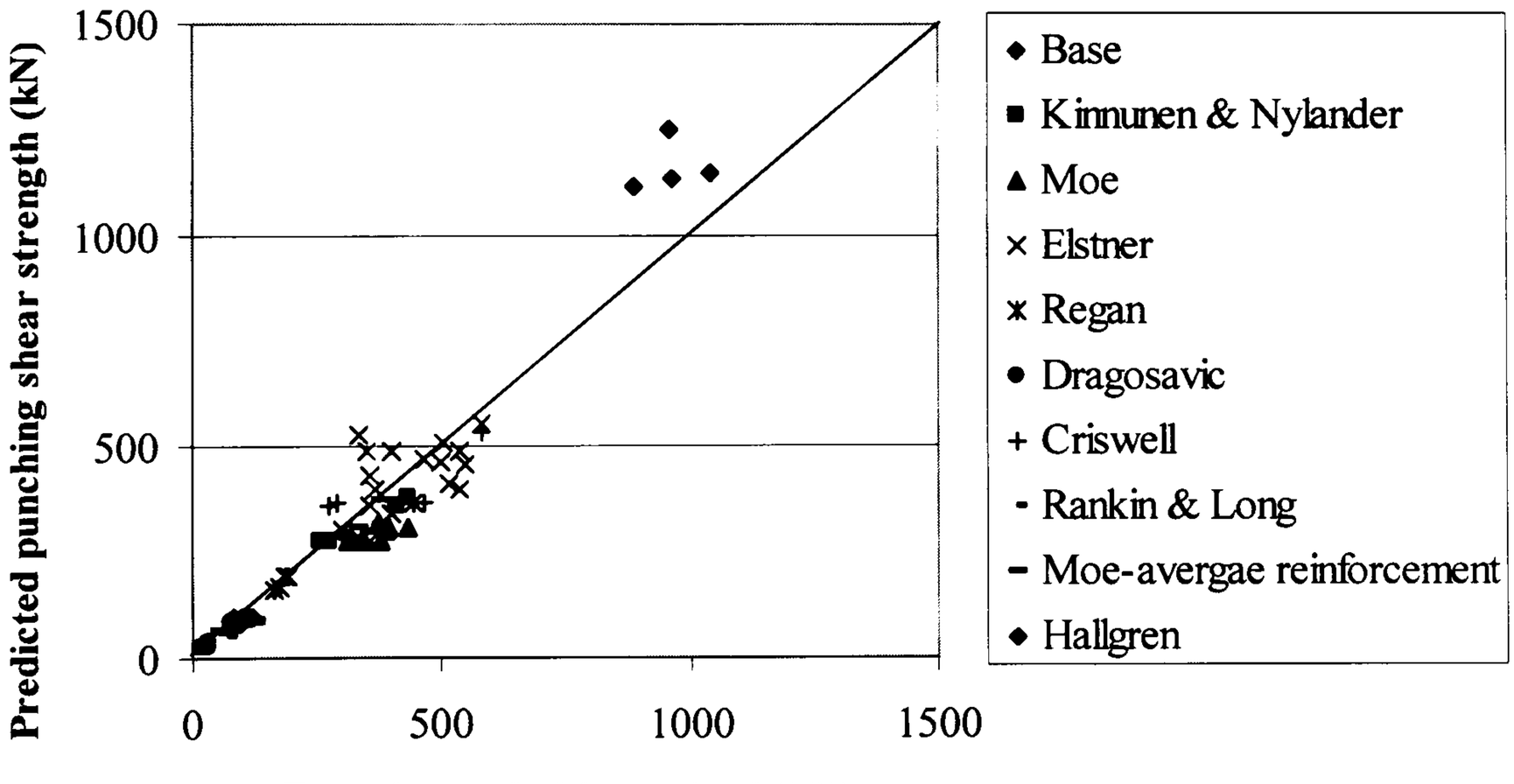

FIG. 3.12(a). Correlation of predictions by simplified method with 97 test results using equations (3.33a & 3.34a)

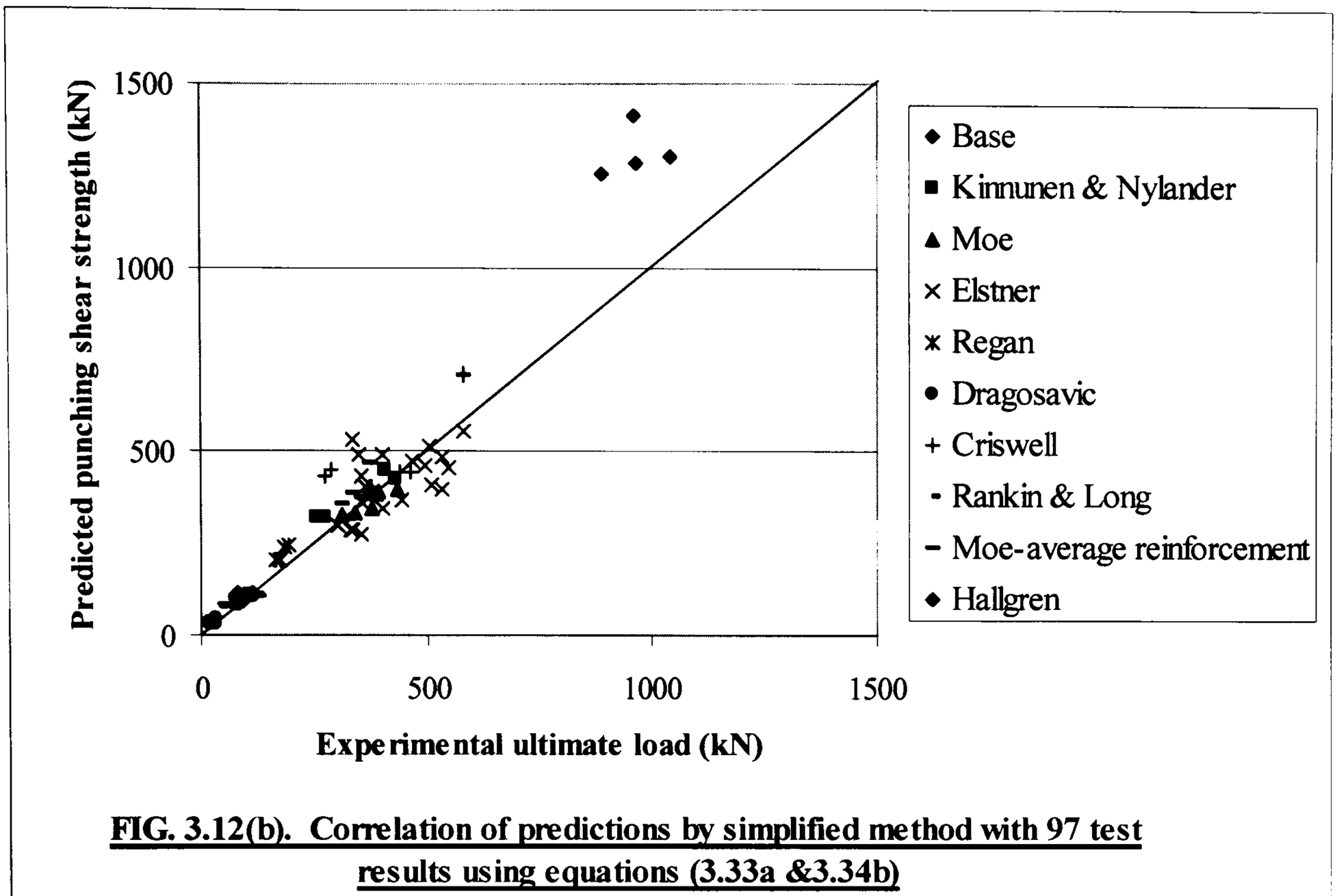

FIG. 3.12(b). Correlation of predictions by simplified method with 97 test results using equations (3.33a &3.34b)

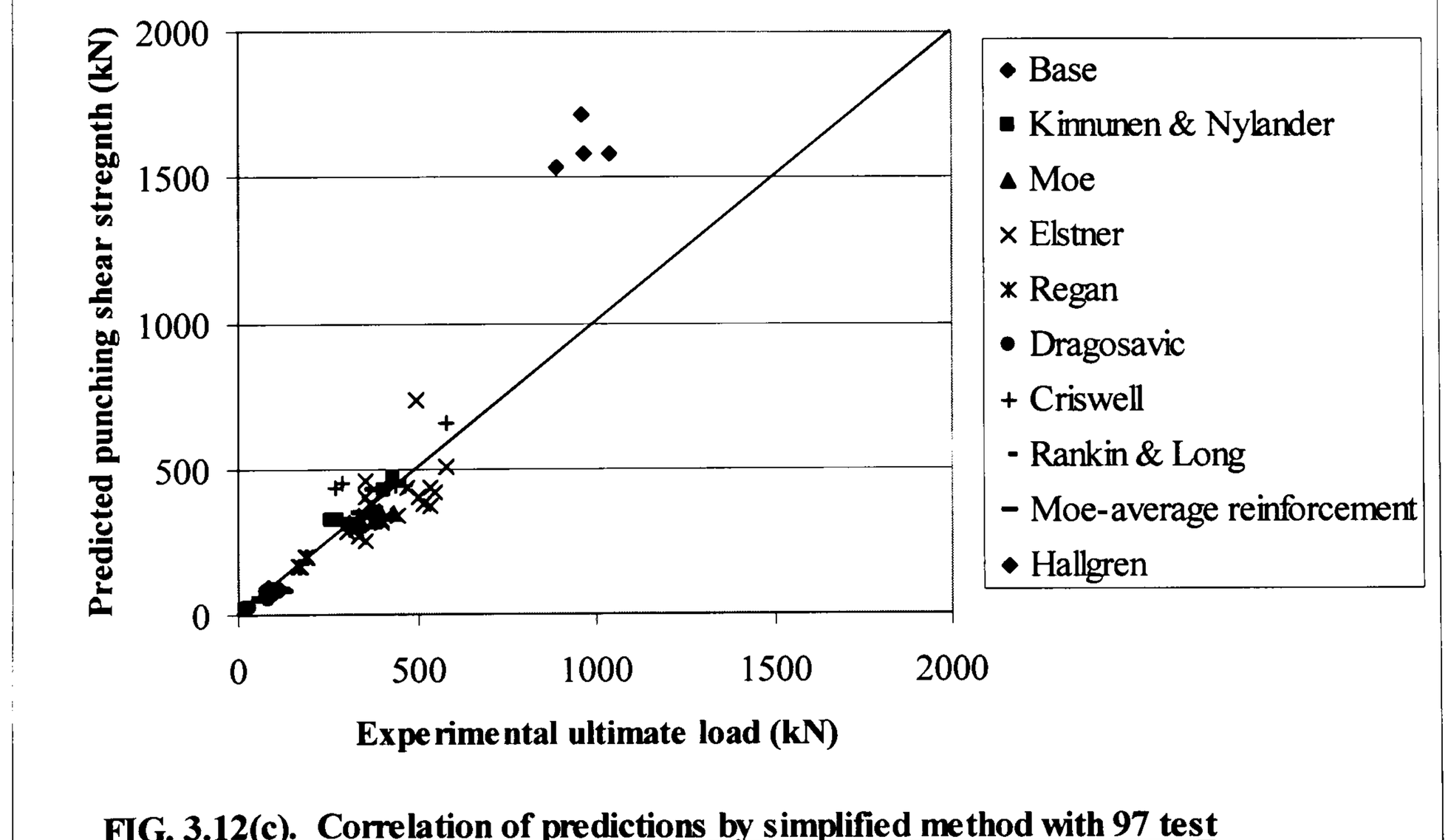

FIG. 3.12(c). Correlation of predictions by simplified method with 97 test results using equations (3.33b &3.34a)

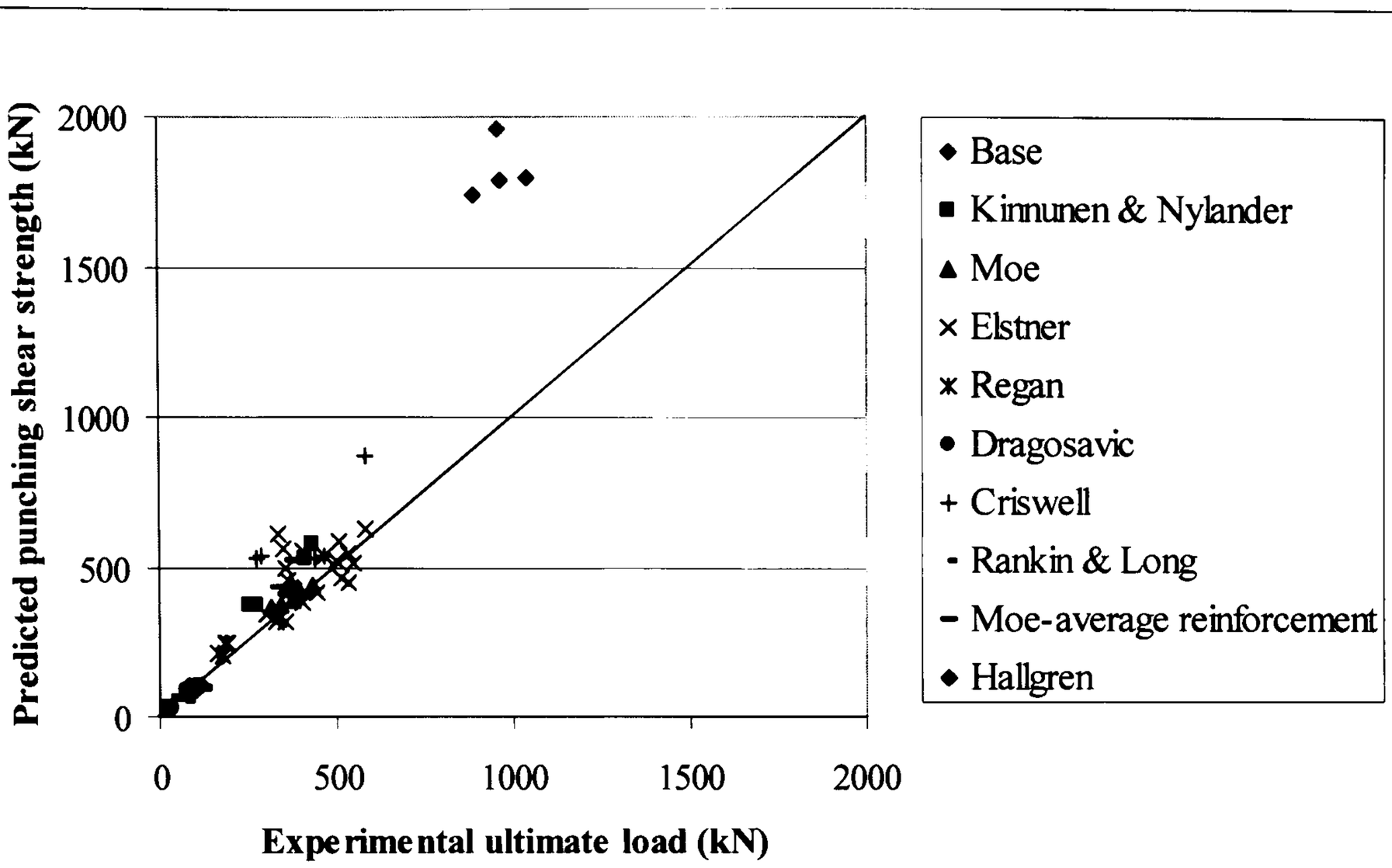

FIG. 3.12(d). Correlation of predictions by simplified method with 97 test results using equations (3.33b & 3.34b)

4

COMPRESSIVE MEMBRANE ACTION ENHANCEMENT TO PUNCHING SHEAR CAPACITIES OF RESTRAINED REINFORCED CONCRETE SLABS

4.1 Introduction

4.2 Parametric Study of the Surround Restraint Stiffness

4.2.1 Influence of Surround Material on Restraint Stiffness

4.2.2 Influence of Effective Young's Modulus of Concrete on Restraint Stiffness

4.2.3 Effect of Variation of Surround Restraint Stiffness on Punching Load

4.3 Arching Action in Restrained Slabs

4.3.1 Nature of Arching Action

4.3.2 Compressive Membrane Forces

4.4 Strength Enhancement due to Compressive Membrane Action

4.4.1 Failure Mechanism

4.4.2 Upper Bound Solution

4.5 Experimental Verification

4.5.1 Tests reported in the literature

4.5.2 Comparison with reported test results

4.6 Conclusions

Chapter Four

COMPRESSIVE MEMBRANE ACTION STRENGTH ENHANCEMENT TO PUNCHING SHEAR CAPACITIES OF RESTRAINED REINFORCED CONCRETE SLABS

4.1 INTRODUCTION

In Chapter 3, a plastic method for predicting the punching shear failure loads of reinforced concrete slabs with no membrane restraint was presented which gave good predictions against experimental results. In the present chapter, the membrane effect in centrally loaded circular slabs with lateral restraint is examined using the flow-theory approach of plasticity. A method of analysis is derived from the theory of plasticity presented in Chapter 3, for predicting the punching shear strength of restrained reinforced concrete slabs with compressive membrane action. In addition, the modified plastic analysis incorporating membrane effect is employed to provide punching shear predictions for some of the slabs considered in Chapter 3, and comparisons are made with predictions based on the plastic theory incorporating nominal effectiveness factors as presented in Chapter 3.

In the membrane-restraint analyses, quantification of the stiffness of the surround restraint is an important issue which requires detailed attention. In practice, the spatial variability in properties of the reinforced concrete surrounding the critical punch zone means that quantification of this restraint stiffness is not straightforward. For this reason, an in-depth mathematical analysis of the variation of surround stiffness with variation in radius of surround concrete material is conducted in this chapter. To that end, Lame axisymmetric analysis is applied to the circular-in-plan slab geometry. The use of an *effective* Young modulus for the surround material as a means of allowing for the co-existing cracked and uncracked surround concretes is explored. The sensitivity of predicted punch load to surround stiffness is also addressed. The following points summarise the objectives of this chapter:

- Illustration of the influence, on the surround restraint stiffness, of varying the amount of surround concrete material and steel hoop material.

- Investigation of the influence, on punching shear capacity, of variation in surround restraint stiffness.

- Investigation of incorporating the membrane effect into the plastic analysis presented earlier in Chapter 3.

- Investigation of the use of this plastic analysis incorporating membrane effect for prediction of punching capacities of the *nominally unrestrained* slabs presented in Chapter 3.

Since quantification of the surround stiffness is of fundamental importance to the ensuing analyses, this surround stiffness is addressed first, in the next section. In doing so, the application of Lame's axi-symmetric analysis to the problem is presented. The influence of this stiffness on punch capacity is then considered, using the analytical models developed later in this chapter. The detailed analyses are then developed and applied to punch load prediction of previously tested slab specimens reported in the literature. Finally, conclusions are drawn on the main findings of the chapter.

4.2 PARAMETRIC STUDY OF THE SURROUND RESTRAINT STIFFNESS

4.2.1 Influence of Surround Material

This section will investigate the effect, on surround restraint stiffness, of altering the amount of surrounding material, via Lame's axi-symmetric analysis. Two distinct cases are considered, namely: (a) the effect of the amount of surround *concrete* material, and (b) the effect of the number of *reinforcing steel hoops*, on the surrounding restraint stiffness. In what follows, σ_r, σ_θ and ε_θ are the radial stress, hoop stress and hoop strain all at a general radius r in the material surrounding the punch zone, E and υ are Young's modulus and Poisson's ratio both for concrete, while a and b are the internal and external radii of the surround zone.

(a) Varying the outer radius of the surrounding concrete material – refer to Fig. 4.1(a).

Considering Lame's equation [103],

$$\sigma_r = A + \frac{B}{r^2} \tag{4.1}$$

$$\sigma_\theta = A - \frac{B}{r^2} \tag{4.2}$$

with boundary conditions, $r = a, \sigma_r = -p$ & $r = b, \sigma_r = 0$ gives:

$$\sigma_r = \frac{pa^2}{\left(b^2 - a^2\right)}\left(1 - \frac{b}{r^2}\right) \tag{4.3}$$

$$\sigma_\theta = \frac{pa^2}{\left(b^2 - a^2\right)}\left(1 + \frac{b}{r^2}\right) \tag{4.4}$$

Also,

$$\varepsilon_{\theta_{r=a}} = \frac{u_{r=a}}{a} = \frac{1}{E}\left(\sigma_{\theta_{r=a}} - \upsilon \cdot \sigma_{r_{r=a}}\right) \tag{4.5}$$

$$\Rightarrow \frac{p}{u_{r=a}} = \frac{(b^2 - a^2) \cdot E}{\left[a^2(1-\upsilon) + b^2(1+\upsilon)\right] \cdot a}$$

$$\Rightarrow S_s = \frac{p}{u_{r=a}} = \frac{E \cdot \left(\phi^2 - 1\right)}{\left(0.8 + 1.2\phi^2\right) \cdot a} \tag{4.6}$$

where:

S is the surround restraint stiffness,

$\phi = \frac{b}{a}$ (a non-dimensional parameter which can be varied) (4.7)

and for concrete $\upsilon = 0.2$ (4.8)

(b) Varying the number of steel hoops – refer to Fig. 4.1(b)

Surround restraint due to hoops (thin-walled cylinder theory) and assuming that the effect due to hoops is smeared uniformly through the thickness of the slab, the equilibrium equation of forces suggests:

$$p \cdot 2R \cdot h = \sigma_h \cdot 2 \cdot A_s \cdot n_{hoop} \tag{4.9}$$

Remembering that $\sigma_h = E_s \cdot \varepsilon_h$ and $\varepsilon_h = \frac{u}{R}$,

$$\frac{p}{u} = \frac{E_s \cdot \pi d^2{}_h \cdot n_{hoop}}{4R^2 \cdot h} \tag{4.10}$$

The above analysis assumes the *elastic* stiffness for the steel hoops. In fact, the hoops may well have gone past first yield when punching failure occurs. However, the test results given in Chapter 6 show that for the examples considered in this study, this excursion of the hoop steel into the plastic regime is not pronounced. In the worst case, it led to a plastic secant modulus only 14% below the elastic modulus. Hence, in the present analysis, the original elastic modulus is assumed to apply to the hoop steel.

Addition of (4.6) & (4.10), leads to the following expression for total surround restraint:

$$S_{total} = \frac{(\phi^2 - 1) \cdot E_c}{(0.8 + 1.2\phi^2)a} + \frac{E_s \cdot \pi d_h{}^2 \cdot n_{hoop}}{4R^2 \cdot h} \tag{4.11}$$

A plot of surround restraint stiffness (S_s) provided by the surrounding concrete material against ϕ is shown in Fig. 4.2(a). Three distinct regimes of behaviour may be identified as follows: (1) Regime A showing a *rapid* and virtually *linear* increase in surround stiffness with increasing ratio of surrounding material to punch radius, (2) Regime B showing a *decrease in tangent stiffness* with increasing ratio of surrounding material to punch radius, and (3) Regime C defined by *levelling-off* of the surround restraint despite an increase in ratio of surrounding material to punch radius. The plot shows that *restraint stiffness increases rapidly when there is little surround material.* This may well lead to significant increase in punch load with little surround material present. Hence, even in cases where the surround restraint is normally considered to be negligible, this restraint may actually provide desirable benefit and so probably should not be ignored. This idea forms the basis of the motivation to apply the membrane-restraint theory developed in this chapter to the test situations analysed in Chapter 3 – where surround material is minimal and so membrane effects are usually neglected.

The other plot of surround restraint stiffness against varying numbers of steel hoop reinforcement, Fig. 4.2(b), indicates a linear increase in the restraint stiffness as the number of hoops increases. However, in practice, there is a limit to the number of hoops which can be physically installed, hence, a maximum number of hoops exists for each specimen considered.

In the above cases where variations in 2 different surrounding materials were considered to investigate the influence of surround restraint, it is necessary to illustrate the influence of surround restraint on punching shear capacities. In particular, there is a need to investigate the presence of a threshold value of surround stiffness beyond

which negligible enhancements in punching capacities may be anticipated. This important issue is addressed below in Section 4.2.3 of this chapter and also will form the basis of Chapter 6 through a carefully designed experimental programme incorporating the above important considerations.

4.2.2 Influence of the *Effective* Young's Modulus of the Surround Concrete

In the previous section, *uniform smearing* of the Young modulus of the surround concrete through the depth of the slab has been tacitly assumed in the derivation of surround restraint stiffness. In actual fact, through the thickness of the surround slab, the concrete is cracked on the tension side and not so on the compression side. Hence, the smeared Young modulus used is an *average*, the value of which clearly depends on the relative quantities of cracked and compression concrete through the thickness of the surround slab. It is also influenced by the extent of cracking, as that will influence tension stiffening levels in the cracked surround concrete. Clearly, there is strong potential for variation in the magnitude of this smeared Young modulus used for the concrete in the present approach. Therefore, it is worth establishing the effect on the surround stiffness of variation of the effective Young modulus of the concrete to represent different ratios of cracked surround concrete to compression surround concrete.

Consider a circular slab with diameter of 1100mm and $E_c = 31kN/mm^2$. This is done by considering Equation (4.6) and Equation (4.10), which generates the plots of surround restraint stiffness (S_s) against ratio of surrounding material to punch radius

shown in Fig. 4.3(a) and 4.3(b) respectively. Figure 4.3(a) shows that variation in effective Young modulus of concrete has a significant effect on surround restraint, with as much as 40% increase in restraint stiffness when the outer radius of the surround material is twice the punch radius and the effective Young modulus increases by 66% (from $0.6E_c$ to E_c in Fig. 4.3(a)).

It is important to note that the above analysis deals with concrete only. In addition, the contribution from steel hoops was dealt with earlier in section 4.2.1(b). Hence, the total surround restraint stiffness is the combined effect of surround concrete and steel hoops. Therefore, it would be instructive to establish an understanding of this variation in effective Young modulus of concrete when considering the total surround restraint which leads to the generation of Fig. 4.3(b). From the figure, the influence of this variation results in as much as 39% difference in the value of total surround restraint stiffness which suggests that the effective Young modulus of concrete does make a significant influence to the overall stiffness as it does on the surrounding concrete alone.

4.2.3 Effect of Variation of Surround Restraint Stiffness on Punching Load

Having established a better understanding of the influence of surround material and variation of effective Young modulus of the concrete on surround stiffness, it is now appropriate to investigate the effect of variation in this stiffness on the punching loads. The theory incorporating the restraint contribution is given later in this chapter. Considering a typical specimen with $f_{cu} = 56MPa$, $d = 113mm$, $\rho = 1.06\%$, by varying the ratio of (b/a) together with the addition of steel hoops reinforcement, Fig.

4.4 shows a plot of non-dimensional punching strength against variation of total surround stiffness due to the effect of hoop reinforcement and surrounding concrete material. The plot eventually demonstrates a levelling off effect of the non-dimensional strength despite an increase in total surround stiffness, suggesting that there may well be a limit (in this case corresponds to 3 hoops) beyond which little or no further enhancements on punching capacities are obtained. Clearly, an experimental verification would be useful in justifying the above findings which stimulates a detailed experimental investigation in Chapter 6.

4.3 ARCHNG ACTION IN RESTRAINED SLABS

4.3.1 Nature of Arching Action

The phenomenon of arching action in reinforced concrete occurs as a result of the great difference between the compressive and tensile strengths of the material. Application of a load causes cracking of the concrete, which leads to a migration of the neutral axis and accompanied by an increase in rotational and lateral deformations. If this lateral movement is restrained, it will significantly enhance the load-carrying capacity of a member by generating an internal arching mechanism. This transfers the loading to the supports by direct compression. An illustration of this type of behaviour has been shown in Figure 2.10.

The term rching action? is widely recognised among researchers of reinforced concrete slabs as it depicts the structural behaviour of a laterally restrained slab (Fig. 4.5) as that of a three-hinged arch as shown in Fig. 4.6. The non-linear load-deflection response of such an arch occurs as a result in the change of geometry of the system.

This point is illustrated in Fig. 4.7. The load carried by the arch at any level of deformation is proportional to the product of the lateral thrust and the lever arm. Up to a certain critical deflection, any load increment is accompanied by a reduction of the internal lever arm. This reduction, however, is offset by greater horizontal reactions and hence stable equilibrium is possible. Beyond an approximate deflection of 0.4 times the thickness of the slab, the system becomes unstable and a sudden collapse will occur.

This sudden collapse behaviour of a laterally restrained slab resembles the 'snap-through' failure of a three-hinged arch, which theoretically occurs at a critical deflection of 42.3% of the arching height (Fig. 4.7).

4.3.2 Compressive Membrane Forces

Consider a clamped circular slab of depth h and radius a, subjected to a concentrated load P at the centre. The restrained slab is treated by the flow theory, lumping the support and in-plane stiffness into a single boundary spring (Fig. 4.8) and assuming membrane action to start at an initial elastic deflection. A conical failure mechanism is assumed, with a central deflection of w_0, as shown in Fig. 4.9. Deformations of the radial segment of the slab are shown in Fig. 4.10. The rotation and middle surface extension are θ and Δ, respectively. The geometrical condition of compatibility can be written as:

$$(a - \Delta_a - \Delta_b + e)^2 + {w_0}^2 = a^2 \tag{4.12}$$

in which subscripts a and b representing the positions at support and mid-span respectively, while e represents the radial displacement, defined by $e = -N/S$, where N is the membrane force and S the restraining stiffness. Using theory consistent with that presented in Section 4.2.1 of this Chapter, an expression of S may be determined as follows:

$$\frac{1}{S} = \frac{aR}{0.8E_c A_b + E_s A_{sb}} + \frac{a}{0.5E_c(x+h)} \tag{4.13}$$

where R is the radius of the edge beam, $x = 1.76d\rho(f_y / f_{cu})$ and E_c and E_s are the elastic moduli of concrete and steel respectively. It is suggested by Hognested [42] that an appropriate value of the elastic modulus of a concrete member subjected to bending and axial load can be obtained from:

$$E_c = 4730\sqrt{f'_c} \cdots (N/mm^2) \tag{4.14}$$

where f'_c is the cylinder strength of concrete.

By differentiating Eqn. (4.12) for small Δ with respect to time, the corresponding kinematical condition is:

$$\dot{\Delta}_a + \dot{\Delta}_b - \dot{e} = \frac{w_0}{a}\dot{w}_0 \tag{4.15}$$

A dot over a variable denotes differentiation with respect to time.

By introducing the dimensionless distance from the middle surface to the axis of rotation (Fig. 4.11a)

$$\eta = \frac{\dot{\Delta}}{h\dot{\theta}} \tag{4.16}$$

and the dimensionless membrane force in mid-depth of the slab (Fig. 4.11b):

$$n = \frac{N}{hf_c} \tag{4.17}$$

Eqn. (4.15) can then be rewritten as:

$$-\eta_a + \eta_b + 2h\phi \frac{dn_a}{dw_0} = \frac{w_0}{h} \tag{4.18}$$

where the value of η is positive when the geometrical neutral axis is above the middle surface and negative when it is below; ϕ is a flexibility factor, defined by:

$$\phi = \frac{af_c}{2hS} \tag{4.19}$$

By using the flow rule and considering the horizontal equilibrium of the slab as well as the kinematical condition [Eqn. (4.18)], the following solutions for the radial membrane forces can be derived:

$$n_a = k\exp\left(\frac{-w_0}{h\phi}\right) - \frac{1}{2}\left(n_0 + \frac{1}{2} + \frac{1}{2}\phi\right) + \frac{1}{4}\left(\frac{w_0}{h}\right) \tag{4.20a}$$

$$n_r = n_a + \frac{w_0}{2h}\left(1 - \frac{r}{a}\right) \tag{4.20b}$$

in which the value of constant k is determined by imposing the condition that $n_a = 0$ for $w_0 = w_i$:

$$k = \left(\frac{1}{2}n_0 + \frac{1}{4} + \frac{1}{4}\phi - \frac{1}{4}\frac{w_i}{h}\right)\exp\left(\frac{w_i}{h\phi}\right) \tag{4.21}$$

where w_i is an initial elastic deflection at which membrane action starts, taken as $0.03h$ empirically [14,67]. If N_0 represents the compressive membrane force corresponding to rotation about mid-depth of the slab (Fig. 4.11b), then:

$$N_0 = \frac{1}{2}hf_c - A_{sh}f_y \tag{4.22}$$

where A_{sh} is the sectional area of steel reinforcement per unit length and the value of n_0 in Eqns. (4.20) and (4.21) is determined from Eqn. (4.17) with $N = N_0$. When there is no flexural reinforcement in the slab, $N_0 = 0.5hf_c$ with $n_0 = 0.5$.

The dimensionless compressive membrane force at the support of the slab can then be determined by Eqn. (4.20a). A plot of compressive membrane force (n_a) against central deflection $\left(\frac{w_0}{h}\right)$ for different flexibility factors (ϕ) is shown in Fig. 4.12.

4.4 COMPRESSIVE MEMBRANE ACTION STRENGTH ENHANCEMENT

4.4.1 Failure Mechanism

Consider a laterally restrained, centrally loaded circular slab in which the failure mechanism of the slab is illustrated by Fig. 4.13, where n_a and n_r represent the membrane restraining forces acting at boundary and on the failure surface respectively.

In this treatment of the collapse of the slab, only translation and no rotation is allowed for the supports.

It is assumed that the failure mechanism consists of the punching out of an axisymmetric, solid cone-like plug at the centre. The generatrix of the failure surface is defined by a function $r = r(x)$, and the relative velocity u is inclined at an angle β to the vertical, as indicated in Fig. 4.14.

For rigidly restrained slabs, it is recognized [67,76,101] that the influence of the level of steel reinforcement on the ultimate capacity is small, which was also confirmed by the results of model tests presented in Ref. [56]. The contribution of flexural reinforcement in the slab is thus neglected in the derivation.

4.4.2 Upper-Bound Plastic Solution

For the assumed failure mechanism, the rate of external work done by the ultimate load associated with the relative displacement is:

$$W_E = Pu\cos\beta \tag{4.23}$$

and the rate of internal work dissipated by the mechanism is:

$$W_A = \int_0^h D_A 2\pi r\sqrt{1+r'^2}\,dx + N_{rs}u\sin\beta \tag{4.24}$$

where N_{rs} is the sum of radial compressive membrane forces acting on the failure surface, which is determined by:

$$N_{rs} = f_c \int_0^h n_r \, 2\pi r dx \tag{4.25}$$

Substituting n_r from Eqn. (4.20b) into Eqn. (4.25) gives:

$$N_{rs} = 2\pi f_c \int_0^h \left[n_a + \frac{1}{2}\frac{w_0}{h}\left(1 - \frac{r}{a}\right) \right] r dx \tag{4.26}$$

and:

$$r' = \tan(\alpha - \beta) \tag{4.27}$$

Therefore it leads to the work equation:

$$Pu\cos\beta = \int_0^h D_A \, 2\pi r \sqrt{1 + r'^2}\, dx + N_{rs} u \sin\beta \tag{4.28}$$

The upper-bound solution for the punching-shear failure load is obtained by substituting D_A and r' from Eqns. (3.41) and (4.27) respectively into Eqn. (4.28):

$$P = 2\pi f_t \int_0^h r\left(r' + \tan\beta\right)\left[1 + \frac{c_k{}^2}{4}\left(\frac{1 - r'\tan\beta}{r' + \tan\beta} \right)^2 \right] dx + N_{rs}\tan\beta \tag{4.29}$$

or is expressed as:

$$P = 2\pi f_t \int_0^h F(r, r')dx + N_{rs}\tan\beta \tag{4.30}$$

where:

$$F(r, r') = r\left[r' + \tan\beta + \frac{c_k{}^2}{4}\frac{\left(1 - r'\tan\beta\right)^2}{r' + \tan\beta} \right] \tag{4.31}$$

The function $r(x)$ which minimizes the ultimate punching load can be found by calculus of variations. The appropriate Euler equation, which is for a function of the form $\int^{h} F(r,r')dx$, in minimizing $r = r(x)$, the function can be written as:

$$\frac{\partial F}{\partial r} - \frac{d}{dx}\left(\frac{\partial F}{\partial r'}\right) = 0 \tag{4.32}$$

Since $F(r,r')$ does not contain x, Euler equation has the first integral:

$$F - r'\frac{\partial F}{\partial r'} = C \tag{4.33}$$

where C is a constant.

Assuming that the value of β is given, by substituting Eqn. (4.31) into Euler equation with consideration of the boundary conditions:

$$r(0) = \frac{d_0}{2} \quad \text{and} \quad r(h) = \frac{d_1}{2} \tag{4.34}$$

and ignoring the higher order terms gives the minimizing function of the generatrix:

$$r = Ae^{Bx} + \frac{\tan\beta}{B} \tag{4.35}$$

where constants A and B can be determined numerically by the following equations:

$$\frac{d_0}{2} = A + \frac{\tan\beta}{B} \tag{4.36a}$$

$$\frac{d_1}{2} = \left(\frac{d_0}{2} - \frac{\tan\beta}{B}\right)e^{Bh} + \frac{\tan\beta}{B} \tag{4.36b}$$

Once the minimizing function of the generatrix has been found, the least upper bound solution for the punching load can then be obtained from Eqn. (4.29):

$$P = 2\pi f_t\left[\frac{A^2}{2}\left(e^{2Bh}-1\right)+\frac{2A}{B}\left(e^{Bh}-1\right)\tan\beta+\frac{h}{B}\tan^2\beta\right]$$
$$+\pi f_t\frac{c_k^{\,2}}{2}\left[\frac{h}{B}-\frac{2A}{B}\left(e^{Bh}-1\right)\tan\beta+\frac{A^2}{2}\left(e^{2Bh}-1\right)\tan^2\beta\right] \qquad (4.37)$$
$$+N_{rs}\tan\beta$$

where the sum of the radial compressive membrane forces acting on the failure surface can be obtained by substituting Eqn. (4.35) into Eqn. (4.26):

$$N_{rs} = 2\pi f_c\left(n_a+\frac{w_0}{2h}\right)\left[\frac{A}{B}\left(e^{Bh}-1\right)+\frac{h}{B}\tan\beta\right]$$
$$-\pi f_c\frac{w_0}{ah}\left[\frac{A^2}{2B}\left(e^{2Bh}-1\right)+\frac{2A}{B^2}\left(e^{Bh}-1\right)\tan\beta+\frac{h}{B^2}\tan^2\beta\right] \qquad (4.38)$$

Consideration of $\frac{\partial P}{\partial\beta}=0$ gives the following equation:

$$2\pi f_t\left[\frac{2A}{B}\left(e^{Bh}-1\right)+\frac{2h}{B}\tan\beta\right]+\pi f_t\frac{c_k^{\,2}}{2}\left[-\frac{2A}{B}\left(e^{Bh}-1\right)+A^2\left(e^{2Bh}-1\right)\tan\beta\right]$$
$$+2\pi f_c\left(n_a+\frac{w_0}{2h}\right)\left(\frac{h}{B}\tan\beta\right)-\pi f_c\frac{w_0}{ah}\left[\frac{2A}{B^2}\left(e^{Bh}-1\right)+\frac{2h}{B^2}\tan\beta\right]\tan\beta+N_{rs}=0 \qquad (4.39)$$

With the values of d_0, h, f_c, f_t and n_a known, the punching shear load can be determined by the following iterative procedures:

(1) Choose a value of d_1, the outer diameter of the failure cone.

(2) Assume a value for the inclined angle β.

(3) Determine the constants B from Eqn. (4.36b) and A from Eqn. (4.36a).

(4) Substitute the values of β, A and B into Eqn. (4.39). If the condition is not satisfied, change the value of β and repeat from step (3).

(5) Calculate the value of N_{rs} from Eqn. (4.38).

(6) Compute the value for the punching failure load, P from Eqn. (4.37).

The initial value for d_1 is usually chosen as a value smaller than that in the case of a simply- supported slab and is then gradually decreased until a minimum value of P is obtained by an iterative process. The value of d_1 for a simply-supported slab is determined by the following expression:

$$\left(\frac{d_1}{d_0}\right)^{d_1} = e^{c_k h}$$

where c_k is obtained from Eqn. (3.20).

4.5. EXPERIMENTAL VERIFICATION

In the following section, the punching shear strengths of concrete slabs with lateral restraint predicted by the proposed method are compared with results from the tests reported in the literature and the author. Although the available test results are not extremely numerous, they do provide valuable information regarding the influence of compressive membrane action on punching shear strength in restrained slabs.

4.5.1 Tests Reported in the Literature

(1) Test by Aoki and Seki [4]

Aoki and Seki conducted tests on approximately 2/3 scale restrained slabs

subjected to concentrated loading over a circular steel platen. The primary intention for conducting the tests served as an attempt to a development of a semi-empirical method for analysing the punching shear failure of restrained concrete slabs. In these tests, the lateral restraints were provided by integral edge beams. The main variable was the level of reinforcement in slabs, with the variation of both the slab span and the size of the boundary frame. Details of the tests and the predicted punching failure loads are presented in Table 4.1.

(2) Test by Holowka, Dorton and Csagoly [43]

As part of the Ontario Ministry of Transportation Investigation into the enhanced punching shear strength of bridge deck panels, Holowka et al reported a series of tests on bridge deck-slab specimens. These isolated circular slabs were subjected to concentrated loading through a circular pad, and the finite lateral restraint was produced by means of a carefully fitted steel ring. The two main variables were the span/depth ration and the level of reinforcement, with the concrete strength remaining constant throughout. The degree of lateral restraint was estimated by consideration of the stiffness of the steel restraining ring. Details of specimens and the predicted punching failure loads are presented in Table 4.2.

(3) Tests by Kuang and Morley [56]

Kuang and Morley conducted punching tests on 12 restrained square reinforced concrete slabs. The slab panels were supported and restrained on all four sides by edge beams. The influence of the degree of edge restraint, percentage of steel reinforcement, and the span/depth ratio were investigated. Details of the tests and the predicted punching failure loads are presented in Table 4.3.

(4) Tests by Taylor and Hayes [101]

The earliest investigation into the influence of lateral restraint on the punching shear strength of concrete slabs was probably reported by Taylor and Hayes. The experimental programme was conducted on approximately 1/3 scale models with edge restraint provided by a rigid frame. The main variables of interest were the column size as well as the level of reinforcement. In particularly, the test results on unreinforced slabs resulted in a substantial punching load before failure. Details of the tests and the predicted punching failure loads are presented in Table 4.4.

(5) Tests by Snowdon [97]

Snowdon conducted a series of tests on full scale specimens at the Building Research Station in Watford. The slabs were tested as interior panels in the surrounding heavily reinforced portion of the cellular runway and the concentrated loading was applied through a circular platen. In the tests, the principal variables were the level of reinforcement and the strength of concrete, with variation in the slab depth and the size of the loading platen. Details of these tests and the predicted punching failure loads are presented in Table 4.5.

(6) Tests by Rankin and Long [81]

Rankin and Long conducted a series of tests on approximately ? scale model specimens which represent the interior slab-column connection. The aim of these tests was to verify the concept of enhanced punching strength due to the development of compressive membrane action in flat slab construction. The type of model ranged from large to full panel specimens and the principal variables were the span/depth ration as well as the percentage of steel reinforcement. Details of the tests and the predicted punching failure loads are presented in Table 4.6.

4.5.2 Comparison with experimental results

Comparison with experimental results

Tables (4.1-4.6) show the correlation of the predictions made by the proposed theory with the experimental results carried out by various researchers [4,43,56,81,97,101]. An overall correlation made by the proposed theory is shown in Fig. 4.15. It can be seen that the overall correlation with the test results is good. The tests analysed by the proposed method have a mean ratio of experimental to predicted ultimate loads of 0.98, with a standard deviation of 0.096 and a coefficient of variation equal to 9.80%. The correlations of the predictions by British and American code methods are presented in Figs. 4.16 and 4.17. The mean ratio of the test to predicted punching loads by the British code (BS 8110) method is 1.42, with a standard deviation of 0.28 and a coefficient equal to 19.72%, and that by the American code (ACI-318) method 1.67 with a standard deviation of 0.27 and a coefficient of variation equal to 16.17%, where the safety factors have been removed. Thus, the overall correlation of the proposed theory with the experimental results is considered to be satisfactory in the view of the wide range of variables involved and the variety of test sources.

In addition, Table 4.7 included some slabs presented in Chapter 3 together with predictions from both the plastic analysis employing the usual effectiveness factors and the membrane modified version plastic analysis. Results clearly indicated that predictions given by the conventional plastic analysis may well incorporate the membrane effect even if they are not physically interpreted as such. This particular finding is crucial for future work where plastic analysis can be employed for predicting the enhanced punching shear capacities with consideration of membrane effect.

4.6 CONCLUSIONS

An upper-bound plastic solution for predicting the punching shear of laterally restrained slabs has been presented, in which concrete was assumed to be rigid-plastic, with yielding controlled by a parabolic Mohr failure criterion. The predictions show good agreement with a wide range of experimental results. Throughout this investigation, ratio of $f_c / f_t = 400$, the diameter of the equivalent circular slabs is equal to 1.1 times the clear span of the corresponding square slabs [4]. The critical deflection of slabs at failure is taken as half the slab depth, which is used to calculate the membrane forces. This value is borne out by an examination on the wide range of measured deflections at failure as cited by Park [76], from results for a series of laterally restrained concrete slabs.

Additional mathematical consideration of the surround stiffness provided by both surround concrete material and hoop reinforcement was presented for the basis of a laboratory simulation of surround restraint via both surround concrete material as well as hoop reinforcement to be presented in chapter 6. The mathematical derivation indicated a limit to restraint stiffness despite further increase in material quantity. Further, it was shown that a threshold stiffness was reached beyond which negligible increase in punch failure load occurred. This important issue of a limit to punching capacities due to increasing surround restraint will also be investigated experimentally in the Chapter 6. Most importantly, the verification of the upper bound approach presented in this chapter for predicting the punching failure loads of restrained slabs against experimental test results conducted by the author will be pursued in Chapter 6.

Slab	f_{cu} (MPa)	f_y (MPa)	d (mm)	p %	c (mm)	N_{rs} (kN)	P_E (kN)	P_P (kN)	P_E/P_P
XC-2	35.7	408	78	0.91	190	1157.0	275	268.8	1.02
XC-3	33.8	408	71	1.00	190	1076.5	275	262.7	1.05
XC-4	24.5	372	62	2.30	190	808.0	147	179.1	0.82
XC-5	24.2	369	73	1.30	190	748.0	206	199.4	1.03
XC-6	23.8	379	63	1.13	190	784.9	153	173.9	0.88
FC-1	33.4	354	75	0.95	190	1082.5	256	251.5	1.02
FC-2	23.5	-	75	-	190	518.2	131	116.3	1.13
FC-3	23.0	-	90	-	190	627.0	132	164.2	0.80
FC-4	23.0	391	73	0.39	190	726.7	186	185.9	1.00
FC-5	22.5	391	70	0.40	190	702.1	185	186.5	0.99
FC-6	22.5	391	73	0.77	190	710.9	177	181.9	0.97
FC-7	20.1	391	70	0.81	190	620.7	186	170.3	1.09
FC-8	29.4	391	74	0.38	190	979.8	177	215.7	0.82

Table 4.1 Laterally restrained slabs tested by Aoki and Seki

Slab	f_{cu} (MPa)	f_y (MPa)	d (mm)	p %	c (mm)	N_{rs} (kN)	P_E (kN)	P_P (kN)	P_E/P_P
A1-A3	27.4	310	38.1	0.20	63.5	98.9	42.4	43.1	0.98
B1/B2	27.7	310	31.8	0.20	63.5	77.6	36.8	37.6	0.98
C1-C3	28.4	310	25.4	0.20	63.5	65	23.1	23.4	0.99
D1-D3	25.9	310	38.1	0.30	63.5	84.9	49.1	49.7	0.99
E1-E3	26.9	310	31.8	0.30	63.5	72.8	34.9	37.9	0.92
F1-F3	27.0	310	25.4	0.30	63.5	60.3	23.8	22.4	1.06
G1	28.1	310	38.1	0.80	63.5	89	44.6	43.1	1.03
H1	28.2	310	31.8	0.80	63.5	69.3	37.9	38	1.00
I1-I3	28.1	310	38.1	1.00	63.5	85.4	47.3	42.2	1.12
J1/J2	27.8	310	31.8	1.00	63.5	64.5	37.2	37.6	0.99
K1/K2	27.9	310	25.4	1.00	63.5	53.4	25.2	22.7	1.11

Table 4.2 Laterally restrained slabs tested by Holowka, Dorton & Csagoly

Slab	f_{cu} (MPa)	f_y (MPa)	d (mm)	p %	c (mm)	d_1 (mm)	P_E (kN)	P_P (kN)	P_E/P_P
S1-C03	48.7	368	49	0.3	120	420	101	114	0.89
S1-C10	33.8	368	49	1.0	120	270	118	120	0.98
S1-C16	41.2	368	49	1.6	120	270	149	143	1.04
S2-C03	48.1	414	31	0.3	120	430	49	55	0.89
S2-C10	45.8	414	31	1.0	120	300	70	65	1.08
S2-C16	42.6	414	31	1.6	120	300	68	59	1.15
S1-B10	45.9	368	49	1.0	120	380	116	117	0.99
S2-B03	50.8	414	31	0.3	120	430	42	58	0.72
S2-B10	59.5	414	31	1.0	120	380	69	71	0.97
S1-A10	46.5	368	49	1.0	120	450	99	106	0.93
S2-A03	47.8	414	31	0.3	120	430	43	54	0.80
S2-A10	60.3	414	31	1.0	120	350	63	75	0.84

Table 4.3 Laterally restrained slabs tested by Kuang

Slab	f_{cu} (MPa)	f_y (MPa)	d (mm)	p %	c (mm)	N_{rs} (kN)	P_E (kN)	P_P (kN)	P_E/P_P
1R2a	36.8	-	-	-	51	444.3	84.9	88.9	0.96
1R2b	32.5	-	-	-	51	320.5	88.9	96.3	0.92
1R3	35.6	-	-	-	76	450.1	129.9	121.5	1.07
1R4	35.6	-	-	-	102	502.8	149.8	155.1	0.97
1R5	27.3	-	-	-	127	458.7	119.4	124.9	0.96
1R6	27.3	-	-	-	152	508.3	143.8	142.3	1.01
2R2	32.5	377	63.5	1.57	51	378.7	83.7	81.0	1.03
2R3	30.8	377	63.5	1.57	76	350.8	114.9	122.8	0.94
2R4	29.0	377	63.5	1.57	102	411.3	139.3	125.4	1.11
2R5	27.6	377	63.5	1.57	127	449.0	144.8	134.9	1.07
2R6	23.0	377	63.5	1.57	152	416.5	157.3	128.0	1.23
3R2	28.5	377	63.5	3.14	51	313.6	79.9	75.1	1.06
3R4	28.4	377	63.5	3.14	102	380.4	134.8	137.6	0.98
3R6	27.1	377	63.5	3.14	152	488.9	172.3	152.3	1.13

Table 4.4 Laterally restrained slabs tested by Taylor and Hayes

Slab	f_{cu} (MPa)	f_y (MPa)	d (mm)	p %	c (mm)	N_{rs} (kN)	P_E (kN)	P_P (kN)	P_E/P_P
1/2	54.1	530	82	0.61	200	1996.3	340	350.5	0.97
3/4	54.7	530	82	0.61	200	2093.9	302	329.1	0.92
5/6	50.3	530	82	0.61	200	1925.5	309	302.6	1.02
7/8	70.5	530	82	0.61	200	2698.8	374	424.1	0.88
10	70.0	400	76	2.64	200	2779.9	359	421.1	0.85
11/12	63.5	400	76	2.64	200	2521.8	358	382.0	0.94
13/14	50.5	530	107	0.47	200	2670.4	413	435.3	0.95
15/16	64.5	400	101	2.00	200	3370.1	537	556.0	0.97
17/18	53.0	400	101	2.00	200	2769.3	442	456.9	0.97
19/20	55.0	395	105	0.85	200	2996.2	427	464.0	0.92
21/22	66.5	395	105	0.85	200	3622.6	503	533.7	0.94
23/24	64.5	530	107	0.47	200	3522.6	448	519.6	0.86
29/30	51.8	400	101	2.00	200	2706.6	433	446.5	0.97
31/32	78.3	400	101	2.00	200	4568.3	507	627.6	0.81
33/34	55.5	530	107	0.47	200	3027.2	451	468.3	0.96
35/36	67.0	530	107	0.47	200	3654.5	508	549.2	0.92
45/46	45.7	-	-	-	200	2497.4	409	392.8	1.04
47/48	45.0	530	107	0.47	300	2841.9	523	517.4	1.01
19/50	44.7	530	107	0.47	100	1552.3	291	293.2	0.99
51/52	59.0	530	107	0.47	200	3218.1	438	497.8	0.88

Table 4.5 Laterally restrained slabs tested by Snowdon

Slab	f_{cu} (MPa)	f_y (MPa)	d (mm)	p %	c (mm)	N_{rs} (kN)	P_E (kN)	P_P (kN)	P_E/P_P
R1-08	37.7	530	40.5	0.802	100	231.5	65.22	64.21	1.02
R2-08	38.9	530	40.5	0.802	100	271.9	64.81	68.19	0.95
R3-08	41.1	530	40.5	0.802	100	321.0	69.66	73.51	0.95
R4-08	33.5	530	40.5	0.802	100	272.3	71.47	66.49	1.07
R5-08	53.8	530	40.5	0.802	100	541.3	77.84	84.27	0.92
R2-11	40.1	530	40.5	1.107	100	280.3	69.73	70.29	0.99
R4-11	43.6	530	40.5	1.107	100	377.4	81.59	77.85	1.05
R5-11	38.9	530	40.5	1.107	100	352.9	87.89	69.15	1.27
R3-05	38.5	530	40.5	0.517	100	300.7	56.16	68.86	0.82
R5-05	38.5	530	40.5	0.517	100	350.1	62.51	68.21	0.92
R3A-08	38.3	530	46.5	0.800	100	333.9	96.41	84.88	1.14
R5A-08	39.6	530	46.5	0.800	100	390.9	95.34	91.57	1.04
R3B-08	36.9	530	35.0	0.799	100	249.4	55.22	55.56	0.99
R5B-08	39.4	530	35.0	0.799	100	300.0	60.34	61.76	0.98
R3C-08	41.3	530	53.5	0.800	100	417.9	112.47	108.57	1.04
R5C-08	44.1	530	53.5	0.800	100	504.3	126.27	121.66	1.04

Table 4.6 Large and full panel specimens tested by Rankin & Long

Slab No	c (mm)	d (mm)	p %	f_{cu} (N/mm^2)	f_y (N/mm^2)	P_E (kN)	$P_{Plastic}$ (kN)	P_P (kN)
1A30a24	300	128.0	1.01	32.4	456	430	381.9	435.7
1A30a25	300	124.0	1.04	30.8	452	408	356.6	428.1
1A15a5	150	117.0	0.80	32.9	442	255	274.9	301.9
1A15a6	150	118.0	0.79	32.1	455	275	274.9	300.9

Table 4.7 Slabs tested by Kinnunen and Nylander

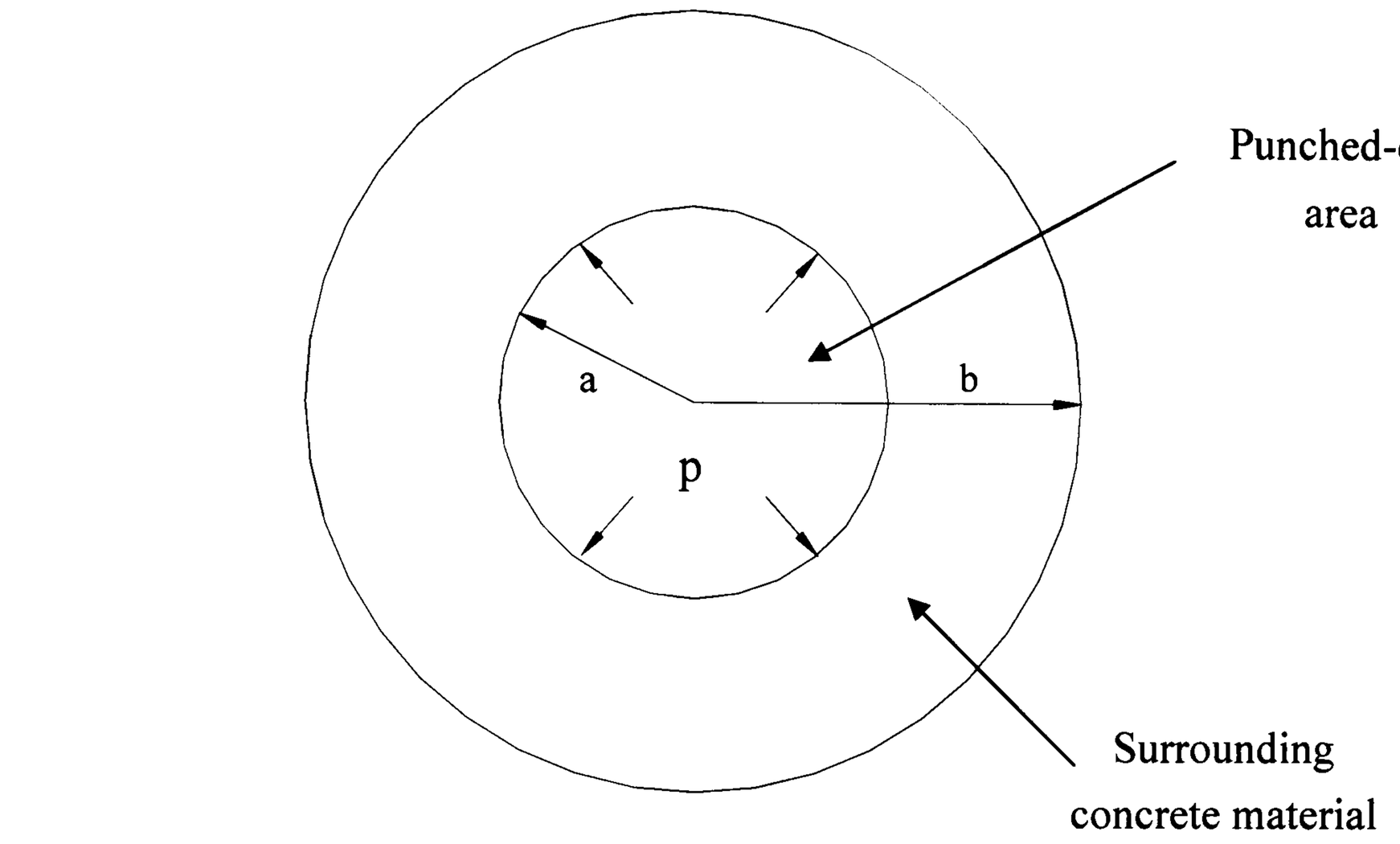

(a) Layout of restrained and restraining zones

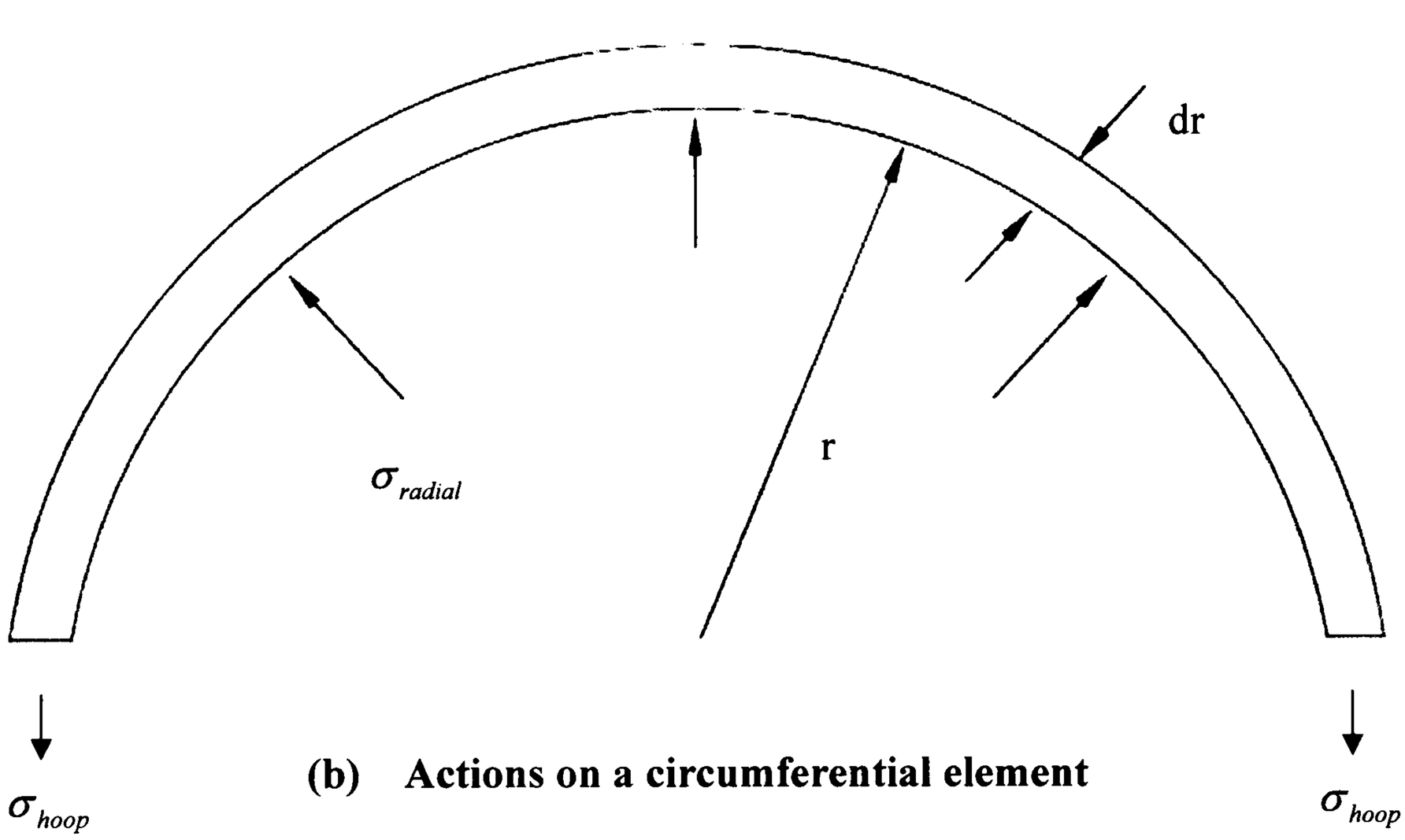

(b) Actions on a circumferential element

FIG. 4.1 Plan of a typical circular slab at punching

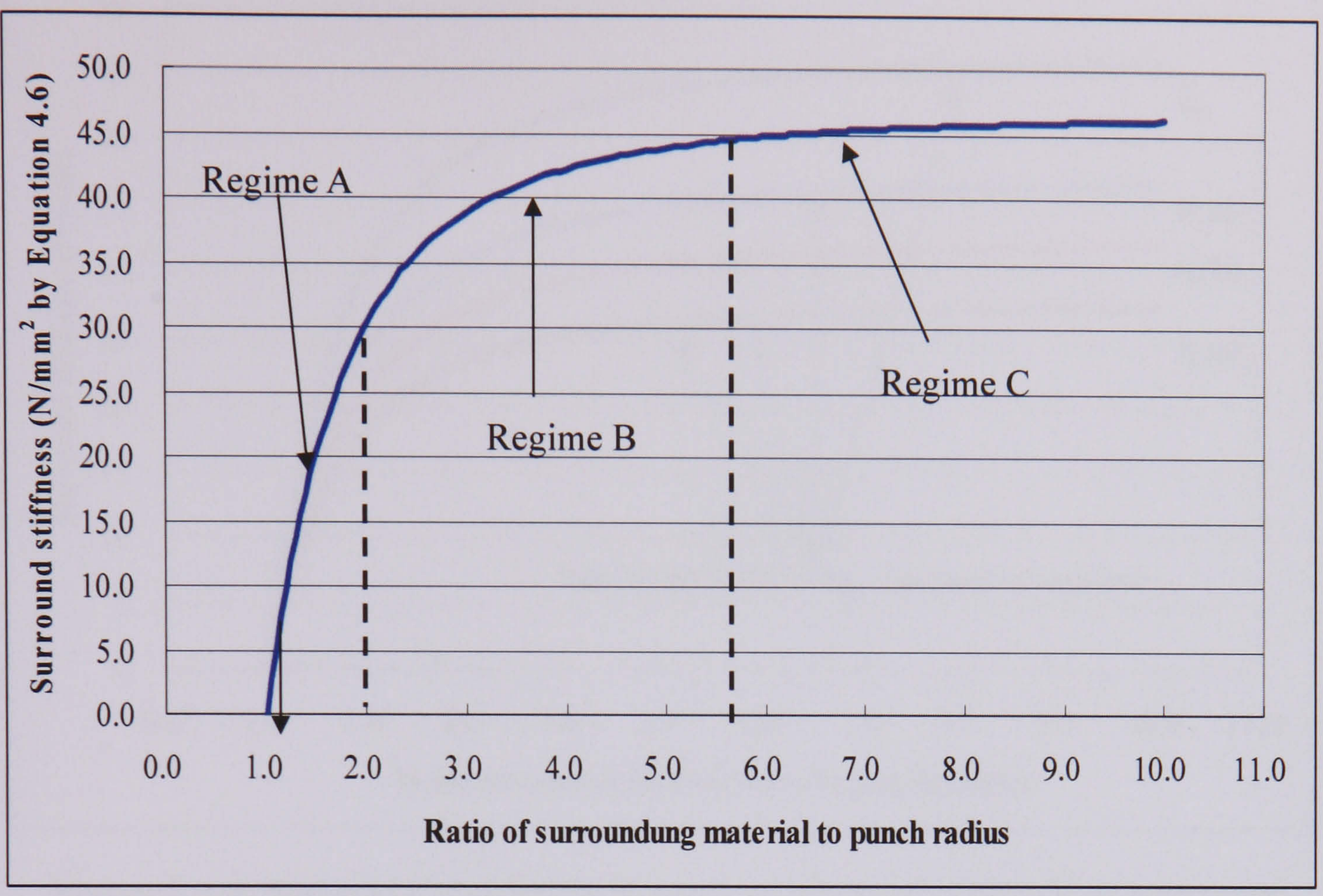

FIG. 4.2(a) Membrane restraint stiffness provided by surround material

FIG. 4.2(b) Membrane restraint stiffness provided by steel hoop

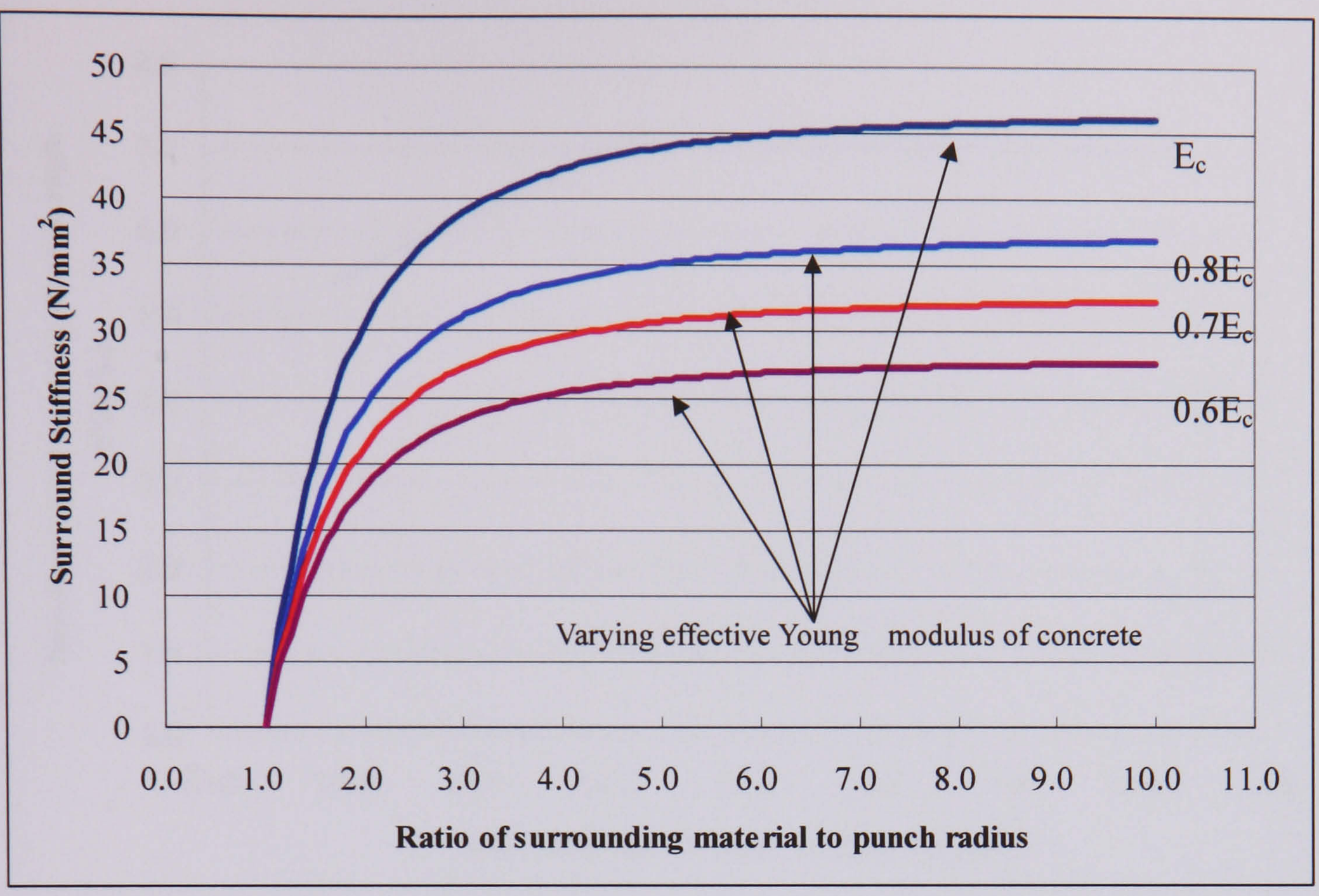

Figure 4.3(a) Influence of effective Young's modulus of concrete on surround stiffness (radius = 550mm)

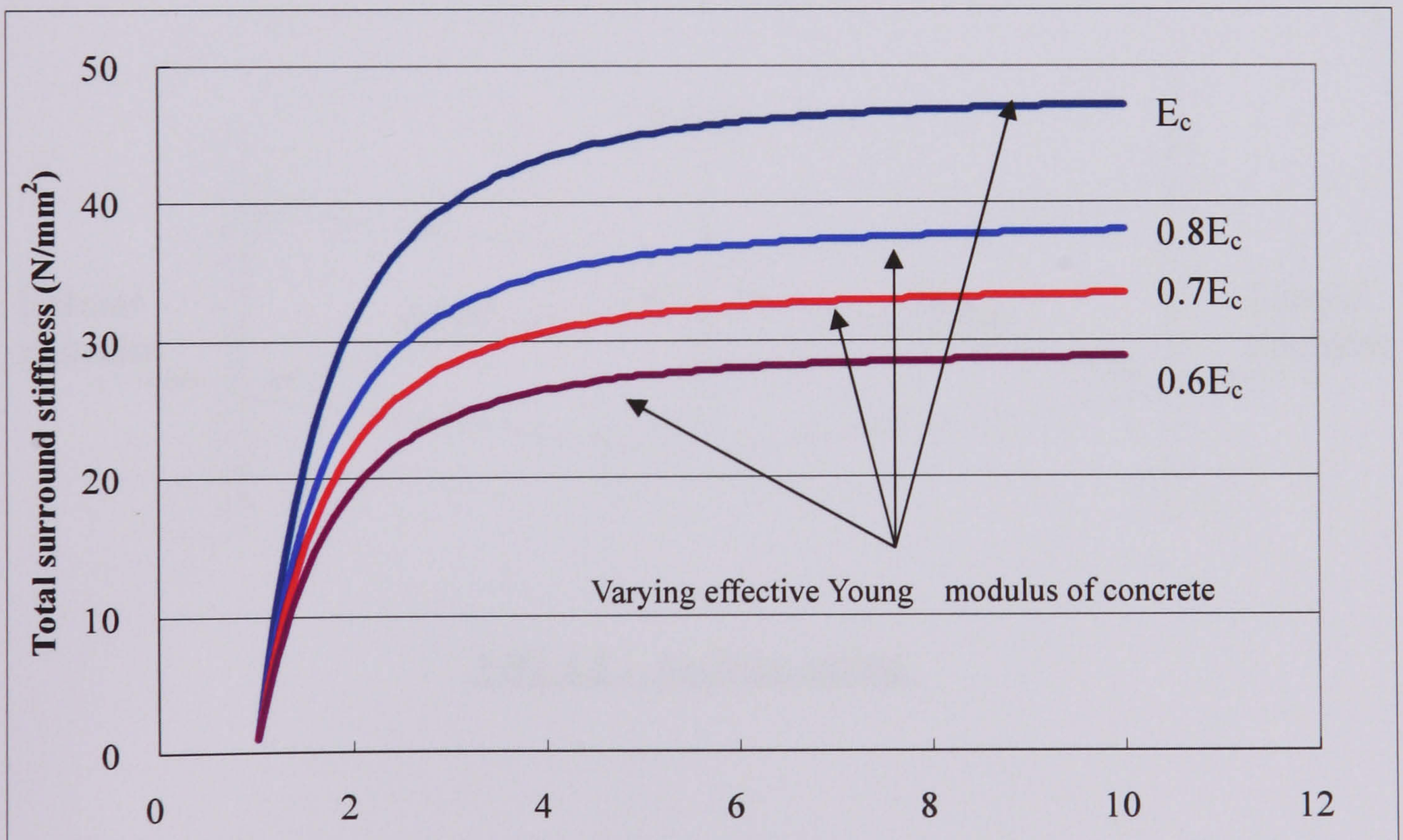

Figure 4.3(b) Influence of effective Young's modulus of concrete on total surround stiffness (same radius as above figure with 3 hoops)

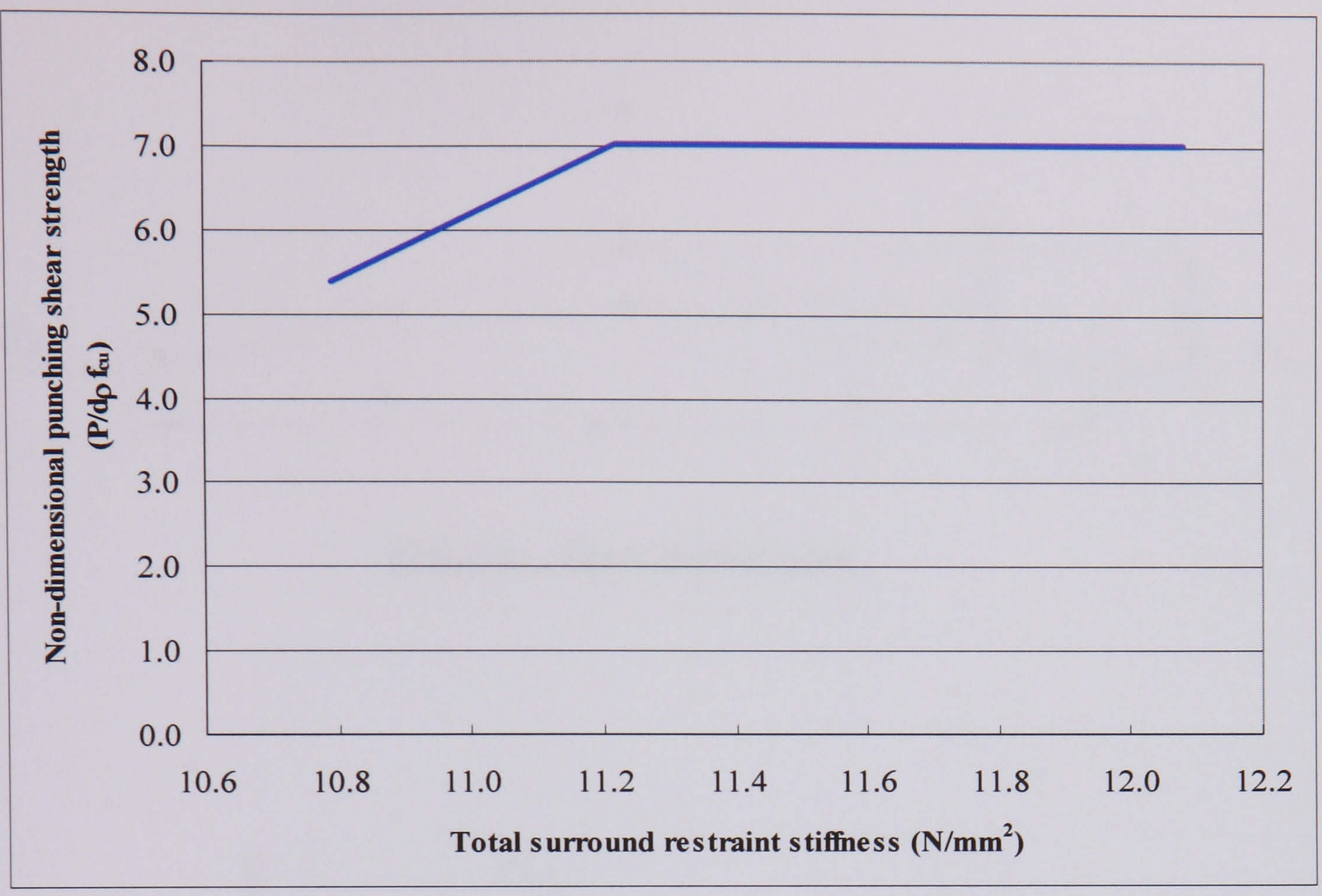

Figure 4.4 Non-dimensional strength against total surround restraint

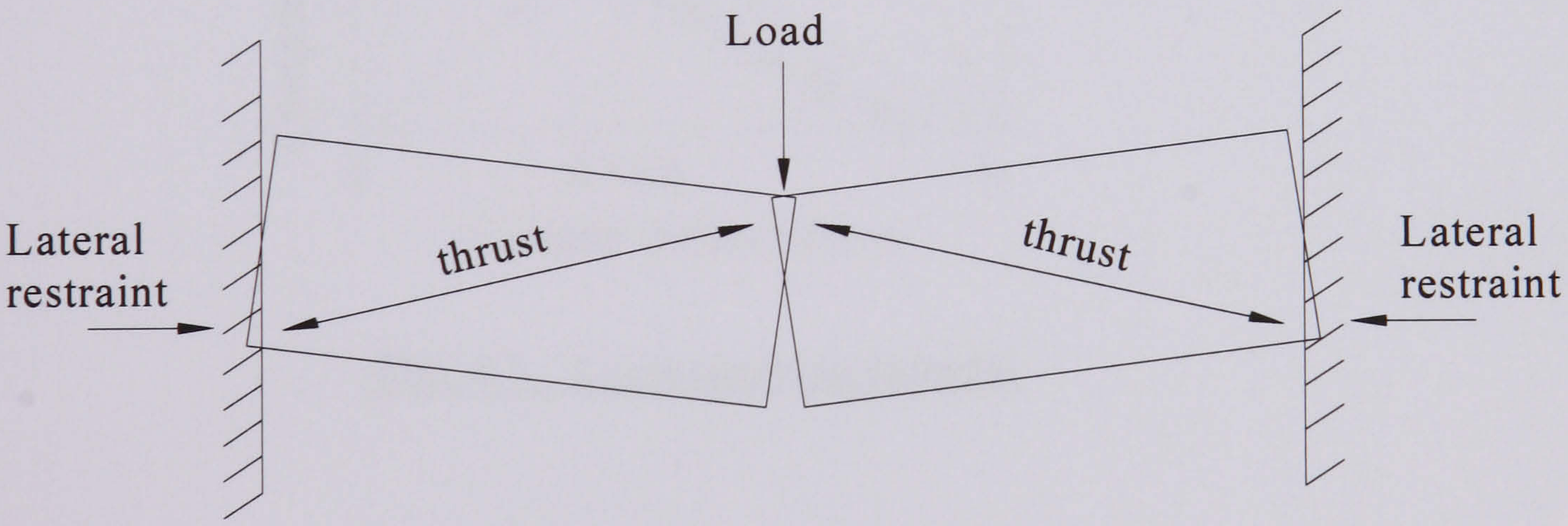

FIG. 4.5 Arching action

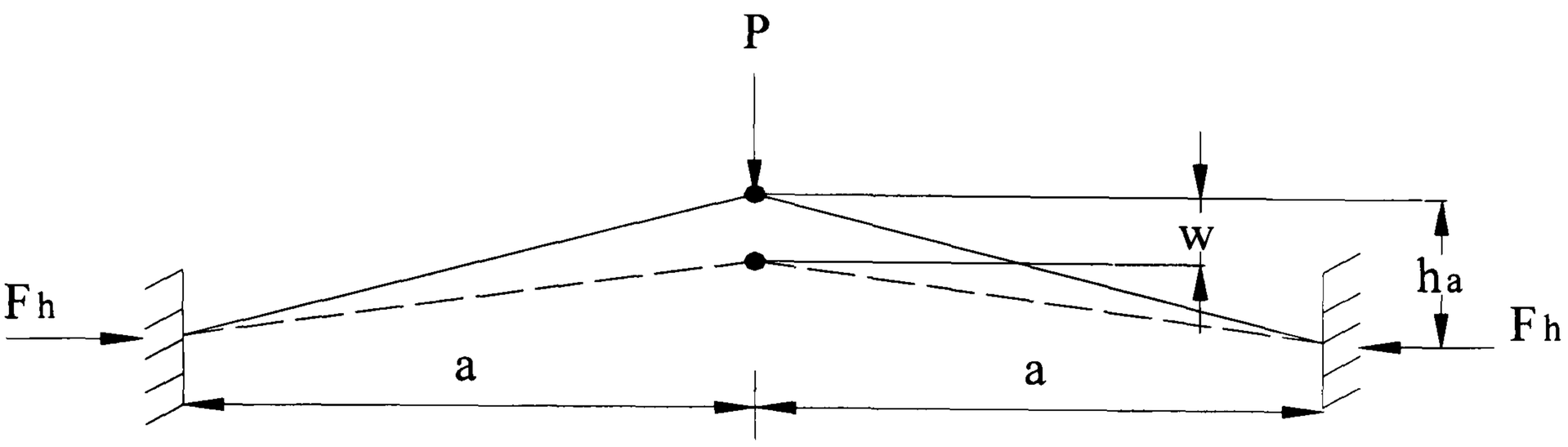

FIG. 4.6 Three-hinged arch

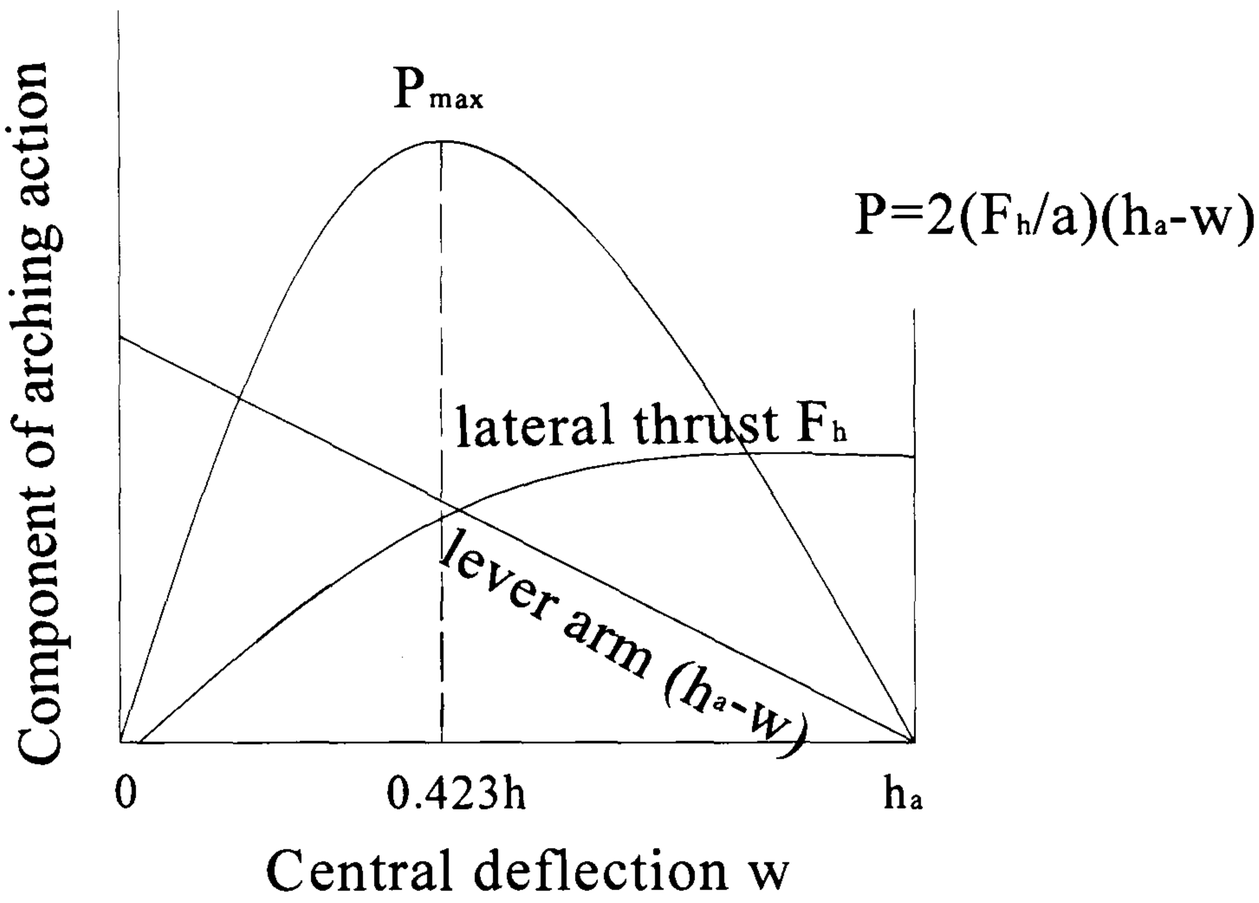

FIG. 4.7 Load-carrying capacity

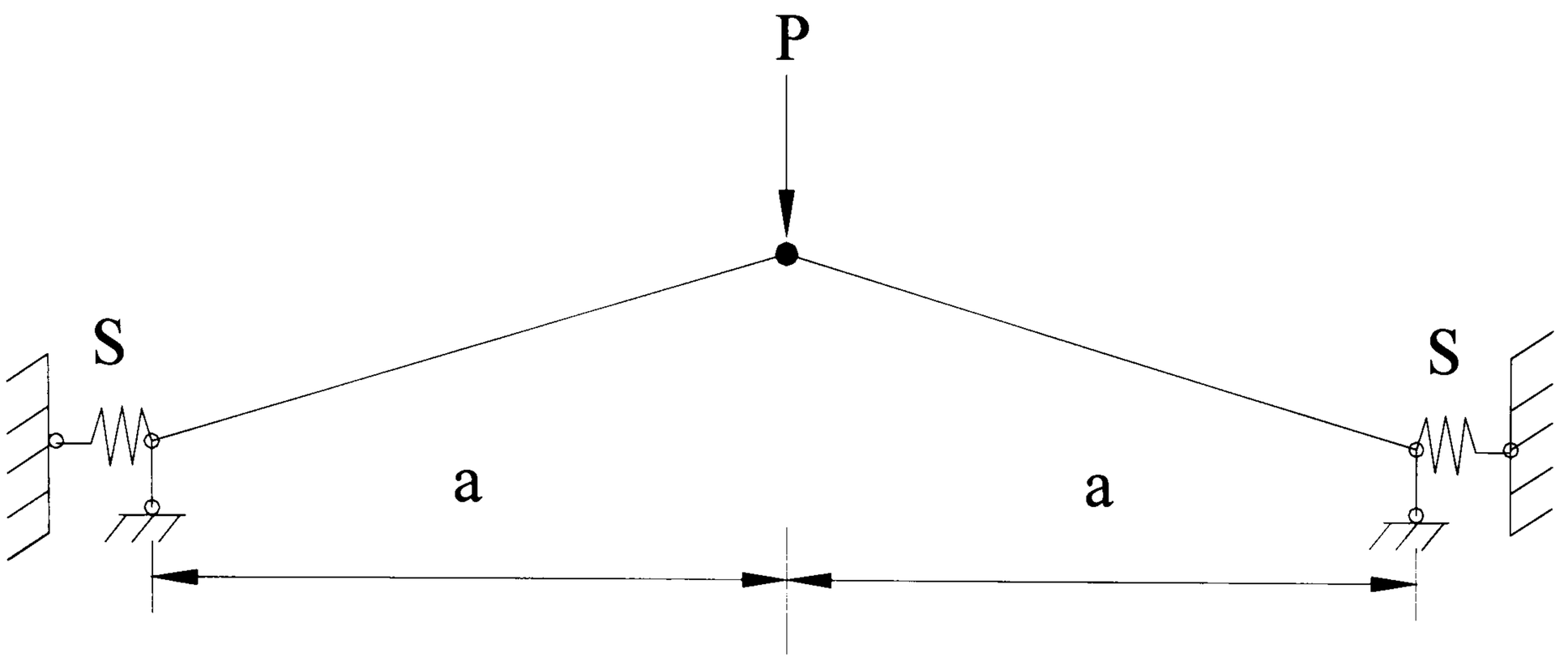

FIG. 4.8 Elastically restrained three-hinged arch

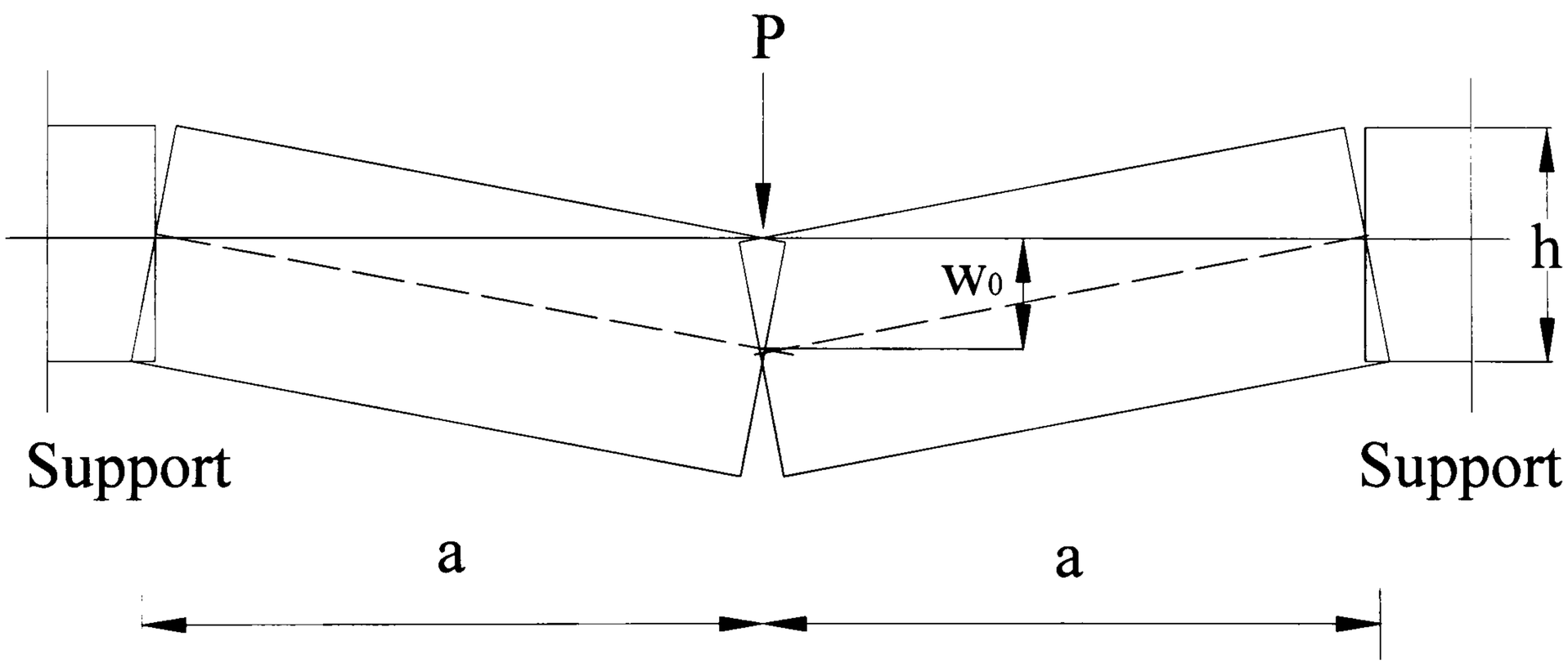

FIG. 4.9 Conical failure mechanism of restrained circular slab subjected to concentrated loading

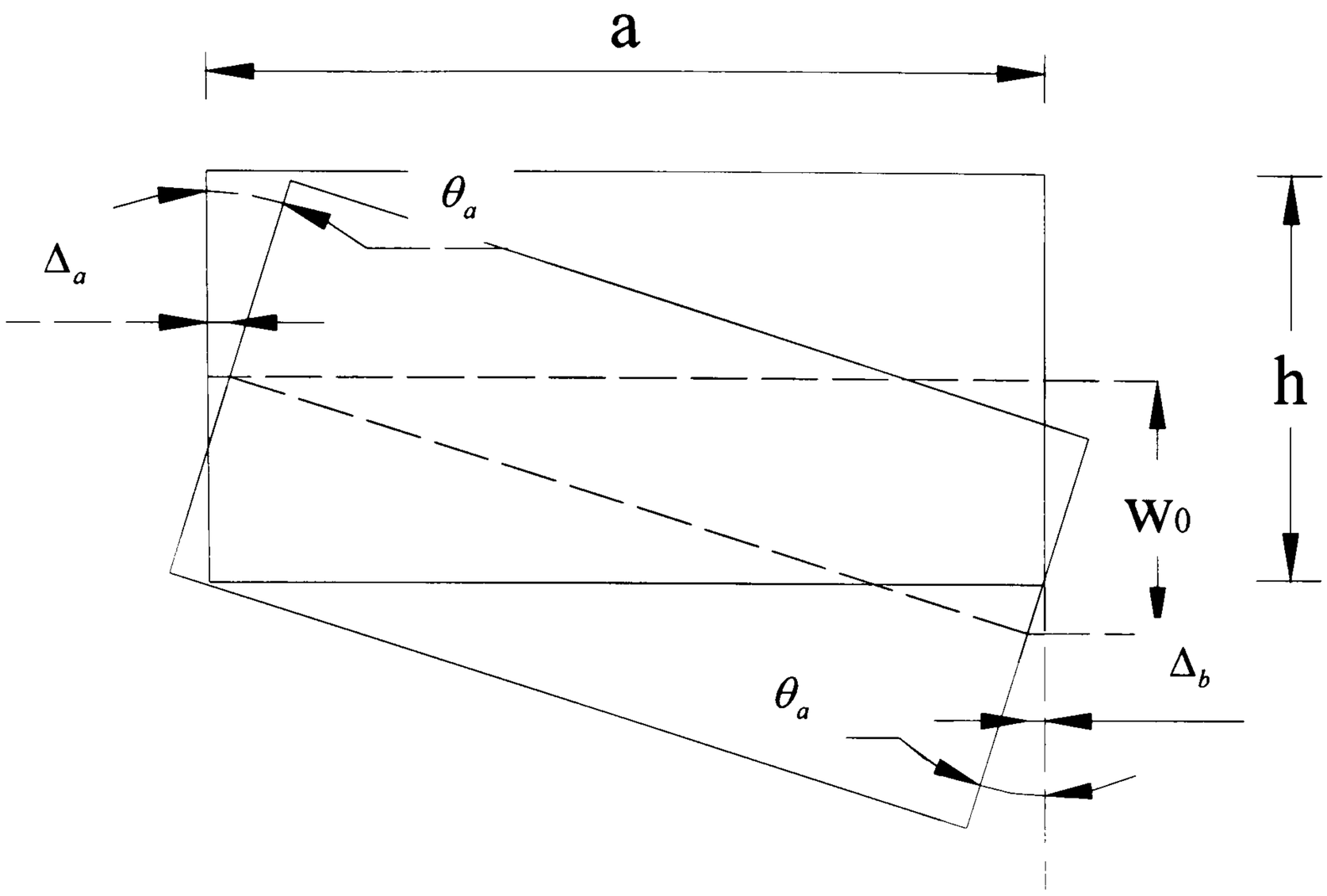

FIG. 4.10 Deformations of radial segment of slab

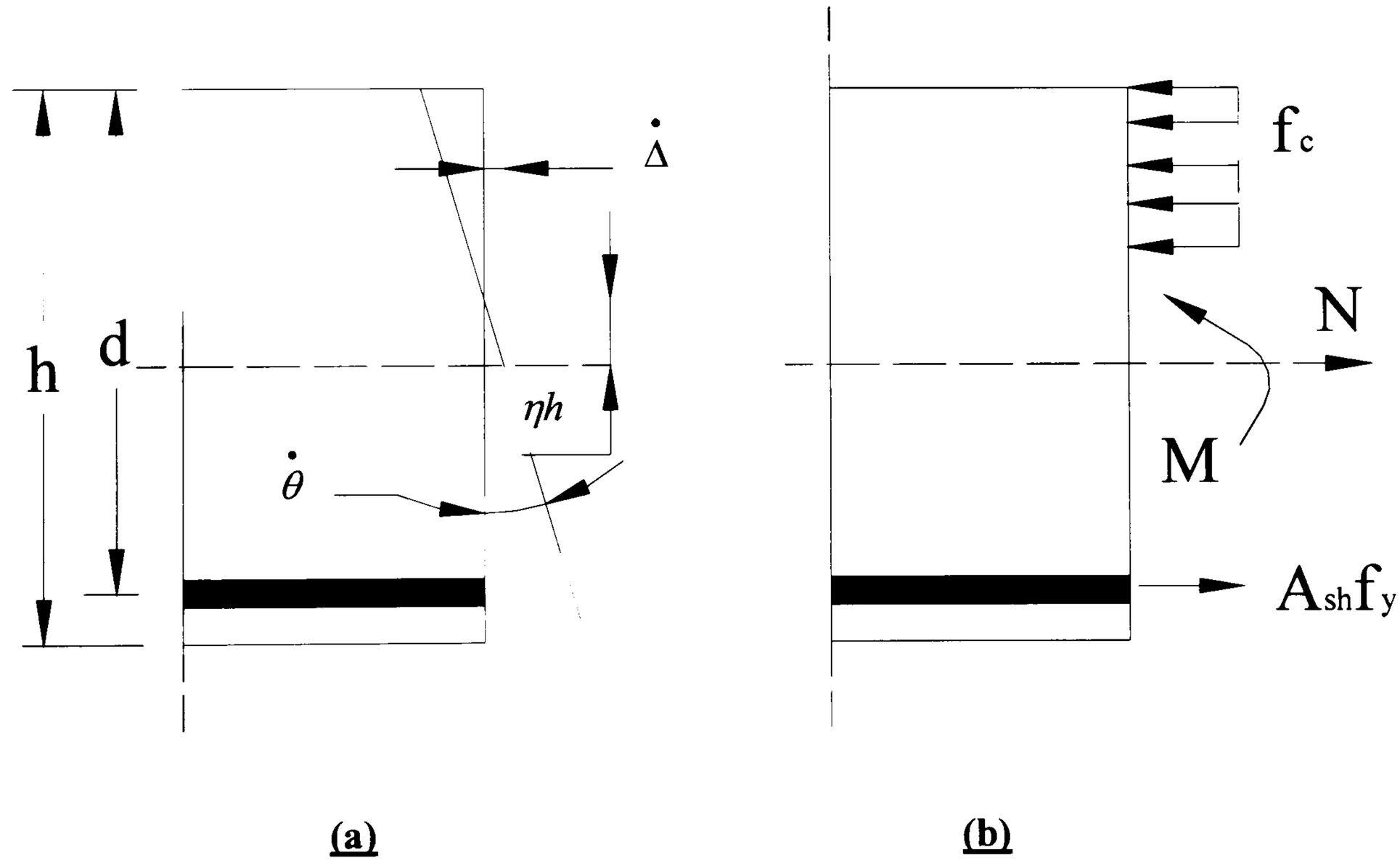

(a) **(b)**

FIG. 4.11 Strain rates and stresses of yielding slab section

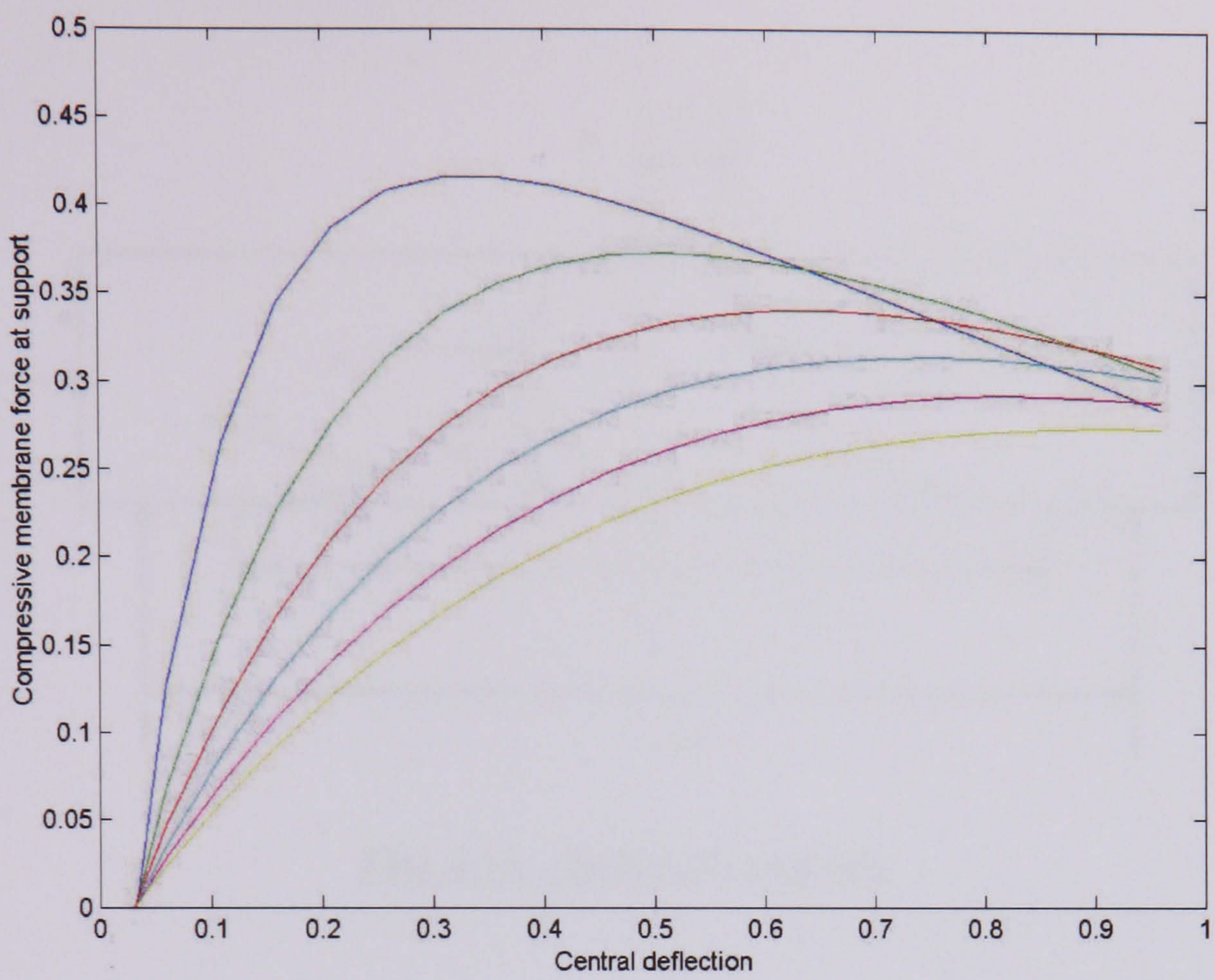

FIG. 4.12 Membrane force-deflection curves for restrained circular slab

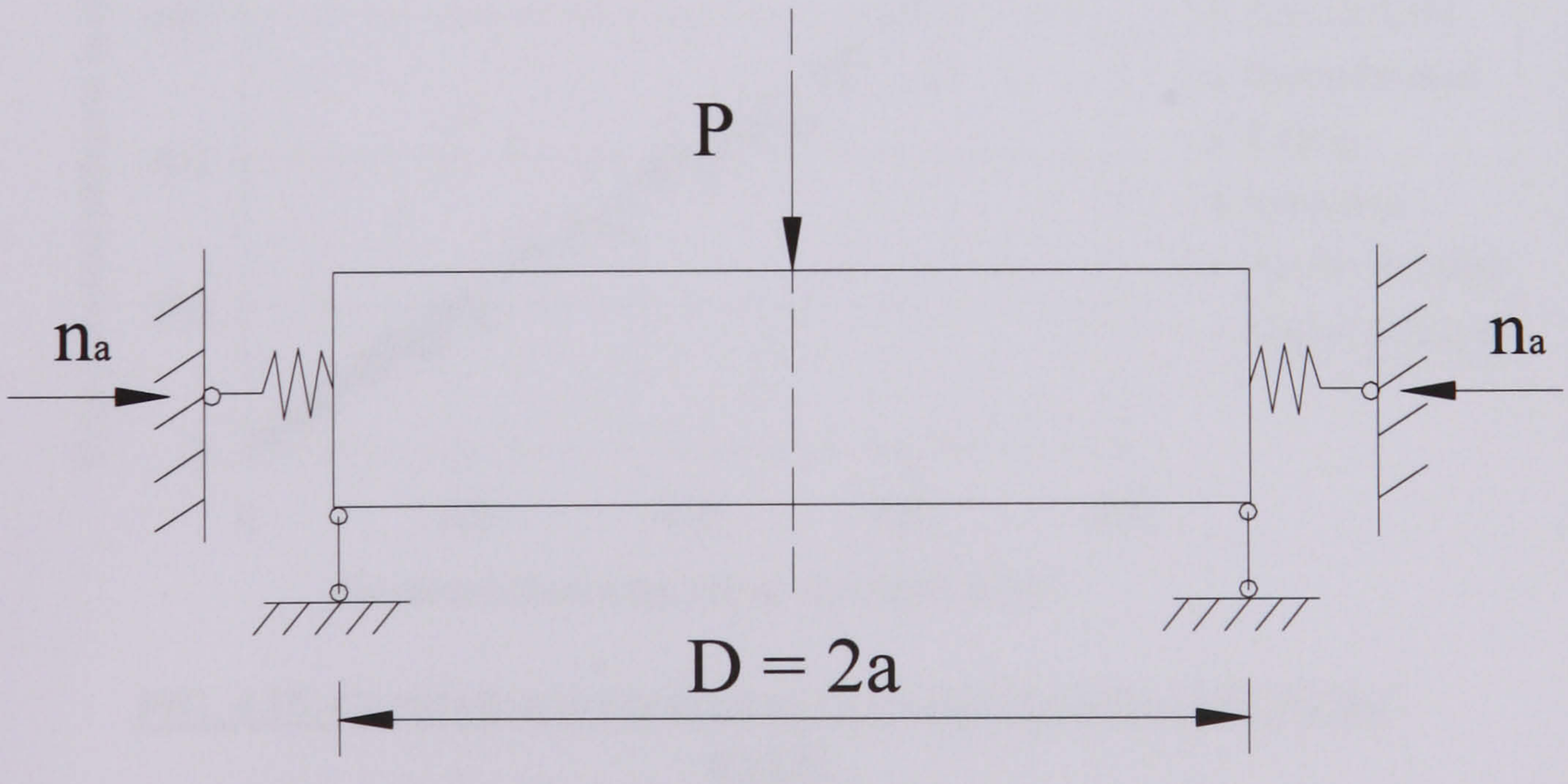

FIG. 4.13 Partially restrained, centrally loaded circular slab

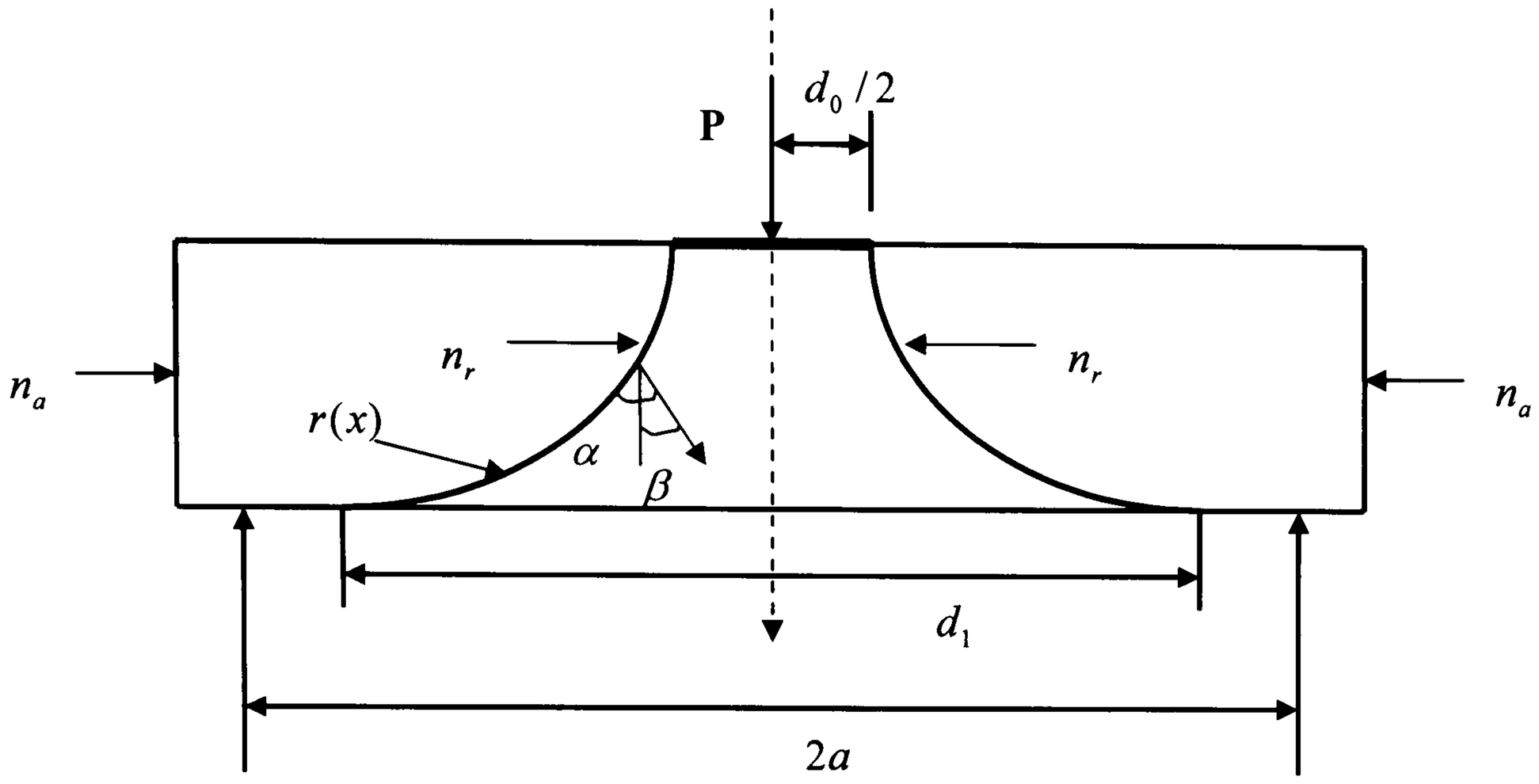

FIG. 4.14 Failure Generatrix

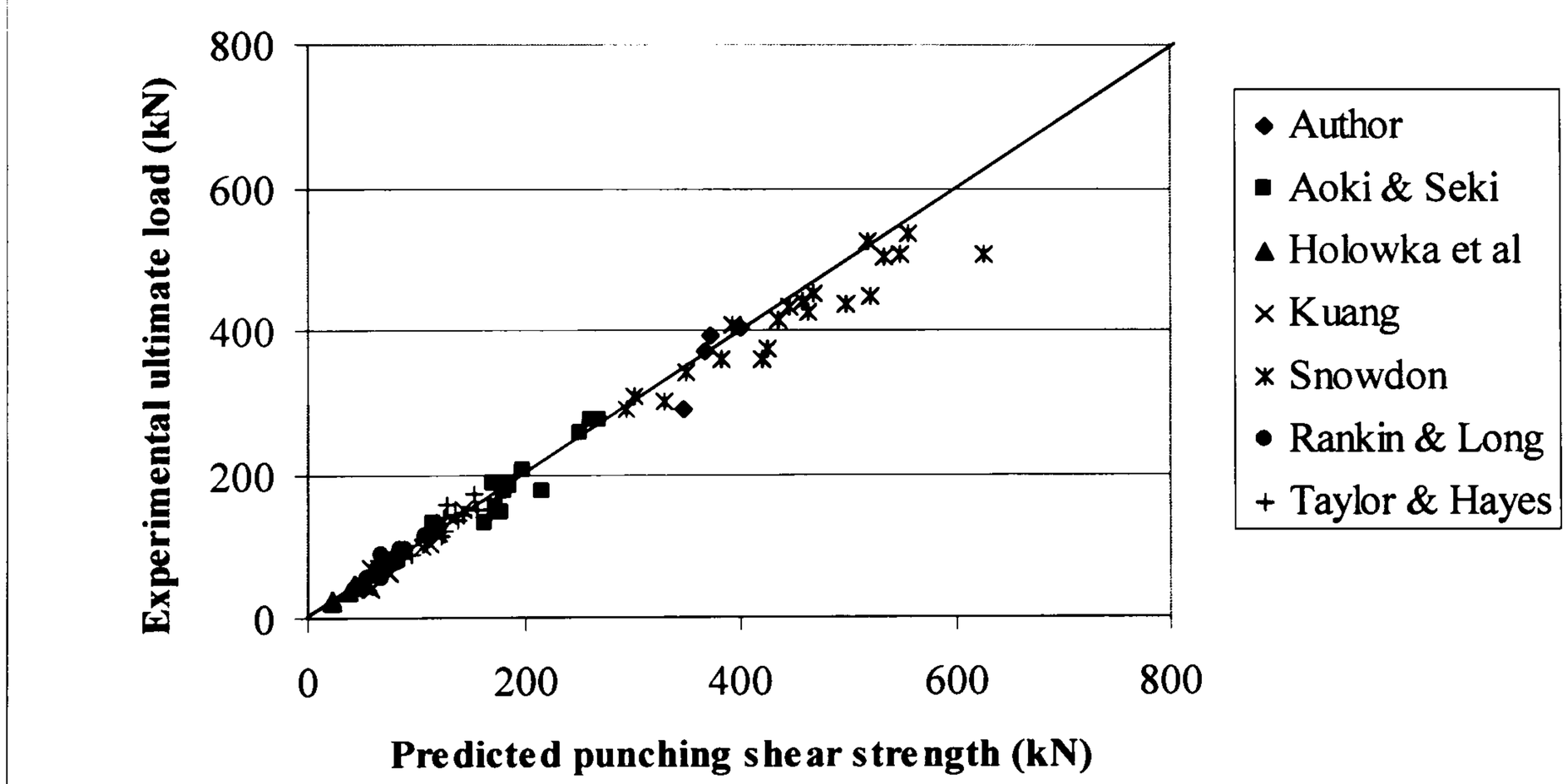

FIG. 4.15. Correlation of predictions by proposed method with 90 test results

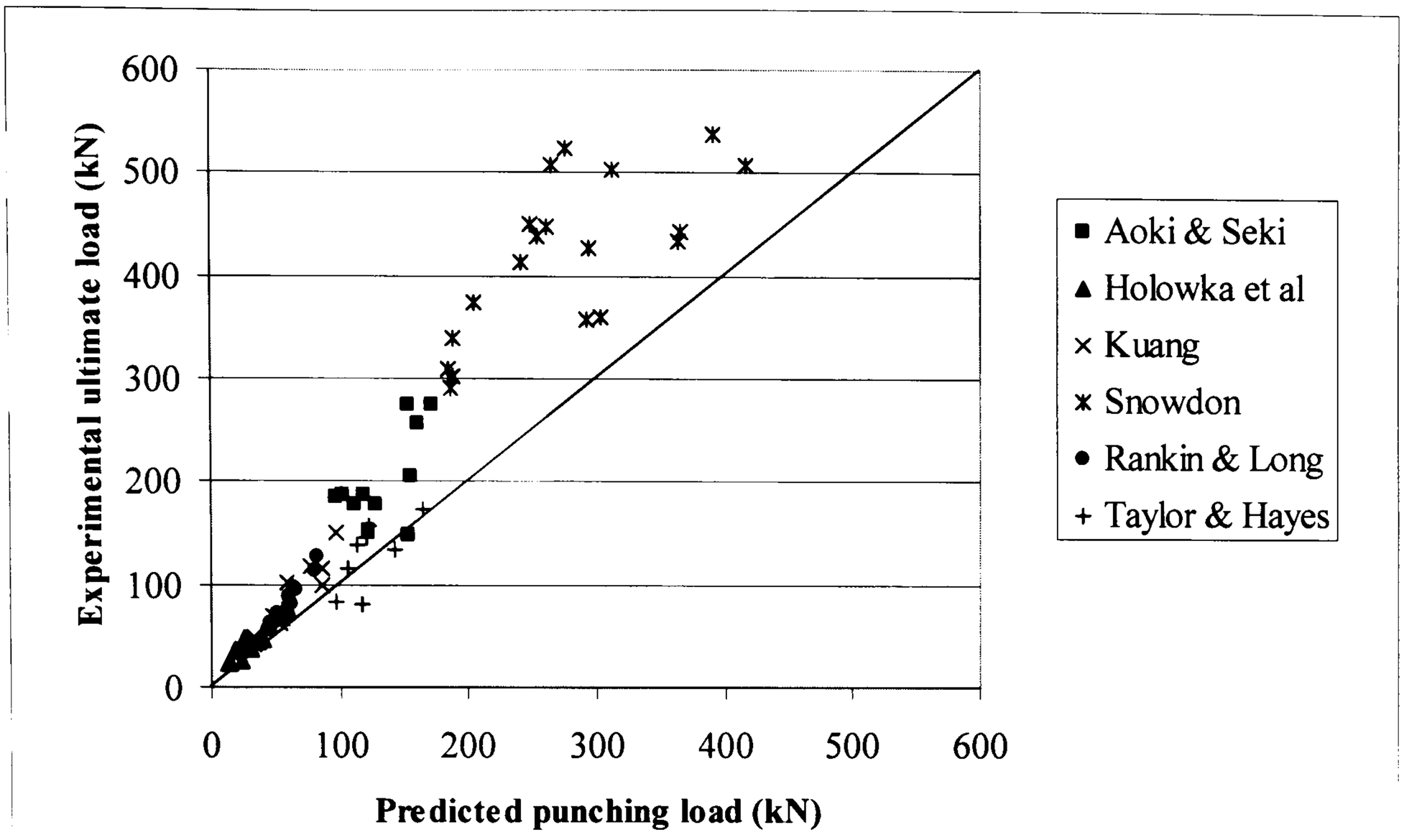

FIG. 4.16 Correlation of predictions by BS 8110 with test results

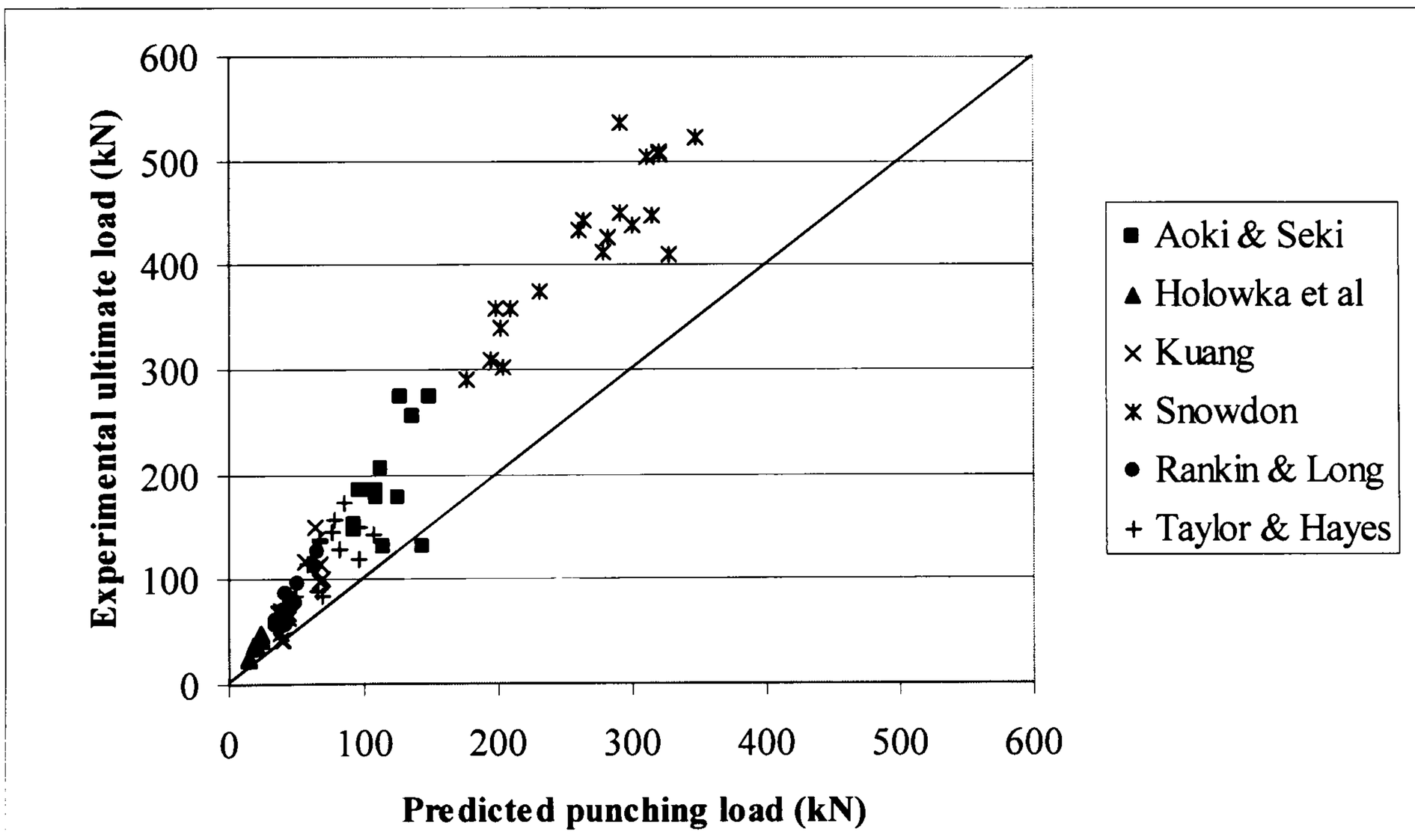

FIG. 4.17 Correlation of predictions by ACI-318 with test results

5

AN EQUILIBRIUM MODEL FOR PREDICTING PUNCHING SHEAR STRENGTHS OF REINFORCED CONCRETE SLABS

Chapter Five

AN *EQUILIBRIUM* MODEL FOR PREDICTING PUNCHING RESISTANCE OF REINFORCED CONCRETE SLABS

5.1 INTRODUCTION

In Chapter 3, an in-depth study of the important factors contributing to the accuracy of the predictive model for punching shear based on plasticity and the work method was pursued. In addition, some refinements were introduced to significantly enhance the predictive capabilities of the model. The present chapter will focus on another approach, namely an equilibrium approach, which builds significantly on that first introduced by Kinnunen and Nylander [50,51]. The approach is developed for predicting the punching shear strength of symmetric slab-column connections in flat slab structures. The preference for the term "equilibrium" as opposed to "lower bound" lies in the fact that firstly, the failure mechanism used in the Kinnunen and Nylander model was only an assumption incorporating *fictitious* material properties supported by experimental results. Secondly, the proposed analysis does not necessarily lead to predictions less than or equal to the experimental failure loads or less

than those predicted by the earlier plasticity models owing to the fact that *different* material models and assumptions were used in the equilibrium approach and the plasticity based analyses. It is, however, appreciated that this approach would generally give lower predictions of failure relative to predictions based on a plasticity model in the work equation using the same material strengths as this equilibrium model.

The important characteristics of the equilibrium model of the present chapter are highlighted by the following points:

- Material models are defined by stress-strain relationships for uniform stress.
- Introduction of a parameter which quantifies the *size effect*.
- Failure criteria expressed in terms of limiting radial and circumferential strains or the limit at which tension is developed in the critical region of concrete.

In what follows, the analytical model is first described, after which comparisons with the plastic analyses presented in Chapter 3 and with test data reported in the literature are put forward. The sensitivity of the results to the assumed *angle* of the net compressive force at the slab-column junction is demonstrated. Finally, conclusions are drawn on the main advances of the chapter.

5.2 ANALYTICAL MODEL

5.2.1 FUNDAMENTALS OF THE MODEL

From the observed typical crack patterns of test specimens (Fig. 5.1) and the linear deflection profiles assumed, it is considered that the slab is divided into rigid radial wedge segments which rotate around a centre of rotation (CR on Fig. 5.3(a)) located at the column face and at the level of the neutral axis. This implies that the bonded

reinforcement crossing the circumferential crack at the column yields. In addition, it is assumed that just before punching failure occurs, a rigid wedge element, bounded by the internal inclined crack and the initial circumferential crack, is detached from each radial segment and rotates independently around the centre of rotation (CR). In Chapter 3, the angle of inclination of the internal crack surface was calculated to be approximately 10° as shown in Fig. 5.2 using the simplified plastic approach. However, that result applied to *select* test data, and in general it is still worth investigating the influence of variation in angle of inclination of the internal crack. Hence a sensitivity study is included in Section 5.3 to illustrate the importance of this parameter to prediction of punching shear failure loads.

From Fig. 5.3, the forces involved in the analysis of each radial segment of the slab are:

1) The external applied load $P(\Delta\phi/2\pi)$, at radius $r = r_p$ (i.e., at support);
2) The circumferential force F_{st} in the steel crossing the radial cracks due to slab deformation;
3) The force F_{ct} in the concrete normal to the radial crack;
4) A force F_{cr} in the concrete at the face of the column;
5) A radial force F_{sr} in the steel crossing the inclined crack due to slab deformation; and;
6) A dowel force F_{dowel} of the steel cutting across the inclined crack. This dowel force is ignored here since in all practical cases, as will be shown later, steel is reaching its yield strength at the time of punching failure and hence the dowel resistance of the bars is negligible.

The vertical and horizontal equilibrium equations of forces in the radial plane lead to,

$$P\left(\frac{\Delta\phi}{2\pi}\right) = F_{cr}\sin\lambda \tag{5.1}$$

$$F_{sr} = F_{cr}\cos\lambda \tag{5.2}$$

In these equations,

$$F_{cr} = A_c \cdot \sigma_b \tag{5.3}$$

$$F_{sr} = \rho_r \cdot r_w \cdot \Delta\phi \cdot d \cdot \sigma_{sr} \tag{5.4}$$

$$A_c = r_0 \cdot \Delta\phi \cdot \left(\frac{x}{\cos\lambda}\right) \tag{5.5}$$

$$\sigma_b = n_c \cdot f'_c \tag{5.6}$$

where x is the neutral axis depth (Fig. 5.3(b), (c)), r_0 is the column radius, d is the effective depth, n_c expresses the enhanced concrete strength under a multi-axial state of stress, and ρ_r is the percentage of radial steel reinforcement.

The neutral axis depth, Fig. 5.3(b), (c), for an ordinary reinforced concrete slab in the elasto-plastic stage has been suggested by Shehata [95] to be calculated from:

$$\frac{x}{d} = 0.8(n_s\rho_e)^{1/2}\left(\frac{35}{f'_c}\right)^{1/2} \tag{5.7}$$

in which f'_c is the cylinder strength in MPa, n_s is the modular ratio defined below and ρ_e is the ratio of reinforcement for a basic yield strength of 500MPa:

$$\rho_e = \rho_r \left(\frac{f_y}{500} \right) \tag{5.8}$$

$$n_s = E_s / E_c \tag{5.9}$$

Shehata [95] suggested a simplified approximate function to obtain the enhanced n_c which is given by:

$$n_c = 1.4 \left(\frac{2d}{r_0} \right)^{1/2} \geq 1.25 \tag{5.10}$$

where the lower limit of 1.25 is relative to the biaxial compressive strength of concrete. This limit is an approximation of the state of stress of thin slabs near a large column, which introduces restriction to the slab deformation in the circumferential direction, reducing the stress state from triaxial compression to biaxial compression in the case of monolithic slab-column connections.

By substituting for F_{cr} into Equation (5.1):

$$P = 2\pi r_0 \cdot x \cdot n_c \cdot f'_c \cdot \tan\lambda \cdot \xi \tag{5.11}$$

where ξ represents the size effect factor which will be discussed in the next section.

In addition, Shehata [95] introduced an approximated expression for determining the neutral axis depth:

$$x \approx 0.8d(n_s \rho_r)^{1/2} \tag{5.12}$$

and with n_c defined as above, using Equation (5.2) after substitution for F_{sr}, gives the ratio of steel reinforcement ρ_y for which the steel within the punching radius r_w is assumed to have yielded:

$$\rho_y = 2.5 n_s \left(\frac{r_0}{r_w}\right)\left(\frac{d}{r_w}\right)\left(\frac{f'_c}{f_y}\right)^2 \tag{5.13}$$

where:

$$r_w = r_0 + (d - x)\cot\lambda \tag{5.14}$$

In equation 5.14, the presence of d is an approximation to using the entire depth of the slab.

For the practical values of $r_0/d = 1$, $n_s = 10$, $f'_c = 40N/mm^2$ and $f_y = 500N/mm^2$, $\rho_y > 1.75\%$. In general, slabs are provided with ratios of steel reinforcement less than this value. This implies that, generally, the steel within the punching radius will be yielding at punching failure and hence, the dowel forces will be zero.

5.2.2 THE SIZE EFFECT FACTOR

Size effects on the strength of concrete components failing in a brittle manner have been observed in different types of concrete structure, and are related to different aspects of the material (i.e. ratio of aggregate size to specimen dimension, type of loading, crack width, shrinkage, internal temperature of concrete during hardening, etc.). The interaction of the parameters makes the total size effect a complicated problem and at present there seems to be no general method to evaluate the effect of the size of the structural element on its strength. The idea of applying fracture mechanics to predict a size effect in punching was proposed by Bazant and Cao [9] as described in the literature review in Chapter 2. For the present (punching shear) problem, another proposal is to relate the punching resistance to the effective depth, d, of the slab.

In this PhD study, an attempt has been made to relate the value of $P_{test} / x \cdot c \cdot \sigma_b \cdot \tan\lambda$ (non-dimensional strength parameter) from tests by other researchers [Base, Kinnunen & Nylander, Moe, Elstner et al, Regan, Rankin & Long] to the effective depths of the slabs, d, as shown in Fig. 5.4. From this plot, a reasonable overall correlation is given by:

$$\xi = \left(\frac{191}{d}\right)^{0.5707} \tag{5.15}$$

where $c = 2\pi r_0$ is the perimeter of the loaded area, σ_b is the concrete bearing capacity given by equation (5.6), and λ is the angle of inclination of the internal crack.

Therefore, by substituting equation (5.15) into equation (5.11), the estimated punching shear strength can be evaluated as :

$$P = 2\pi r_0 \cdot x \cdot n_c \cdot f'_c \cdot \tan\lambda \cdot \left(\frac{191}{d}\right)^{0.5707} \tag{5.16}$$

5.3 A SENSITIVITY STUDY OF VARIATION IN ANGLE OF INCLINATION OF THE INTERNAL CRACK

The plasticity approach presented in Chapter 3 suggested that the angle λ of the compressive force is approximately 10°. In addition, a perusal of Equation (5.16) suggests that the value of λ could well significantly influence the magnitudes of the predicted failure loads. Therefore, it is worth investigating the effect of varying the angle λ to investigate which value would give the best overall correlation to be adopted in the punching shear equation. In the present study, three different values were chosen: $\lambda = 8^\circ$, 10° and 12°.

Table 5.1(a) shows the sensitivity of the punching predictions to different values of λ. It appears that the mean value of predicted to experimental loads increases as the value of λ increases, suggesting that λ plays an important role in the sensitivity of the punching shear predictions. In particular, when λ exceeds 10°, the correlation mean (1.31) furthest away from 1 suggests an unsafe solution. On the other hand, when λ is limited to values less than 10°, the correlation mean points to the conservative regime.

5.4 EXPERIMENTAL VERIFICATION

Predictions from the presently-proposed analysis have been compared with the results of 97 tests conducted by various researchers (Base [8], Kinnunen & Nylander [51], Moe [65], Dragosavic et al [28], Elstner et al [30], Criswell [22], Regan [85], Rankin & Long [81], Hallgren & Kinnunen [39]). The comparisons between predicted and measured punching shear failure loads are given in Table 5.2 to Table 5.11, together with a statistical summary of the correlations of employing the plasticity approach as well as the equilibrium approach. The data of Table 5.2 to Table 5.11 were obtained by implementing the present analyses in EXCEL. Note the following points in relation to the implementations of the analyses:

- The present analyses assume a circular punch, but some of the experiments used square punches. In such cases, an effective diameter (d_0) 10% greater than the side length of the square is assumed (after Aoki & Seki [4]. This gives a circular punch of equal plan area to the experimentally-employed square punch.

- Table 5.1(b) shows the comparisons based on the plasticity and equilibrium analyses respectively based on applying the most appropriate set of effectiveness factors (plasticity approach), and the most suitable value for the angle of inclined crack λ (equilibrium approach).

A scrutiny of Tables 5.1 – 5.11 reveals the following essential points:

- Both the plasticity and equilibrium theoretical analyses show decent correlation with the test data. The best correlation (based on the mean & coefficient of variation) occurs for the plasticity approach. This gives a mean correlation of 0.93 and coefficient of variation of 16.1% (Table 5.1(b)).

- The mean correlations for the equilibrium analyses are appreciably sensitive to variation in the angle of inclined crack λ (refer to Table 5.1) with the best correlation having a mean of predicted to experimental failure loads of 0.86 and a coefficient of variation equal to 34.0%, at a value of $\lambda = 8^\circ$ (Table 5.1(a)).

- The equilibrium predictions sometimes *exceed* the corresponding plastic predictions. See for example the second specimen in Table 5.3. This is because the "effectiveness" factors for the plasticity approach and the "size effect" factors for the equilibrium approach have been arrived at via different routes. It is for this reason that the terms "Lower Bound" and "Upper Bound" have been ignored in favour of the terms "equilibrium" and "plasticity" respectively.

These results clearly suggest that the equilibrium approach gives a reasonable correlation (0.86 mean) overall. In the light of that, the simplified approach with a value of $\lambda = 8^\circ$ is strongly recommended because it also gives the best correlation for slabs made of high strength concrete (Table 5.11). In addition, the value of $\lambda = 8^\circ$ agrees reasonably well with the results of $\alpha \approx 80^\circ$ or $\lambda = 10^\circ$ calculated from

plasticity theory (see figure 5.2) which reinforced the confidence of applying both approaches for prediction of punching capacities of reinforced concrete slabs. The excellent mean of value 0.86 points to a conservative approach. This conservatism, coupled with the ease of implementation in a computer, renders this version of the simplified analysis particularly useful in a design office environment.

5.5 CONCLUSIONS

Significantly building on a theoretical framework initially proposed by Kinnunen and Nylander, an equilibrium analysis for the punching shear failure of reinforced concrete slabs has been presented in this chapter as part of the present PhD study. Results from Tables 5.2 – 5.11 show that the approach does not necessarily lead to predictions less than or equal to the experimental loads. Therefore, it seems reasonable to name the approach as "Equilibrium" rather than "Lower Bound" in the present PhD study.

As far as the predictive capabilities of the equilibrium approach is concerned, the overall correlation made by the analysis against experimental results showed reasonably good predictions with a mean ratio of predicted against experimental loads of 0.86, a standard deviation of 0.292, and a coefficient of variation equal to 34.0%. On the other hand, the tests analysed by the plasticity theory have a mean ratio of 0.93, with a standard deviation of 0.15, and a coefficient of variation equal to 16.1%. Clearly, these figures suggested that the plasticity theory performed only slightly better in terms of its predictive capabilities.

In the next chapter, an experimental programme was conducted to investigate the influence of the degree of restraint on the punching failure loads. In particular, the reliability of the analyses based on membrane action as presented in Chapter 4 will be assessed thoroughly in terms of both the validity of the assumed failure surface and the predicted punching loads.

λ (in degrees)	Mean	Standard of Deviation	Coefficient of Variation (%)
8	0.86	0.292	34.0
10	1.09	0.376	34.5
12	1.31	0.442	33.7

Table 5.1(a) Comparison of Mean, Standard Deviation & Coefficient of Variation for ratio of predicted to experimental failure loads using different values of angle of compressive stress with 97 test results [8, 22, 28, 30, 39, 51, 65, 81 and 87]

Analysis	Mean	Coefficient of Variation %
Plasticity theory	0.93	16.1
Equilibrium analysis	1.09	34.5

Table 5.1(b) Comparison of ratio of predicted to experimental failure loads using Plastic against Equilibrium analysis with 97 test results [8, 22, 28, 30, 39, 51, 65, 81 and 87]

Slab No	c (mm)	d (mm)	ρ %	f_{cu} (N/mm^2)	P_E (kN)	$P_{plastic}$ (kN)	$P_{equilibrium}$ (kN)
A	102	57.3	1.083	33.1	93.9	93.0	95.1
B	102	57.3	1.083	35.7	103.9	96.2	96.9
C	102	57.3	1.083	32.8	97.9	92.4	94.9
D	102	57.3	1.083	34.2	103.9	94.5	95.9
E	102	57.3	0.725	37.3	81.9	98.7	80.2
F	102	57.3	0.725	34.7	81.9	95.2	78.7
G	102	57.3	1.635	36.4	112.9	97.3	119.7
H	102	57.3	1.635	33.0	99.9	93.4	97.3
J	102	57.3	3.270	35.1	117.9	95.9	139.8

Slab size = 610 x 610 mm; Span = 559 mm

Table 5.2 Slabs tested by Base [8]

Slab No	c (mm)	d (mm)	ρ %	f_{cu} (N/mm^2)	P_E (kN)	$P_{plastic}$ (kN)	$P_{equilibrium}$ (kN)
1A30a24	300	128.0	1.01	32.4	430	380.5	416.7
1A30a25	300	124.0	1.04	30.8	408	357.9	401.8
1A15a5	150	117.0	0.80	32.9	255	274.2	234.7
1A15a6	150	118.0	0.79	32.1	275	275.0	240.5

Slab diameter = 1829 mm; Span = 1710 mm

Table 5.3 Slabs tested by Kinnunen and Nylander [51]

Slab No	c (mm)	d (mm)	ρ %	f_{cu} (N/mm^2)	P_E (kN)	$P_{plastic}$ (kN)	$P_{equilibrium}$ (kN)
S1-60	254	114.3	1.06	29.3	390.0	302.3	317.2
S5-60	203	114.3	1.06	27.8	343.0	274.4	279.9
S1-70	254	114.3	1.06	30.6	393.0	309.4	388.0
S5-70	203	114.3	1.06	28.9	379.0	278.7	342.0
H1	254	114.3	1.15	32.6	372.0	320.7	278.3
M1A	305	114.3	1.50	26.1	434.0	307.8	484.1

Slab size = 1829 mm; Span = 1778 mm

Table 5.4 Slabs tested by Moe [65]

Slab No	c (mm)	d (mm)	ρ %	f_{cu} (N/mm^2)	P_E (kN)	$P_{plastic}$ (kN)	$P_{equilibrium}$ (kN)
SS2	200	77	1.20	29.3	176	164.5	216.1
SS4	200	77	0.92	40.4	194	192.1	205.1
SS6	200	79	0.75	27.4	165	163.4	165.2
SS7	200	79	0.80	38.0	186	193.8	185.2

Slab size = 2000 x 2000 mm; Span = 1892 mm

Table 5.5 Slabs tested by Regan [87]

Slab No	c (mm)	d (mm)	ρ %	f_{cu} (N/mm^2)	P_E (kN)	$P_{plastic}$ (kN)	$P_{equilibrium}$ (kN)
1	60	30	1.20	38.4	32.0	36	42.8
2	60	30	1.20	38.4	33.0	35.9	42.8
3	60	60	1.20	34.1	78.0	86.7	79.0
4	40	30	1.20	38.4	26.0	31.7	34.9
5	60	30	0.50	27.5	18.0	25.7	25.4
6	60	30	1.20	27.7	31.2	25.8	39.4
15	60	30	0.60	31.1	21.1	28.9	28.7
16	60	30	0.90	29.5	26.0	27.4	34.7
17	60	30	1.30	29.5	26.0	27.4	41.7
18	60	30	1.70	29.5	30.0	27.5	47.6
19	60	30	2.10	29.5	30.0	27.5	52.9

Slab diameter = 475 mm; Span = 425 mm

Table 5.6 Slabs tested by Dragosavic and van den Beukel [28]

Slab No	c (mm)	d (mm)	ρ %	f'_c (N/mm^2)	P_E (kN)	$P_{plastic}$ (kN)	$P_{equilibrium}$ (kN)
A1a	254	117.6	1.15	14.1	303	300.0	248.7
A1b	254	117.6	1.15	25.3	366	402.2	287.9
A1c	254	117.6	1.15	29.1	357	430.1	298.1
A1d	254	117.6	1.15	36.9	352	488.9	316.3
A1e	254	117.6	1.15	20.3	357	360.6	272.4
A2a	254	114.3	2.47	13.7	334	285.5	340.8
A2b	254	114.3	2.47	19.6	401	342.7	372.7
A2c	254	114.3	2.47	37.5	468	472.7	438.4
A7b	254	114.3	2.47	28.0	513	410.4	407.5
A3a	254	114.3	3.70	12.8	357	276.7	341.8
A3b	254	114.3	3.70	22.7	446	368.6	394.4
A3c	254	114.3	3.70	26.6	535	399.3	492.4
A3d	254	114.3	3.70	34.6	549	457.5	525.8
A4	356	117.6	1.15	26.2	401	489.0	343.8
A5	356	114.3	2.47	27.8	535	486.4	481.6
A6	356	114.3	3.70	25.1	499	462.0	478.8
B4	254	114.3	0.99	47.8	334	530.2	278.4
B9	254	114.3	2.00	44.0	506	511.1	436.1
B11	254	114.3	3.00	13.5	330	284.5	397.1
B14	254	114.3	3.00	50.7	580	552.4	527.4

Slab size = 1829 x 1829 mm; Span = 1778 mm

Table 5.7 Slabs tested by Elstner and Hognestad [30]

Slab No	c (mm)	d (mm)	ρ %	f_{cu} (N/mm^2)	P_E (kN)	$P_{plastic}$ (kN)	$P_{equilibrium}$ (kN)
1	100	40.5	0.423	38.4	36.42	62.8	56.6
2	100	40.5	0.558	38.4	49.08	62.9	65.1
3	100	40.5	0.691	38.4	56.55	62.8	72.4
4	100	40.5	0.821	43.5	56.18	66.9	78.9
5	100	40.5	0.883	43.5	57.27	67.4	84.4
6	100	40.5	1.026	43.5	65.58	66.9	91.0
7	100	40.5	1.163	37.1	70.94	62.2	93.1
8	100	40.5	1.292	37.1	71.09	62.4	98.1
9	100	40.5	1.454	37.1	78.60	61.9	104.1
10	100	40.5	0.517	37.4	43.59	62.3	62.2
11	100	40.5	0.802	37.4	55.00	62.5	77.5
12	100	40.5	1.107	37.4	67.06	62.1	91.0
13	100	40.5	0.601	42.5	49.39	66.7	69.2
14	100	40.5	0.691	42.5	52.45	66.4	74.2
15	100	40.5	1.994	42.5	84.84	66.3	126.1
2A	100	46.5	0.691	36.0	66.24	72.8	81.0
3A	100	46.5	1.293	36.0	89.72	72.9	110.8
4A	100	46.5	1.992	38.6	97.43	75.5	139.9
3B	100	35.0	1.292	47.1	56.67	58.4	91.0
4B	100	35.0	1.994	38.6	72.52	52.9	107.5
1C	100	53.5	0.423	34.8	62.74	85.9	71.6
2C	100	53.5	0.690	40.5	87.86	93.5	94.9
3C	100	53.5	1.288	40.5	124.14	93.3	129.7
4C	100	53.5	1.993	34.8	125.94	86.9	155.4

Slab size = 700 x 700 mm; Span = 640 mm

Table 5.8 Slabs tested by Rankin and Long [81]

Slab No	c (mm)	d (mm)	ρ %	f'_c (N/mm^2)	P_E (kN)	$P_{plastic}$ (kN)	$P_{equilibrium}$ (kN)
S2075-1	254	120.6	0.75	32.5	291	368.4	251.9
S2075-2	254	122.2	0.75	29.1	273	359.2	248.0
S2150-1	254	124.0	1.50	29.7	464	368.3	357.4
S2150-2	254	122.2	1.50	30.2	441	364.5	354.0
S4150-1	508	125.5	1.50	35.5	581	533.0	534.4
S4150-2	508	125.5	1.50	35.8	582	533.9	545.2

Slab size: S2075 to S2150 = 2134 x 2134 mm; Span = 2032 mm

Slab size: S4075 to S4150 = 2388 x 2388 mm; Span = 2286 mm

Table 5.9 Slabs tested by Criswell [22]

Slab No	c (mm)	d (mm)	ρ %	f'_c (N/mm^2)	P_E (kN)	$P_{plastic}$ (kN)	$P_{equilibrium}$ (kN)
S2-60	254	114.3	1.53 0.84	22.1	357	295.0	330.5
S3-60	254	114.3	2.30 0.54	22.7	365	299.2	364.2
S4-60	254	114.3	3.45 2.65	23.9	334	306.4	450.6
S3-70	254	114.3	2.30 0.54	25.4	379	315.8	377.7
S4-70	254	114.3	3.45 2.65	35.2	375	375.0	600.6

Slab size: S4075 to S4150 = 2388 x 2388 mm; Span = 2286 mm

Table 5.10 Slabs tested by Moe-Concentrated Reinforcement [65]

Slab No	c (mm)	d (mm)	ρ %	f'_c (N/mm^2)	P_E (kN)	$P_{plastic}$ (kN)	$P_{equilibrium}$ (kN)
HSC0	250	200	0.8	90.3	965	1135.3	805.2
HSC2	250	200	0.8	85.7	889	1111.3	794.8
HSC4	250	200	1.2	91.6	1041	1144.0	989.8
HSC6	250	200	0.6	108.8	960	1246.8	730.7

Slab size: HSC0-6 = 2540 x 2540 mm; Span = 2400 mm

Table 5.11 Slabs tested by Hallgren and Kinnunen [39]

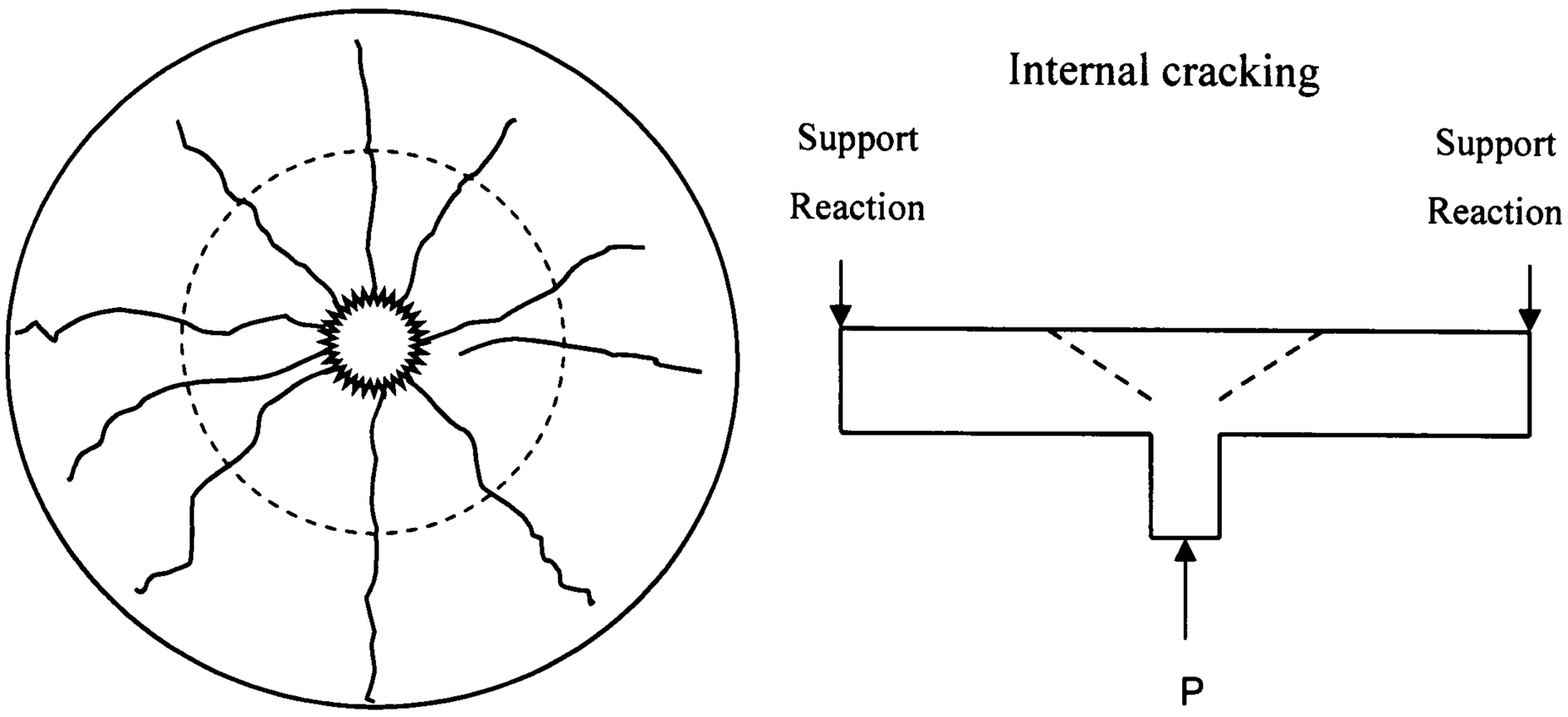

Figure 5.1 Typical test specimen in punching shear

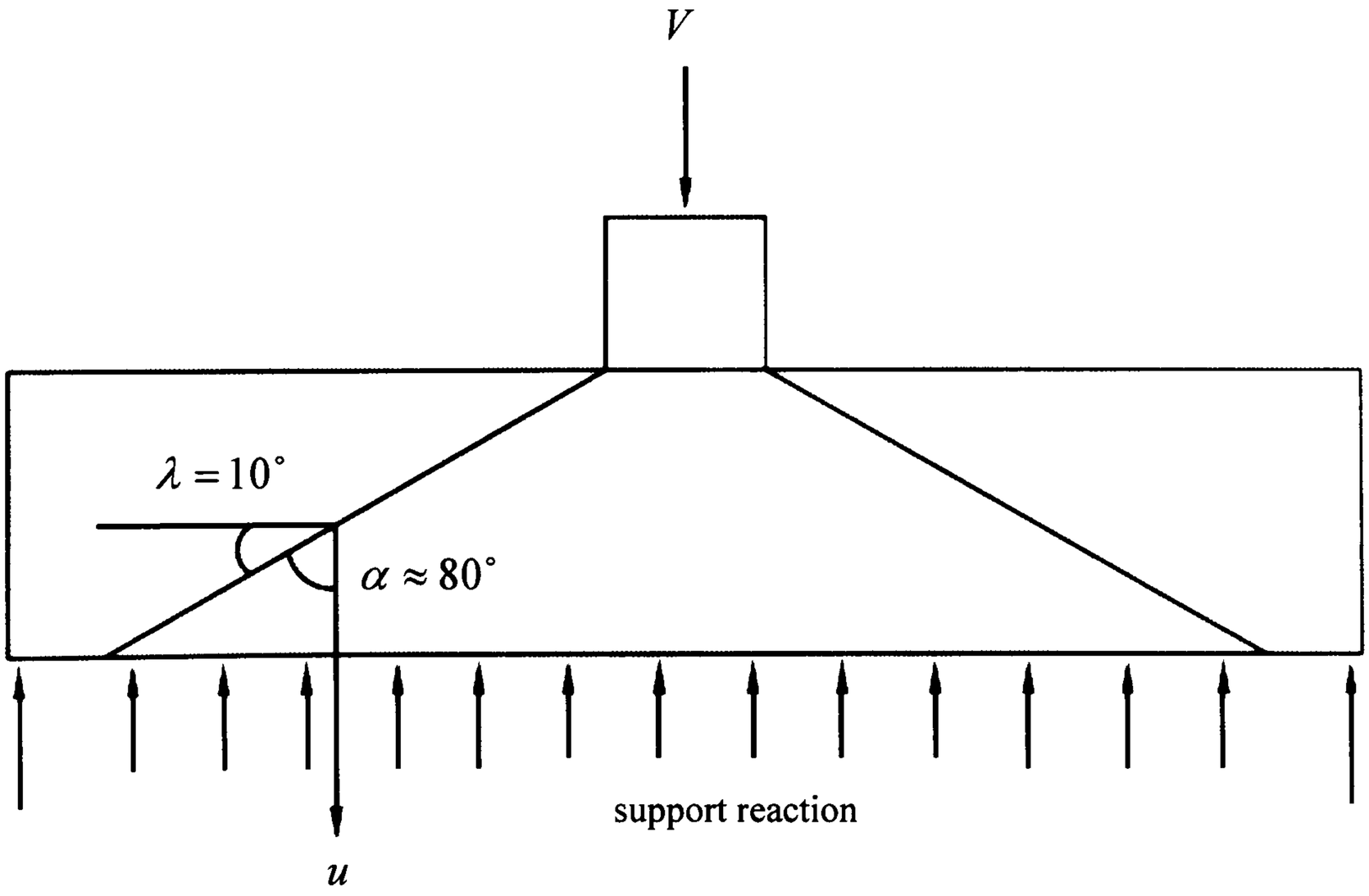

Figure 5.2 Punching shear failure model adopted in plasticity theory

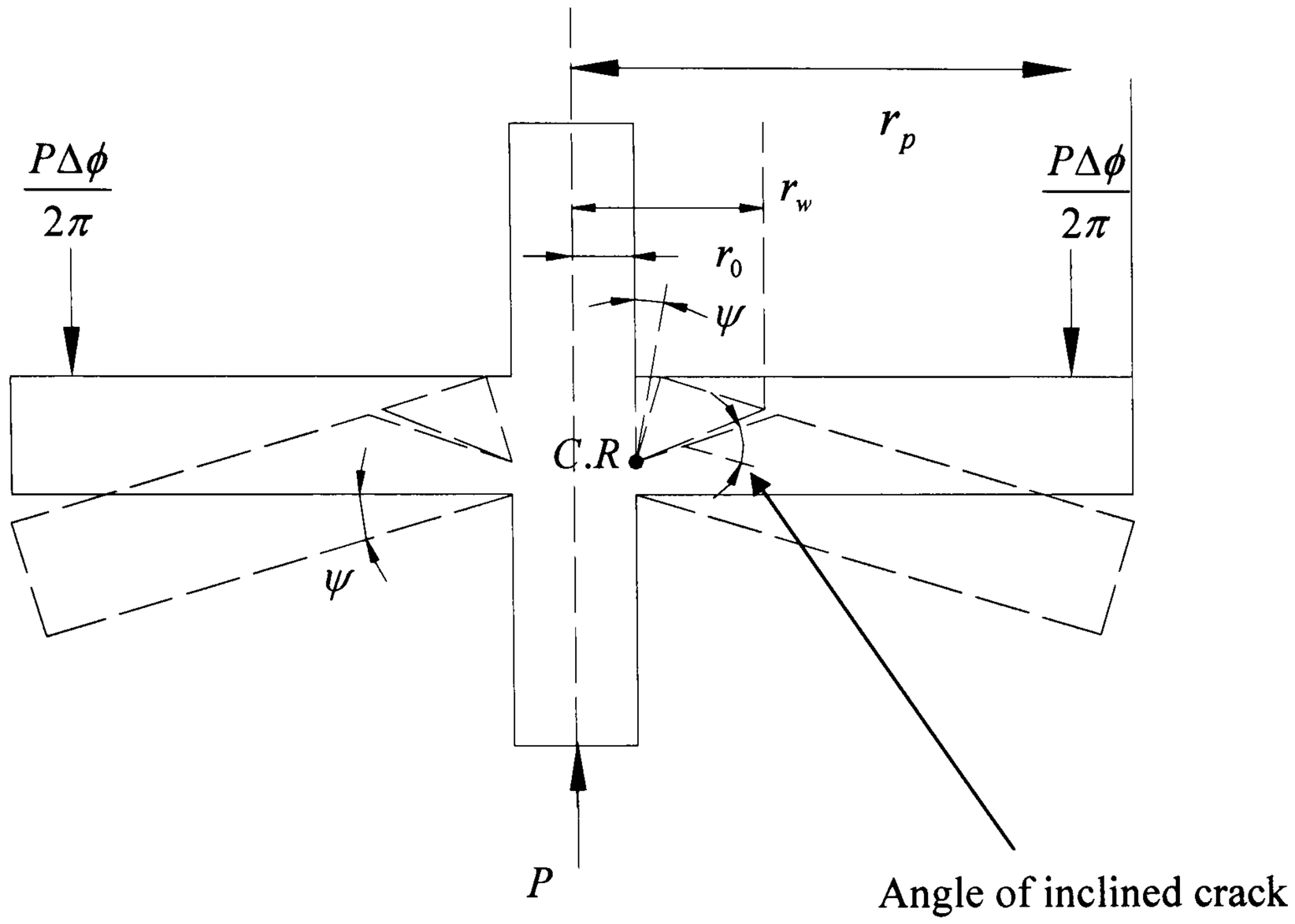

FIG. 5.3(a)

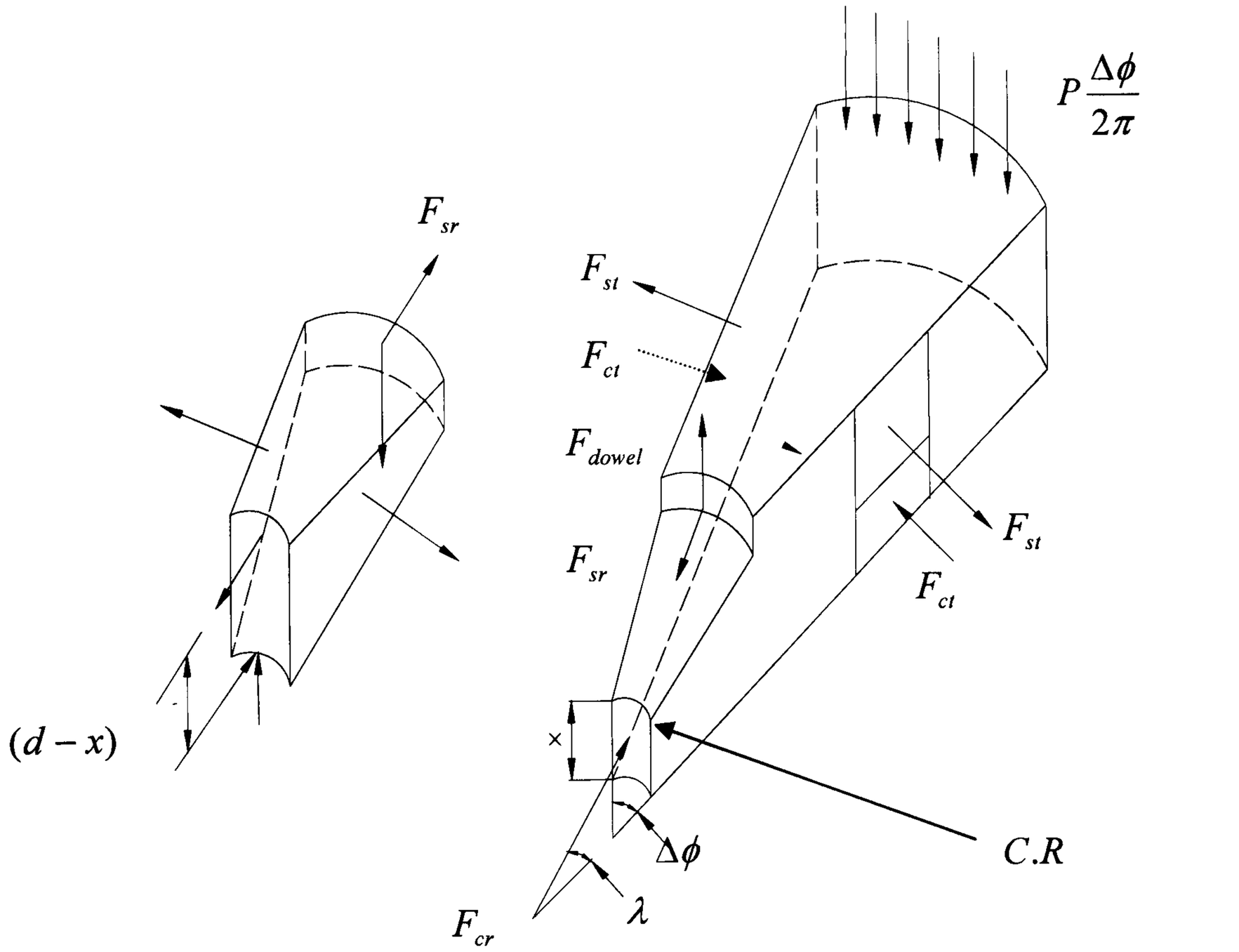

FIG. 5.3(b)

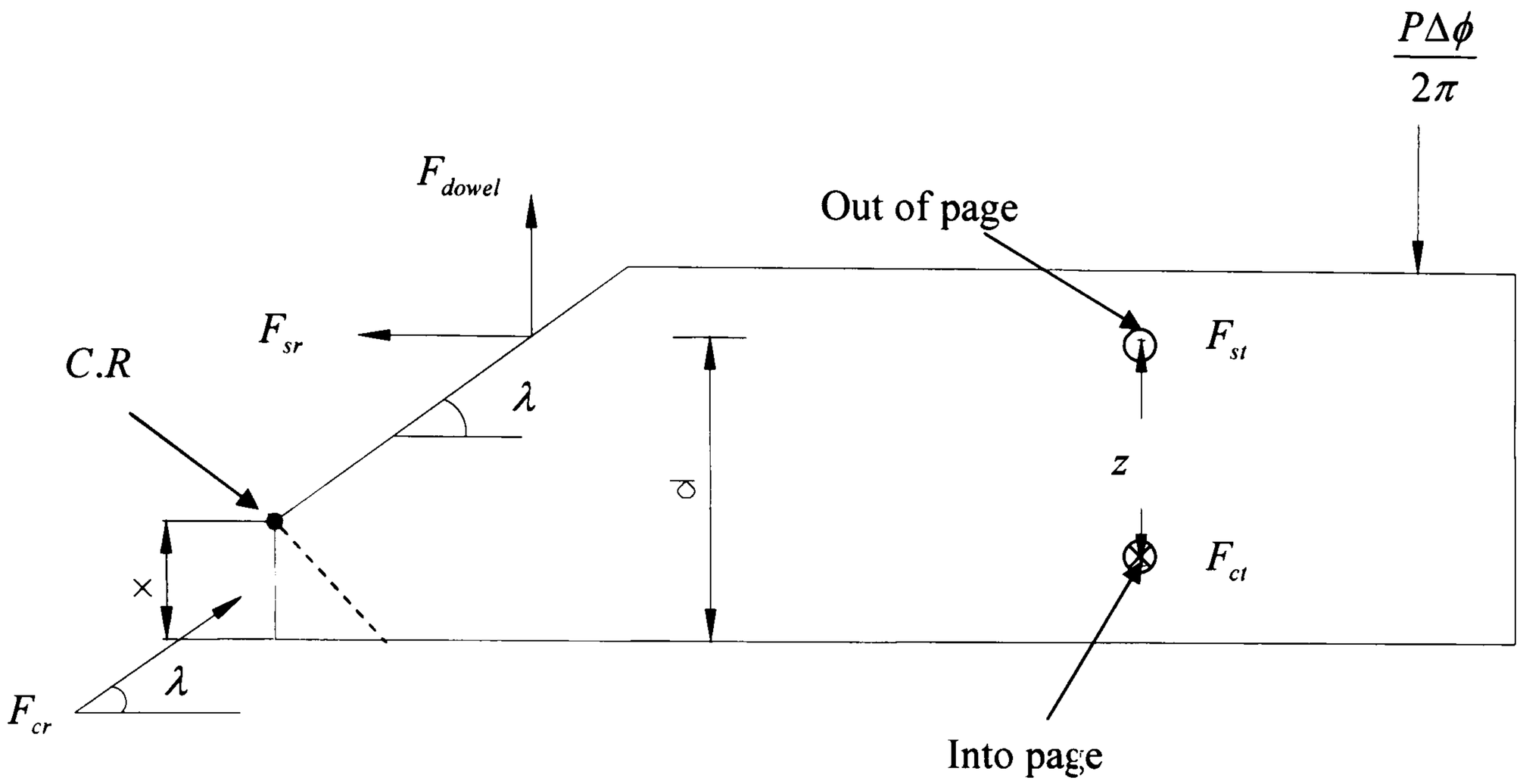

(c)

Figure 5.3 Punching failure model and forces involved

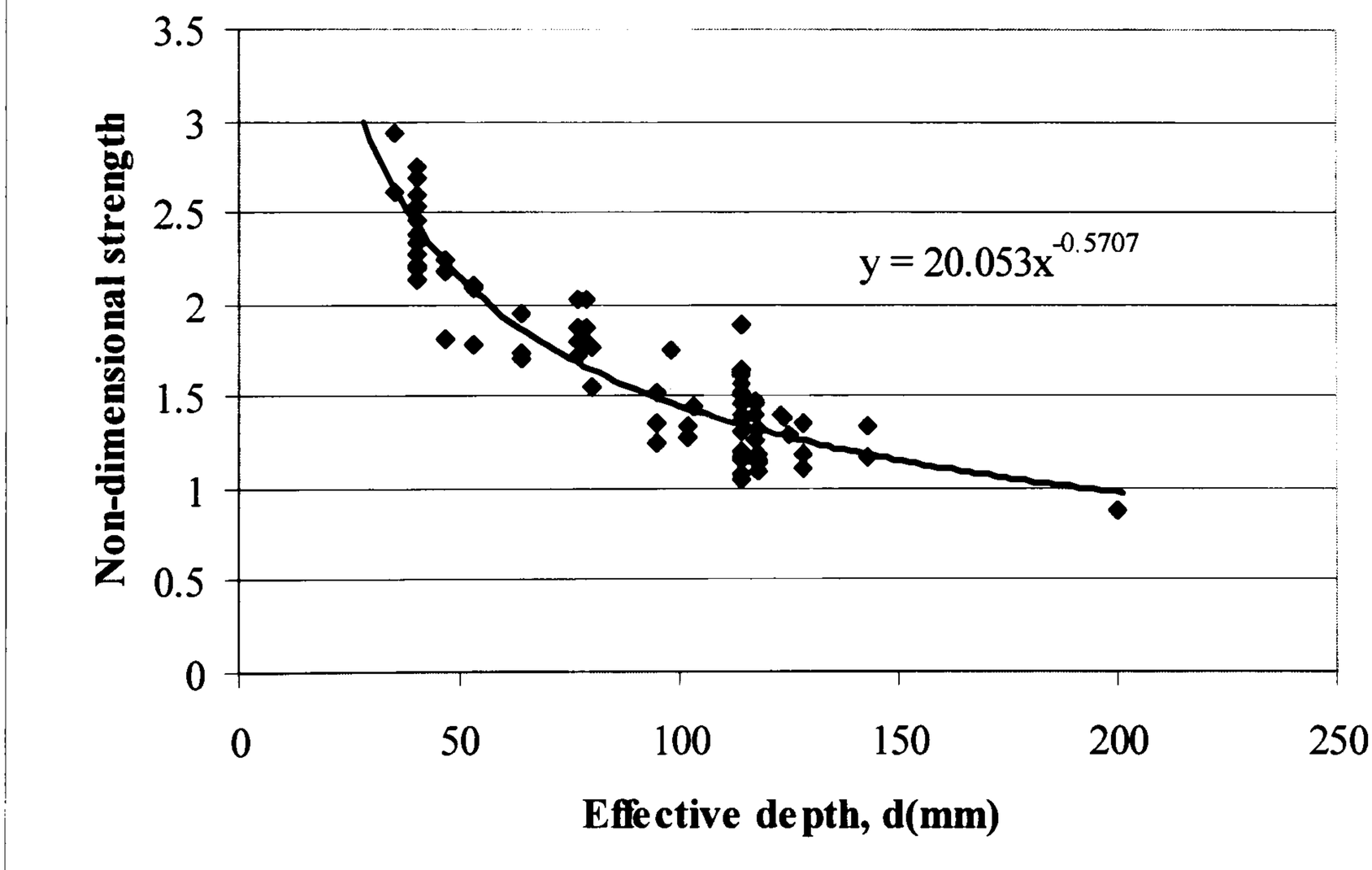

Figure 5.4 Influence of slab depth on punching resistance

6

EXPERIMENTAL PROGRAMME

Chapter Six

EXPERIMENTAL PROGRAMME

6.1 INTRODUCTION

In Chapter 2, it was identified that research into some important aspects of the effect of surrounding restraint on punching failure loads of reinforced concrete flat slabs was still outstanding. In this chapter, experimental work conducted within this PhD study is presented to address the following among these outstanding issues:

- Verification of theoretical predictions against experimental results in terms of both the validity of the *failure surface* as well as the predicted punching failure loads.
- Investigation of the influence of increasing levels of surround restraint on the punch loads.
- Assessment of the effects – on the punching failure surface and load – of the statical indeterminacy of the tested slab along with any asymmetry of the slab due to asymmetric crack patterns developing under load.

The following general ideas have formed the basis of the experimental methodology employed to obtain the results discussed henceforth, namely:

- Use of realistic scale concrete slab specimens utilising a suitable depth of cover concrete.
- Imposition of boundary conditions within the experimental setup which permit reliable knowledge of the critical locations for measurement and visual observation of the failure mechanisms, without unduly altering the failure modes.
- Identification and careful recording of the critical crack patterns and strain profiles, and the use of these patterns and profiles to help explain the influence of different degrees of surround restraint on the punching failure loads of the tested specimens.

In the next section, an in-depth description of the manner in which the above scientific considerations influenced the final details of the test specimens is presented. Afterwards, the experiments, the results of these experiments and the inferences drawn from these results are discussed. Finally, conclusions are drawn on the work presented in this chapter.

6.2 SCIENTIFIC CONSIDERATIONS IN DESIGN OF EXPERIMENTS

6.2.1 General specimen details

The range of types of specimen which can be used for punching tests is quite large, and any reinforced model, in which a failure of the right type can be produced, is a legitimate subject of study. A complete theory would take into account the differences between different models and should be able to be checked, albeit only partially, by comparisons between its predictions and the experimental results from any model. An attempt at a theoretical approach incorporating compressive membrane action has been presented in Chapter 4 which gives reasonably good correlation against other researchers?experimental results.

Further to that work of Chapter 4, the experimental programme reported in this Chapter has been pursued to assess 3 issues, namely: (1) any effects of *loss of axisymmetry* on the actual punch loads and on the validity of the theoretical predictions of both strength and failure surface; (2) the effectiveness of *thin* and *few* steel hoops as substitutes for *considerable amounts* of surround concrete material, thus reducing the slab specimen sizes and so making these specimens more manageable and cheaper in the lab (hence use of the steel hoops as a beneficial research tool). (3) study of the potential for such hoops as effective *shear capacity-enhancers* in practice.

The initial step was to decide upon the geometry of the slab, the specimens being required to be large enough to be realistic but small enough to be tested effectively. A 1.2 m square slab with an overall thickness of 150 mm was deemed appropriate. The slab and reinforcement details are presented in the next section. The design is such

that the slab is loaded through a monolithic stub column at its centre and reacted against corner supports to observe variations in strains, ultimate load and deflections. Corner supports were chosen rather than line supports to achieve lower failure loads together with the consideration that the test rig cannot support loads higher than 500 kN. The plan dimensions of each corner support were arrived at by consideration of shear failure at those supports. This led to a 150 mm square-in-plan support at each corner with the support reaction being 25% (assuming axi-symmetric distribution of stiffness in the slab) of the applied load hence the danger of punching at the reaction points was avoided. For the collected data to be judged realistically with minimum scaling effects, a 1.2 m square slab was chosen with a thickness of 150 mm, a little on the thin side for a real building but nonetheless within real bounds. The stub column needed to be kept small in order to retain the punching problem so 150 mm square was deemed appropriate. The stub was introduced as a monolithic feature through which the load is applied. A circular slab of slightly higher plan dimensions was also tested.

6.2.2 Degree of Indeterminacy

Given the support conditions, the slab is statically indeterminate. If we assume axisymmetry of both the structure and the load, then all support reactions are equal. However, as shown later in this chapter, the failure crack pattern, and hence the structure, can deviate from this axisymmetry at the higher loads. Differential vertical stiffnesses between the supports would also introduce asymmetry to structural action. This is because differential stiffness between supports can result in redistribution of reactions between supports, which in turn give deviation from axisymmetry in the failure behaviour of the slab. The influences of this behaviour on the failure *surface* and on the failure *load* (especially regarding comparisons between theoretical and

measured) are of interest.

This possibility was recognised before the tests were done, and a decision was initially made to place a load cell at one support, to render the structure statically determinate. However, when this was attempted, the test set-up showed signs of instability and so for safety reasons this idea was abandoned. The later discussions show that *study* of the influences of lack of symmetry on the failure surface and load was only *mildly* inhibited by this inability to use a load cell at a support.

6.2.3 Degree of Surrounding Restraint

The theory for compressive membrane action is fairly well developed and the main concern devotes to the ability of quantifying the restraint properly. Some work has focused on the influence of the degree of restraint by restraining the specimens laterally to simulate the practical surrounding boundary conditions. However, it is believed that the inherent stiffness of the slab should also provide this restraint which stimulates the idea of introducing circular steel hoop reinforcement as a mean of providing surrounding restraint in the present research. By varying the amount of hoop steel reinforcement, the limits beyond which little or no further enhancements on punching capacities are obtained can be established. If a threshold value of surround stiffness does exist and this threshold is small, then there is a real potential for such hoops to be used as shear capacity-enhancers in practice – particularly useful for edge columns. On the other hand, it would be interesting to establish an understanding of the influence of surround restraint provided by surround concrete material *alone* as opposed to the use of steel hoops reinforcement. Hence, the motivation of introducing a final specimen with ratios of surround material to punch radius of 1.8 as shown in Figure 6.1.

The final specimens used in the present study incorporated strong features of all the above important considerations, whilst inevitably having to allow for some small constraints imposed by existing laboratory space and facilities. The crucial statistics of many of these lab specimens tested in the present study can be summarised as follows:

- Plan dimensions of 1200 mm x 1200 mm for square slabs ;
- A plan radius of 1800 mm for the circular slab ;
- An overall thickness of 150 mm ;
- Varying concrete cube strengths of 40 MPa – 60 MPa ;
- Steel reinforcement ratios of 1.06% (square specimens) and 0.89% (circular specimen) ;
- A column size of 150 mm square for square specimens and 175 mm circular for circular specimen ;
- Supports were kept at same locations relative to central stub column for all specimens in order to avoid introducing another variable here ;
- Varying the degree of surrounding restraint by means of incorporating steel hoop reinforcement for square specimens ;
- Introducing the surrounding restraint by means of providing extra surrounding material outside the critical punch out zone for circular specimen ;
- A 25mm depth of cover concrete ;
- A Span-to-depth ratio of 6.7.

6.3 TEST SPECIMENS

Details of the five slab specimens, including four square specimens of dimensions 1200 x 1200 x 150 mm and 1 circular specimen of dimensions 1800 diameter x 150 mm are presented in Table 6.1. The plan view and cross section of a typical specimen are shown in Fig. 6.3(a) for the square specimen and in Fig. 6.3(b) for the circular specimen. The experimental model consists of a typical slab-column system, with the slab supported on four corners. Corner supports were chosen so that a lower failure load can be anticipated and due to the limitations that the loading frame cannot support loads which exceed 500 kN. To simulate the possible in-plane restraint, the first 4 specimens were cast internally with hoop reinforcement (Fig. 6.2). The different degrees of restraint were provided by having three different numbers of layers of hoop reinforcement. As for the final specimen, extra surrounding material was provided with a total surround restraint stiffness as much as 2.7 times to that of specimen S1.

In this investigation, the major variable was devoted to the degree of restraint provided by having different numbers of layers of steel hoop reinforcement which ranges from 0 (control specimen) to 3.

6.4 MATERIALS AND FABRICATION OF MODELS

6.4.1 Model Concrete and Reinforcing Steel

The concrete used was supplied by the local ready-mixed plant. The mix resulted in cube strengths ranging from 40 MPa to 63 MPa measured on both 150 x 150 x 150 mm and 100 x 100 x 100 mm cubes at a test age of 28 days.

12 mm diameter steel, suitable for the desired scale modelling work, was used in the slab panels with an average yield strength of 500 N/mm^2. Hoop reinforcement was provided by 10 mm diameter mild steel bars with an average yield strength of 250 N/mm^2.

6.4.2 Specimen Fabrication

The formwork for the square specimens was constructed using plywood whereas steel formwork was used for the circular specimen. The formwork consisted of a flat base, stiffened underneath, on which the detachable side forms were bolted. Details of the mould for the specimens are shown in Fig. 6.4(a) and Fig. 6.4(b).

For all the models, the formwork was given a light coating of mould oil before any concrete was poured. This facilitated easy removal of the specimen once the concrete had cured sufficiently.

After the cutting and bending of the reinforcing bars to their desired lengths, they were assembled and positioned within the formwork by means of plastic and concrete spacers to ensure accurate control of the effective depth at the slab section. Afterwards, spring binding clips were employed to achieve a rigid reinforcing mesh. Four lifting sockets were installed symmetrically to allow lifting of the concrete specimens after curing.

During the casting stage, two vibrating pokers were used for compaction and a steel float was used to achieve a smooth surface finish. The concrete was then covered with hessian and plastic sheet and allowed to cure for a desired period.

6.4.3 Material properties

In order to obtain accurate knowledge of the material properties, careful monitoring of sample specimens was required. In the case of reinforcement, tensile testing was frequently carried out particularly as a consistency check between different bundles of steel.

For the measurement of concrete compressive and tensile strength, cubes and cylinders were used respectively. While ideally the specimens?sizes should perhaps be scaled in the same proportion as the model in the prototype, in practice very small samples tend to exhibit higher strengths due to the effect of aggregate size and of machine stiffness being relatively large. Suitable sizes for which this trend was not expected were 100 mm cubes and 100 mm x 200 mm cylinders. For each specimen, at least three cubes were made. Owing to the relationship $(f'_c = 0.8 f_{cu})$, it was not adjudged necessary to cast cylinder specimens for each model.

6.5 TEST APPARATUS

The test rig for the slab models are shown in Fig. 6.5(a) for square specimens and 6.5(b) for the circular specimen. The slab was placed on four steel pedestals at the corners. Loading was applied at the geometric centre of the slab by a stiff screw jack with capacity 1000 kN, through an 150 mm square or circular, 20 mm thick steel plate, simulating a concentrated load.

6.6 INSTRUMENTATION

6.6.1 Measurement of Load

An accurately calibrated 500 kN load cell was used to take measurements and provide a direct indication of the load from the data logger. The load cell was located between the mechanical jack and the loading plate.

For all the slab specimens, care was taken to ensure that the load was applied at the precise location intended, which was marked out before testing. In addition, a 150 mm diameter spherical seating was included to minimise any possible eccentricity of the loading apparatus. A view of the loading arrangement is shown in Fig. 6.6.

6.6.2 Measurement of Deflection

For all the slab specimens tested, deflections were measured along the central line. A particular type of measuring device named the "Draw Wire" displacement transducer was preferred to conventional LVDT due to an exceptionally large travelling distance which made precise measurements possible even under large deflections. Displacement transducers were clamped firmly to rigid supporting frames with the tips of the drawing wires placed in contact with the slab. Fig. 6.7(a), (b) exhibit the arrangement of displacement transducers on the models.

6.6.3 Measurement of Strain

For most of the slab specimens tested, strains in the steel reinforcement were measured at the positions shown in Fig. 6.8. Electrical resistance strain gauges (TML

Type FLA-2-11 mm) as shown in Fig. 6.9, were used to measure the strain profile of reinforcement around the central and exterior areas. All the ERS gauges were bonded to the surfaces of the carefully prepared steel bars using a suitable adhesive. A layer of elastomeric coating was added over the gauges for waterproofing and protection from damage during fabrication.

6.6.4 Data Acquisition

The readings of the load cell, transducers and electrical strain gauges were monitored and recorded by means of an electric data acquisition system. This system has a display with front panel controls and a built in paper-strip. The data logger proved invaluable due to the large number of measurements involved. Fig. 6.10 shows the data logger and instruments in place before commencement of a test, and an overall view of a slab specimen in position ready for the testing can be seen in Fig. 6.11.

6.7 SPECIMEN PREPARATION AND TESTING

6.7.1 Preparation for Testing

After removal of the formwork, the slab specimens were painted with a thin coat of white emulsion to facilitate crack detection during testing. The subsequent placing of the model into the test rig was achieved as described below:

The slab was lifted up and carefully positioned on the pedestals by means of a crane, which was attached to lifting hooks embedded in the slab. With the specimen in position, the precise location of the deflection measuring apparatus was marked out.

The instrumentation was then installed and assembled and finally connected to the data acquisition system, leaving the model ready for testing.

6.7.2 Testing Procedure

After the measuring equipment had been accurately and firmly installed, initial readings from all the bits of instrumentation were recorded at the unloaded stage. Loading was initially applied to the specimens in increments of 50 kN, reducing to 10-20 kN increments near failure. After each increment, any new crack patterns on the plan and sides of the slabs were marked out, and the deflection and rebar strain data were recorded onto the data logger system. Once the slab was punched, the test terminated.

6.8 PRESENTATION AND DISCUSSION OF TEST RESULTS

All the slab panels failed in a punching shear mode as shown in Figs. 6.12(a) to 6.12(e). In this section, physical observations and experimental measurements are presented and discussed in general terms, to promote a clear understanding of the punching shear behaviour, compressive membrane action and its effect on punching load capacity of restrained reinforced concrete slabs. A summary of the test results of all the specimens is presented in Table 6.2. Comparisons are made between the test strengths and the predictions of proposed analysis presented in Chapter 4 and design codes.

6.8.1 Slab Cracking

Initial cracking on the bottom surfaces occurred at an early stage of load application. The formation of flexural cracks started at a load of approximately 25% to 45% of the corresponding ultimate load, depending on the amount of steel reinforcement and the degree of restraint. The cracking initially formed on the underside of the slab, and then developed as a series of radial cracks from the central loaded area. As the load increased so did the widths of the cracks.

In the strongly restrained slab specimen S4, the cracks were fine but large in number (Fig. 6.13) whereas wider but fewer cracks formed in a weakly restrained slab S2 (Fig. 6.14).

In general, the crack widths of all the slabs were small until near the failure load. The typical discontinuity on the top surface of the slabs after shear failure is shown in Fig. 6.15. No crack was seen around the periphery of the loading plate until failure.

6.8.2 Slab Deflection

The variations of the slab deflections with the applied load are shown in Fig. 6.16. This shows the central deflections of the five sets of slabs with different degrees of restraint, including one control specimen (S1) with no restraint provided. From this Figure, it was noted that the deflections were relatively similar for the all the specimens considered in this study irrespective whether they were restrained or not. Therefore, it would appear that compressive membrane forces do not play an important part in the control of slab deflection.

6.8.3 Reinforcement strain

Typical radial strain variations of steel at different loading stages are shown in Fig. 6.17. Load-strain curves for the steel reinforcement under the periphery of the loaded area are shown in Fig. 6.18. Fig. 6.18 indicates that the steel has yielded at failure around the column area for all five specimens considered in the present study. An additional strain gauge (G6) was positioned as indicated in Fig. 6.8 which shows that the steel is close to the yielding point (Fig. 6.19). Therefore, it is reasonable to predict that the slab is undergoing an elasto-plastic stage where the punching radius is greater than the radius within which all steel is yielding.

In addition, smaller strains were exhibited in the slabs restrained by more hoops than in the weakly restrained ones. However, reinforcement generally reached yield point before failure at between 70% and 90% of ultimate load. This is one fact which may be considered to contribute to the justification for the use of plastic theory to prediction of punching failure loads in steel-reinforced concrete flat slabs.

Load-strain curves for the hoop reinforcement are shown in Fig. 6.20-6.22. Fig. 6.20 indicates that the hoop steel has nearly yielded for Slab 4 with the strongest restraint. Tensile strains in the hoop steel suggest compressive membrane restraint to the enclosed concrete as per the diagram at the bottom right of Fig. 6.20. Fig. 6.21 indicates that the hoop steel for Slab 4 has gone from tensile to compressive strains at failure. Fig. 6.22 indicates that the hoop steel has again undergone a transition from tensile to compressive regime at a load of approximately 290kN which was in fact the failure load of Slab 2 with one hoop. This clearly showed signs of the existence of compressive membrane forces.

6.8.4 Ultimate Load Capacity

A summary of the test results and the comparisons between the experimental strengths and the ultimate loads predicted by both the proposed plasticity analysis as well as the design codes is presented in Table 6.2, where the non-dimensional punching shear strength of each specimen is also given, calculated by dividing the corresponding ultimate punching loads by the product of the compressive strength of concrete and the critical surface located at half the effective depth away from the perimeter of the load. The Table shows that the plasticity approach gave reliable predictions against the present experimental results. In particular, it is important to note that the plasticity approach appears to be capable of predicting the levelling-off effect on the punch loads at 3 hoops (Figure 6.23(a)). BS 8110 gave decent predictions, while the ACI code gave significant underestimates of failure load.

6.8.5 Effect of surrounding restraint

Table 6.1 shows that there was a definite increase in ultimate punching load of the slab panels as the degree of restraint increased. This trend is very evident in Fig. 6.23 which shows the corresponding enhancements of ultimate non-dimensional strength. Figure 6.23(a) shows that the load-carrying capacity increased significantly from 1 to 2 hoops, tending to flatten out in 3 hoops. An increase of 38% of non-dimensional capacity occurs in proceeding from 1 to 3 hoops. This reveals that the restraint provided by the hoop reinforcement has a significant effect on the ultimate punching load of reinforced concrete slabs, resulting in promotion of shear resistance in the slabs and enhancing effectively the load-carrying capacity. Fig. 6.23(b) also shows that Slab 5 failed at a similar punching load to that experienced by Slab 1, bearing in mind that

Slab 5 exhibits approximately 2.7 times total surround restraint stiffness than that of S1. This explicitly suggests that concrete strength and percentage of reinforcement are important parameters to be considered in future research.

6.8.6 Comparison with Proposed Plastic Analysis and Design Codes

The ratios of the experimental strengths to the predicted values using the plastic analysis and the code-specified methods for each specimen are listed in Table 6.2. It can be seen that the predictions made by using the plastic analysis showed extremely good correlation against experimental results conducted within this PhD study. In addition, Table 6.3 shows a comparison between the predicted and experimentally observed diameters of the punched-out cones. The comparisons are reasonable in the main, except for slabs S4 and S5, which show much higher diameters than those predicted.

The level of success achieved via the use of plasticity theory to prediction of punching capacities was demonstrated earlier in Chapter 3 and Chapter 4 for both cases of slabs with and without membrane restraint. The essence of plasticity theory lies in 2 major assumptions namely: the use of appropriate sets of effectiveness factors and an assumed failure mechanism. The first factor was already discussed in detail earlier in Chapter 3 and the remainder of this section aims to verify the assumption of the axi-symmetric failure profile employed in the plastic theory. The failure surface obtained from the specimen was shown in Fig. 6.25(a) and (b). A series of points were taken and measured along the failure surface of the specimen to form a comparison with the assumed theoretical failure surface as shown in Fig. 6.26(a), 6.26(b) and 6.26(c). It

can be seen that the experimental failure surface observed from the specimen indicated an asymmetric profile of the failure surface which contradicted the assumptions of a symmetric failure surface made in the plastic analysis. Potential contributing factors to this profile as discussed earlier in section 6.2.2 include differential flexibilities of the supports which hinder the uniform distribution of forces to the four supports, as well as possible variation on concrete material properties throughout the slab. It is important to note that despite a disparity between the predicted and measured failure surface, a good comparison between the predicted and measured failure loads was still achieved. Therefore, the application of plasticity theory to prediction of punching failure loads of reinforced concrete slabs was still considered satisfactory.

The code-specified strength of the specimens was also calculated according to the British and American codes using the following expressions, from which the partial safety factor $(\gamma_m = 1.25)$ in BS 8110 and capacity reduction factor $(\phi = 0.85)$ in ACI 318 have been removed:

$$P_{BS8110} = 3.16 \cdot \sqrt[3]{100\rho} \cdot \sqrt[3]{\frac{f_{cu}}{25}} \cdot \sqrt[4]{\frac{400}{d}} \cdot (c + 3d) \cdot d \qquad (6.1)$$

for BS 8110, and

$$P_{ACI318} = 1.33 \cdot \sqrt{f'_c} \cdot (c + d) \cdot d \qquad (6.2)$$

for ACI 318-89.

It can be seen from Fig. 6.24 that no code-specified method predicts an enhancement in punching shear strength of a restrained concrete slab with an increase in the degree of restraint provided by hoop reinforcement, with BS 8110 providing

predictions closer to the reality than does ACI 318-89. In reality, there is a definite enhancement in punching shear strength as the degree of edge restraints increases. The codes do not give accurate predictions of the punching shear capacity of restrained slabs, and in the view of the magnitude of the strength enhancement, it would evidently be beneficial if the effect of compressive membrane action could be allowed for in design codes.

6.9 CONCLUSIONS

Five reinforced concrete slab specimens, including four 1.2 m square and one 1.8 m specimens have been fabricated and tested to failure. The parameters varied between the specimens include the degree of surrounding restraint simulated by incorporating steel hoop reinforcement for the case of square specimens, and by introducing extra surround concrete material outside the critical punch out zone. All slabs failed in a punching shear mode.

From the physical observations made and data collected during the experiments, the following general points may be made:

- All the restrained reinforced concrete slabs together with one control specimen, failed in a punching shear mode when subjected to concentrated loading.

- Compressive membrane forces were developed in the slabs due to the in-plane restraint given by the hoop reinforcement (Slabs 2-4) as well as the surrounding restraint (Slab 5). This is deduced from the strain readings obtained from the hoop reinforcement followed by enhancement in load-carrying capacities.

- The degree of restraint has a significant effect on ultimate punching load of a concrete slab, resulting in a greater promotion of shear resistance in the slab and enhancement of the load-carrying capacity. The magnitude of the strength enhancement depends on the degree of restraint – the stiffer the restraint, the higher the enhancement but only up to a certain threshold number of hoops

beyond which there is little, or no further increase in punching load as indicated by Fig. 6.23.

- The use of plasticity theory for prediction of punching failure loads resulted in good correlation against experimental results. Most importantly, a good correlation between the predicted and measured failure loads was achieved despite the disparity between the predicted and measured failure surfaces.

- The measured experimental strengths of the specimens are significantly greater than the code predictions. The enhanced punching shear strengths of the specimens are presumably attributable to the development of compressive membrane action. Present code methods underestimate the punching load capacity of the specimens, as no account is taken of the considerable enhancement due to the in-plane restraint.

- The introduction of a final circular specimen with a total surround stiffness equivalent to a ratio of surround to punch radius of 1.8 resulted in punching strength sufficiently close to tested value of specimen S1 despite having lower concrete strength and percentage of steel reinforcement.

Slab	f_{cu} (MPa)	f_y (MPa)	d (mm)	ρ (%)	c (mm)	P_E (kN)	no. of hoops
S1	63.0	500	113	1.06	150	369.4	0
S2	52.0	500	113	1.06	150	290.6	1
S3	56.0	500	113	1.06	150	402.2	2
S4	53.0	500	113	1.06	150	394.1	3
S5	40.0	500	113	0.89	175	372.4	2.7 times total surround restraint of S1

Table 6.1 Restrained slabs tested by the author

Slab	f_{cu} (MPa)	f_y (MPa)	d (mm)	ρ (%)	P_E (kN)	$\frac{P_E}{d\rho f_{cu}}$	$\frac{P_E}{P_P}$	$\frac{P_E}{P_{BS8110}}$	$\frac{P_E}{P_{ACI}}$
S1	63.0	500	113	1.06	369.4	4.90	1.00	1.11	1.32
S2	52.0	500	113	1.06	290.6	4.67	0.84	0.93	1.14
S3	56.0	500	113	1.06	402.2	6.00	1.00	1.26	1.52
S4	53.0	500	113	1.06	394.1	6.21	1.06	1.26	1.53
S5	40.0	500	113	0.89	374.2	9.30	0.99	1.32	1.53

Table 6.2 Details of slab models and predictions

Slab Model	Measured punched out cone diameter (mm)	Predicted punched out cone diameter (mm)
S1	1000	1027
S2	1000	1027
S3	900	1027
S4	800	572
S5	800	582

Table 6.3 A comparison between experimental and predicted punched out cone diameter

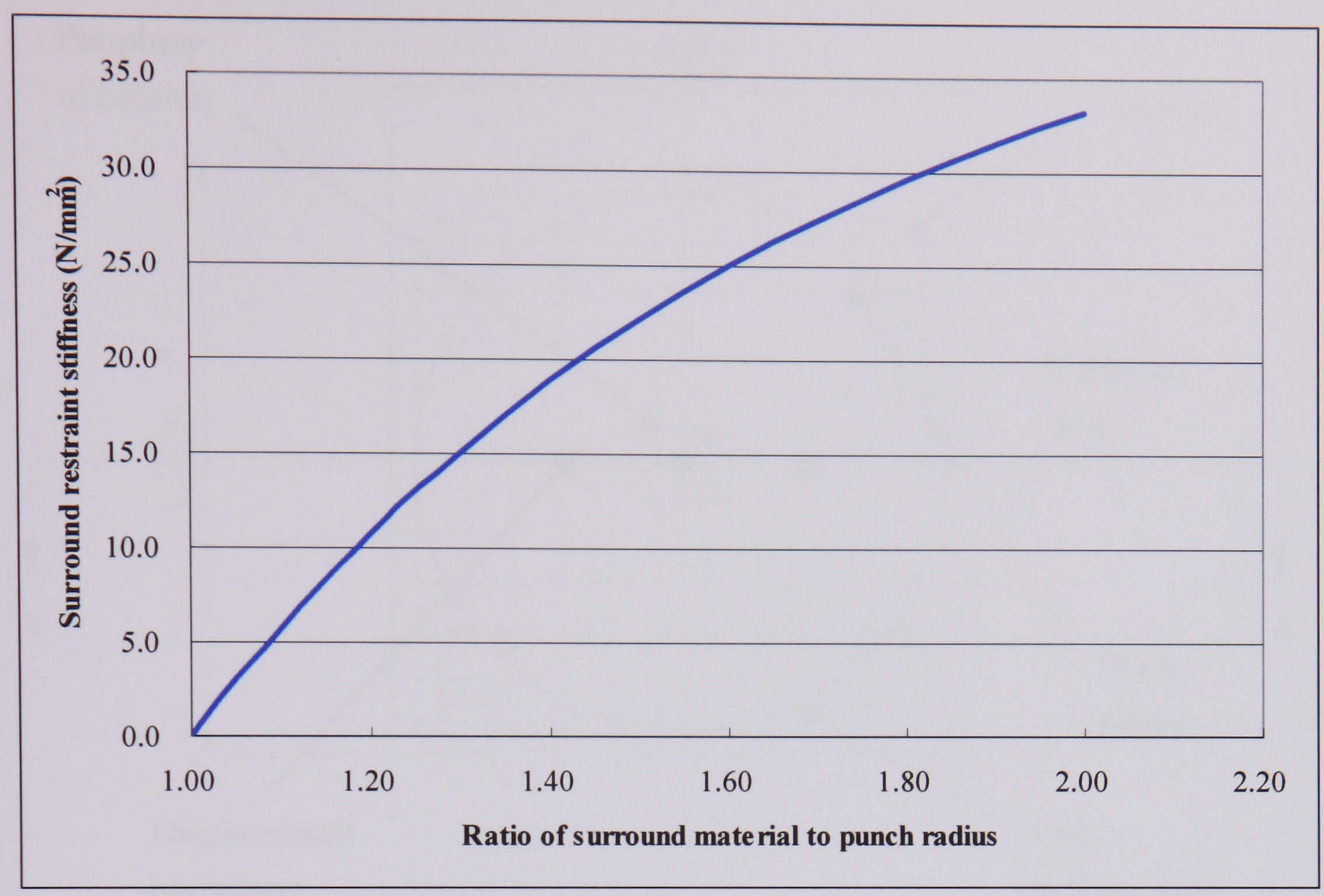

FIG. 6.1 Membrane restraint stiffness provided by surround concrete material

FIG. 6.2 Hoop reinforcement

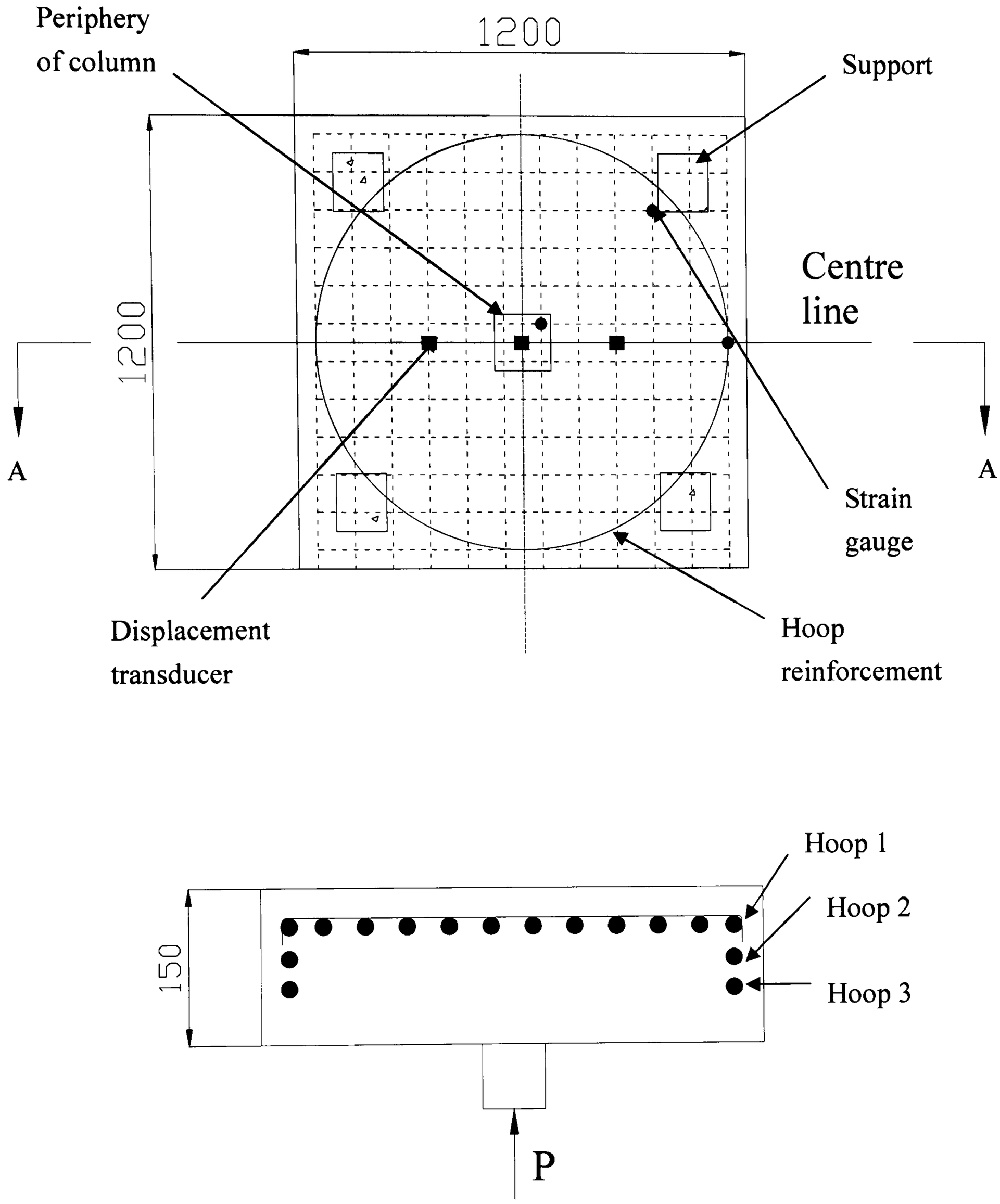

Spacing between hoop 1 and 2 = 25mm

Spacing between hoop 2 and 3 = 25mm

FIG. 6.3(a) Plan view and cross-section of typical specimen (S1-S4)

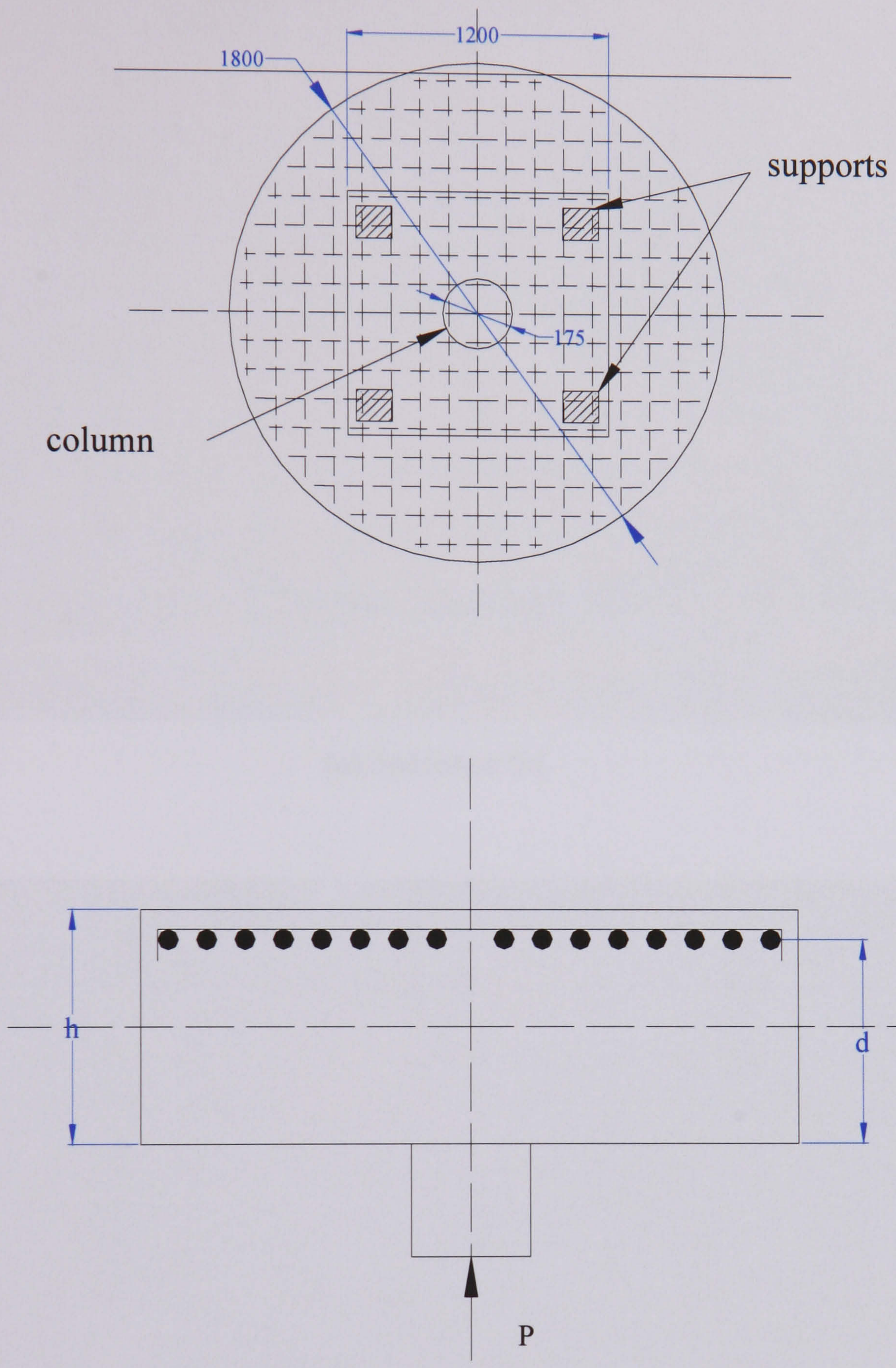

$h = 150mm$

$d = 113mm$

FIG. 6.3(b) Plan view and cross-section of specimen (S5)

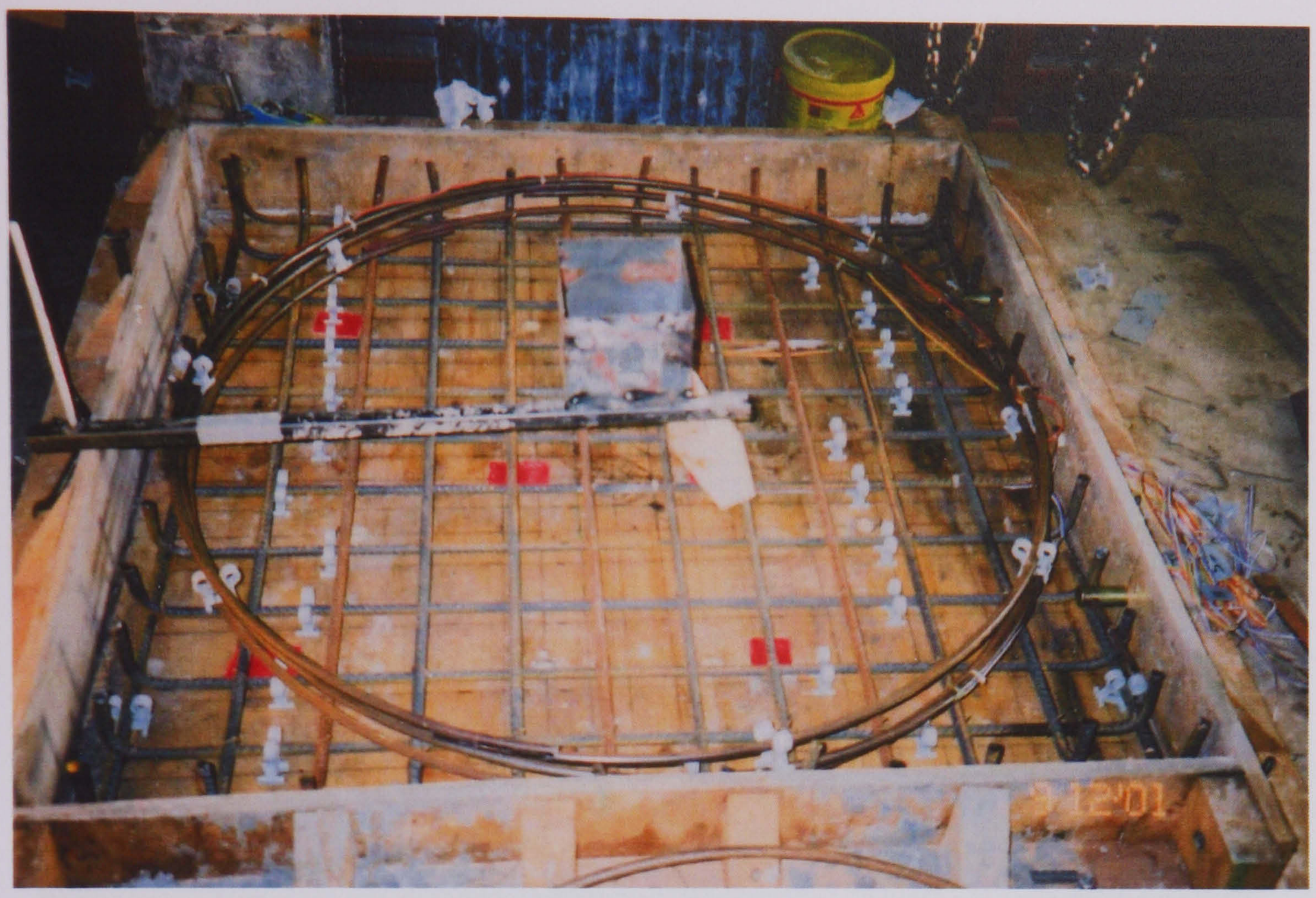

(a) Specimen S4

(b) Specimen S5

FIG. 6.4 Mould for specimens

(a)

(b)

FIG. 6.5 Test rig

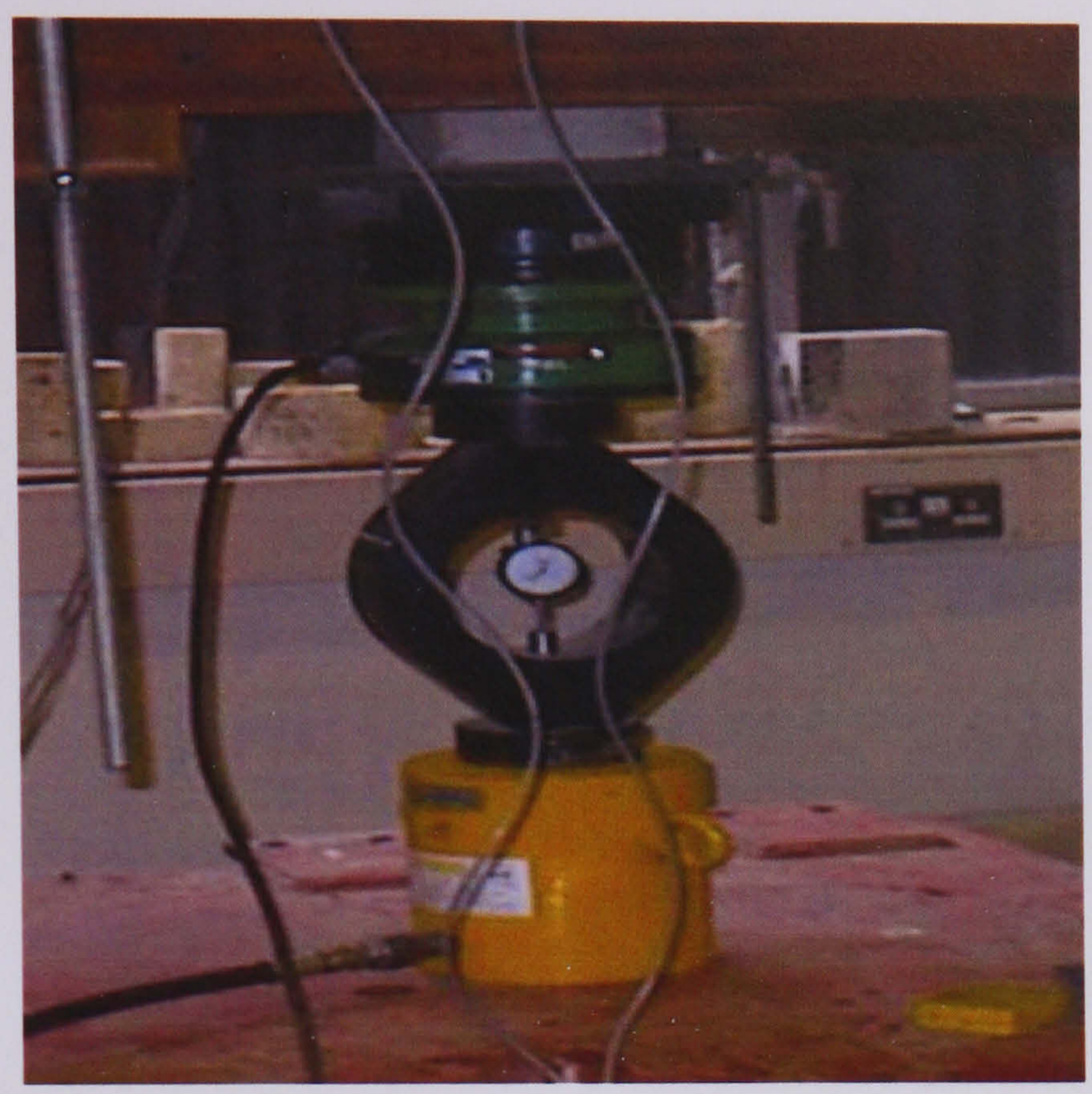

FIG. 6.6 Loading configuration

(a)

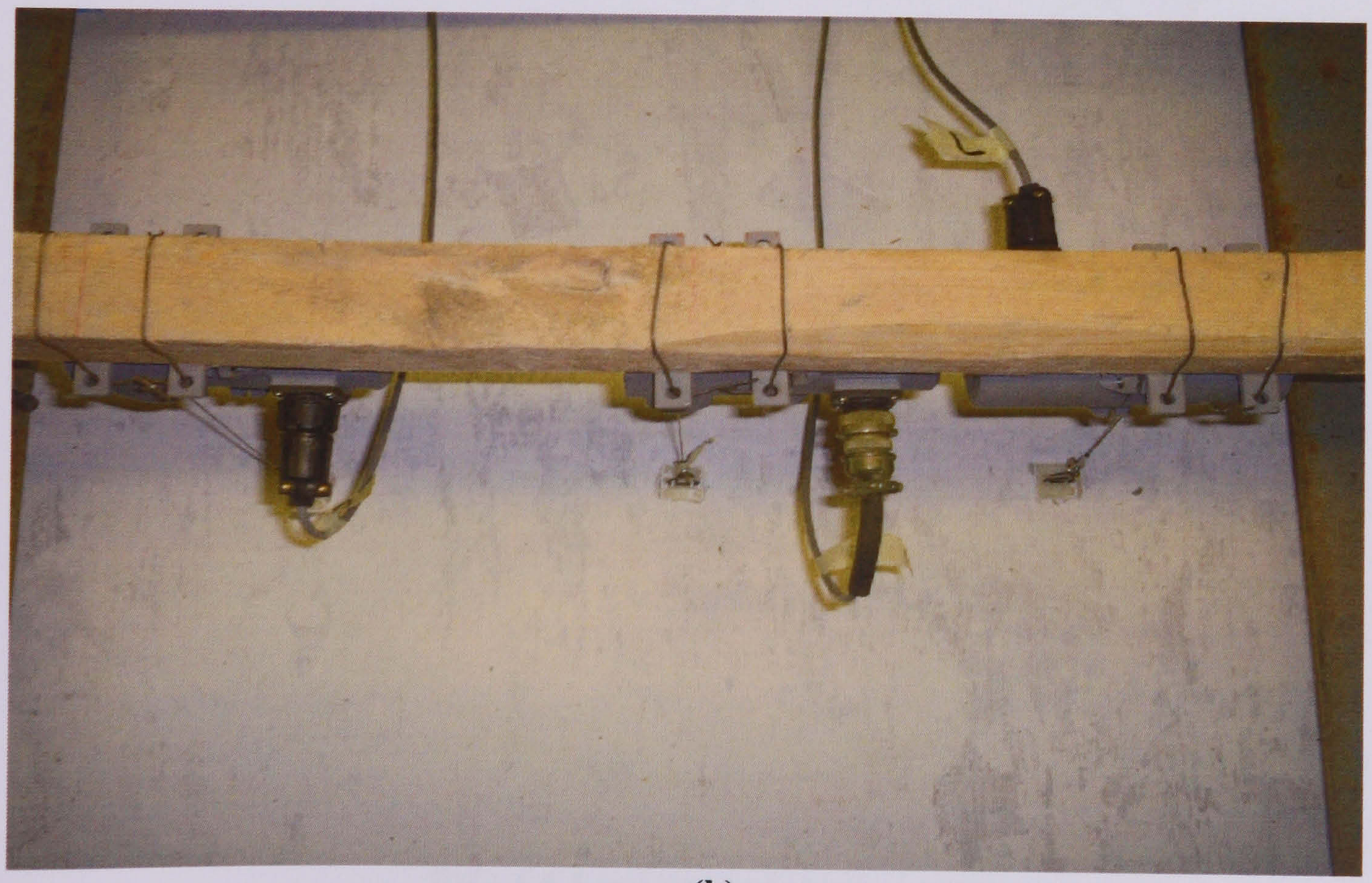

(b)

FIG. 6.7 Displacement transducers

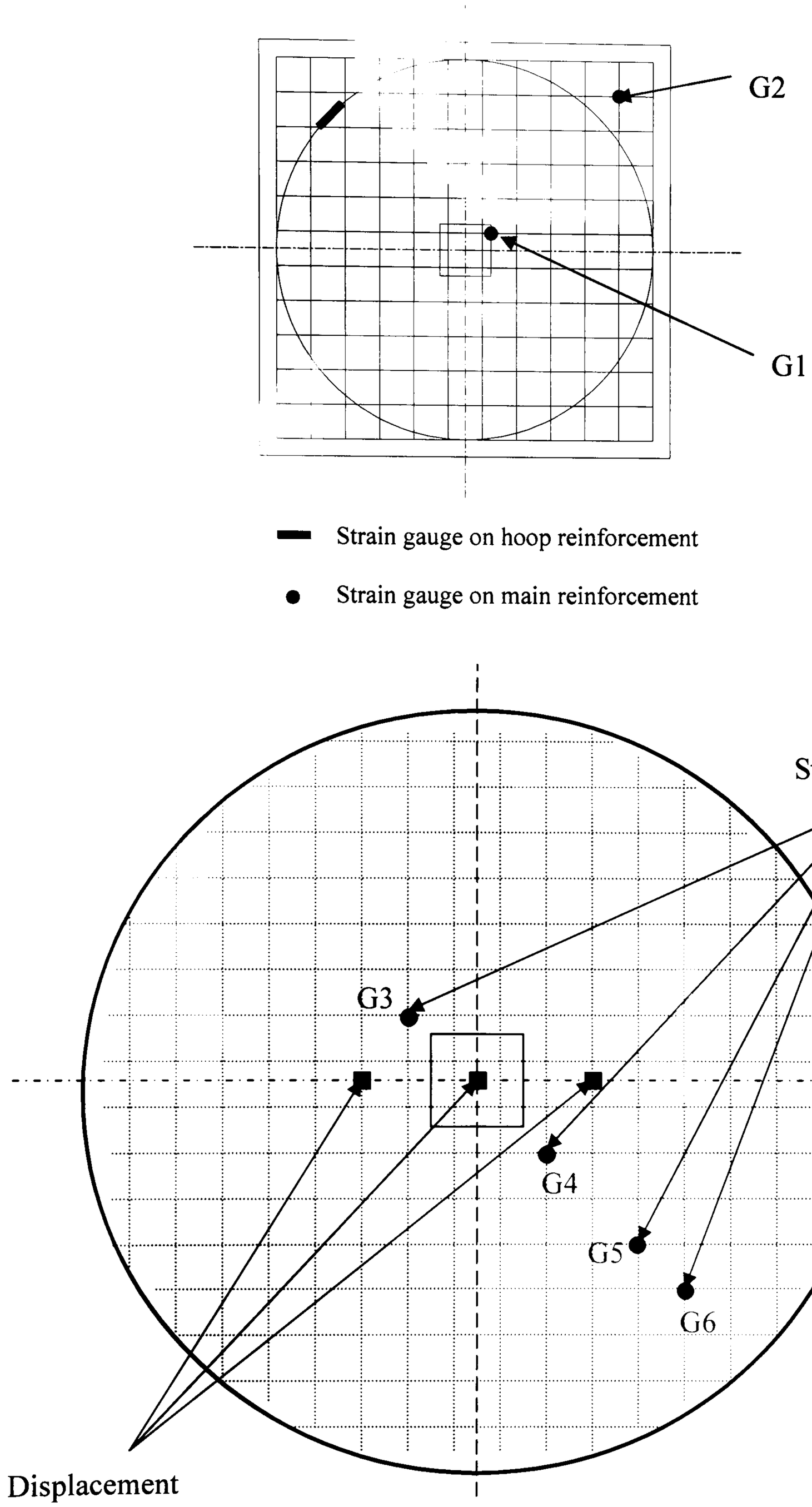

FIG. 6.8 Locations of strain gauges

FIG. 6.9 Electrical strain gauges (TML Type FLA-2-11)

FIG. 6.10 Data-logger

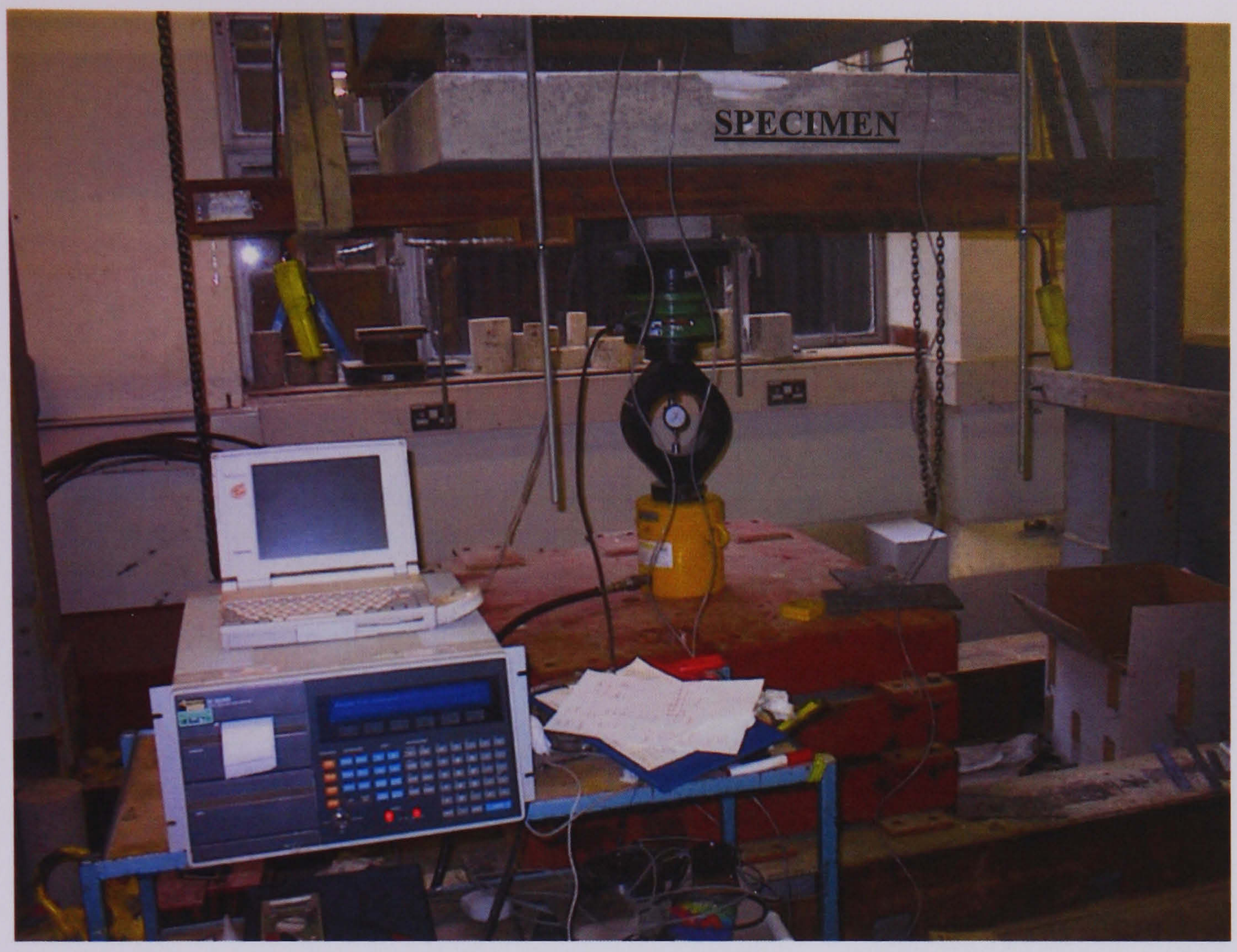

FIG. 6.11 An overall view of a specimen in position for testing

(a) Specimen S1

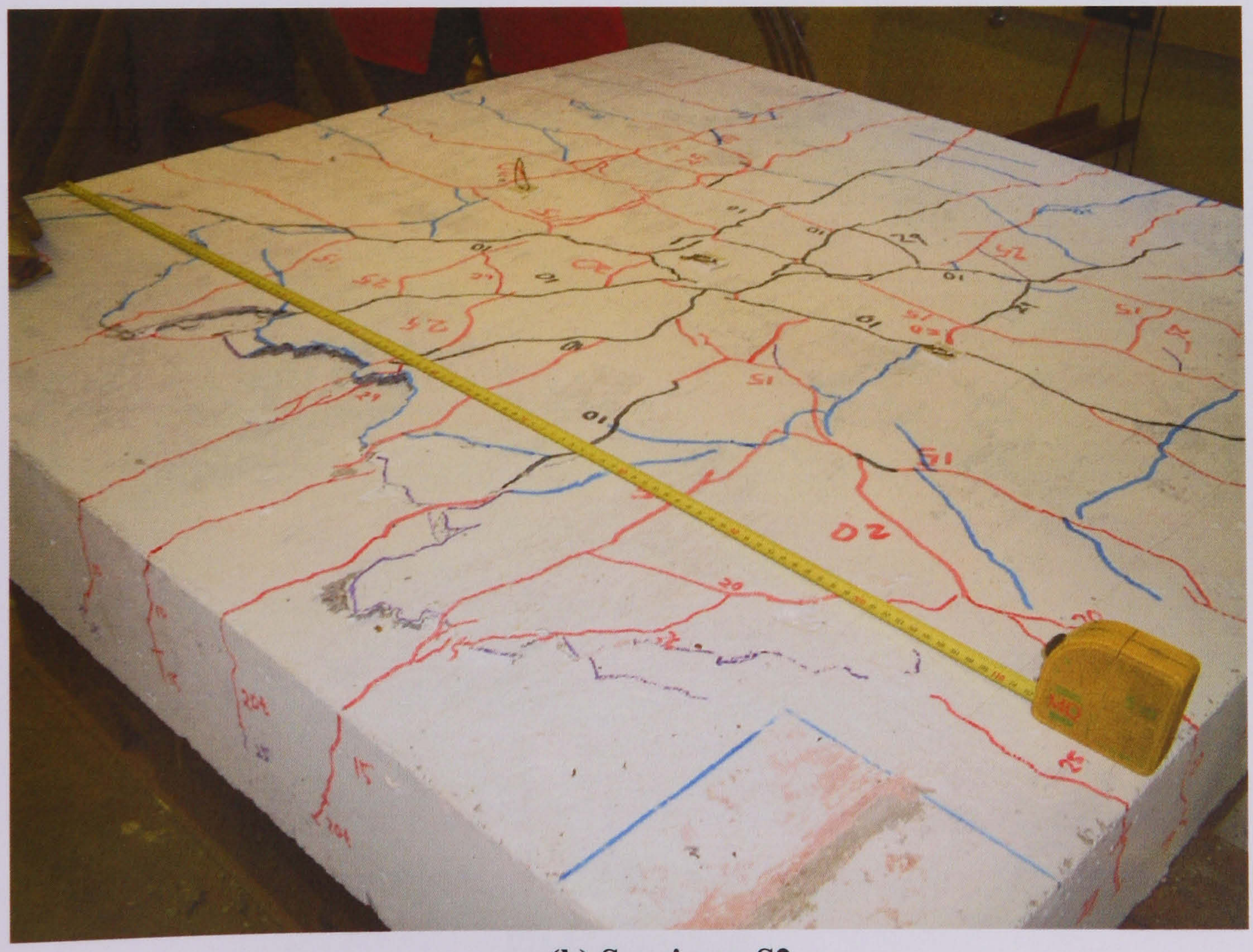

(b) Specimen S2

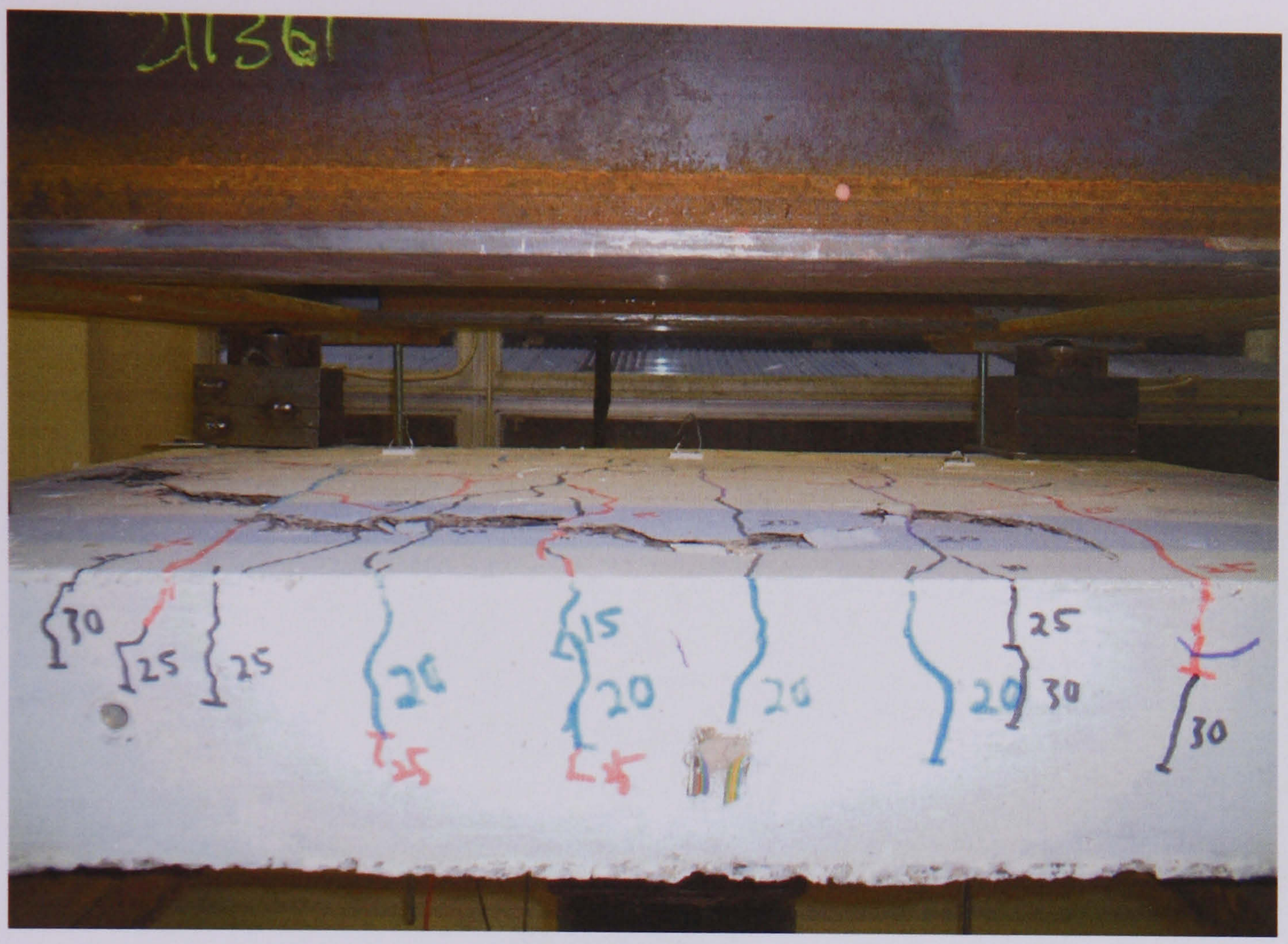

(c) Specimen S3

(d) Specimen S4

(e) Specimen S5

FIG. 6.12 Typical punching shear failure in slabs (S1-S5)

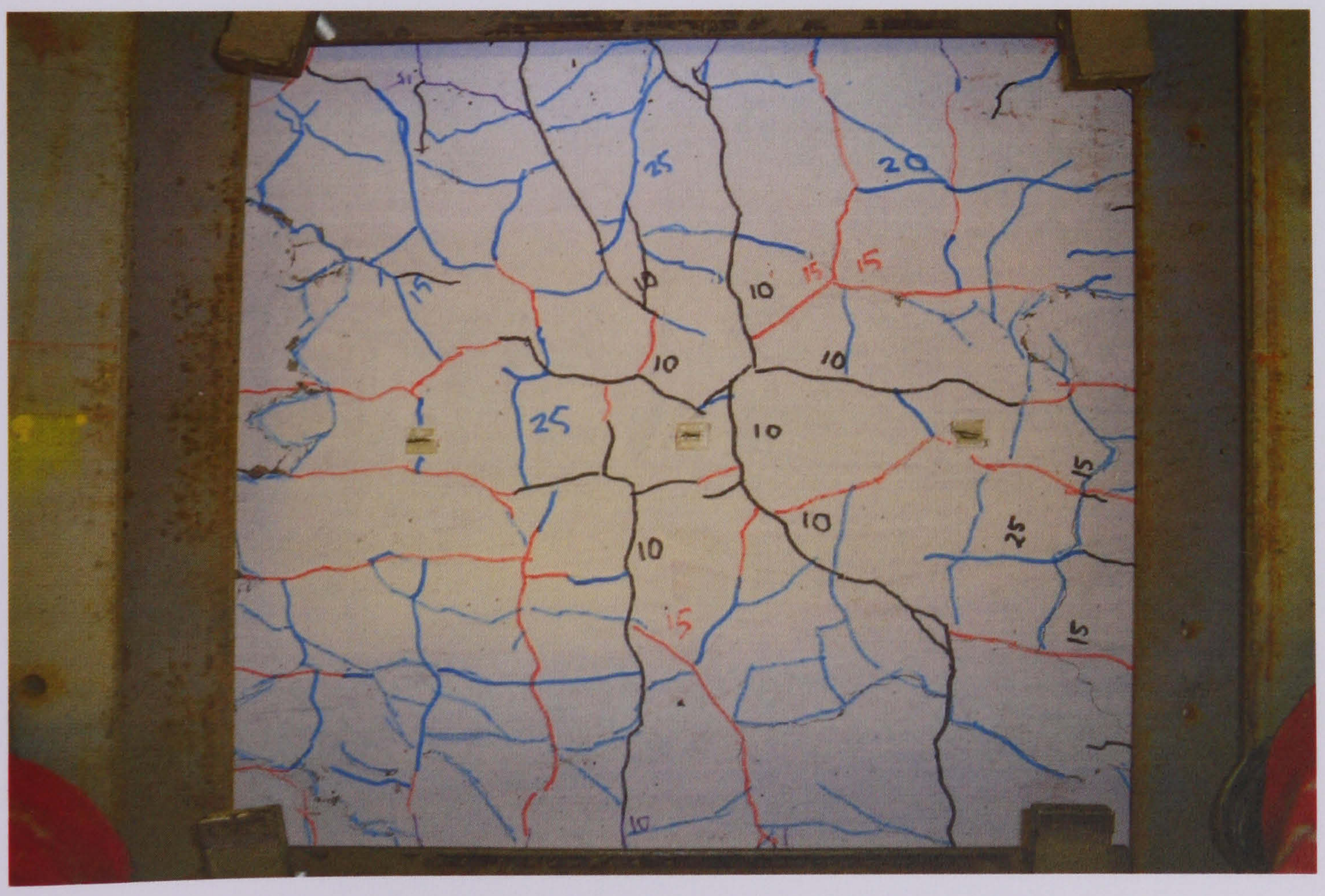

FIG. 6.13 Typical crack pattern of slab specimen which is strongly restrained (Specimen S4)

FIG. 6.14 Typical crack pattern of slab specimen which is weakly restrained (S1)

FIG. 6.15 Typical discontinuity on top surface of slabs after failure

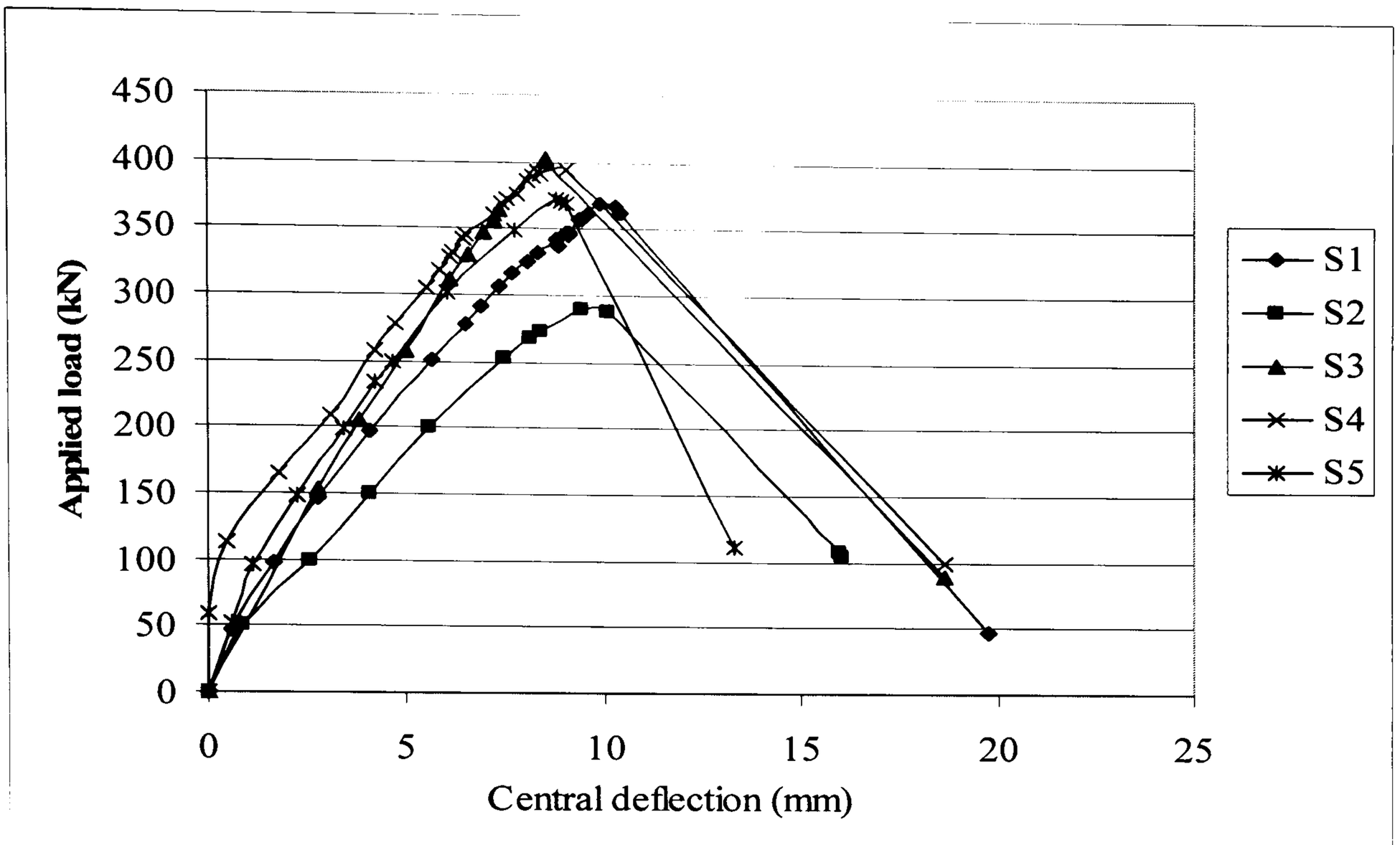

FIG. 6.16 Load-Deflection relationship of slabs

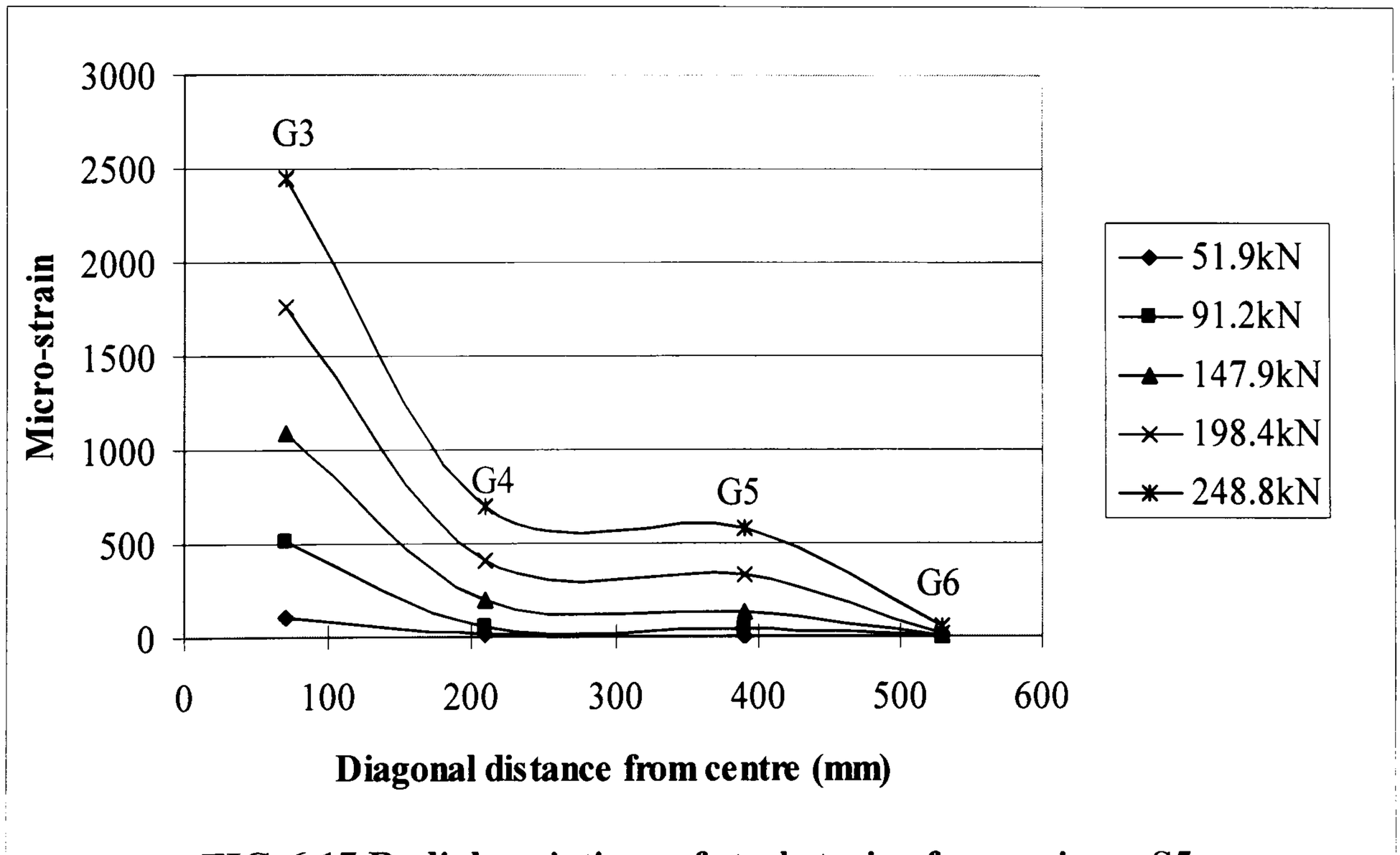

FIG. 6.17 Radial variations of steel strains for specimen S5

See Fig. 6.8 for locations of reinforcement gauges G3 – G6

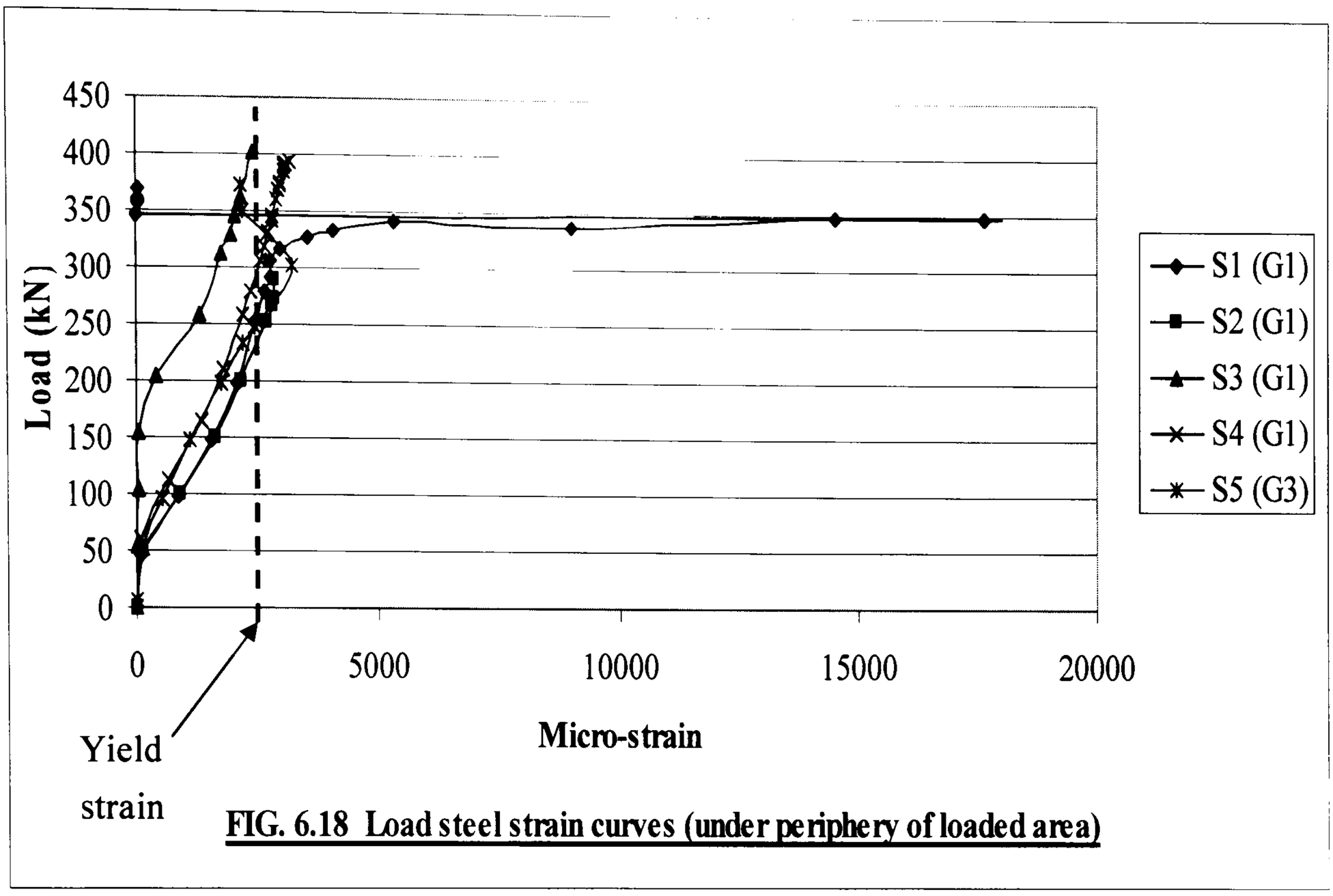

FIG. 6.18 Load steel strain curves (under periphery of loaded area)

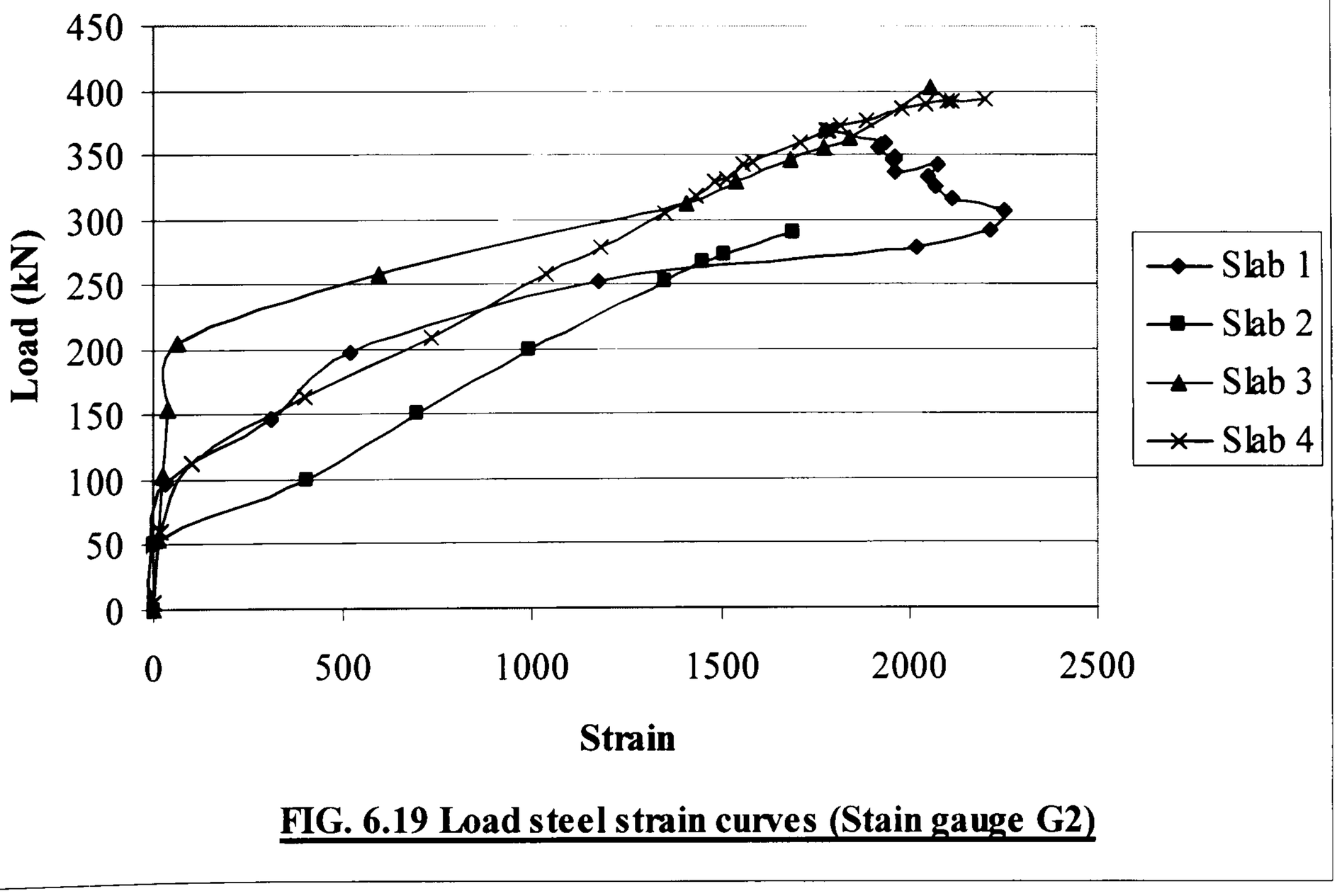

FIG. 6.19 Load steel strain curves (Stain gauge G2)

See Fig. 6.8 for locations of reinforcement gauges G1 and G2

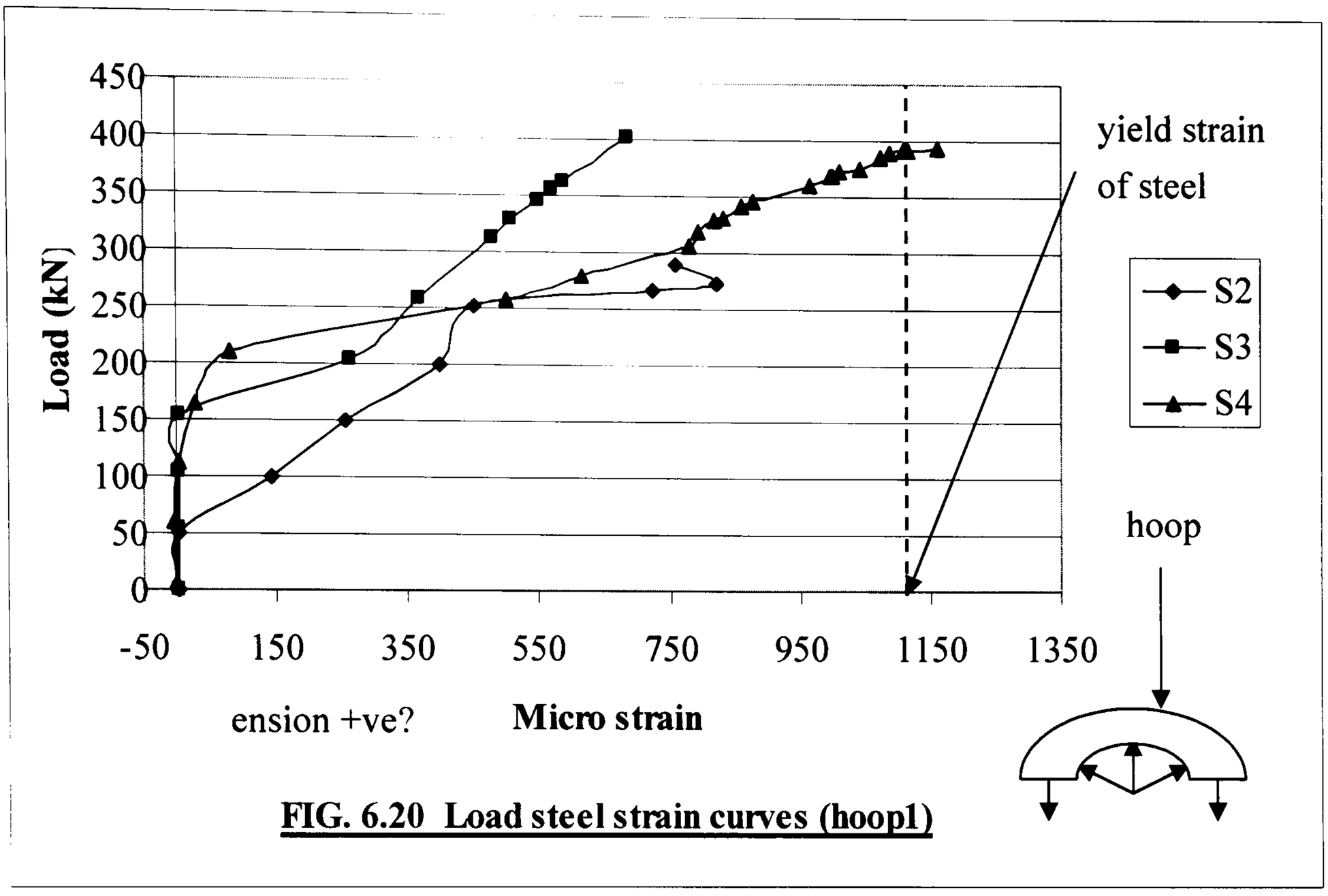

FIG. 6.20 Load steel strain curves (hoop1)

See Fig. 6.8 for gauge locations

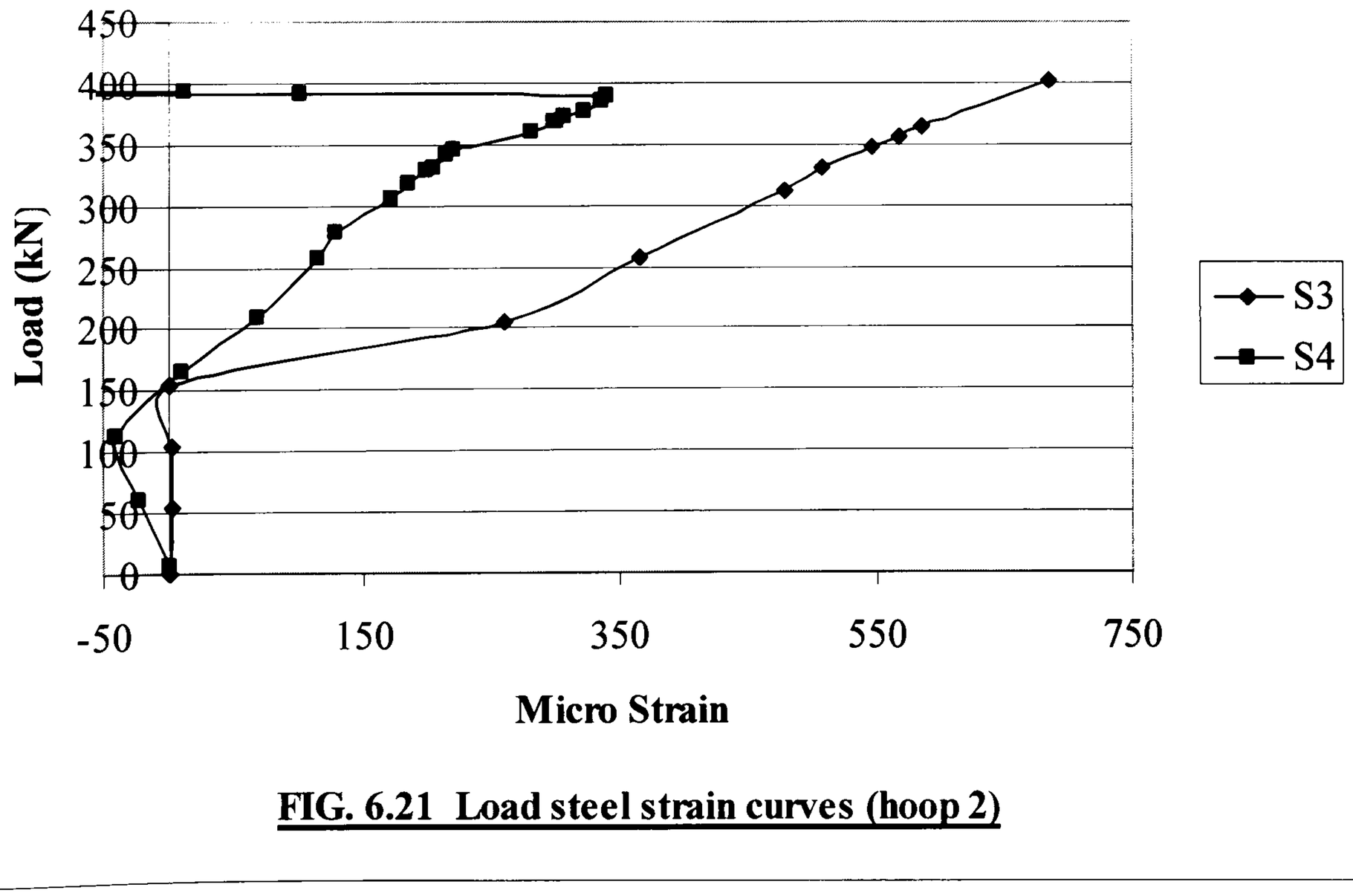

FIG. 6.21 Load steel strain curves (hoop 2)

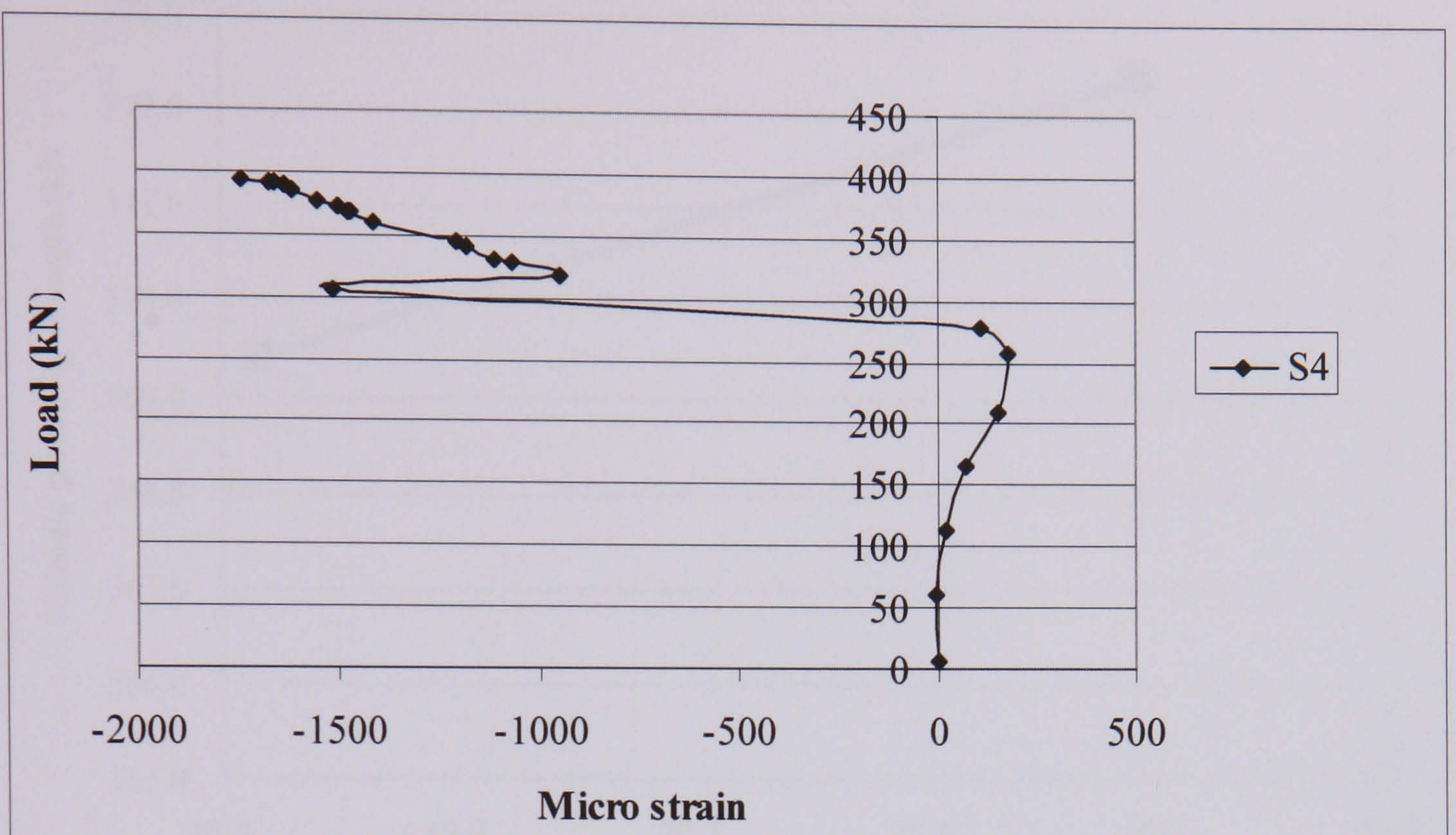

FIG. 6.22 Load steel strain curves (hoop 3)

Fig. 6.23(a) Non-dimensional strength against different degrees of restraint

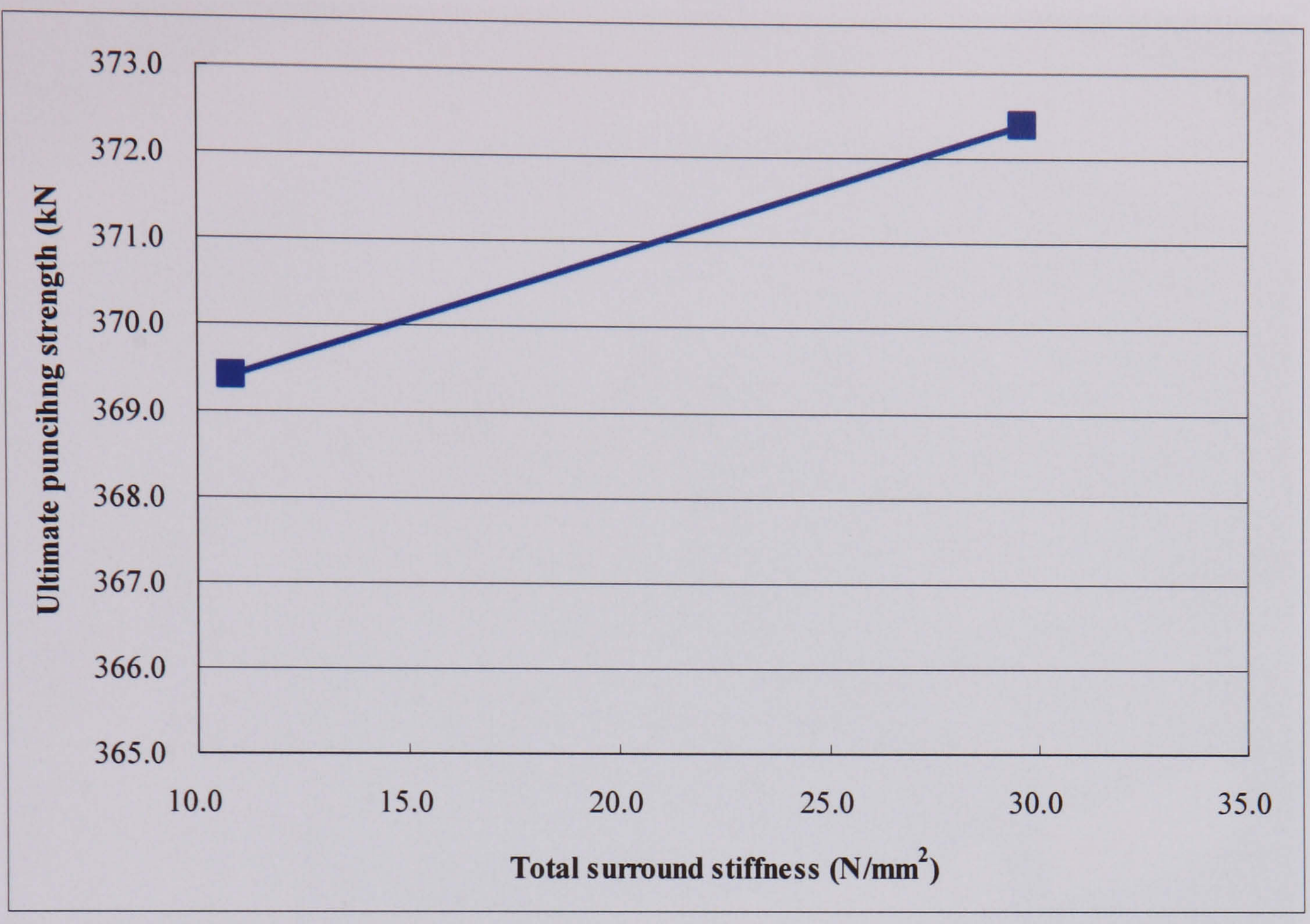

Figure 6.23(b) Effect of surround concrete material on punching capacities

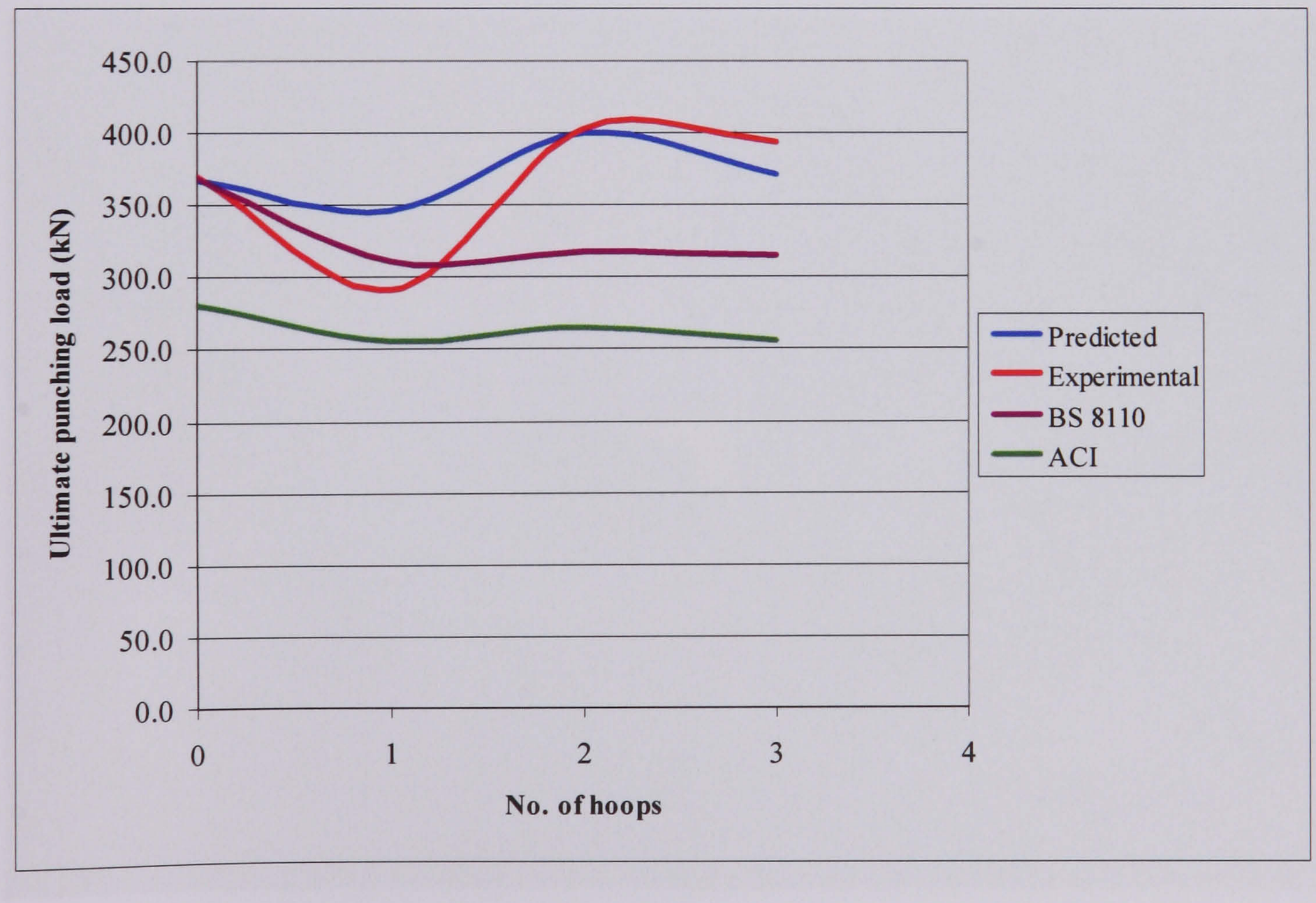

Figure 6.24 Comparison between test strength, proposed analysis and code predictions

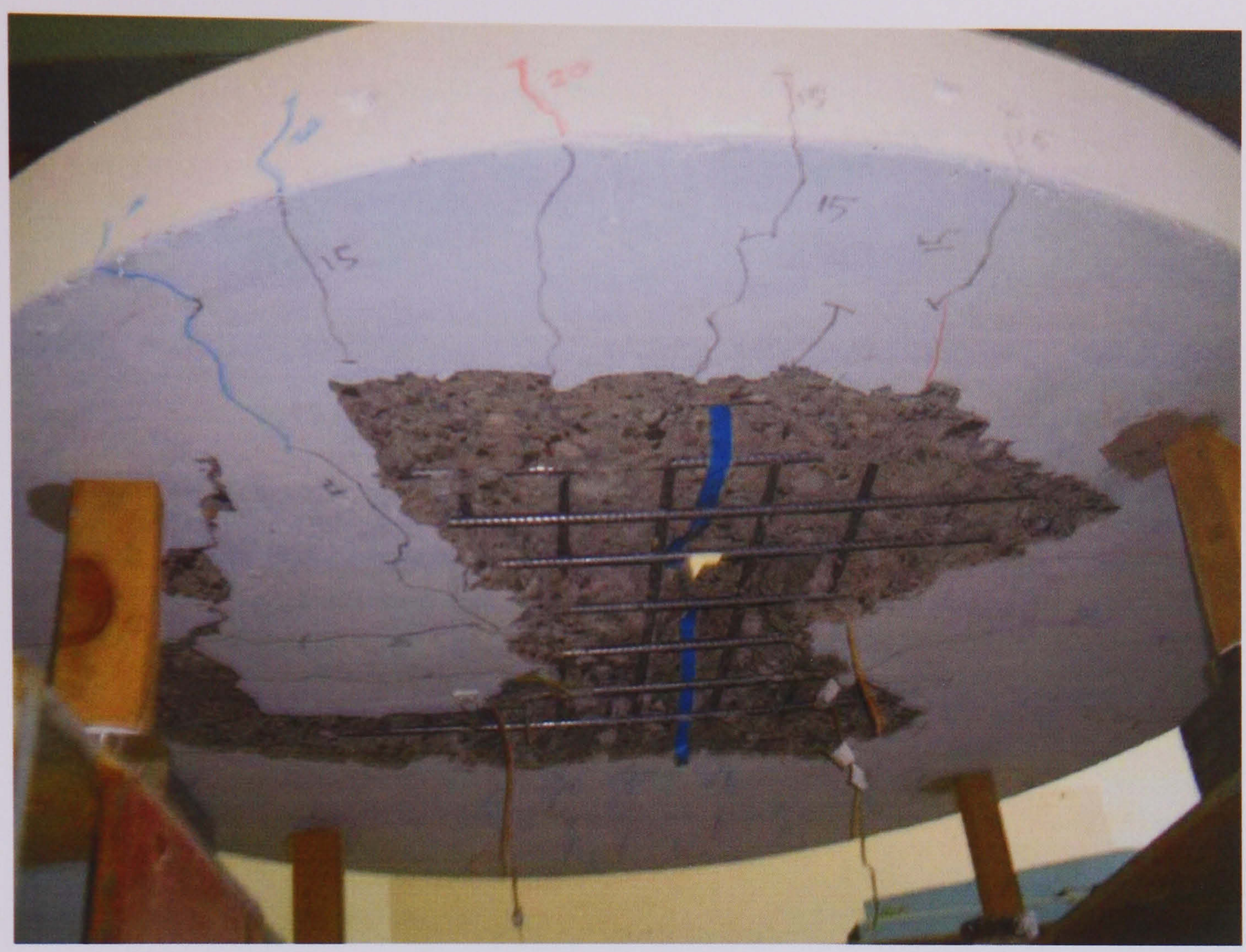

FIG. 6.25(a) A plan view of the failure surface

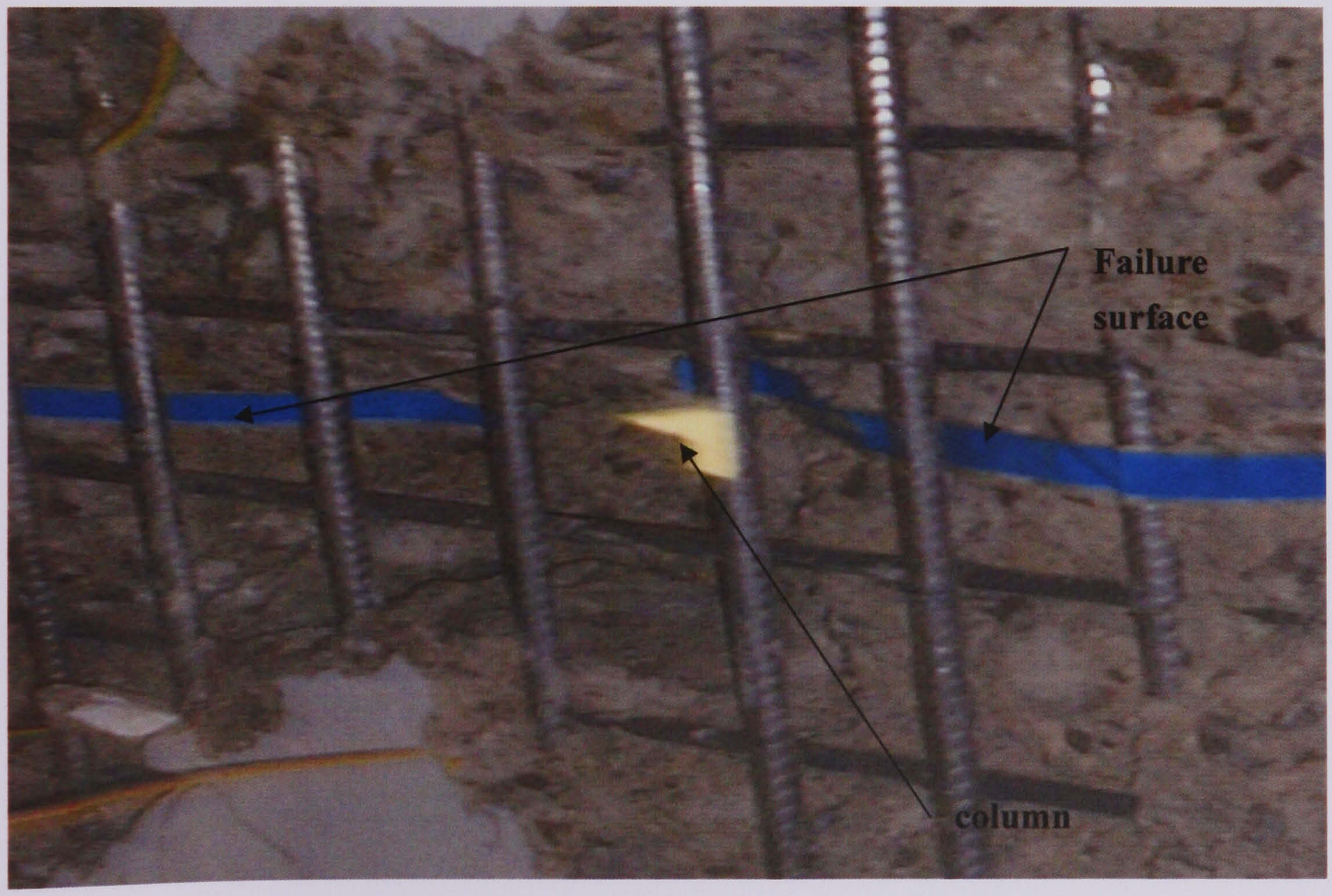

FIG. 6.25(b) A bottom view showing the profile of the failure surface

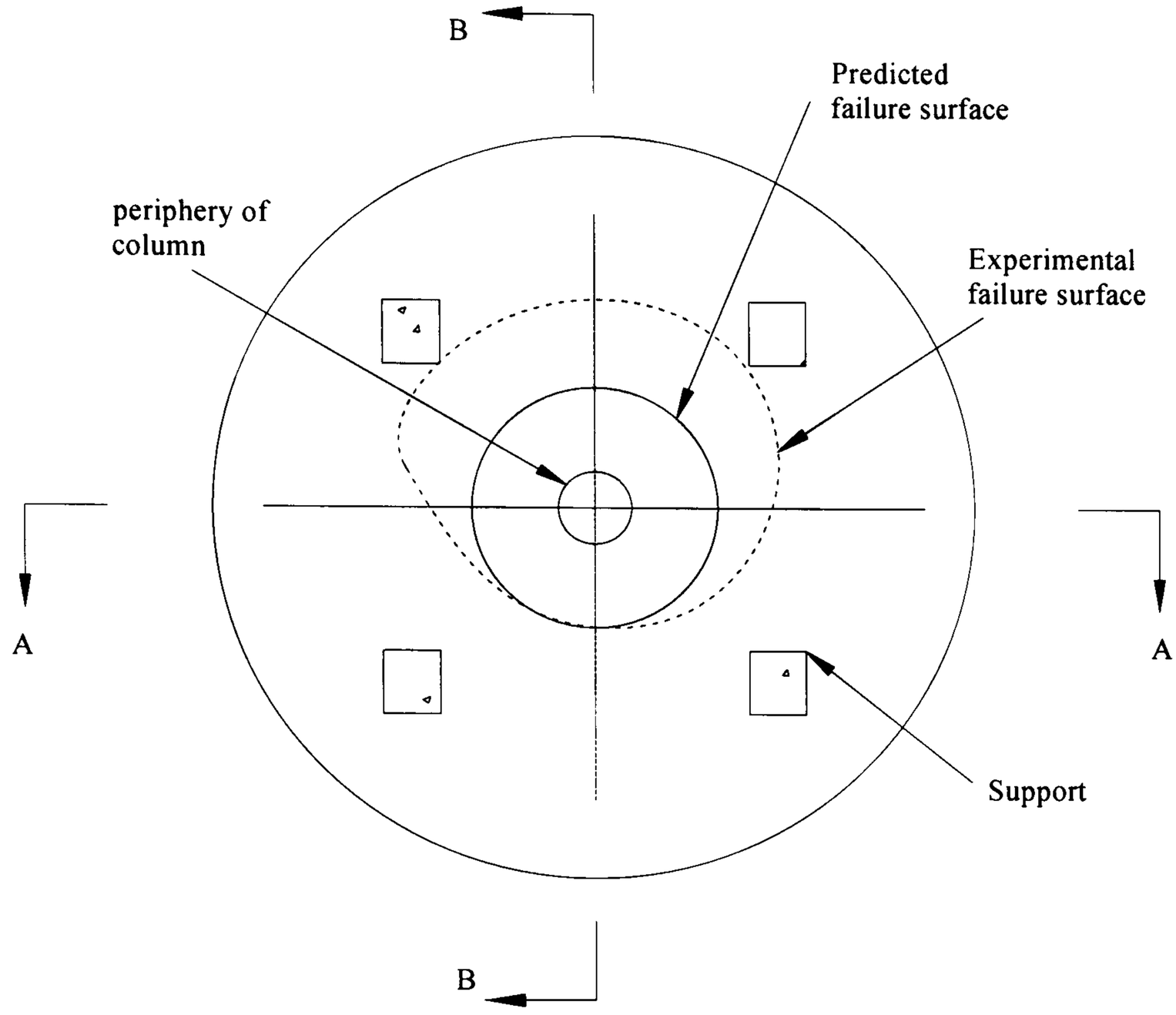

FIG. 6.26(a) A comparison of predicted and experimental failure surface (plan view)

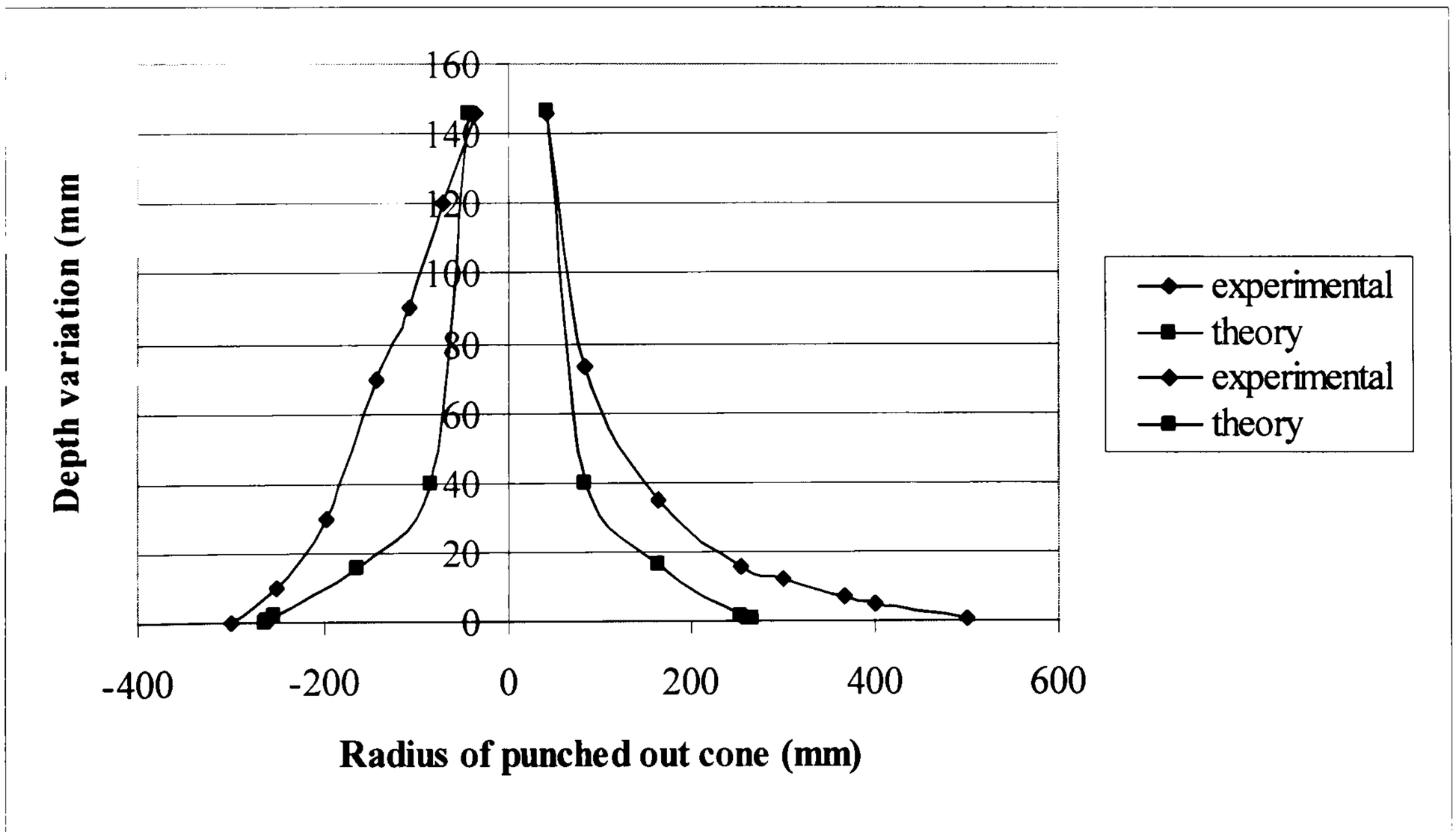

FIG. 6.26(b) Comaprison of predicted against experimental failure surface (section AA)

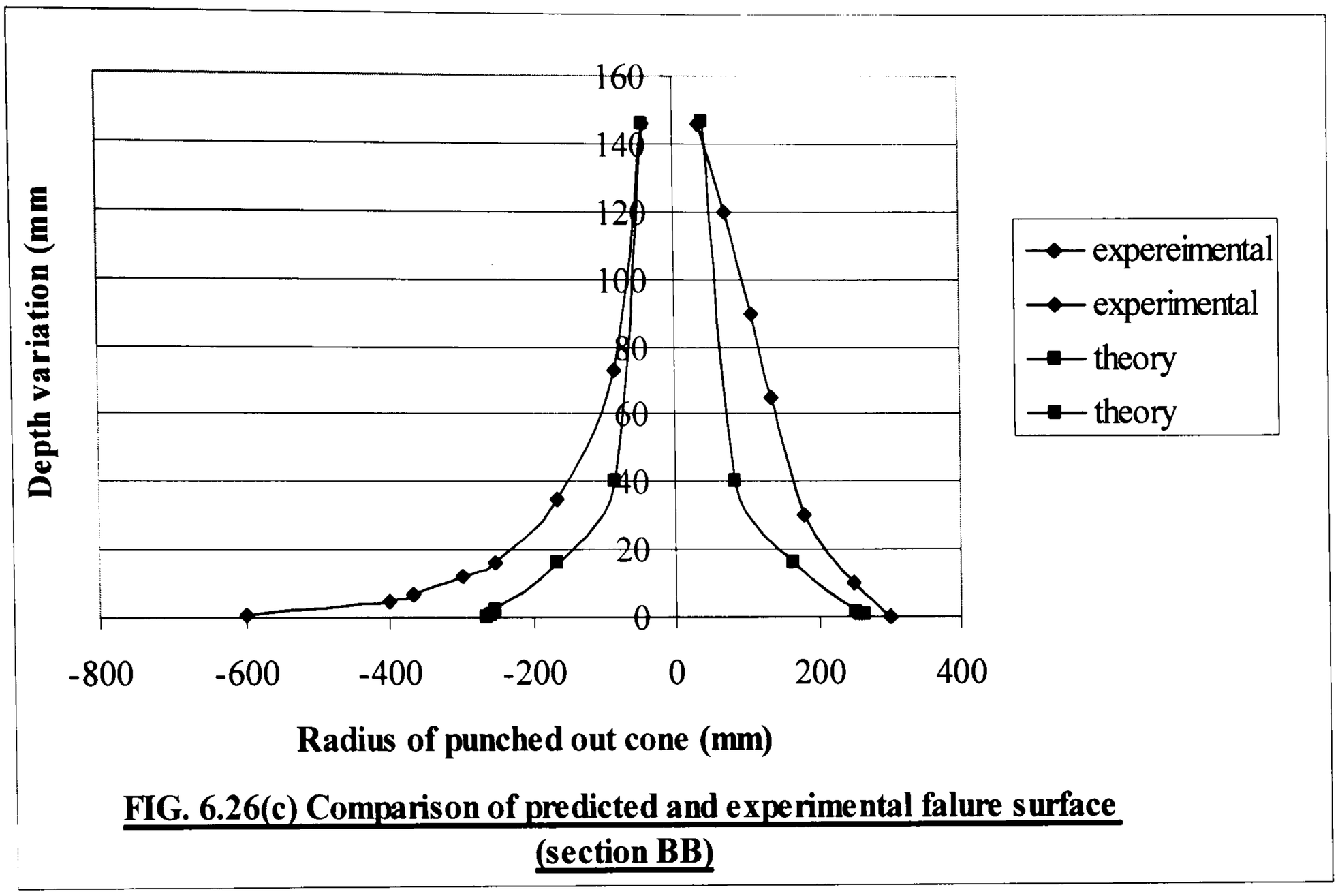

FIG. 6.26(c) Comparison of predicted and experimental falure surface (section BB)

7

CONCLUSIONS

7.1 Summary

7.2 Conclusions

7.3 Suggestions for Future Work

Chapter Seven

CONCLUSIONS

7.1 SUMMARY

This chapter summarises the issues addressed throughout the thesis, and outlines the main findings of the work. Finally, suggestions are made for extension of this work.

There is currently a need for a better understanding of the enhancing effect of compressive membrane action on the punching shear capacities of reinforced concrete flat slabs. Due largely to the economic advantages of incorporating this important phenomenon, a number of theoretical and experimental investigations have been carried out. This thesis is concerned with 2 important approaches, namely: the plasticity theory based on the parabolic failure criterion for concrete and the equilibrium analysis based on the work of Kinnunen & Nylander.

A survey of the literature identified that there was considerable scope for further research to achieve the following:

- Gaining a better understanding of the role of *effectiveness factors* of concrete in compression and in tension, on punching shear predictions;
- Introduction of a *simplified* plastic approach whilst still retaining the predictive capabilities of that approach;
- Investigating the reliability of the plastic approach in terms of both the validity of the *failure surface* and the punching shear predictions;
- Assessing the influence of deviations from axisymmetry on the failure surface and load;
- Quantification of surround restraint stiffness;
- Understanding the influence of increasing levels of surround restraint provide via both steel hoop reinforcement and surround concrete material on punch loads;

In order to investigate these issues, five reinforced concrete slab specimens were fabricated and tested to failure at the Bristol University concrete laboratory. The specimens incorporated nominally grade 40 concrete of practical aggregate sizes and grading, along with high yield (flexural) and mild steel (hoops) reinforcement. In addition, 2 analyses based on plasticity theory and the equilibrium approach, were conducted to provide punching shear predictions of reinforced concrete slabs where membrane restraint is not significant. Sensitivity studies were conducted to establish the levels of robustness of the plasticity-based predictions to the actual effectiveness factors used. An important extension to plastic analysis was made to incorporate the enhancing effect as a result of compressive membrane action.

The main conclusions drawn from these experimental and theoretical studies are presented in the next section.

7.2 CONCLUSIONS

The principal objectives of the research into punching shear failure and compressive membrane action in reinforced concrete slabs have been attained. As the major points of importance have been presented in details at the end in the relevant chapters, it is now appropriate to take an overall perspective on the work. On the basis of this combined experimental and theoretical study of the behaviour of reinforced concrete slabs subjected to concentrated loading, the following general conclusions have been drawn:

1. By adopting a parabolic failure criterion for concrete, a rigid-plastic solution for predicting the punching shear strength of simply-supported concrete slabs is derived. In addition, the derived solution can be simplified by assuming that the yield line is straight in elevation. The proposed method is less empirical and relatively easy to use, and provides consistently reliable predictions. Most importantly, it is less conservative than the code predictions.

2. A study to investigate the role of the effectiveness factors themselves, in particular the range of values over which these may be varied without significantly influencing the predictions has been done to assess the robustness of the plastic predictions in light of the variability of the effectiveness factors. In addition, the sensitivity of the predicted punching capacities via the application of plasticity theory to the effectiveness factors used for the concrete material was investigated.

Based on this work, a suitable set of effectiveness factors giving the best correlation against experimental results was suggested.

3. An extension to the rigid-plastic theoretical model is presented for predicting the compressive membrane action strength enhancement of restrained reinforced concrete slabs subjected to concentrated loading. The proposed method of enhanced punching shear strength predictions showed good correlation with experimental test results reported in the literature as well as test results conducted by the author.

4. The degree of restraint has a significant effect on the ultimate load of a concrete slab, resulting in a greater promotion of shear resistance in the slab and enhancement in load-carrying capacities. The magnitude of strength enhancement depends on the degree of restraint ; the stiffer the restraint, the higher the enhancement but only up to a certain threshold restraint stiffness beyond which there is little, or no further increase in punching load.

5. The use of plasticity theory to prediction of punching failure loads resulted in good correlation against experimental results conducted by the author despite the disparity between the predicted and experimentally observed failure surface.

6. Present code methods significantly underestimate the punching shear strength of restrained slabs that are more representative of the slabs in the actual structure, such as continuous slab floors, flat slab construction and bridge decks, than simply-supported slabs.

7. Following the idea of the Kinnunen and Nylander model, a simplified equilibrium analysis for predicting the punching shear strength of reinforced concrete slabs is presented. The final expression incorporates important parameters including a *size effect* parameter which significantly enhances the predicted punching failure loads.

7.3 SUGGESTIONS FOR FUTURE WORK

- Further verification with experimental results covering a wider range of variables, is required to validate the use of plasticity theory to prediction of punching capacities of reinforced concrete slabs. In particular, demonstration of the accuracy of the predictions over a wider range of slab depths, to assess the reliability of the size effect factor, is important.

- The solution for predicting punching shear strength of concrete slabs can be extended to represent a transition between plasticity and fracture mechanics.

- Further study should be devoted to an extensive investigation of effectiveness factors which together provide consistently accurate predictions of punching shear failure surface and capacity in situations of asymmetric failure.

- Further study of the quantification of surrounding restraint stiffness is necessary by establishing an equivalence of restraint stiffness from surrounding material to hoop reinforcement.

REFERENCES

REFERENCES

[1] ACI Committee 318, *Building Code Requirements for Reinforced Concrete (ACI 318-83)*, American Concrete Institute, Detroit, 1983, 111 pp.

[2] American Association of State Highway and Transportation Officials, *Standard Specifications for Highway Bridge*, 12th Edition, Washington DC, 1977.

[3] Andra, H., "Zum Tragverhalten des Auflagerbereichs von Flachdecken" (On the strengths of support regions of flat slabs), DR. Ing. Thesis, Universitat Stuttgart, 1982.

[4] Aoki, Y. and Seki, H., "Shearing strength and cracking in two-way slabs subjected to concentrated load. In *Cracking, Deflection, and Ultimate Load of Concrete Slab Systems*, American Concrete Institute SP-30, 1971, pp. 103-126.

[5] ASCE-ACI Committee 426, "The shear strength of reinforced concrete member – slabs", *Journal of the Structural Division*, ASCE, Vol. 100, No. ST8, Aug., 1974, pp. 1543-1591.

[6] Ashour, A.F. and Morley, C.T., "Effectiveness factor of concrete in continuous deep beams", *Journal of Structural Engineering*, ASCE, Vol. 122, No. 2, Feb., 1996, pp. 169-178.

[7] Batchelor, B. de V., and Tissington, I.R., "Shear strength of two-way bridge slabs", *Journal of the Structural Division*, ASCE, Vol. 102, ST12, Dec., 1976, pp. 2315-2331.

[8] Base, G.D., "Some tests on the punching shear strength of reinforced concrete slabs", *Technical Report* TRA/321, Cement and Concrete Association, London, July, 1959.

[9] Bazant, Z.P., and Cao, Zhiping, "Size effect in punching shear failure of slabs", *ACI Structural Journal*, American Concrete Institute, Vol. 84, Jan.-Feb., 1987, pp. 44-51.

[10] Beal, D., "Load capacity of concrete of concrete bridge decks", *Journal of the Structural Division*, ASCE, Vol. 108, ST4, 1982.

[11] Bortolotti, L., "Punching shear strength in concrete slabs", *ACI Structural Journal*, American Concrete Institute, Vol. 87, No.2, March-April, 1990, pp.208-219.

[12] Braestrup, M.W., Nielsen, M.P., Jensen, B.C., and Bach, F., "Axisymmetric punching and reinforced concrete", *Report* No. R-75, Structural Research Laboratory, Technical University of Denmark, 1976, 33 pp.

[13] Braestrup, M.W., "Dome effect in reinforced concrete slabs: rigid-plastic analysis", *Journal of the Structural Division*, ASCE, Vol. 106, No. ST6, June, 1980, pp. 1237-1253.

[14] Braestrup, M.W., and Morley, C.T., "Dome effect in reinforced concrete slabs: elastic-plastic analysis", *Journal of the Structural Division*, ASCE, Vol. 106, No. ST6, June, 1980, pp. 1255-1262.

[15] Braestrup, M.W., "Punching shear in concrete slabs", *Plasticity in Reinforced Concrete*, Introductory Report, Colloquium of International Association for Bridge and Structural Engineering, Copenhagen, Aug., 1979, pp. 115-136.

[16] British Standards Institution, *Code of Practice for Design and Construction*, BS 8110: Part 1, London, 1985.

[17] British Standards Institution, *Code of Practice for Design of Concrete Bridge*, BS 5400: Part 4, London, 1984.

[18] British Standards Institution, *Code of Practice for the Structural Use of Concrete*, CP 110: Part 1, London, 1972, 154 pp.

[19] CEB, *CEB-FIP Model Code for Concrete Structures*, Comite Euro-International du Beton, Paris, 1978, 348 pp.

[20] Christiansen, K.P., and Frederiksen, V.T., "Tests on rectangular concrete slabs with horizontal restraints on three sides only", *Nordic Concrete Research*, Vol. N1, Dec., 1982, pp. 11-21.

[21] Collings, D., "Design of bridge decks using arching effects", *Proceedings of the Institution of Civil Engineers-Structures and Buildings*, Vol. 152, Issue 3, August, 2002, pp. 277-282.

[22] Criswell, M.E., Static and dynamic response of reinforced concrete slab-column connections", *Shear in Reinforced Concrete*, SP-42, V. 2, American Concrete Institute, Farmington Hills, Mich., 1974, pp. 721-746.

[23] Csagoly, F., "Design of thin concrete deck slabs by the Ontario highway bridge design code", *SRR-79-11*, Ontario Ministry of Transportation and Communications, Toronto, 1979, 22 pp.

[24] Department of the Environment for Northern Ireland, *Design of M-beam Bridge Decks*, Amendment 3 to B.D.C. Northern Ireland Roads Service Headquarter, 1986, pp. 11.1-11.5.

[25] Department of Transport, *Technical Memorandum (Bridge) No. BE1/77*, Standard Highway Loadings, London, 1977.

[26] Design Manual for Roads and Bridges BD 81/02 Volume 3, Section 4, Part 20, Use of Compressive Membrane Action in Bridge Decks May 2002.

[27] Dorton, R.A., Holowka, M., and King, J.P.C., "The Connestogo River Bridge-design and testing", *Canadian Journal of Civil Engineering*, Vol. 4, Issue 1, 1977.

[28] Dragosavic, M., and van den Beukel, A., "Punching shear", *Heron*, V. 20, No. 2, Delft, 1974, 48 pp.

[29] Ekeberg, P.K., Sjursen, A., and Thorenfeldt, E., "Load-carrying capacity of continuous concrete slabs with concentrated loads", *Journal of the Nordic Concrete Federation*, FIP congress edition, June, 1982, pp. 183-186.

[30] Elstner, R.C., and Hognestad, E., "Shearing strength of reinforced concrete slabs", *Journal of the American Concrete Institute*, Vol. 53, No. 2, July, 1956, pp. 29-58.

[31] Eyre, J.R., "Membrane action in plain concrete slabs under concentrated loading", *Proceedings of the Institution of Civil Engineers-Structures and Buildings*, Vol. 140, Aug., 2000, pp. 207-217.

[32] Fenwick, R.C., and Dickson, A.R., "Slabs subjected to concentrated loading", *ACI Structural Journal*, American Concrete Institute, Vol. 86, No. 6, Nov.-Dec., 1989, pp. 672-678.

[33] Forsell, C., and Holmberg, A., "Concentrated loads on concrete slabs", Betong, Vol. 31, No. 2, Stockholm, Feb., 1946, pp. 95-123.

[34] Gesund, H., and Dikshit, O.P., "Yield line analysis of the punching problem at slab/column intersections", *Cracking, Deflection and Ultimate Load of Concrete Slab Systems*, Publication SP-30, American Concrete Institute, Detroit, 1971, pp. 177-201.

[35] Gomes, R., and Regan, P.E., "Punching strength of slabs reinforced for shear with offcuts of rolled steel I-section beams", *Magazine of Concrete Research*, Vol. 51, No. 2, April, 1999, pp. 121-129.

[36] Graf, O., "Strength tests of thick reinforced concrete slabs supported on all sides under concentrated loads", *Deutscher Ausschuss fur Eisenbeton*, Vol. 88, 1938, pp. 1-26.

[37] Graf, O., "Tests of the strength of reinforced concrete slabs supported at all sides and subjected to concentrated loads", Deutscher Ausschuss fur Eisenbeton, Heft 38, Berlin, 1938.

[38] Gvozdev, A.A., "Comments on Clause 33 of the Russian code for reinforced concrete", (in Russian), *Stroitelnaya Promyshlennost*, Vol. 17, No. 3, 1939.

[39] Hallgren, M., and Kinnunen, S., "Increase of punching shear capacity by using high strength concrete", *4th International Symposium on Utilization of High-Strength/High-Performance Concrete*, Paris, 1996, pp. 1015-1026.

[40] Hewitt, B.E., and Batchelor, B. deV., "Punching shear strength of restrained slabs", *Journal of the Structural Division*, ASCE, Vol. 101, No. ST9, Sept., 1975, pp. 1837-1853.

[41] Hognested, E., "A study of combined bending and axial load in reinforced concrete members", Bulletin No. 339, Engineering Experiment Station, University of Illinois, 1951.

[42] Hognestad, E., "Shearing strength of reinforced concrete column footings", *Journal of the Structural Division*, Vol. 50, Nov., 1953, pp. 189-208.

[43] Holowka, M., Dorton, R., and Csagoly, P., "Punching shear strength of restrained circular slabs", The Ontario Ministry of Transportation and Communications, Toronto, 1979.

[44] Hyttinen, E., "Dome action in reinforced concrete slabs", *Nordisk Betong*, Vol. 15, Stockholm, Sweden, 1971, pp. 111-128.

[45] Jackson, P.A., "The global and local behaviour of bridge deck slabs", *The Structural Engineer*, Vol. 68, No. 6, March, 1990, pp. 112-116.

[46] Jiang, D.-H. and Shen, J.-H., "Strength of concrete slabs in punching shear", *Journal of Structural Engineering*, ASCE, Vol. 112, No. 12, Dec., 1986, pp. 2578-2591.

[47] Jiang, D.-H. and Shen, J.-H., "Strength of concrete slabs in punching shear discussion)", *Journal of Structural Engineering*, ASCE, Vol. 114, No. 9, Sept., 1988, pp. 2160-2167.

[48] Johansen, K.W., *Yield-Line Theory*, translated by Cement and Concrete Association, London, 1962, 181 pp.

[49] Kamaraldin, K., *Punching Shear And Moment Transfer In Reinforced Concrete Flat Slabs*, PhD. Thesis, University of Westminster, 1990.

[50] Kinnunen, S., "Punching of concrete slabs with two-way reinforcement with special reference to dowel effect and deviation of reinforcement from polar symmetry", *Transactions of the Royal Institute of Technology*, Stockholm, Sweden, No. 198, 1963, 109 pp.

[51] Kinnunen, S., and Nylander, H., "Punching of concrete slabs without shear reinforcement", *Transactions of the Royal Institute of Technology*, Stockholm, Sweden, No. 198, 1960, 112 pp.

[52] Kinnunen, S., Nylander, H. and Tolf., "Undersokningar rorande genomstansning vid. Istitutionen for byggnadsstatik, KTH, *Journal of the Nordic concrete federation*, 1978.

[53] Kirkpatrick, J., Rankin, G.I.B., "and Long, A.E., "Strength evaluation of M-beam bridge deck slabs", *The Structural Engineer*, Vol. 62B, No. 3, Sept., 1984, pp. 60-68.

[54] Kirkpatrick, J., Rankin, G.I.B., "and Long, A.E., "The influence of compressive membrane action on the serviceability of beam and slab bridge decks", *The Structural Engineer*, Vol. 64B, No. 1, March, 1986, pp. 6-9.

[55] Kuang, J.S., *Punching Shear Failure of Concrete Slabs with Compressive Membrane Action*, PhD. Thesis, University of Cambridge, 1991.

[56] Kuang, J.S., and Morley, C.T., "Punching shear behaviour of restrained reinforced concrete slabs", *ACI Structural Journal*, American Concrete Institute, Vol. 89, Issue 1, 1992, pp. 13-19.

[57] Kuang, J.S., and Morley, C.T., "A plasticity model for punching shear of laterally restrained slabs with compressive membrane action", *International Journal of Mechanical Sciences*, Vol. 35, Issue 5, 1993, pp. 371-385.

[58] Leon, A., "Ueber die scherfestigkeit des betons", *Beton und Eisen*, V. 34, No. 8, April, 1935, pp. 130-135.

[59] Long, A.E., "A two-phase approach to the prediction of the punching strength of slabs", *Journal of the American Concrete Institute*, Vol. 72, No. 2, Feb., 1975, pp. 37-45.

[60] Marzouk, H., Osman, M., and Hussein, A., "Punching shear of slabs: crack size and size effects", *Magazine of Concrete Research*, Vol. 53, No. 1, February, 2002, pp. 13-21.

[61] Masterson, D.M., and Long, A.E., "The punching strength of slabs, a flexural approach using finite elements", *Shear in Reinforced Concrete*, Publication SP-42, Vol. 2, Part 4, American Concrete Institute, Detroit, 1974, pp. 747-768.

[62] Menetrey, P., "Analytical computation of the punching strength of reinforced concrete", *ACI Structural Journal*, Vol. 93, No. 5, September, 1996, pp. 503-511.

[63] Menetrey, P., Walther, R., Zimmermann, T., William, K.J., and Regan, P.E., "Simulation of punching failure in reinforced concrete structures", *Journal of Structural Engineering*, Vol. 123, No. 5, May, 1997, pp.652-659.

[64] McDowell, E.L., McKee, K.E., and Sevin, E., "Arching action theory of masonry walls", *Journal of the Structural Division*, ASCE, Vol. 82, No. ST2, March, 1956, pp. 915.1-915.8.

[65] Moe, J., "Shearing strength of reinforced concrete slabs and footings under concentrated loads", *Development Department Bulletin D47*, Portland Cement Association, Skokie, III, April, 1961, 130 pp.

[66] Morley, C.T., "Punching shear failure of hollow concrete spheres", *Plasticity in Reinforced Concrete*, Final Report, Colloquium of International Association for Bridge and Structural Engineering, Copenhagen, August, 1979, pp. 167-174.

[67] Morley, C.T., "Some experiments on circular concrete slabs with lateral restraint", Paper presented at the International Conference on Engineering Mechanics, Warsaw, 1974.

[68] Newmark, N.M., Siess, C.P., and Penman, R.R., "Studies of slab and beam highway bridge, Part 1", *Bulletin No. 363*, Engineering Experiment Station, University of Illinois, March, 1946, 130 pp.

[69] Newmark, N.M., Siess, C.P., and Peckham, W.M., "Studies of slab and beam highway bridges, Part 2", *Bulletin No. 375*, Engineering Experiment Station, University of Illinois, Jan., 1948, 60 pp.

[70] Nielsen, M.P., Braestrup, M.W., Jensen, B.C., and Bach, F., "Concrete plasticity – beam shear – punching shear – shear in joints", Danish Society for Structural Science and Engineering, Copenhagen, Oct., 1978.

[71] Nielsen, M.P., "*Limit Analysis and Concrete Plasticity*, Prentice-Hall, New Jersey, 2000.

[72] Ockleston, A.J., "Arching action on a three-storey reinforced concrete building in Johannesburg", *The Structural Engineer*, Vol. 33, Oct., 1955, pp. 304-322.

[73] Ockleston, A.J., "Arching action in reinforced concrete slabs", *The Structural Engineer*, Vol. 36, No. 6, June, 1958, pp. 197-201.

[74] Ontario Ministry of Transportation and Communications, Ontario, Canada. *Ontario Highway Bridge Design Code*, 1983.

[75] Ontario Ministry of Transportation and Communications, Ontario, Canada. *Ontario Highway Bridge Design Code*, 1991.

[76] Park, R., "Ultimate strength of rectangular concrete slabs under short-term uniform loading with edges restrained against lateral movement", *Proceedings of the Institution of Civil Engineers*, Vol. 28, June, 1964, pp. 125-150.

[77] Polak, M.A., "Modelling punching shear of reinforced concrete slabs using layered finite elements", *ACI Structural Journal*, Vol. 95, No. 1, January, pp. 71-80.

[78] Pucher, A., *Influence Surfaces of Elastic Plates*, Springer Verlag, Wien and New York, 1964, 33 pp and 93 chs.

[79] Rankin, G.I.B., *Punching Failure and Compressive Membrane Action in Reinforced Concrete Slabs*, PhD. Thesis, Queen's University of Belfast, 1982.

[80] Rankin, G.I.B., and Long, A.E., "Predicting the punching strength of conventional slab-column specimens", *Proceedings of the Institution of Civil Engineers*, Part 1, Vol. 82, April, 1987, pp. 327-346.

[81] Rankin, G.I.B., and Long, A.E., "Predicting the enhanced punching strength of interior slab-column connections", *Proceedings of the Institution of Civil Engineers*, Part 1, Vol. 82, 1987, pp. 1165-1186.

[82] Rankin, G.I.B., "Arching action strength enhancement in laterally-restrained slab strips", *Proceedings of the Institution of Civil Engineers-Structures and Buildings*, Vol. 122, Nov., 1997, pp. 461-467.

[83] Regan, P.E., "A comparison of British and ACI 318-71 treatments of punching shear", *Shear in Reinforced Concrete*, Publication SP-42, Vol. 2, American Concrete Institute, Detroit, 1974, pp. 881-904.

[84] Regan, P.E., "Design for punching shear", *The Structural Engineer*, Vol. 52, No. 6, Dec., 1974, pp. 197-207.

[85] Regan, P.E., "Design of reinforced concrete flat slabs", *Technical Note to Project Record 220*, Construction Industry Research and Information Association, London, 1978.

[86] Regan, P.E., "Behaviour of reinforced concrete slabs", CIRIA Report 89, 1980.

[87] Regan, P.E., "Symmetric punching of reinforced concrete slabs", *Magazine of Concrete Research*, Vol. 38, No. 136, Sept., 1986, pp. 115-128.

[88] Richart, F.E., "Reinforced concrete wall and footings", *Journal of the American Concrete Institute*, Vol. 45, Oct., 1948, pp. 97-127.

[89] Richart, F.E., "Reinforced concrete wall and footings", *Journal of the American Concrete Institute*, Vol. 45, Nov., 1948, pp. 237-260.

[90] Richart, F.E., Brandtzaeg, A., and Brown, R.L., "A study of the failure of concrete under combined compressive stresses", *Bulletin No. 185*, Engineering Experiment Station, University of Illinois, 1928.

[91] Richart, F.E., and Kluge, R.W., "Tests of reinforced concrete slabs subjected to concentrated loads", *Bulletin No. 134*, Engineering Experiment Station, University of Illinois, June, 1939, 75 pp.

[92] Shehata, I.A.E.M., *Theory of punching in concrete slabs*, PhD. Thesis, Polytechnic of Central London, U.K, 1985.

[93] Shehata, I.A.E.M., and Regan, P.E., "Punching in reinforced concrete slabs", *Journal of Structural Engineering*, Vol. 115, No. 7, July, 1989, pp. 1726-1740.

[94] Shehata, I.A.E.M., "Simplified model for estimating the punching resistance of reinforced concrete slabs", *Materials and Structures*, Vol. 23, No. 137, 1990, pp. 364-371.

[95] Sigurdsson, T.G., Punching shear by eccentric loading", MSc thesis, Department of Structural Engineering, Technical University of Denmark, July, 1991.

[96] Skates, A.S., *Development of a design method for restrained concrete slab systems subjected to concentrated and uniform loading*, PhD. Thesis, The Queen's University of Belfast, U.K, 1986.

[97] Snowdon, L.C., "Some tests on the strength in punching shear of restrained concrete slabs", Building Research Station, Watford, 1983.

[98] Sozen, M.A., and Siess, C.P., "Investigation of multi-panel reinforced concrete slabs: Design methods – Their evolution and comparison", *Proceedings of the American Concrete Institute*, Vol. 60, Aug., 1963, pp. 999-1028.

[99] Talbot, A.N., "Reinforced concrete wall footings and column footings", Bulletin No. 67, Engineering Experiment Station, University of Illinois, Urbana, 1913.

[100] Taylor, F.W., Thompson, S.E., and Smulski, E., *Concrete Plain and Reinforced*, Vol. 1, 4th Edition, John Wiley and Sons, New York, 1925.

[101] Taylor, R., and Hayes, B., "Some tests on the effect of edge restraint on punching shear in reinforced concrete slabs", *Magazine of Concrete Research*, Vol. 17, No. 50, March, 1965, pp. 39-44.

[102] Tong, Y.P., and Batchelor, B. deV., "Compressive membrane enhancement in two-way bridge slabs", *Cracking, Deflection and Ultimate Load of Concrete Slab Systems*, American Concrete Institute, Detroit, 1971, 271 pp.

[103] Timoshenko, S., and Goodier, J.N., *Theory of elasticity*, McGraw Hill Companies, 3rd Edition, 1970.

[104] Turner, C.A.P., "Concrete steel construction, Part 1 – Buildings", Farnham Printing and Stationery Co., Minneapolis, Minnesota, (*Publication SP-52*, American Concrete Institute, Detroit, 1976, pp. 245-284).

[105] Westergaard, H.M., "Computation of stresses in bridge slabs due to wheel loads", *Public Roads*, Vol. 11, No. 1, March, 1930, pp. 1-23.

[106] Westergaard, H.M., and Slater, W.A., "Moments and stresses in slabs", *Journal of the American Concrete Institute*, Vol. 17, 1921, pp. 415-438.

[107] Whitney, C.S., "Ultimate shear strength of reinforced concrete flat slabs, footings, beams and frame members without shear reinforcement", *Journal of the American Concrete Institute*, Vol. 54, No. 4, Oct., 1957, pp. 265-298.

[108] Wood, J.G.M., Pipers Row Car Park, Wolverhampton – Quantitative Study of the Causes of the Partial Collapse on 20th March 1997.

[109] Yankelevsky, D., and Leibowitz, O., "Punching shear in concrete slabs", *International of Mechanical Sciences*, Vol. 41, 1999, pp. 1-15.

LIST OF TABLES AND FIGURES

A. LIST OF TABLES

B. LIST OF FIGURES